Reliability – based Performance Assessment of Damaged Ships

By

Fei Sun, Y. Pu, H.S Chan and R.S. Dow
School of Marine Science and Technology, Newcastle University,
Newcastle Upon Tyne NE1 7RU United Kingdom

M. Shahid and P.K. Das
Department of Naval Architecture and Marine Engineering,
Universities of Glasgow and Strathclyde, Henry Dyer Building,
100 Montrose Street, Glasgow G4 OLZ United Kingdom

September 2008

REPORT DOCUMENTATION PAGE	Form Approved OMB No. 0704-0188

PLEASE DO NOT RETURN YOUR FORM TO THE ABOVE ADDRESS.

1. REPORT DATE *(DD-MM-YYYY)*	2. REPORT TYPE	3. DATES COVERED *(From - To)*
10-02-2009	Technical, Research	15-JUL-2006 to 14-OCT-2008

4. TITLE AND SUBTITLE

Reliability - Based Performance Assessment of Damaged Ships

5a. CONTRACT NUMBER

N00014-06-1-0669

5b. GRANT NUMBER

N00014-06-1-0669

5c. PROGRAM ELEMENT NUMBER

06PR07158-01

6. AUTHOR(S)

Sun, F.; Pu, Y.; Chan, H.; Dow, R.S.;
Shahid, M.; Das, P.K.

5d. PROJECT NUMBER

5e. TASK NUMBER

5f. WORK UNIT NUMBER

7. PERFORMING ORGANIZATION NAME(S) AND ADDRESS(ES)

a) Newcastle University, Newcastle Upon Tyne NE1 7RU United Kingdom
b) Universities of Glasgow and Strathclyde, Henry Dyer Building, 100 Montrose Street, Glasgow G4 OLZ United Kingdom

8. PERFORMING ORGANIZATION REPORT NUMBER

9. SPONSORING/MONITORING AGENCY NAME(S) AND ADDRESS(ES)

Office of Naval Research, Ballston Centre Tower One, 800 North Quincy Street, Arlington VA 22217 - 5660

10. SPONSOR/MONITOR'S ACRONYM(S)

ONR

11. SPONSOR/MONITOR'S REPORT NUMBER(S)

12. DISTRIBUTION/AVAILABILITY STATEMENT

Approved for Public Release; distribution is Unlimited.

13. SUPPLEMENTARY NOTES

14. ABSTRACT

The objective of this project is to develop a procedure and tools for operators and decision makers to assess the residual ultimate hull girder strength of damaged ships for a given damage scenario. In this study, some tools for predicting wave-induced loads and assessing ultimate hull girder strength have been further developed. In particular, 2D linear and non-linear methods have been applied to a ship model to calculate the wave-induced loads in regular waves. The numerical results have been compared with the experimental results. The extreme design loads at sea states 3 - 7 have been calculated using short term prediction. An 'equivalent wave system' has been used to combine vertical bending moment, horizontal bending moment and torsion moment. The ultimate hull girder strength was calculated using MARS (Bureau Veritas software for structural calculation) and ANSYS (FE analysis Software). The reliability of the hull girder was predicted by a First Order Reliability Method (FORM) and Monte Carlo Simulation (MCS).

15. SUBJECT TERMS

Residual strength of damaged ships; Wave-induced loads on damaged ships; Hull girder strength; Reliability analysis of damaged ships; Model tests of hydrodynamic loads; Interaction of vertical and horizontal bending moment.

16. SECURITY CLASSIFICATION OF:			17. LIMITATION OF ABSTRACT	18. NUMBER OF PAGES	19a. NAME OF RESPONSIBLE PERSON
a. REPORT	b. ABSTRACT	c. THIS PAGE			Dr Yongchang Pu
UU	UU	UU	UU	220	19b. TELEPHONE NUMBER *(Include area code)* +44-191-222 6243

CONTENTS

List of Figures

List of Tables

1. EXECUTIVE SUMMARY

When a ship is damaged, the operators need to decide the immediate repair actions by evaluating the effects of the damage on the safety of the ship using residual strength assessment procedure. The objective of this project is to develop a procedure and tools for operators and decision makers to assess the residual ultimate hull girder strength of damaged ships for a given damage scenario. This study is a continuation of NICOP project (Lee, et al 2006), in which an assessment procedure was developed. In order for the readers to understand the significance of the current project, the assessment procedure is briefly described here. This procedure consists of four steps: (1) Identify the location and size of the openings; (2) Calculate the still water bending moment and wave-induced loadings including vertical bending moment, horizontal bending moment and torsion; (3) Calculate the ultimate hull girder strength of the damaged cross-section considering the interaction of vertical bending moment, horizontal bending moment and torsion; (4) Assess the structural integrity by deterministic and probabilistic approaches. In Step 1, once a ship is damaged, the location and size in terms of length, height and depth of the penetration of the opening should be determined. So the degree of water ingress could be predicted. In Step 2, the floating conditions of the ship need to be calculated. The stillwater bending moment and wave-induced loads are then estimated. Because it is desirable to install the developed tools on board of ships for a quick and reliable assessment, computational time is a very important factor in choosing a particular method for both loading calculations and strength assessment. In Step 3, the ultimate hull girder strength of the damaged cross-section needs to be assessed. The interaction of vertical bending moment, horizontal bending moment and torsion should be considered. In addition, the strength of other cross-sections (not the damaged one), where the total load including stillwater bending moment and wave-induced loads under the damage conditions exceed that in intact condition, should also be assessed. In Step 4, reliability of the damaged ship is calculated. So a well-informed decision could be made based on this information.

In the current project, some tools for predicting wave-induced loads and assessing ultimate hull girder strength have been further developed. In particular, a 2D linear and non-linear method have been applied to the ship model to calculate the wave-induced loads in regular waves at the cut where the force gauge is installed to measure the loads in the experimental tests. The numerical results have been compared with the experimental results.

The 2D linear method can accurately predict wave-induced vertical bending moment in head seas and stern quartering seas, but the accuracy is deteriorating with the increase of wave amplitude. The accuracy in predicting horizontal bending moment is not as good as that for vertical bending moment, but is acceptable in most cases. However, the predictions of torsion moment are not satisfactory.

The experimental results have revealed that majority of the response RAOs show non-linear trend, in which the non-dimensional responses are decreasing as wave amplitude increases in most frequency range, especially at the frequency where the responses achieve the maximum. For vertical bending moment this trend is very remarkable. It may be said that the high non-linearity is an inherent feature of the sample vessel with a very fine hull form.

Because the damage on the ship is unsymmetrical transversely, it is expected that the wave-induced loads might be different when the wave is approaching the ship model from different sides due to the dynamic behaviour of the flooded water in the damaged compartment. The test results have shown that the vertical bending moment at 45° wave heading at most of frequencies was slightly larger than that at 315° wave heading. There was no clear trend for

horizontal bending moment at 45° and 315° wave headings. However, the horizontal bending moment in beam seas at 90° wave headings is slightly larger than that at 270° wave headings. The torsion moment at 315° wave headings is larger than that at 45° wave headings.

The 2D nonlinear method does not produce satisfactory results for vertical bending moment, horizontal bending moment and torsion moment in regular waves. Although this conclusion was largely based on the analysis of the results of 2 metres wave height, it was equally applicable to the results of 2.5 metres wave height. Again the predictions of torsion moment are the worst among the three components of the wave-induced loads, while the predictions of vertical bending moment have similar level of accuracy to those of horizontal bending moment. The nonlinear method tends to produce better results at the resonant frequencies than at the other frequencies. However it should be pointed out that the measured wave heights were not equal to 2.0 metres, which was used in the numerical calculations, at most frequencies.

Model uncertainties of both 2D linear and non-linear method have been calculated. For the 2D linear method, it is observed that the accuracy, which is measured by the mean and COV of the model uncertainty factor, of vertical bending moment is generally better than that of horizontal bending moment and torsion moment, and the accuracy for loads in head seas is mueh better than those in stern quartering seas and beam seas. This could be mainly caused by the underwater hull form of the ship model with a small C_b compared with conventional ships. The COV of horizontal bending moment is almost as twice as that of vertical bending moment. The COV of torsion moment is the largest of the three. Because of the large difference in COV for different force components it is more rational to consider the model uncertainties for vertical bending moment, horizontal bending moment and torsion moment separately in reliability analysis rather than using one combined model uncertainty for all the components. It can be seen that the 2D linear method has better mean and COV of X_m in the predictions of vertical bending moment and horizontal bending moment in both intact condition and damage scenario 2 than the 2D nonlinear method, and both 2D linear and nonlinear methods have produced unsatisfactory results in torsion moment. Based on the current results, it may be said that the 2D linear method is more accurate than the nonlinear method. However the nonlinear method can distinguish the difference between the positive and negative responses, but linear methods can't. This advantage of the nonlinear method is especially important for ships with small block coefficient, such as frigate etc. For a frigate the ratio of sagging bending moment to hogging bending moment could be as large as 1.78 (Clarke, 1986). In addition, hull girder strength in hogging is normally different from that in sagging. Therefore the nonlinear method is preferred. This slight preference of the nonlinear method was also based on another fact that the nonlinear method tends to produce better results in the resonant region than at other frequencies. Based on the current method for combining different load components, the accuracy in resonant region is more important than that at other frequencies.

Extreme design loads in irregular waves based on the RAO from the 2D linear method, 2D non-linear method and experiment have been calculated for the ship model at the cut under intact condition and damage scenario 2. The formulae recommended in the Lloyds Register's rule for Navy vessels (Lloyds Register of shipping, 2002) have also been used to calculate the wave-induced extreme design loads. The results have demonstrated that the difference of extreme design loads (both hogging and sagging) between 2m and 2.5m wave height was increasing with the increase of sea roughness, but always less than 6.62% in intact condition and 6.60% in damage scenario 2. For hogging bending moment, the extreme design value based on 2m wave height is greater than that based on 2.5m wave height, but it was opposite for sagging bending moment. Hence the effects of wave amplitude on the prediction of extreme design loads are modest.

Both 2D linear and nonlinear methods overestimate extreme design loads. The results are slightly in favour of the 2D linear method in intact condition, while the accuracy of the 2D linear method is almost as good as that of the 2D nonlinear method in damage scenario 2. Both hogging and sagging bending moments predicted by the 2D nonlinear method agree well with those of LR Rules' formulae. However hogging bending moment of the 2D linear method agrees well with that of LR Rules' formulae, but agreement in sagging bending moment is not as good as in hogging bending moment because in the 2D linear method the sagging bending moment is the same as hogging bending moment. It should be noted that the extreme design value predicted by LR Rules is the maximum value for the ship model. In another word, the extreme design value at the cut is the same as that of the sections at the amidships because the cut is not far away from amidships. However the extreme design value predicted by the 2D nonlinear method at the cut could potentially be quite different from that of the sections at amidships, where the maximum vertical bending moment would occur. This might, at least partly, explain that LR Rules produces the largest extreme design hogging and sagging moments in intact condition.

The ratio of sagging bending moment to hogging bending moment of the 2D nonlinear method is in good agreement with that of the experimental tests. This is an advantage of the 2D nonlinear method over the 2D linear method. It should be pointed out that the reason for using the RAO of the 2D linear method rather than 2D non-linear method in strength assessment in this project is that the 2D non-linear results were not available at that moment.

The 2D linear method has also been applied to the original ship (not the model) in order to predict the extreme design loads for the strength assessment. The extreme design loads at sea states 3 - 7 have been calculated using short term prediction. An 'equivalent wave system' has been used to combine vertical bending moment, horizontal bending moment and torsion moment.

The Ultimate Hull Girder Strength was calculated using MARS (Bureau Veritas software for structural calculation) and Ansys (FE analysis Software). Calculations were made for both intact and damage. The MARS software provides different failure mode algorithms for calculation of ultimate strength that include Elastic Ideally Plastic (EIP) failure mode and Beam-Column (BC) failure mode, apart from the others. The ultimate bending moment capacity for combination of vertical and horizontal moments for elastic-plastic failure mode and for beam-column method were found and interaction formula's were derived based on that. . It may be observed that for hogging condition when the bending curvature ratio is small and, consequently, predominantly curvature is in vertical direction depicting predominant vertical bending moment, the difference between ultimate moment for damaged and intact condition is small.

The Finite element analysis was carried out using ANSYS, since no FE based design assessment of intact ship is available to compare the results with that of the damaged ship. The FE analysis for ultimate strength of hull girder is carried out for both intact and damaged conditions. Two types of moment interaction functions were developed, one set of two combinations of moments such as interaction of vertical and horizontal moments, and one set for interaction of all the moments viz. vertical, horizontal and torsion moment. The vertical and horizontal moment interaction function obtained from finite element analysis is compared with that of MARS beam-column and elastic-plastic interaction diagram. The ultimate moment estimates obtained using beam-column method is higher than that from the two frame finite

element analysis. The difference between the two results diminishes as M_v/M_h moment ratio increases.

The reliability analysis was carried out using CALREL software, the First Order Reliability Method (FORM) and Monte Carlo Simulation (MCS). The results from the finite element analysis were used for deriving the limit state function. The reliability based assessment of hull structure was made for both intact and damaged condition. The reliability assessment for intact condition is made for worse case scenario i.e. sea state 7 including three combinations as identified from ship loading analysis.

2. INTRODUCTION

2.1 Background

A large number of ship accidents continue to occur despite the advance with the navigation system. These accidents would cause the loss of cargos, pollution of environment, even loss of human beings. Based on statistical data of Lloyd's Register of Shipping (Lloyd's Register, 2000), a total of 1336 ships were lost with 6.6 million gross tonnage cargo loss between 1995 and 2000. 2727 people were reported killed or missing as a result of total losses in this period. A survey on the accidents of Greek ships over 100 GRT from 1993 to 2002 has revealed that about 48% of the loss were caused by grounding, collision and excessive loading (Samuelides, et al, 2007). So it is very important to ensure an acceptable safety level for damaged ships. Unfortunately adequate structural strength in intact condition does not necessarily guarantee an acceptable safety margin in damaged conditions. Conventionally only the structural strength in intact condition was assessed in the design.

Recognising the importance of the residual strength of ships, International Maritime Organisation (IMO) has proposed an amendment, which states: 'All oil tankers of 5000 tonnes deadweight or more shall have prompt access to computerised, shore-based damage stability and residual structural strength calculation programmes.'

When a ship is damaged, the operators need to decide the immediate repair actions by evaluating the effects of the damage on the safety of the ship using residual strength assessment procedure.

Various publications have concerned at, as summarised in the following, the local and overall structural behaviour of a damaged ship. Smith and Dow (1981) carried out pioneer work in assessing residual strength of damaged ships and offshore structures. Strength reduction of dented stiffened panels was investigated. The effect of this reduction on the ultimate strength of hull girder was further assessed.

Qi, et al (1999) have derived a simplified method for assessing residual strength of hull girders of damaged ships. Reliability of the ship was also estimated by a first order and second moment method.

Wang, et al (2002) have tried to use the section modulus to indicate the residual strength of damaged ships. Both section modulus and ultimate strength of damaged ships were calculated. A regression analysis was carried out to derive an empirical formula for predicting safety level of damaged ships.

A few more papers (Ghoneim and Tadros, 1992, Paik, 1992, Paik, et al, 1995, Zhang, et al,1996, Paik, et al, 1998, Ghose, et al, 1995) have discussed the residual strength of damaged ships from different view points.

All the above work only studied the ultimate vertical bending moment capacity without considering the effect of horizontal bending moment and torsion and critical load case was not evaluated. This means that the worst load case was assumed to be the vertical bending moment, and the horizontal bending moment and torsion are negligible. This methodology was, strictly speaking, only valid for ships in intact condition.

In the design of ships, structural strength is conventionally assessed only in intact condition. Under this condition, the critical load case for mono-hull ship is the vertical bending moment, which reaches maximum in head seas. Both horizontal bending moment and torsion are insignificant. The torsion will be considered only when there are large openings on ships. This methodology has been successfully applied to ship design for many years. Because of this, the prediction of environmental loads and assessment of structural strength were normally carried out separately by two groups of people. When the ultimate strength of hull girder is assessed, only vertical bending moment is considered. Although some researchers have tried to evaluate the effect of horizontal bending moment and shear on the ultimate strength (Paik, et al, 1996), it is concluded that these effects are insignificant. But this conclusion is only valid for intact condition.

When a ship is in damaged conditions its floating conditions could be changed dramatically. Its draught is increased and it may heel. It could also have large holes in the structure. If the methodology used for intact condition is blindly applied to damaged conditions, the results could be misleading. Ideally the environmental loads should be calculated together with the assessment of the residual strength of the ship. In another words, a systematic approach should be used for a more accurate assessment of residual strength of a damaged ship. Chan, et al, (2001) have shown that the most critical condition for a damaged Ro-Ro ship is in quartering seas. Although the vertical bending moment in quartering seas is smaller than that in head seas, the horizontal bending moment is quite large. The ratio of horizontal bending moment to vertical bending moment could be as large as 1.73. So the combined effect of vertical bending moment and horizontal bending moment is more serious. In addition, torsion, which is not considered in the above study, normally reaches maximum in quartering seas. So the effect of horizontal bending moment and torsion on the ultimate hull girder strength should be considered in the assessment of residual strength of damaged ships.

From 2004 to 2006 Office of Naval Research (USA) sponsored a project, NICOP, which shares the same title as the current project, to address some of the important issues associated with damaged ships (Lee, et al, 2006). The participants include Y.W. Lee, Y. Pu, H.S. Chan, A. Incecik and R.S. Dow in Newcastle University, I. Khan and P.K. Das in the University of Glasgow and Strathclyde, and P.E. Hess in Naval Surface Warfare Center Carderrock Division (NSWCCD) in USA. In this study, a procedure has been developed to assess structural integrity of damaged ships. The procedure consists of four steps: (1) Identify the location and size of the openings; (2) Calculate the still water bending moment and wave-induced loadings including vertical bending moment, horizontal bending moment and torsion; (3) Calculate the ultimate hull girder strength of the damaged cross-section considering the interaction of vertical bending moment, horizontal bending moment and torsion; (4) Assess the structural integrity by deterministic and probabilistic approaches. The state of the art of the methods for predicting environmental loads and assessing the structural safety has been reviewed. The developed procedure is applied to a sample vessel, HULL5415, to demonstrate the applicability of the proposed procedure.

The hydrodynamic loads in regular waves have been calculated by a 2D linear method. Experimental tests on a ship model with a scale of 1/100 have also been carried out to predict the hydrodynamic loads in regular waves. The results of the theoretical method and experimental tests are compared to validate the theoretical method and to calculate the model uncertainties of the theoretical method for probabilistic strength assessment. The comparison of theoretical results with experimental results has revealed that the prediction of vertical bending moment of the 2D linear method agrees reasonably well with the experimental results, while the prediction of horizontal bending moment is acceptable. However the accuracy of

torsion moment is generally poor. Further research is required to improve the accuracy in this area.

The extreme wave-induced loads have been calculated by short term and long term predictions. For the loads in intact condition, long term prediction with duration of 20 years is used, while for loads in damaged conditions short term prediction is used. The maximum values of the most probable extreme amplitudes of dynamic wave induced loads in damaged conditions are much less than those in intact condition, because the most probable extreme load in intact condition is based on long term prediction, while the most probable extreme load for damaged conditions is based on short term prediction under sea state 3 for 96 hours.

An opening could change the distribution of not only stillwater bending moment but also wave-induced bending moment. It is observed that although some cross sections are not structurally damaged, the total loads (including stillwater bending moment and wave-induced bending moment) acting on these cross sections after damage (in other locations) may be increased dramatically compared to the original design load in intact condition. In this case the strength of these cross sections also needs to be assessed.

The ultimate strength of the hull 5415 has been predicted using the progressive analysis, the results of which compare well with those of another program developed by Bureau Veritas (BV). Although the strength assessment of all the critical cross sections should be carried out in practice, not all the cross sections have structural details for this hypothetical vessel. Therefore only those critical cross sections with structural details are assessed to demonstrate the applicability of the developed methods.

The residual strength in 4 different damage scenarios has been compared. In damage scenarios 1 and 2, since the locations of the damages have been around the elastic neutral axis, the residual strength has been about 96.6% and 93 % of the ultimate strength during hogging condition. Similarly the residual strength at damage scenarios 3 and 4 shows significant decrease compared to the ultimate strength.

Deterministic strength assessment of the damaged ships is carried out by considering the interaction of vertical and horizontal bending moments for intact condition and damage scenario 2. It is found that the damaged ship is quite safe with a fairly high safety margin. This is due to the relatively small wave-induced loads, which is based on a short term prediction, and at the same time the extent of damage is fairly moderate, which does not reduce the ultimate strength too much.

The residual strength has also been assessed by a probabilistic approach. The limit state function used for reliability analysis is derived from the interaction equation including vertical and horizontal bending moments, which was developed in the deterministic strength assessment. The reliability index for HULL 5415 in intact condition has been calculated.

Overall the developed procedure and the methods are working well. It also reveals the needs for further research in some areas.

2.2 Objectives and Scope of Work

The objective of this project is to develop a procedure and tools for operators and decision makers to assess the residual ultimate hull girder strength of damaged ships for a given damage scenario. To achieve this objective, the following work packages are planned:

- Develop a method for predicting wave-induced loading on damaged ships, and validate the method by comparing with experimental results so that its model uncertainty could be determined.
- Develop the damaged ship structural strength predictions with a focus on hull girder bending using numerical analysis.
- Develop reliability-based analysis procedure for determining the recoverability and operability of damaged ships.

This project is a continued effort of NICOP project (Lee et al, 2006). While these two projects share the same objectives, the current project will focus on the following tasks:

Task 1: To apply the 2D linear method to predict wave-induced loads on the ship model;

In this task, an in-house program, which is based on a 2D linear theory (Chan, 1992), was chosen to predict wave-induced loads in regular waves. This method is capable of dealing with unsymmetrical floating conditions, which is a unique feature of damaged ships. The details of this method are described in Section 3.1.1, while the results are presented in Section 5.2.

Task 2: To apply the 2D non-linear method to predict wave-induced loads on the ship model;

In this task, another in-house program, which is based on a 2D non-linear method (Chan, et al, 2003), has been used to predict wave-induced loads in regular waves. This method calculates wave-induced loads in time domain. Unsymmetrical floating conditions can also be considered in this method. The details of the method will be described in Section 3.1.2, and the results will be presented in Section 5.3.

Task 3: To carry out more experimental tests to validate both 2D linear and non-linear methods;

Experiments have been carried out to investigate the structural responses of the ship model with a scale of 1/100. The results can reveal important phenomena at various damaged conditions, and also be used to validate both the 2D linear and non-linear methods. The test facilities and other details of running the tests will be shown in Section 3.1.4, and the results will be presented in Chapter 5.

Task 4: To calculate model uncertainties of both 2D linear and non-linear methods for reliability analysis;

In this task, model uncertainties of both 2D linear and non-linear methods are calculated. These are important parameters which influence reliability of strength assessment. The method is presented in Section 3.1.5 and the results are presented in Section 5.4.

Task 5: To calculate extreme design loads in irregular waves using short term prediction;

Extreme design loads in irregular waves have been calculated using short term prediction for the original sample vessel at amidships. RAOs of the 2D linear method have been used. These results are used for strength assessment in Task 7. In addition, RAOs of 2D linear method, 2D non-linear method and experiment have also been used to calculate extreme design load of the ship model at the cut, where the force gauge is installed, in order to compare the results of different methods. The formulae recommended by Lloyds Register of

Shipping (Lloyds Register of Shipping, 2002) are also used to predict the extreme design loads. The method is presented in Section 3.1.3, and the results are in Section 5.5.

Task 6: To combine different load components, such as vertical bending moment, horizontal bending moment and torsion, in order to assess structural integrity under combined load conditions;

One of the aims of this project is to investigate the effects of horizontal bending moment and torsion on the ultimate hull girder strength of damaged ships. In this task, vertical bending moment, horizontal bending moments and torsion are combined. These results have been passed onto the research team of the University of Glasgow and Strathclyde to assess the strength of the sample vessel. The method is presented in Section 3.2 and the results are in Section 5.5.3.

Task 7: Develop the damaged ship structural strength predictions with a focus on hull girder bending using numerical analysis.

The ultimate hull girder strength of the damaged cross-section needs to be assessed .This task was accomplished using Ansys (FE analysis Software) and MARS (Bureau Veritas software for structural calculation). The interaction of vertical bending moment, horizontal bending moment and torsion were considered. In addition, the strength of other cross-sections (not the damaged one), where the total load including stillwater bending moment and wave-induced loads under the damage conditions exceed that in intact condition, should also be assessed. The method and results can be found in Section 5.6.2 and Section 5.6.3

Task 8: Develop reliability-based analysis procedure for determining the recoverability and operability of damaged ships.

The reliability based assessment of hull structure was made for both intact and damaged condition. The reliability assessment for intact condition is made for worse case scenario i.e. sea state 7 including three combinations as identified from ship loading analysis. The reliability analysis was carried out using CALREL software, the First Order Reliability Method (FORM) and Monte Carlo Simulation (MCS). The reliability index and relevant probabilities as calculated are given in table 5.6.3.6.1 for both intact and damaged case.

This research has been jointly carried out by Newcastle University, and the University of Glasgow and Strathclyde. Tasks 1 – 6 are executed by Newcastle University, while the others by the University of Glasgow and Strathclyde.

This report consists of 6 chapters. Chapter 1 summarises the major findings of the current project. Chapter 2 presents the background, objectives and scope of the project. The state of the art of the techniques has been reviewed in NICOP project (Lee, et al, 2006), so it will not be presented in this report. The details of the methods, which are used in this project, are presented in Chapter 3. Chapter 4 shows the particulars of the sample vessel and its model, and describes briefly 3 damage scenarios used in the following calculations. In Chapter 5 all the methods have been applied to both the sample vessel and its model. The results have been analysed and discussed. Finally conclusions have been drawn in Chapter 6.

3. METHODOLOGIES

3.1 Methodologies for Wave-Induced Loading

To predict the motion and load responses of a vessel to waves, either results of experimental measurements or those obtained mainly from linear frequency domain methods may be used. However, the frequency domain method is not adequate for large-amplitude motion predictions because it is assumed not only that the free surface condition is linearised but also that the ship motions are small relative to the ship dimensions. Large-amplitude motions and resulting global wave loads, which cannot be predicted accurately by linear theory, are associated with non-linear effects. In particular, the wetted surface of a ship's body varies significantly in large-amplitude motions and becomes asymmetrical during roll motion. The variation of the wetted surface can lead to different absolute values of positive and negative responses. Moreover, flood water dynamics inside a damaged compartment will alter the inertia characteristics of a damaged vessel. There is a need to use time-domain methods to take these effects into account. In the present study a linear two-dimensional method in a frequency domain, a non-linear time-domain method and model experiments have been employed for the predictions of motion and global load responses of a notional US Navy destroyer hull 5414 in regular waves in an intact and various damaged conditions.

3.1.1 Linear two-dimensional method

Fig. 3.1-1 shows the right-hand coordinate system o-*xyz* with its *x*-axis pointing toward bow, and the *z*-axis pointing vertically upward through the centre of gravity of the intact body with the origin o in the plane of mean free surface. The body is assumed rigid and oscillates in six degrees of freedom about its mean position with complex amplitudes η_k. Here, the index $k = 1, 2, 3, 4, 5, 6$ refer to surge, sway, heave, roll, pitch and yaw modes of motion respectively.

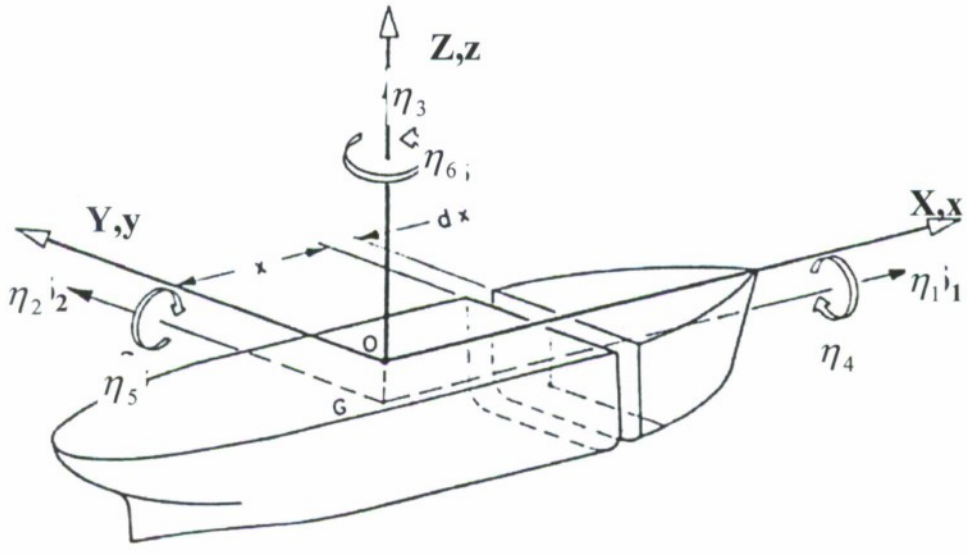

Figure 3.1-1: Co-ordinate system and modes of motions

For dynamic equilibrium the coupled linear equations of motion of the rigid body can be written as

$$\sum_{k=1}^{6}[(M_{jk}+A_{jk})\cdot\ddot{\eta}_k+B_{jk}\cdot\dot{\eta}_k+C_{jk}\cdot\eta_k]=F_j \qquad \text{for } j=1, 2, \ldots 6 \tag{3.1-1}$$

where $\ddot{\eta}_k$ and $\dot{\eta}_k$ are motion acceleration and velocity respectively; M_{jk} is the generalised mass; A_{jk} is the added mass; B_{jk} is the damping; C_{jk} is the restoring coefficients; F_j is the wave exciting force or moment. The indices j and k indicate the direction of force and the mode of motion respectively.

The generalised mass matrix $[\boldsymbol{M}]$ of a damaged ship whose centre of gravity is at (x_G, y_G, z_G) is given by

$$[M]=\begin{bmatrix} M & 0 & 0 & 0 & Mz_G & -My_G \\ 0 & M & 0 & -Mz_G & 0 & Mx_G \\ 0 & 0 & M & My_G & -Mx_G & 0 \\ 0 & -Mz_G & My_G & I_{44} & -I_{45} & -I_{46} \\ Mz_G & 0 & -Mx_G & -I_{54} & I_{55} & -I_{56} \\ -My_G & Mx_G & 0 & -I_{64} & -I_{65} & I_{66} \end{bmatrix} \tag{3.1-2}$$

in which M is the mass of the ship including flood water, I_{jj} is the moment of inertia about the origin in the jth mode of motion and I_{jk} is the cross-product of inertia about the origin.

The added mass, damping coefficients, and wave exciting forces can be calculated by integration of the sectional values over the ship length L, and can be expressed respectively as

$$A_{jk}=\int_L a_{jk}(x)dx \tag{3.1-3}$$

$$B_{jk}=\int_L b_{jk}(x)dx \tag{3.1-4}$$

$$F_j=\int_L f_j(x)dx \tag{3.1-5}$$

where a_{jk}, b_{jk} and f_j are respectively the sectional values of added mass, damping coefficient and wave-exciting force. The details of calculations of a_{jk}, b_{jk} and f_j can be found in Chan et al 2002.

The global wave-induced loads P_j on a particular transverse cross-section x of the ship body can be expressed as

$$P_j=\sum_{k=1}^{6}[(m_{jk}+A_{jk}(x))\cdot\ddot{\eta}_k+B_{jk}(x)\cdot\dot{\eta}_k+C_{jk}(x)\cdot\eta_k]-F_j(x) \quad \text{for } j=1, 2, \ldots 6 \tag{3.1-6}$$

where P_1, P_2 and P_3 represent wave-induced longitudinal force, horizontal shear force and vertical shear force respectively, while P_4, P_5 and P_6 are wave-induced torsional moment, vertical bending moment and horizontal bending moment respectively. m_{jk} is generalised mass for the portion aft the cross-section.

$$A_{jk}(x) = \int_x a_{jk}(\xi) d\xi \tag{3.1-7}$$

$$B_{jk}(x) = \int_x b_{jk}(\xi) d\xi \tag{3.1-8}$$

$$F_j(x) = \int_x f_j(\xi) d\xi \tag{3.1-9}$$

The integration is performed from aft end of the ship body to the cross-section x.

3.1.2 Non-linear time-domain method

To describe flow fields and motions of a rigid body floating in waves in a time-domain, it is convenient to refer the rigid body motion to a space-fixed coordinate system O-XYZ as well as a body-fixed coordinate system o-xyz as shown in Figure 4.1-2. The position and orientation of the body should be described with respect to the space-fixed system O-XYZ while the linear and angular velocities and accelerations of the body should be expressed in the body-fixed system o-xyz. The space-fixed system O-XYZ is the inertia system with the origin O lying on undisturbed free surface and the Z-axis pointing vertically upward. The body-fixed system o-xyz is moving rectangular co-ordinate system with the origin o being coincident with the centre of gravity of the intact body. The x, y and z axes are directed respectively toward the bow, the port side and the sky (Chan, 1998; Chan et al, 2003).

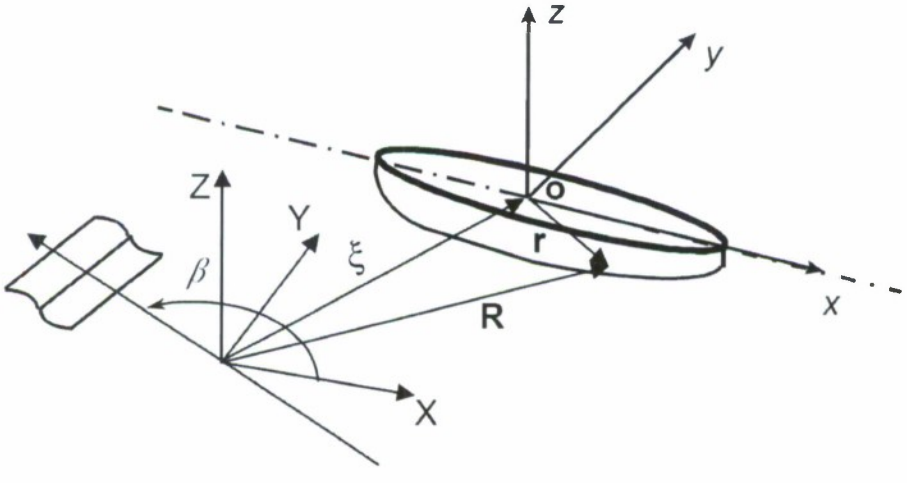

Figure 3.1-2: Co-ordinate systems (Chan at al, 2003)

The position and orientation vectors of the body-fixed axes with respect to the space-fixed frame are defined respectively in the form

$$\boldsymbol{X} = (\eta_1, \eta_2, \eta_3) \tag{3.1-10}$$

$$\boldsymbol{\Omega} = (\eta_4, \eta_5, \eta_6) \tag{3.1-11}$$

The relationship between a body-fixed position vector $\boldsymbol{r}$ and a space-fixed position vector $\boldsymbol{R}$ can be written as

$$\boldsymbol{R} = \boldsymbol{X} + \boldsymbol{T}\,\boldsymbol{r} \tag{3.1-12}$$

where $\boldsymbol{T}$ is an orthogonal transformation matrix (Chan 1998).

The Euler equations of motion of a rigid body in six degrees of freedom with respect to the body-fixed co-ordinate system are defined by Chan 1998 as

$$\dot{m}\left(\mathbf{v} + \boldsymbol{\omega} \times r_G\right) + m\left(\dot{\mathbf{v}} + \boldsymbol{\omega} \times \mathbf{v} + \dot{\boldsymbol{\omega}} \times \boldsymbol{r}_G + \boldsymbol{\omega} \times \left(\boldsymbol{\omega} \times r_G\right)\right) = \boldsymbol{F} \tag{3.1-13}$$

$$\boldsymbol{I}\boldsymbol{\omega} + \dot{m}\boldsymbol{r}_G \times \mathbf{v} + \boldsymbol{I}\dot{\boldsymbol{\omega}} + \boldsymbol{\omega} \times \boldsymbol{I}\boldsymbol{\omega} + m\boldsymbol{r}_G \times \left(\dot{\mathbf{v}} + \boldsymbol{\omega} \times \mathbf{v}\right) = \boldsymbol{M} \tag{3.1-14}$$

in which m is the body mass; $\boldsymbol{I}$ is the matrix of second moment of inertia; $\mathbf{v}$ and $\boldsymbol{\omega}$ are linear and angular velocity vectors respectively; the dot stands for time derivative with respect to the body-fixed frame; $\boldsymbol{r}_G$ is a position vector of the centre of gravity of the body; $\boldsymbol{F}$ and $\boldsymbol{M}$ are the external force and moment vectors respectively. The body-fixed angular velocity vector $\boldsymbol{\omega}$ and the Euler angular velocity vector $d\boldsymbol{\Omega}/dt$ can be related through a transformation matrix Γ (Chan 1998).

$$d\boldsymbol{\Omega}/dt = \Gamma\boldsymbol{\omega} \tag{3.1-15}$$

Equations (3.1-13) and (3.1-14) represent a set of six second-order ordinary differential equations and can be solved by numerically integration over time using 4th order Runge-Kutta method.

Within the framework of linear potential flow theory the components of the external force $\boldsymbol{F}$ and moment $\boldsymbol{M}$ can be generalised in the form

$$\widetilde{F}_j = F_j - \sum_{k=1}^{6}\left(A_{jk}\dot{\mathrm{v}}_{\mathrm{j}} + B_{jk}\mathrm{v}_{\mathrm{j}}\right) + C_j - W_j \tag{3.1-16}$$

where j and k indicate the direction of external force and velocity (acceleration) respectively in the body-fixed co-ordinate system; F_j is the wave exciting force; A_{jk} is the added mass; B_{jk} is the damping coefficient; C_j is the buoyancy force; W_j is the force due to gravitation. These hydrodynamic forces due to radiation and wave excitation at each time step can be calculated by integration of sectional values at the incident wave profile. The sectional values of hydrodynamic coefficients and wave exciting forces at various ship sections can be obtained by means of two-dimensional source distribution technique (Kim et al, 1980). The buoyancy force and moment of submerged body are calculated by integration of sectional area and momcnt of submerged section. For a damaged hull loss of buoyancy can be accounted for the calculations

of buoyancy force and moment by means of loss buoyancy method or added weight method. The external force $\boldsymbol{F}$ and moment $\boldsymbol{M}$ are time dependent and become non-linear. The hydrodynamic coefficients are coupled with each other when the ship sections are no longer symmetrical.

The position vector $\boldsymbol{r}_G$ of an intact ship is equal to zero as the origin of the body-fixed system is defined at the centre of gravity of intact ship and the ship mass m and inertia matrix $\boldsymbol{I}$ is constant. The dynamic effects of flooding water in damaged compartment on ship motion are taken into account by adding time dependent mass of flooding water into the ship mass m. Consequently the mass m, inertia matrix $\boldsymbol{I}$ and the position vector $\boldsymbol{r}_G$ of a damaged ship varies with time. As it is difficult to simulate the free surface of flooding water, the sloshing effects are not considered in the present study. For simplicity the level of flooding water is assumed to be the same height as that of the incident wave profile.

Since the ship body is free to drift, she will inevitably drift away from the nominal heading angle β. In order to maintain the wave heading angle within a reasonable range, an artificial restoring yaw moment c_6 is introduced in the equations of motion and may be expressed by

$$c_6 = -a\zeta\omega_o^2 I_{zz} \tag{3.1-17}$$

where a is a constant; ζ is wave amplitude and I_{ZZ} is yaw moment of inertia. In the present study the constant a of 0.1 is used outside roll resonant region. In addition to potential roll damping B_{44}, viscous roll damping b_{44} obtained from roll decay test is used in the prediction of roll motion in roll resonant region.

Although the equations of motion are fully non-linear, the hydrodynamic forces due to incident waves, radiation waves and diffraction waves are still linear and calculated up to the incident wave profile. No radiation and diffraction waves are considered on the free surface. As a consequence, drift motions predicted by the present numerical model may be unrealistic.

After solving the non-linear Euler equations of motion at each time step, the dynamic global wave loads can be easily calculated. They are expressed by Chan 1998 as

$$\begin{aligned}(P_1,P_2,P_3) &= \overline{\boldsymbol{F}} - \overline{\boldsymbol{F}_S} - \int_x \dot{m}(\mathrm{v} + \omega \times \boldsymbol{r})dx \\ &- \int_x m(\dot{\mathrm{v}} + \omega \times \mathrm{v} + \omega \times \boldsymbol{r} + \omega \times (\omega \times \boldsymbol{r}))dx\end{aligned} \tag{3.1-18}$$

$$\begin{aligned}(P_4,P_5,P_6) &= \overline{\boldsymbol{M}} - \overline{\boldsymbol{M}}_S - \boldsymbol{r}_c \times \boldsymbol{P} - \bar{\boldsymbol{I}}\dot{\omega} + \int_x \dot{m}\boldsymbol{r} \times \mathrm{v}\,dx \\ &- \bar{\boldsymbol{I}}\dot{\omega} - \omega \times \bar{\boldsymbol{I}}\omega - \int_x m\boldsymbol{r} \times (\dot{\mathrm{v}} + \omega \times \mathrm{v})dx\end{aligned} \tag{3.1-19}$$

where the over-bar implies that the integration is carried out from one end to the particular cut. $\boldsymbol{F}_S$ and $\boldsymbol{M}_S$ are shear force and bending moment vectors due to still water loads. $\boldsymbol{r}_c$ is the position vector of the point of interest at which the dynamic shear force vector $\boldsymbol{P}$ acts.

3.1.3 Responses under irregular waves

The elevation of the ocean waves is irregular and has a random nature in seaway. In practice linear theory is used to simulate irregular sea and to obtain statistical estimates. The wave spectrum can be estimated from wave measurements during limited time period in the range from ½ hour to around 10 hours. In the literature this is often referred to as a short-term description of the sea. ITTC spectrum can be used to calculate significant values and other characteristics of wave exciting forces and responses in short term prediction method (Hasselmann at al, 1973; DNV, 2000).

The variance (m_0) is the area below the spectral density function.

$$m_0 = \int_0^\infty S(\omega)d\omega \tag{3.1-20}$$

From equation (3.1-20), the following characteristic parameters can be defined as follows (Ochi, 1973 and 1981; DNV, 2000).

Significant wave height is

$$H_s = 4\sqrt{m_0} \tag{3.1-21}$$

Average wave height is

$$H_{av} = \sqrt{2m_0} \tag{3.1-22}$$

Highest one tenth of all waves is

$$H_{1/10} = 5.1\sqrt{m_0} \tag{3.1-23}$$

Extreme design wave height is

$$H_{\max} = \sqrt{8m_0 \ln\frac{N}{0.01}} \tag{3.1-24}$$

where N is the number of waves.

Related to the wave spectrum $S(\omega)$ of the seaway, the response spectrum $RS(\omega)$ represents the energy distribution of the output signal.

$$\sigma_R{}^2 = \int_0^\infty S(\omega)\left|H(\omega)\right|^2 d\omega \tag{3.1-25}$$

If the wave height values are assumed to be Rayleigh distributed so are the response values. The probability density function of a response amplitude value R_0 can be written as (Faltinsen, 1990)

$$p(R_0) = \frac{R_0}{\sigma_R{}^2} e^{-R_0{}^2/2\sigma_R{}^2} \tag{3.1-26}$$

The probability of exceeding the value of R_0 is

$$Q(R > R_0) = e^{-R_0^2/2\sigma_R^2} \tag{3.1-27}$$

The most probable extreme response amplitude value in N waves can be written as

$$R_{\max} = \sqrt{2\sigma_R^2 \ln(N)} \tag{3.1-28}$$

The probability of exceeding the response value given in equation (4.1-26) for large N values is 0.632 (Ochi, 1973). The design extreme response amplitude value that will not be exceeded in N encounters with a probability of 0.99 is given by

$$R_{design} = \sqrt{2\sigma_R^2 \ln(N/0.01)} \tag{3.1-29}$$

3.1.4 Experimental investigation

3.1.4.1 Introduction

The facilities and test procedure used in this project is the same as those in NICOP project. Detailed descriptions of them can be seen in the report of Lee, et al (2006). A brief description is provided here for the readers to understand the test results.

The tests have been carried out at the Newcastle University towing tank, which is 37 metres long, 4 metres wide and 1.2 meters deep, and is equipped with a wave-maker at one end and an energy-absorbing beach at the other end. In order to measure the wave-induced loads, the model is cut into two pieces at the cross-section, which is located 545.43 mm from the after perpendicular longitudinally. The two pieces are linked together by a force gauge, which is bolted to two substantial bulkheads mounted in the fore and aft parts of the model and the two sections are made waterproof by the provision of a thin membrane across the cut. The force gauge is capable of measuring five force components, namely F_y, F_z, M_y, M_z and M_x. Due to the limit of the budget, the forces are measured at only one cross-section.

Waves were generated by seven rolling seal hinged paddle type wave makers normally operating in unison and driven by a sinusoidal source at the desired period and amplitude. The wave profile was monitored and recorded using two Churchill resistance probes, which were placed in the front of the model, and an associated monitor.

3.1.4.2 Test conditions and procedures

In all the tests, wave-induced loads in the five directions at the cut of the model along with wave height and period were measured at a zero forward speed. As shown in Figure 3.1-3, four mooring lines were attached to the ship model at the fore and stern ends, each of which has two mooring lines, in order to keep the model from drifting too far away from its original position and to maintain the intended orientations.

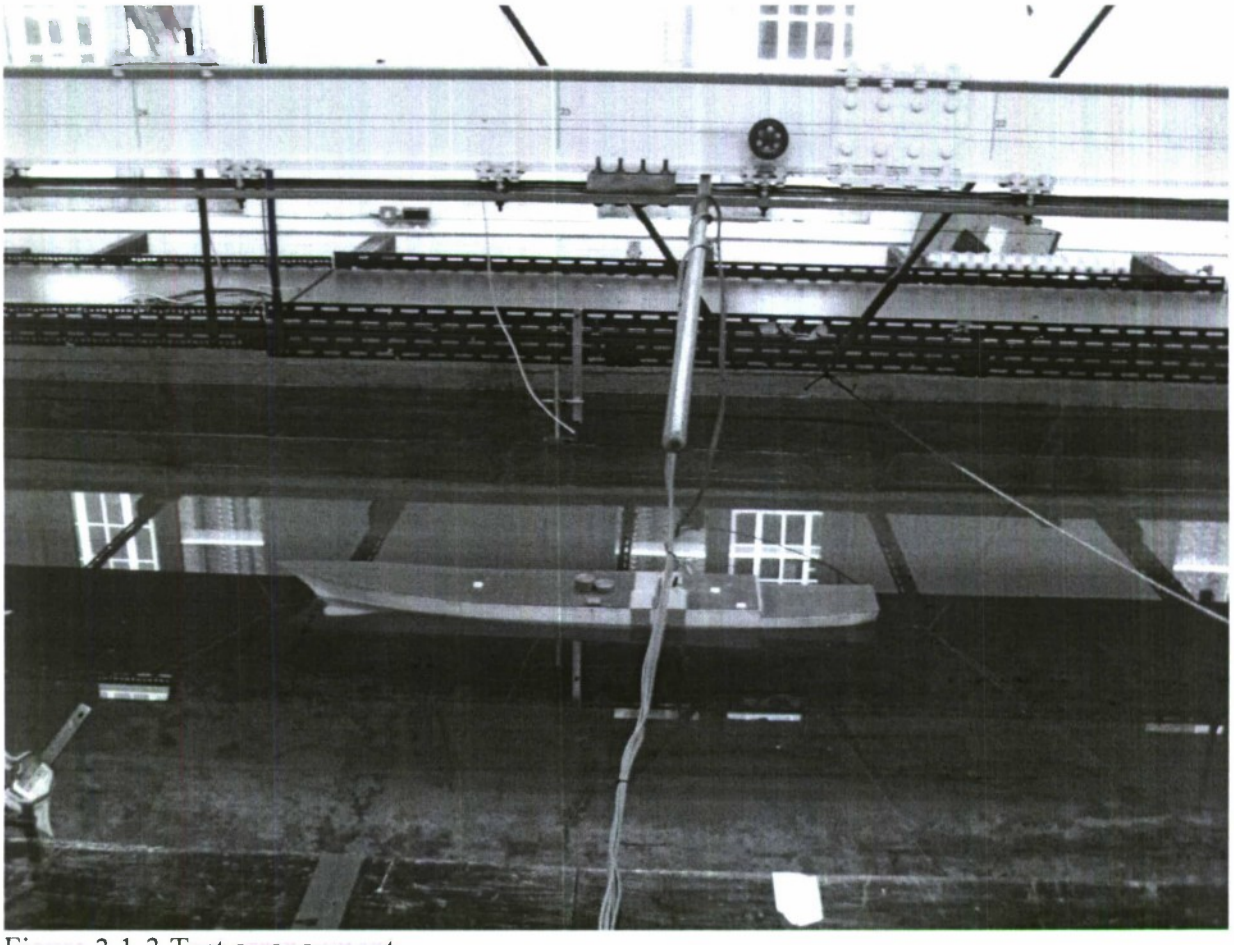

Figure 3.1-3 Test arrangement

The original data were processed by a filter to remove the high frequency noise and high frequency forces, such as slamming and green water effects under severe wave conditions, and then by FFT. The RAOs of each force components could then be calculated and plotted for further analysis.

Initially a total number of 324 tests have been planned as shown in Table 3.1-1 Basically 3 floating conditions, namely intact condition, damage scenarios 2 and 3, were considered. For each floating condition, various wave headings, 3 different wave heights and 9 wave frequencies have been chosen. In the intact condition, 4 wave headings, which include head seas, bow quartering seas, stern quartering seas and beam seas, have been chosen. In damage scenario 2, 5 wave headings, namely, head seas, stern quartering seas from the port, stern quartering seas from the starboard, beam seas from the port and beam seas from the starboard are selected. The reason for having two stern quartering seas is due to the fact that the damage (opening) of the ship model is on the starboard side only. So when a wave is approaching the model from different sides, the dynamic responses of the model might be quite different. For the same reason, two different beam seas are considered. In damage scenario 3, only 3 wave headings, namely head seas, stern quartering seas from the starboard and beam seas, have been selected due to the limited availability of time to the towing tank. Three different wave heights, namely small, large and very large, are defined in Table 3.1-2.

Table 3.1-1: Test Conditions of the First Batch of Wave-induced Loads Tests

Floating conditions	Wave heights	Number of wave headings	Number of wave frequencies	Total
Intact	small	4	9	36
	large	4	9	36
	very large	4	9	36
Damage scenario 2 (DS2)	small	5	9	45
	large	5	9	45
	very large	5	9	45
Damage scenario 3 (DS3)	small	3	9	27
	large	3	9	27
	very large	3	9	27
Total				324

Table 3.1-2 Definitions of Different Categories of Wave Heights in Table 3.1-1

Category of wave height	For the ship model (mm)	For the ship (m)
Small	5.74 – 7.88	0.574 – 0.788
Large	11.64 – 23.72	1.164 – 2.372
Very large	10.44 – 47.45	1.044 – 4.745

After the first batch of tests was completed and the results were analysed, it appeared that there was a need to carry out additional tests to investigate the nonlinearity in some frequencies. Therefore another 86 tests have been carried out. Basically for a given frequency, four different wave amplitudes have been used in order to indicate how the wave-induced loads vary against the wave amplitude.

3.1.5 Model uncertainties of numerical methods

Model uncertainty is a very important source of uncertainties in structural design process. A coefficient of variation (COV) of a typical strength prediction could be about 10 – 15%, while a COV of wave-induced load prediction could be well above 30%. This means that model uncertainties of wave-induced load prediction is a major uncertainty in structural strength assessment.

Model uncertainty of wave-induced loads is defined as the ratio of real load to the predicted load, which could be expressed as:

$$X_{m0} = \frac{M_{exp}}{M_{pred}} \qquad (3.1-30)$$

where X_{m0} is model uncertainty of the formula or numerical method for predicting wave-induced loads. In this project model uncertainty of the 2D linear method for predicting wave-induced loads will be calculated. M_{exp} and M_{pred} are real and predicted extreme design wave-induced loads respectively. In practice the real extreme design wave-induced loads are very

difficult to be obtained, so the experimental results would be used as the real values if the experiment is properly executed.

When the model uncertainty is calculated, the number of sample data should be fairly large so that reliable statistical mean and standard deviation could be obtained. However if the definition in Eq. (3.1-30) is directly used in model uncertainty calculation, there would be only one set of data for each wave headings, so the total number of sample data would be too few to calculate the model uncertainty of wave-induced load prediction. In addition, wave-induced loads for a given period can not be measured in the test. Therefore another definition is introduced, which is expressed as:

$$X_{m1} = \frac{RAO_{exp}}{RAO_{pred}} \tag{3.1-31}$$

where RAO stands for Response Amplitude Operator. Obviously X_{m1} is a function of wave frequency. However it is a good indicator of model uncertainty associated with wave-induced loads. When X_{m1} is a constant, it is equal to X_{m0} if the extreme design wave-induced load is calculated by a short term analysis. This can be proved as follows:

Substitute Eq. (3.1-28) into Eq. (3.1-30), so

$$X_{m0} = \frac{M_{exp}}{M_{pred}} = \frac{(\sigma_R)_{exp}\sqrt{2\ln(N)}}{(\sigma_R)_{pred}\sqrt{2\ln(N)}} = \frac{(\sigma_R)_{exp}}{(\sigma_R)_{pred}} \tag{3.1-32}$$

Because

$$(\sigma_R^2)_{exp} = \int_0^\infty S(\omega)|RAO_{exp}|^2 d\omega = \int_0^\infty S(\omega)|X_{m1} \times RAO_{pred}|^2 d\omega = X_{m1}^2 \int_0^\infty S(\omega)|RAO_{pred}|^2 d\omega = X_{m1}^2 \times (\sigma_R^2)_{pred} \tag{3.1-33}$$

Combine Eqs. (3.1-32) and (3.1-33)

$$X_{m0} = X_{m1} \tag{3.1-34}$$

Hence in this project X_{m1} is used as model uncertainty of wave-induced loads.

3.2 Methodologies for combining different loads

There are various types of loads acting on ships, such as stillwater bending moment, wave-induced loads, slamming forces, etc. In this project, only stillwater bending moment and wave-induced loads will be considered. It is very important to properly combine all these loads in the strength assessment. In the ship design rules the maximum loads for each type of load are simply added together (Wang and Moan, 1996). This could introduce unnecessary conservatism in the design. In the context of load combination of ship structures, there are two issues. The first issue is how to combine different components of wave-induced loads. The second issue is how to combine stillwater bending moment and wave-induced loads.

Bearing in mind that the objectives of the project is to develop a procedure and tools for operators and decision makers to assess the residual ultimate hull girder strength of damaged ships for a given damage scenario, the loads required for strength assessment are at the given

operational conditions. So the stillwater bending moment will be calculated at the given operational conditions, and be then directly added to the combined wave-induced loads.

Wave-induced loads have generally six components, among which 5 components will be predicted by the 2D methods in this project. Of these load components, vertical and horizontal bending moments, torsion and vertical shear force are potentially important in the strength assessment of damaged ships. Because all these load components have different phase angles, they reach maximum at different time. If the maximum amplitudes of each components are simply added together to assess the structural strength, the results could be too conservative. For this reason, an "equivalent wave system" is used to combine all the load components. The concept of equivalent wave system was introduced by Reilly (1988). It was used by Pu (1995) to calculate the instantaneous pressure distribution of a SWATH vessel.

In this study, three load components, namely vertical bending moment (M_y), horizontal bending moment (M_z) and torsion moment (M_x), will be considered. However this concept could be applied to all the five load components.

Before combining these load components, the following results need to be produced:
1). RAO of all the load components;
2). Extreme design loads for each components based on short term prediction.

There are three possible load combinations for three load components. For load combination 1 vertical bending moment will take maximum value. The procedure to combine them is as follows:

Step 1: read the values of the following parameters
ω_1 - the wave frequency, at which RAO of M_y achieves maximum;
RAO^{My}_{max} - the maximum RAO of M_y ;
M_y^{max} - extreme design value of M_y

Step 2: Calculate the amplitude of the equivalent wave H_{eq1}

$$H_{eq1} = \frac{M_y^{max}}{RAO^{My}_{max}} \tag{3.2-1}$$

Step 3: find out the RAO values of M_z and M_x at ω_1

Assume RAO_1^{Mz} - RAO value of M_z at ω_1;
RAO_1^{Mx} - RAO value of M_x at ω_1

Step 4: combine the load components

$$LC1 = M_y^{max} + H_{eq1} \times RAO_1^{M_z} + H_{eq1} \times RAO_1^{M_x} \tag{3.2-2}$$

Where LC1 is load combination 1. Note that it is vector addition in Eq.(3.2-2) because all the components have different directions.

The same procedure is applied to calculate load combinations 2 and 3. For load combination 2, horizontal bending moment takes maximum value. If ω_2 is the wave frequency, at which RAO of M_Z achieves maximum, $RAO_{max}^{M_z}$ is the maximum RAO of M_Z , M_z^{max} is extreme design value of M_Z , H_{eq2} is the wave amplitude of the equivalent wave for load combination 2,

$$H_{eq2} = \frac{M_z^{max}}{RAO_{max}^{Mz}} \tag{3.2-3}$$

So

$$LC2 = H_{eq2} \times RAO_2^{M_y} + M_z^{max} + H_{eq2} \times RAO_2^{M_x} \tag{3.2-4}$$

Where
LC2 is load combination 2, $RAO_2^{M_y}$ and $RAO_2^{M_x}$ are RAO values of M_y and M_x at ω_2 respectively.

For load combination 3, torsion moment takes maximum value. If ω_3 is the wave frequency, at which RAO of M_X achieves maximum, $RAO_{max}^{M_x}$ is the maximum RAO of M_X , M_x^{max} is extreme design value of M_X , H_{eq3} is the wave amplitude of the equivalent wave for load combination 3,

$$H_{eq3} = \frac{M_x^{max}}{RAO_{max}^{Mx}} \tag{3.2-5}$$

So

$$LC3 = H_{eq3} \times RAO_3^{M_y} + H_{eq3} \times RAO_3^{M_z} + M_x^{max} \tag{3.2-6}$$

Where
LC3 is load combination 3, $RAO_3^{M_y}$ and $RAO_3^{M_z}$ are RAO values of M_y and M_z at ω_3 respectively.

3.3 Methodologies for Ultimate Strength of Hull Girders

The response of ship structure depends on a variety of influencing factors that includes geometric configuration, material composition and resulting physical properties, production related imperfections such as initial deflections and residual stresses, degradation related to in service issues such as corrosion, ship and environmental load characteristics. This makes the ship structural system a complex problem for analysis and design. The overall ship structure may be considered as a girder to determine the overall loading effects.

The most common overall failures of a ship hull girder are normally buckling in compression flange or plastic collapse of the girder flange in tension. Depending on the loading, especially if horizontal moment or torsion loading is considerable, the failure may sometimes initiate in the side shell stiffened panels.

There are different methods available for determination of ultimate strength of hull girder that may broadly be classed into two types:

Nonlinear Finite Element Method
Structural Unit Idealization Method

The nonlinear finite element method can be used to analyze the detailed nonlinear response of ship structures involving both the geometric and material nonlinearities to determine ultimate collapse strength of the hull girder. This is a versatile technique but need enormous effort and computing resources in FE modelling and analysis. A number of established commercial and public domain finite element analysis software are available to carry out nonlinear finite element analysis. The ANSYS commercial FE software for nonlinear structural analysis was used for this research work.

An alternative to nonlinear finite element analyses is Structural Unit Idealization Method that was suggested by Ueda & Rashed (1974, 1984) to reduce the computational effort by modelling the ships structure using large idealized structural unit instead of fine finite element mesh. This method of using large idealize structural units between nodes is called Idealized Structural Unit Method (ISUM) that efficiently model the actual nonlinear behaviour of large structural units and considerably reduce the computational effort and time.

Smith (1977) developed another method some what similar to ISUM in that stiffened panel is idealized as independent beam-column made up of plate-stiffener combination. Total ultimate strength of stiffened panel is estimated from cumulative ultimate strength of beam-column units. Load shortening curves are developed and used to idealize plate-stiffener combination response as beam-column. This method is also computationally very efficient and accuracy of results depends upon how well plate-stiffener combination behaviour is depicted in the load shortening curves used in determination of ultimate strength analysis. The load shortening curves may be developed to count for all possible load combinations, nonlinearity in material as well as in spatial response, residual stress due to production related processing of material, imperfection in shape etc. This method is commonly used by the classification societies for determination of ultimate strength of hull girder. The MARS software from Bureau Veritas is used to calculate ultimate hull girder strength using beam-column idealization as of Smith Method. The MARS software provides different failure mode algorithms for calculation of ultimate strength that include Elastic Ideally Plastic (EIP) failure mode and Beam-Column (BC) failure mode, apart from the others.

For EIP failure mode, material beyond elastic limit is considered fully plastic in both under tension and compression. Beam-Column method of MARS uses the following load-end shortening curves to determine ultimate bending moment capacity of ship section:

$$\sigma_{CR1} = \Phi \sigma_{C1} \frac{A_s + 10 b_E t_p}{A_s + 10 s t_p} \qquad (3.3\text{-}1)$$

where Φ is edge function, σ_{C1} is critical stress, A_S is net sectional area, b_E effective width of plating attached to stiffener, t_P net thickness of plating and s is spacing of stiffeners. The detail of the methods may be found in BV Rules, Part B, Chapter 6, Appendix 1.

As mentioned earlier, the structural strength of ship is conventionally assessed only in intact condition. Under this condition, the critical load case for mono-hull ship is the vertical bending

moment, which reaches maximum in head seas. For intact ship, often horizontal bending moment and torsion are insignificant. The conventional design tools for intact ship such as Smith Method with load shortening curves depicting behaviour of beam-column for dominant vertical bending moment is not likely to give accurate results for damaged section where horizontal bending and torsion along with residual stress out of damage incident shall be present to a significant level.

For analysis of residual strength of damaged ship structure, the application of ISUM or Smith Method requires that the behaviour of idealized structural units or beam-column idealization be modelled for loading of damaged condition. In context of Smith Method, this simply suggests that load shortening curves may be developed for dominant loading conditions for damaged structure in order to get good estimate of ultimate strength of damaged section.

For this project, in order to determine reduction in ultimate strength of ship due to damage, following approach is adopted:

Full plastic moment of intact ship section is calculated that give the maximum load bearing capacity of the ship in intact condition.

Ultimate hull girder strength of intact ship is calculated using Smith Method, (MARS software)

Ultimate hull girder strength of intact ship calculated using nonlinear finite element method (ANSYS software)

Ultimate hull girder strength of damaged ship is calculated using Smith Method with the same load shortening curves as used for intact condition (MARS software). The hull damage is simply simulated by removing of material from the damaged part of ship section.

Explicit finite element method is used to simulate actual ships collision scenario in order to get requisite damage condition for further ultimate strength analysis (ANSYS/LS-DYNA software).

Ultimate hull girder strength of damaged ship section obtained from explicit dynamic collision simulation is calculated using nonlinear FEM (ANSYS software)

The results of ultimate hull strength for intact ship using Smith Method and nonlinear FEM shall enable to correlate Smith Method and nonlinear FEM. This correlation shall be helpful to deduce validity of results of Smith Method as described at'd' above for damaged condition comparing the ultimate strength of damaged ship obtained using the FEM

3.3.1 Reliability Base assessment of damaged ship Residual strength

The reliability analysis is essentially evaluation of probability of failure (P_f) of a component which is defined by:

$$P_f = \int_{g(X)\leq 0} f(X)dX \qquad (3.3\text{-}2)$$

where X is the vector of random design variables for the component and f(X) is joint probability density function of X. The g(X)=0 is called limit state dividing performance of the component into failure state (i.e. g(X) <0) and safe state (i.e. g(X) > 0). The g(X) ≤0 defines

the failure domain over which integration of (3.3-2) is performed to determine probability of failure of the component.

The probability of failure of system is similarly given by:

$$P_f = \int_{G(X)\leq 0} f(X)dX \tag{3.3-3}$$

where G(X) is the limit state function for the system given by:

$$G(X) = \bigcup \bigcap g_i(X) \tag{3.3-4}$$

and $g_i(X)$ is the limit state of ith component of the system made up of series of parallel combination of components, appropriately.

A number of established methods to solve (3.3-2) and (3.3-3) are available such as Monte Carlo's Simulation (Crude or Adaptive) (MCS), First Order Reliability Method (FORM), Second Order Reliability Method (SORM), etc. For details, see for example Thoft-Christensen & Murotsu (1986), Ditlevsen & Madsen (1996) and Melchers (1999).

It is apparent that determination of probability of failure of component or system requires evaluation of limit state g(X) or G(X). In structural design, finite element methods are commonly used and evaluation of g(X) (or G(X)) may be based on these methods. There are number of methods available for reliability analysis based on Finite Element Methods as discussed in reference Shahid & Das (2007) which includes:

- Direct FEA Limit State Methods
- Statistical Response Characterisation Methods
- Limit State Simulation
- Response Surface Methods
- Artificial Neural Network Methods

For large and complex structures needing enormous computing effort it is cost effect to use limit state simulation such as Response Surface Method for reliability analysis instead of using direct FEM for evaluation of limit state.

The Response Surface Method was first introduced by Box et al (1951), which are being used in many applications to simulate response for systems needing considerable cost and/or effort for real experimental test and analysis. The response surface is fundamentally regression fit of a polynomial function to the structure response data obtained through experiments or FE analysis as given in equation (3.3-5) below.

$$\overline{Y} = C_0 + \sum_{i=1}^{n} C_i X_i + \sum_{i=1}^{n}\sum_{j=1}^{n} C_{ij} X_i . X_j \tag{3.3-5}$$

where $\overline{Y}$ is the estimated response of the system to n number of system parameters X. C_0 is a constant, C_i are coefficients of first order terms and C_{ij} are coefficients of second order and cross terms in the approximating polynomial function where i & j are 1…n.

The response surface approximation of a linear system is essentially a linear polynomial only involving first order terms in equation (3.3-5) and are straight forward to develop and use in system response simulation. Unfortunately, most of real systems are non-linear in nature

requiring higher order polynomial to represent their response. It is mostly sufficient to use 2nd order polynomial to represent the non-linear system response. Sometime it is also possible to use a suitable transformation on the response data in order to improve regression fit. Nevertheless, accuracy of the response surface approximation depends on the nature of response of the system that may not be easily representable by polynomial function.
The accuracy of system response simulation on one hand and minimizing the number of data points needed in development of appropriate response surface on the other hand are active field of research since first introduction of response surface methods. There are a number of techniques available for design of experiment and response surface generation detailed description of those may be found in literature, see for example Høyland & Rausand (1994), Myers (1999), Das & Zheng (2000), Myers & Montgomery (2002), Zheng et al (2000, 2005), etc.

The schematic in Figure (3.3-1) shows how the response surface method is used for reliability analysis based on FE methods. In this case, the limit state function is the response surface developed through regression of FEA response data. Obviously, the accuracy of the results depends upon how well the response surface simulates the actual response of the system.

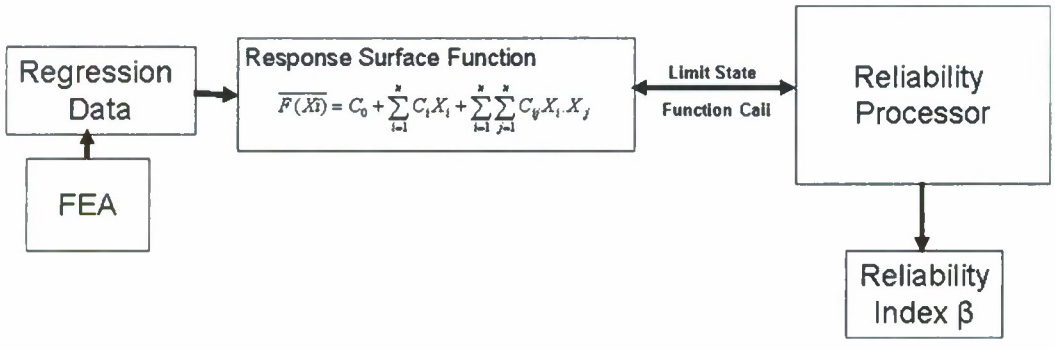

Figure 3.3-1: Reliability analysis using FEA response surface

The number of FE analysis required to generate response surface depends upon the number of random parameters for the FE model. The number of FE runs may considerably be reduced by a suitable choice of data generation techniques such as Central Composite Design with partial factorial points that allows sufficient samples to maintain resolution for V-design where none of the second order terms of the approximation function are confined with each other.

The response surface methods are very efficient in term of computational efforts needed to simulate a system response. However, for highly non-linear system the accuracy may be an issue which may or may not be predictable by statistical measures of goodness of fit of the regression polynomial, especially for higher order polynomial having oscillation between data points, Bucher et al (2006).

The good accuracy in fitting of response surface function with comparatively fewer data point may be achieved if type of response of structural system is known a prior. For example, interaction of ultimate hull girder bending strength for combined vertical and horizontal moments is characterise by the following relation (Paik & Thayamballi, 2003)

$$\left(\frac{M_V}{M_{VU}}\right)^{C1} + \left(\frac{M_H}{M_{HU}}\right)^{c2} = 1 \qquad (3.3\text{-}6)$$

Where M_{VU} and M_{HU} are ultimate vertical and ultimate horizontal bending moment capacities of ship section; M_V and M_H are vertical and horizontal bending moments, respectively.

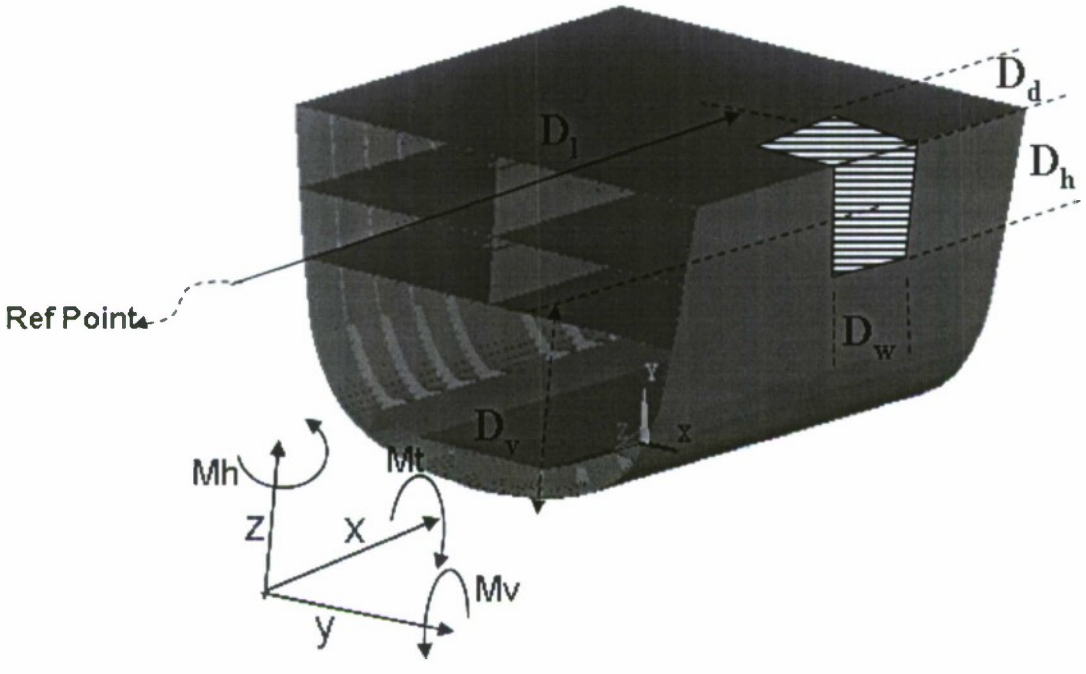

Figure 3.3-2 : Damaged ship structure, variables relevant for reliability based assessment of residual structural strength.

In general, the ultimate strength of damaged ship essentially depends upon physical characteristics of structural damage such as location of damage that include distance of centre of damage from appropriate ship reference axis, and size of damaged part of hull structure that include damaged depth, damaged height and damaged width as shown in Figure (3.3-2) above. And also variation in properties of material used in construction of hull and aging effect such as corrosion and accumulation of stress during ship in active service (fatigue cycles). Accordingly, the residual ultimate strength of damaged ship depicted by ultimate moment capacity M_u may be given by the following:

$$M_u = f(M_v, M_h, M_t, F_s, D_h, D_w, D_d, D_l, D_v, T_{age}, \sigma_y, E) \qquad (3.3\text{-}7)$$

Where f(...) is the ultimate strength response function which depends on the following parameters:

M_v - vertical moment load
M_h – horizontal moment load
M_t – torsion load
F_s – shear force load
D_h – height of damaged structural part
D_w – width of damaged structural part

D_d – depth of damaged structural part
D_l – longitudinal location of structural damage
D_v – vertical location of structural damage
T_{age} – aging related structural degradation
σ_y – yield strength of material
E – Modulus of elasticity of the material

The first four parameters pertaining to load and load combinations are essentially stochastic in nature because of random nature of sea environment in which ship operate along with random operating profile of ship experienced in service. The parameters relevant to size and location of structural damage are also random in nature and depends upon the type and nature of incident that caused the damage. The aging related degradation in structural strength of ship may also be accounted for while making reliability based assessment of residual strength of ship having considerable time in service. The last two parameters, yield strength and modulus of elasticity of material used in construction of ship are also random in nature and therefore should be part of statistical/probabilistic assessment.

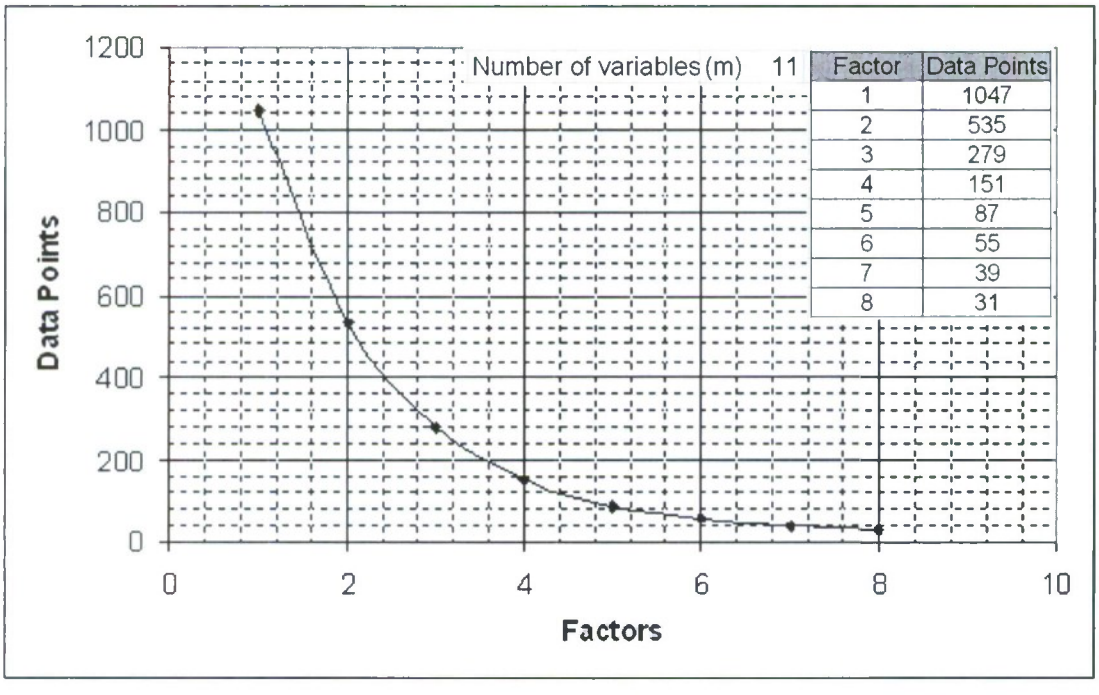

Figure 3.3-3: Number of random variables & computational effort

For an objective to provide quick assessment of residual ultimate strength of damaged ship for decision support based on reliability and risk analysis to ensure her safe passage subsequent to damage incident, the ultimate strength response function in (3.3-7) is considered appropriate formulation. However, the ultimate objective of the presently proposed research is to develop a reliability-based design procedure for better survivability of damaged ships and, accordingly, response function may be modified to reduce number of parameters that are directly relevant to design development. This also considerably reduce the computational effort required in development of ultimate strength response function (see figure 3.3-2).

As far as, conventional design approach and difference in evaluation of damaged ship structure is concerned, the major deviation is in load combinations that arise because of large ship side opening subsequent to ships structure damage in collision. Such opening is mostly asymmetric

giving way to stress field in the damaged structure that shall be much different from that of an intact ship. Further, considerable residual stress is expected to exist subsequent to plastic rapture and damage of structure in collision impact. As discussed earlier, the conventional design tools are developed for loading conditions that are predominant for intact ship viz. vertical bending moment and horizontal bending moment, respectively in order of precedence, for ultimate strength of ships hull girder. For damaged condition, the torsional moment is also likely to be dominant load. In order to develop ultimate strength model for damaged ship hull girder, the following response model is adopted for reliability based assessment of residual strength:

$$M_u = f(M_v, M_h, M_t) \tag{3.3-8}$$

Where M_v, M_h and M_t as mentioned earlier are vertical, horizontal and torsion moment, respectively.

A fixed size of structural damage as per recommendation of classification society Lloyd's Register given in table 0-1 is considered in this study. The random variations in material properties for reliability analysis are taken care, along with other factors related to production such as residual stress, through modelling uncertainties parameter in performance function.

Table 3.3-1: LR Rules; collision damage extent

Military threats	The extent of damage due to military threats defined as the minimum of the shock or blast damage that is likely to result from a specified weapon threat.	
Collision damage to the side shell	Level A	- 5 m longitudinally between bulkheads
		- from the waterline up to the main deck
		- inboard for B/5 m

4. A SAMPLE VESSEL, ITS MODEL AND DAMAGE SCENARIOS

Descriptions of the Sample Vessel and Its Model

A sample vessel, which is a Notional US Navy Destroyer Hull 5415, was initially designed by NSWCCD. The principal dimensions of the vessel are shown in Table 4-1. Division of the compartment of the vessel is presented in Figure 4-1. The other details of Hull 5415 can be seen in Lee et al (2006).

Table 4-1: Main particulars of Hull 5415 and its model

Particulars	Ship	Model (1/100)
Length between perpendiculars (L_{oa}) in meters	151.18	1.5118
Length between perpendiculars (L_{pp}) in meters	142.04	1.4204
Breadth moulded (B) in meters	20.03	0.2003
Depth to public spaces deck (D) in meters	12.74	0.1274
Design draft (T) in meters	6.31	0.06124
Maximum section area (Ax) in m^2	96.7923	0.009679
Block coefficient (C_B)	0.4909	0.4909
Prismatic coefficient (C_P)	0.6409	0.6409
Midship section coefficient (C_M)	0.7658	0.7658
KM (Height of metacentre above keel) in m	9.47	0.0947
Height of gravity centre above keel (KG) in meters	6.283	0.06817
Metacentric height (GM) in meters	3.187	0.02602
Longitudinal position CoG from A.P. (LCG) in meters	71.02	0.7168
Roll radius of gyration (k_{xx}) in meters		0.0612
Pitch radius of gyration (k_{yy}) in meters		0.3250
Yaw radius of gyration(k_{zz}) in meters		0.3250

A ship model with a scale of 1/100 has been made from fibreglass based on the offsets of Hull 5415. Using such a small model scale is due to the dimensions of the towing tank facility. The main particulars of the model are presented in Table 4-1, while a view of the model is shown in Figure 4-2. As described in Chapter 3, in order to measure the wave-induced loads, the model is cut into two pieces at the cross-section, which is located 545 mm from the after perpendicular longitudinally. The two sections are linked together by a force gauge, which is bolted to two substantial bulkheads mounted in the fore and aft parts of the model and the two sections are made waterproof by the provision of a thin membrane across the cut.

Although every effort has been made to construct a ship model with the same longitudinal weight distribution as the original ship, it proves being very difficult to achieve this due to the general arrangement of the ship model, especially around the location of the force gauge, whose weight is a large percent of the total weight of the ship model. So the ship model has slightly different longitudinal weight distribution from the original ship. The longitudinal weight distributions of the original ship and ship model are presented in Figures 4-3 and 4-4.

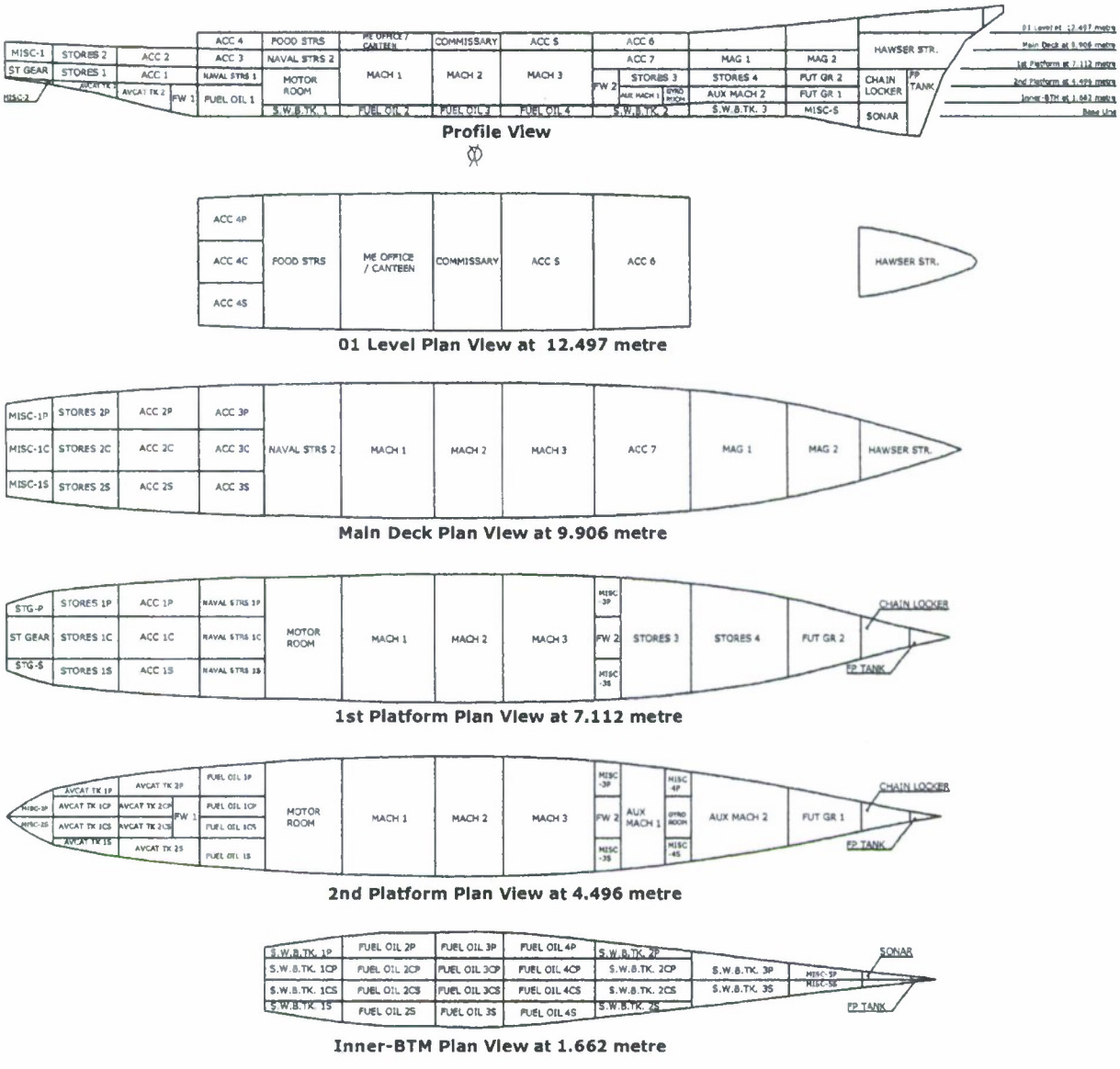

Figure 4-1: Division of the compartments of the vessel

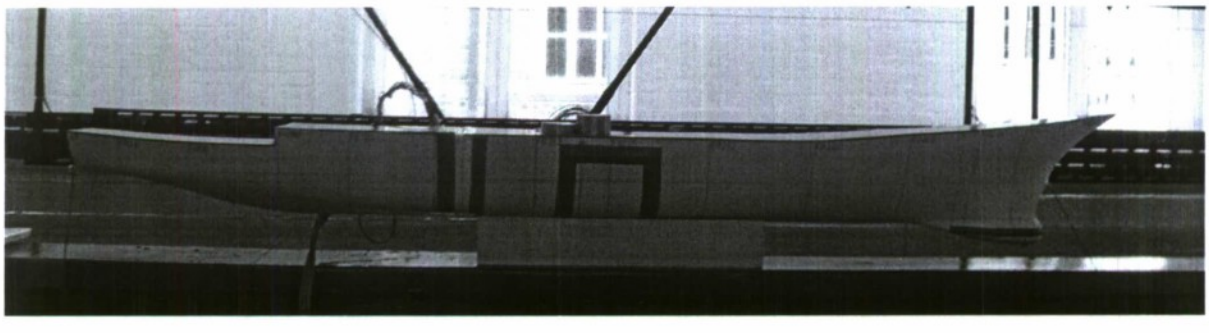

Figure 4-2: The ship model (Lee, et al 2006)

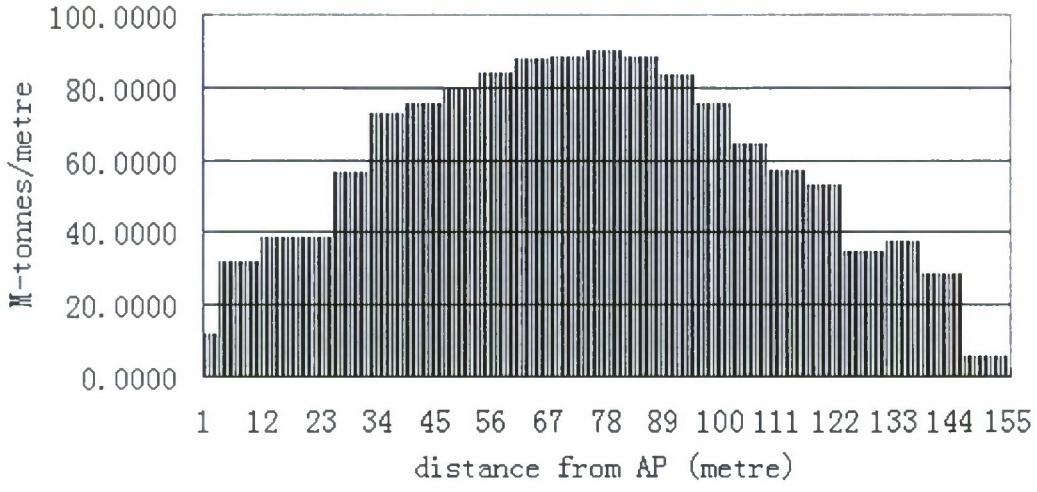

Figure 4-3: Weight distribution of the intact sample vessel

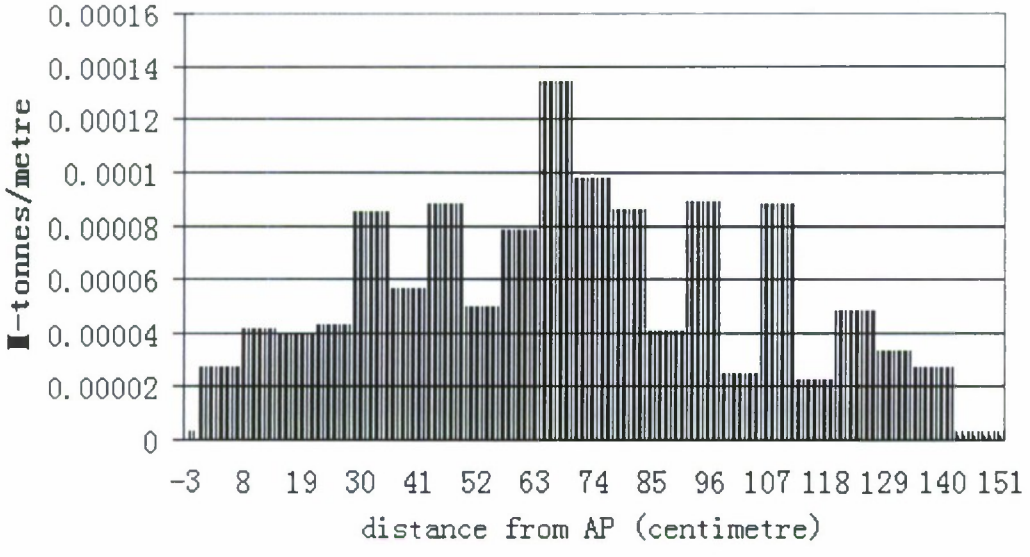

Figure 4-4: Weight distribution of the intact model

It should be pointed out that the ship model in this project was the same as that in NICOP project except for the way that the cut was sealed. Figures 4-5 and 4-6 show how the cling film was applied in both NICOP and the current projects. In NICOP project the film was applied as a flat surface, although it was fairly loose to minimise the effects of the cling film on the measurement of loads. However the cling film was still subject to, to some extent, loads. It should be noted that the effects of the cling film were very small (may be negligible) when the magnitude of loads was relatively large, such as vertical bending moment in head seas, etc. However the maximum torsion on the ship model was only about 0.3 Nm. The effects of the

cling film on torsion could be significant. In the current study, the cling film was tucked into the gap, so it would not be subject to any loads (ideally).

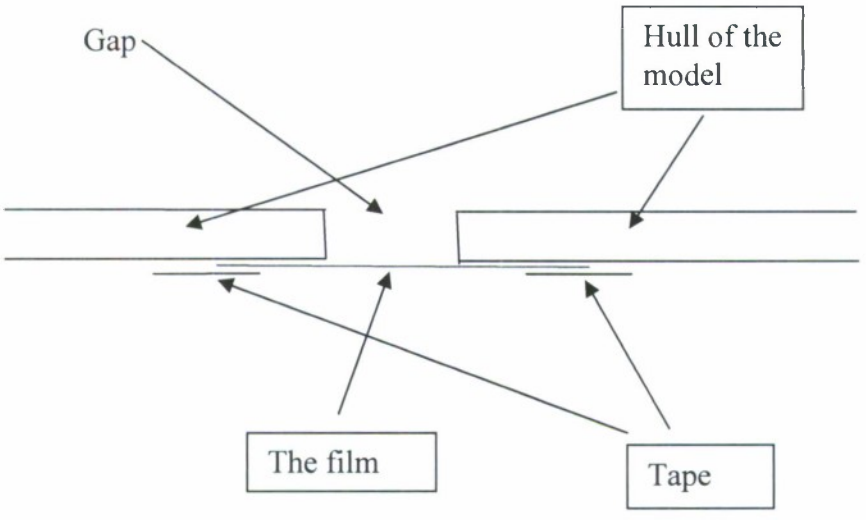

Figure 4-5 The cling film in NICOP project

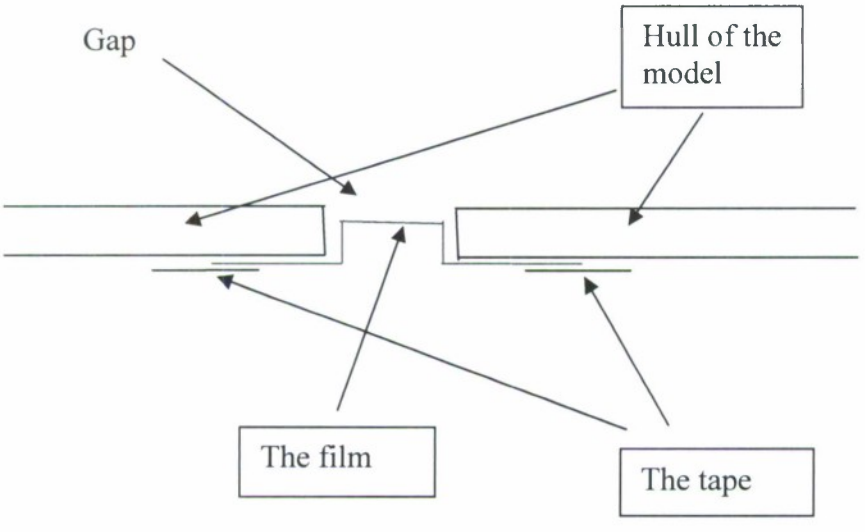

Figure 4-6 The cling film in the current project

Damage Scenarios

In this project, three damage scenarios have been used and been shown in Figures 4-7 ~ 4-9. Detailed explanations of determining these damage scenarios can be seen in the report of Lee, et al (2006). Presented in Figure 4-7 is damage scenario 1, which has a 5 metres (long) by 5.5 metres (high) opening on the starboard side shell in the middle of machine room 2

longitudinally as indicated by a rectangular window with dashed line. Because the lower edge of the opening is below the draught, water could enter the damaged machine room, which is indicated by the shaded areas. Water ingress is symmetrical transversely, so heel angle is zero at this scenario. This damage scenario simulates a possible collision at Level A, which is recommended in Lloyd's Register Rules (Lloyd's Register of Shipping, 2002). Model tests have not been carried out for this damage scenario due to the limited availability of the towing tank. However structural strength assessment has been applied to this scenario because damage is limited in only one compartment so that the size of finite element model is more manageable.

Figure 4-8 shows damage scenario 2, which is similar to the damage on USS Cole destroyer (*http://archives.cnn.com*), which suffered from a 12 metres by 12 metres hole in the ship's side shell caused by a suicide attack. Hence in this damage scenario, a 12 meters (long) by 9 meters (high) opening on starboard side shell is introduced as indicated by a rectangular window with dashed line. The opening equally extends into machine rooms 2 and 3 longitudinally, and penetrates into the double bottom causing water ingress in four fuel tanks on the starboard side. Both experimental tests and numerical calculations have been applied to this damage scenario and damage scenario 3, which is shown in Figure 4-9. It simulates a raking damage at Levels B & C recommended in Lloyd's Register Rules (Lloyd's Register of Shipping, 2002). The damage is mainly in the bow and is symmetrical transversely.

Table 4-2 presents the floating conditions of the sample ship at intact and damage conditions, while its intact stability is summarised in Table 4-3. Similarly the floating conditions of the ship model at intact and damage conditions are shown in Table 4-4, and its intact stability is presented in Table 4-5. From those Tables it can be seen that the sample vessel and its model have also different draughts apart from their difference in longitudinal weight distribution and total weight at design draught. Damage scenario 2 has led to an increase of draught by 1.121 meters and a heel angle of 1.1 degree towards starboard. The reason for such a small heel angle is that the major flooding in machine rooms 2 and 3 is transversely symmetrical. The only unsymmetrical flooding is at the four small fuel tanks within the double bottom. This is the most severe damage among all the 3 damage scenarios. In damage scenario 3, the draught has increased the least by only 0.143 meters and it is not heeling. The transverse GM of the sample ship is 3.126 metres, so it has adequate stability.

DEMAGE SCENARIO 1

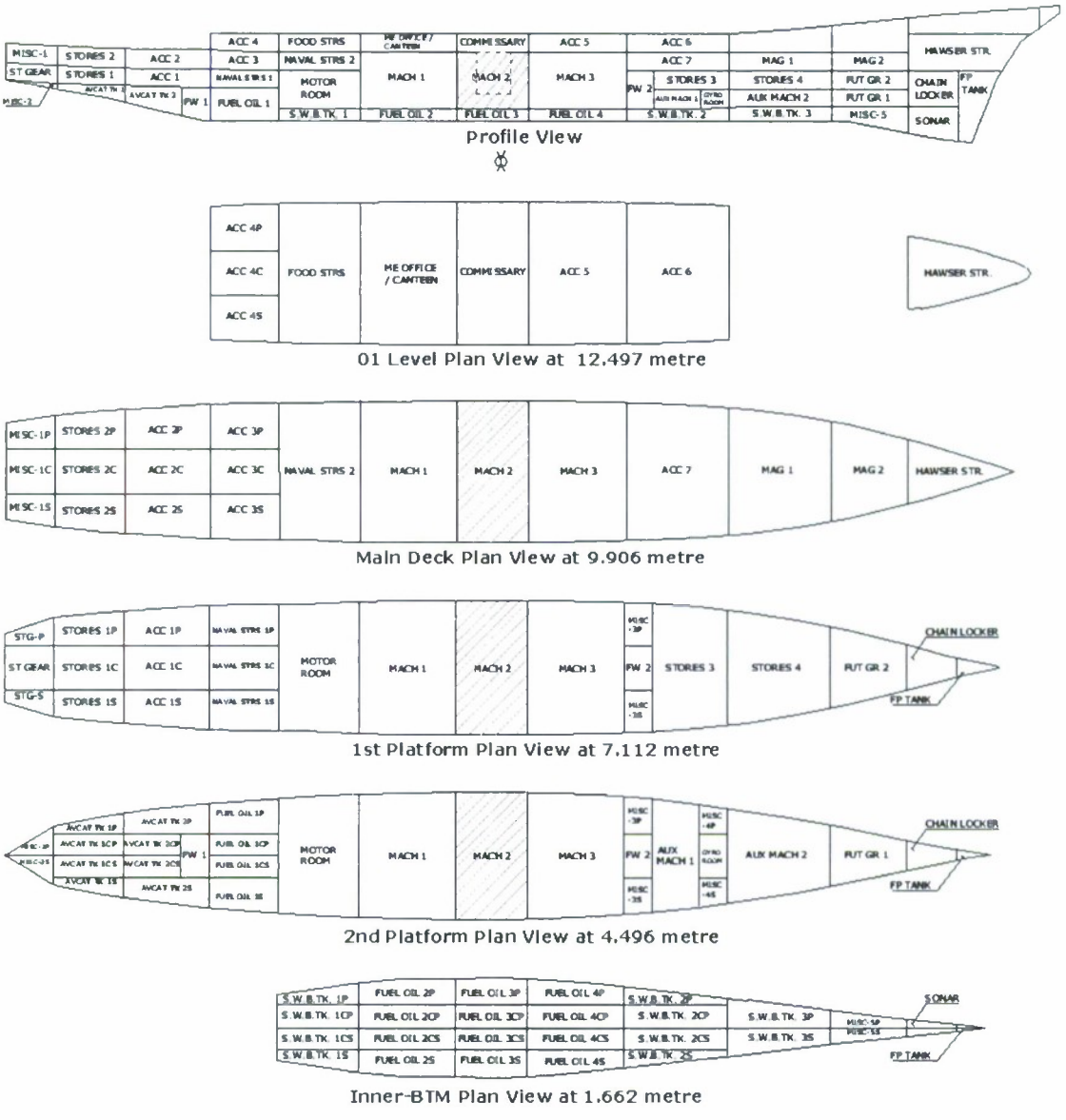

Figure 4-7: Damage scenario 1

DEMAGE SCENARIO 2

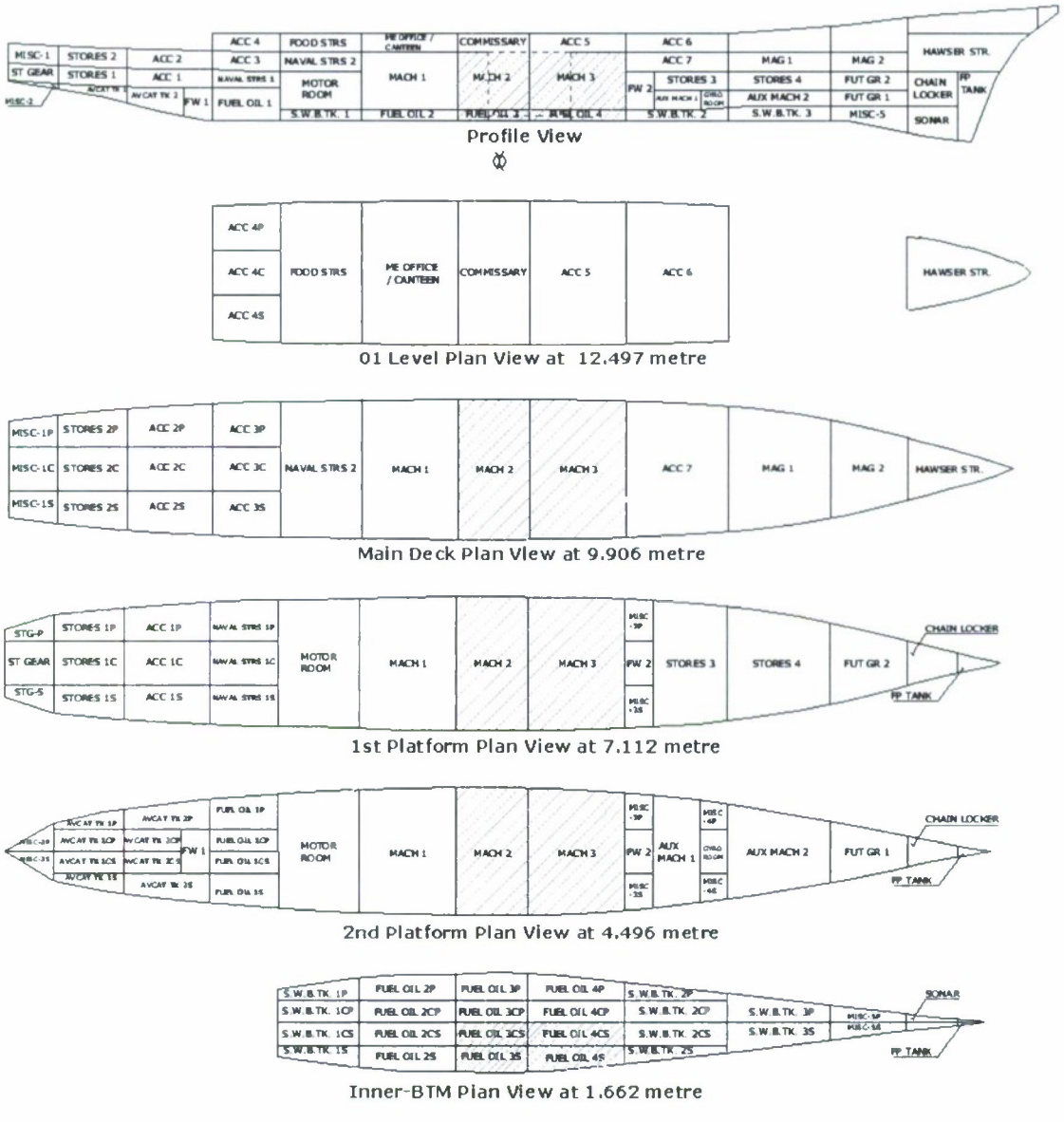

Figure 4-8: Damage scenario 2

DEMAGE SCENARIO 3

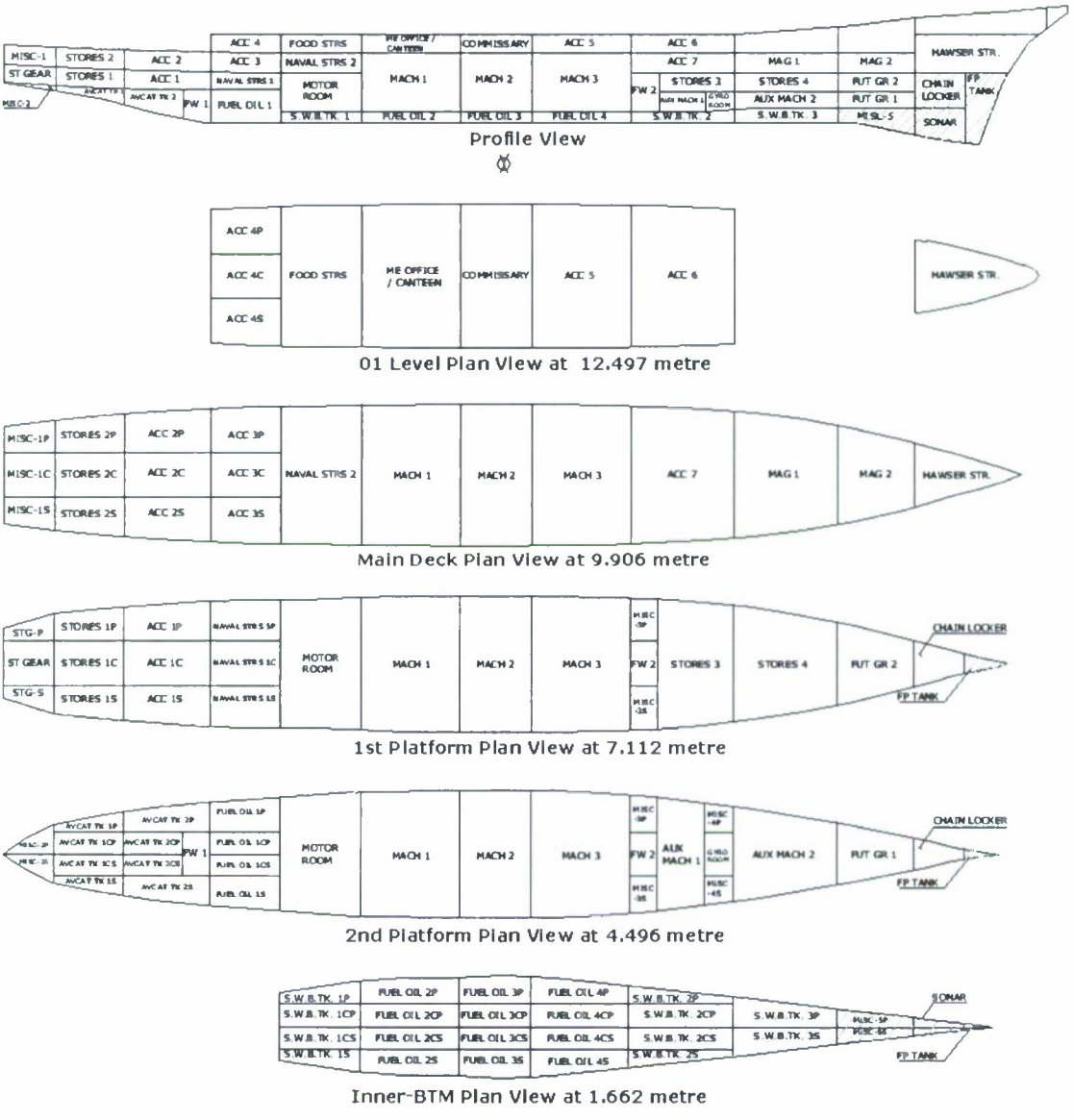

Figure 4-9: Damage scenario 3

Table 4-2: Intact and damage conditions of the design ship

Intact and Damaged Conditions to be Investigated						
Case	Condition	Displ. (tonne)	Mean draught (m)	Trim (m)	Heel (deg.)	Heading angle (deg.)
1	Intact	9114	6.309	0	0	180
2	Intact	9114	6.309	0	0	45
3	Intact	9114	6.309	0	0	90
4	Damage Scenario 1	9914	6.6875	0.2450F	0	180
5	Damage Scenario 1	9914	6.6875	0.2450F	0	45
6	Damage Scenario 1	9914	6.6875	0.2450F	0	90
7	Damage Scenario 2	11450	7.4295	1.4570F	1.100S	180
8	Damage Scenario 2	11450	7.4295	1.4570F	1.100S	45
9	Damage Scenario 2	11450	7.4295	1.4570F	1.100S	90
10	Damage Scenario 2	11450	7.4295	1.4570F	1.100S	270
11	Damage Scenario 2	11450	7.4295	1.4570F	1.100S	315
12	Damage Scenario 3	9336	6.4515	0.8530F	0	180
13	Damage Scenario 3	9336	6.4515	0.8530F	0	45
14	Damage Scenario 3	9336	6.4515	0.8530F	0	90

Table 4-3: Intact stability and trim summary of the design ship

Stability Calculation			**Trim Calculation**		
KMt	9.470	metres	LCF Draft	6.309	metres
VCG	6.293	metres	LCB	70.113F	m-AP
GMt (Solid)	3.177	metres	LCF	64.551F	m-AP
FSc	0.083	metres	MT1cm	182.000	m-MT/cm
GMt (Corrected)	3.126	metres	Trim	0.000	m-F
			List	0.000	deg
Specific Gravity	1.025	MT/cu.m			

Drafts		
Draft at A.P.	6.309	metres
Draft at M.S.	6.309	metres
Draft at F.P.	6.309	metres
Draft at Aft Marks	6.309	metres
Draft at Mid Marks	6.309	metres
Draft at Fwd Marks	6.309	metres

KMt – Transvers metacementric height above baseline
VCG – Vertical centre of gravity
GMt (Solid)- The metacentric height
FSc – Free surface correction
GMt (Corrected) – The metacentric height with correction
MT1cm – Moment to trim 1cm

Table 4-4: Intact and damage conditions of the ship model

Intact and Damaged Conditions to be Investigated						
Case	Condition	Displ. (tonne)	Mean draught (m)	Trim (m)	Heel (deg.)	Heading angle (deg.)
1	Intact	0.008503	0.06124	0	0	180
2	Intact	0.008503	0.06124	0	0	45
3	Intact	0.008503	0.06124	0	0	90
7	Damage Scenario 2	0.01145	0.072085	0.013350F	1.000S	180
8	Damage Scenario 2	0.01145	0.072085	0.013350F	1.000S	45
9	Damage Scenario 2	0.01145	0.072085	0.013350F	1.000S	90
10	Damage Scenario 2	0.01145	0.072085	0.013350F	1.000S	270
11	Damage Scenario 2	0.01145	0.072085	0.013350F	1.000S	315
12	Damage Scenario 3	0.008771	0.062635	0.007610F	0	180
13	Damage Scenario 3	0.008771	0.062635	0.007610F	0	45
14	Damage Scenario 3	0.008771	0.062635	0.007610F	0	90

Table 4-5: Intact stability and trim summary of ship model

Stability Calculation			**Trim Calculation**		
KMt	0.09486	metres	LCF Draft	0.06128	metres
VCG	0.06868	metres	LCB	0.70336F	m-AP
GMt (Solid)	0.02618	metres	LCF	0.64563F	m-AP
FSe	0	metres	MT1em	0.000174	m-MT/em
GMt (Corrected)	0.02618	metres	Trim	0.086	m-F
			List	0	deg
Specific Gravity	1.000	MT/cu.m			

Drafts		
Draft at A.P.	0.06167	metres
Draft at M.S.	0.06124	metres
Draft at F.P.	0.06081	metres
Draft at Aft Marks	0.06167	metres
Draft at Mid Marks	0.06124	metres
Draft at Fwd Marks	0.06081	metres

5. RESULTS AND DISCUSSIONS

5.1 Introduction

As mentioned in chapter 2, this study is a continuation of NICOP project (Lee, et al 2006), in which an assessment procedure was developed. In order for the readers to understand the significance of the current project, the assessment procedure is briefly described here. This procedure consists of four steps: (1) Identify the location and size of the openings; (2) Calculate the still water bending moment and wave-induced loadings including vertical bending moment, horizontal bending moment and torsion; (3) Calculate the ultimate hull girder strength of the damaged cross-section considering the interaction of vertical bending moment, horizontal bending moment and torsion; (4) Assess the structural integrity by deterministic and probabilistic approaches. In Step 1, once a ship is damaged, the location and size in terms of length, height and depth of the penetration of the opening should be determined. So the degree of water ingress could be predicted. In Step 2, the floating conditions of the ship need to be calculated. The stillwater bending moment and wave-induced loads are then estimated. Because it is desirable to install the developed tools on board of ships for a quick and reliable assessment, computational time is a very important factor in choosing a particular method for both loading calculations and strength assessment. In Step 3, the ultimate hull girder strength of the damaged cross-section needs to be assessed. The interaction of vertical bending moment, horizontal bending moment and torsion should be considered. In addition, the strength of other cross-sections (not the damaged one), where the total load including stillwater bending moment and wave-induced loads under the damage conditions exceed that in intact condition, should also be assessed. In Step 4, reliability of the damaged ship is calculated. So a well-informed decision could be made based on this information.

In the current project, some tools for predicting wave-induced loads and assessing ultimate hull girder strength have been further developed. In particular, a 2D linear and non-linear method have been applied to the ship model to calculate the wave-induced loads in regular waves at the cut where the force gauge is installed to measure the loads in the experimental tests. The numerical results have been compared with the experimental results. These are presented in sections 5.2 and 5.3. Model uncertainties of both 2D linear and non-linear method have been calculated in section 5.4. Model uncertainties of the numerical methods are needed in reliability analysis of the hull girder strength. At the same time they are also important measures of accuracy of both numerical methods. Through the above calculations, it is hoped that the accuracy of the numerical methods could be adequately addressed.

Extreme design loads in irregular waves based on the RAO from the 2D linear method, 2D non-linear method and experiment have been calculated for the ship model at the cut under intact condition and damage scenario 2. The formulae recommended in the Lloyds Register's rule for Navy vessels (Lloyds Register of shipping, 2002) have also been used to calculate the wave-induced extreme design loads. The results have been compared in section 5.5. Because the structural strength needs to be assessed on the original sample vessel at the cross-section, where the damage was incurred, under intact condition and damage scenario 1, the extreme design loads have also been calculated using the RAO of the 2D linear method for those scenarios in section 5.5. These data were passed onto the research team in the University of Glasgow and Strathclyde for strength assessment. It should be pointed out that the reason for using the RAO of the 2D linear method rather than 2D non-linear method in strength assessment is that the 2D non-linear results were not available at that moment. The wave-induced loads have been combined in section 5.5.3 in order to consider the interaction of

vertical bending moment, horizontal bending moment and torsion in both deterministic and probabilistic assessment of ultimate hull girder strength.

The ultimate hull girder strength of the sample vessel has been predicted in section 5.6 by a progressive collapse analysis method and non-linear finite element method in order to assess the accuracy of the chosen progressive collapse analysis method.

The ultimate hull girder strength of the sample vessel has been predicted in section 5.6 by a progressive collapse analysis method using MARS and non-linear finite element method using ANSYS in order to assess the accuracy of the chosen progressive collapse analysis method. The MARS software from Bureau Veritas is used to calculate ultimate hull girder strength using beam-column idealization as of Smith Method. The MARS software provides different failure mode algorithms for calculation of ultimate strength that include Elastic Ideally Plastic (EIP) failure mode and Beam-Column (BC) failure mode, apart from the others. The MARS calculations are performed for both intact and damaged condition. The ultimate bending moment capacity for combination of vertical and horizontal moments for elastic-plastic failure mode and for beam-column method are obtained and based on which the MV and MH interaction formula for Intact and Damage conditions are derived. The results and graphs are shown in section 5.6.2

Since no FE based design assessment of intact ship is available to compare the results with that of the damaged ship. The FE analysis for ultimate strength of hull girder is carried out for both intact and damaged conditions. Two types of moment interaction functions were developed, one set of two combinations of moments such as interaction of vertical and horizontal moments, and one set for interaction of all the moments viz. vertical, horizontal and torsion moment. The vertical and horizontal moment interaction function obtained from finite element analysis is compared with that of MARS beam-column and elastic-plastic interaction diagram.
The results and graphs are shown in section 5.6.3.

The Reliability analysis which followed used the results of Finite element analysis to derive the Limit state function. The analysis was carried out using CALRel. The reliability index and relevant probabilities as calculated are given in table 5.6.3.6.1 for both intact and damaged case.

5.2 Predictions of Global Dynamic Wave-induced Loads Using 2D Linear Method

In this section, the 2D linear method has been applied to the ship model to calculate the RAO of all the force components at the cut, which is 545 mm from AP. The numerical results are compared with the experimental results.

5.2.1 Effects of transverse location of gravity centre

As mentioned in Chapter 2, the differences between the 2D linear method and the experimental measurements of dynamic torsion moments are significant in the previous research (Lee, et al, 2006). Although these phenomena could be caused by the effects of sloshing and slamming within the damaged compartments, which could change the global dynamic wave load components, other factors, such as transverse distribution of weight, should also have effects on torsion. Hence the effects of transverse distribution of weight on torsion moment have been investigated. In the 2D linear method this effects can be considered by using a transverse location of the weight centre of the whole vessel or of each section. In the current study a transverse location of gravity centre (TCG) in each transverse section was used. Three different TCG, namely 0, 2 and 4 centimetres apart from the central plane of the ship

model, for each transverse section are assumed to calculate torsion moment of the ship model at the cut. The results were presented in Figures 5.2.1-1 to -5.

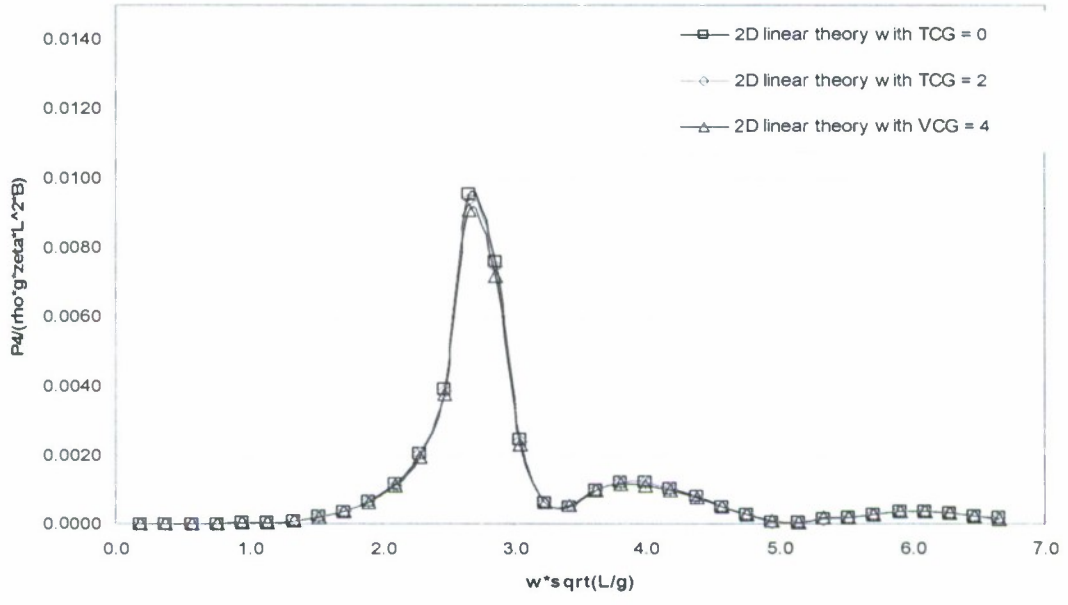

Figure 5.2.1-1: Torsion moment RAO in intact condition at stern quartering waves

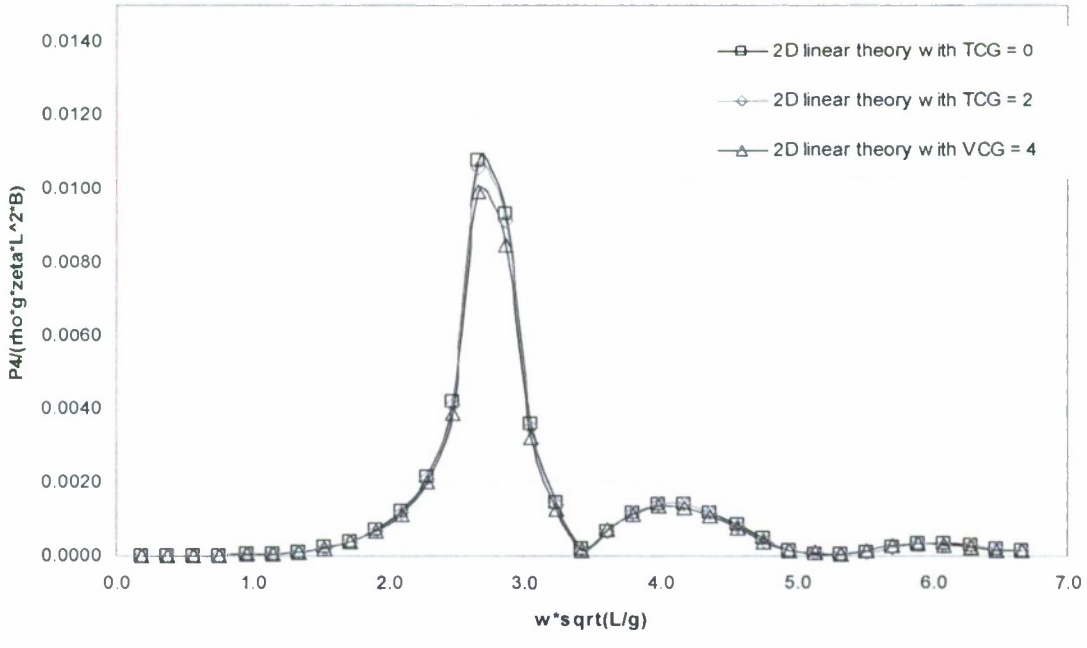

Figure 5.2.1-2: Torsion moment RAO in intact condition at bow quartering waves

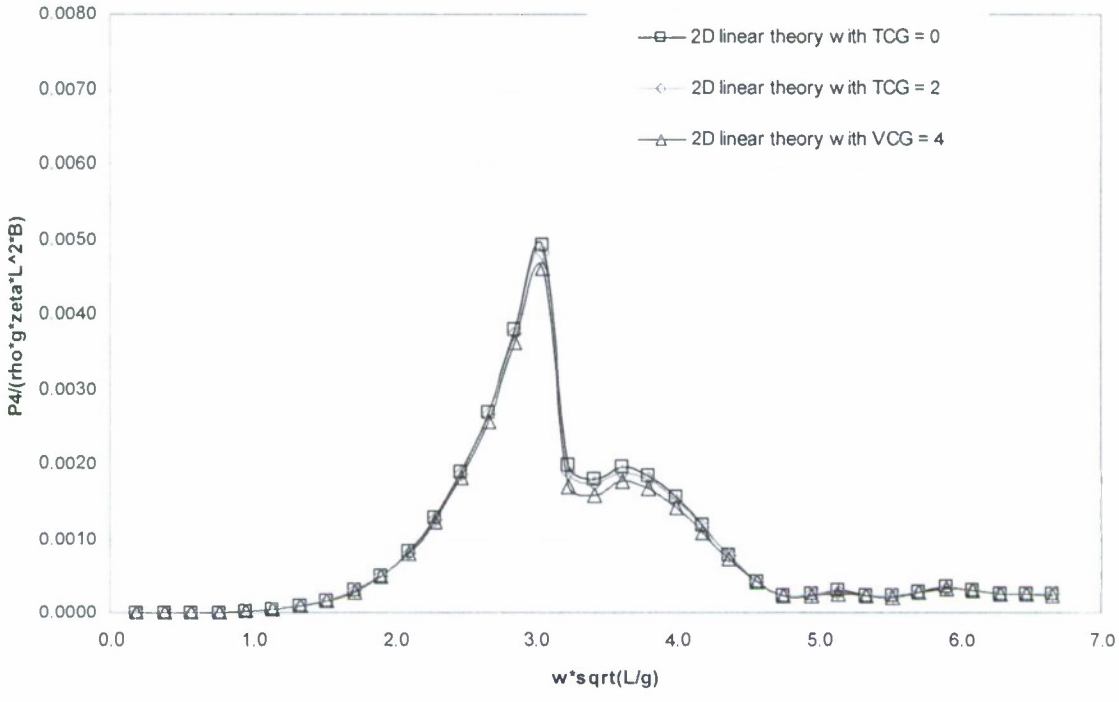

Figure 5.2.1-3: Torsion moment RAO in DS2 at stern quartering waves (heading 45)

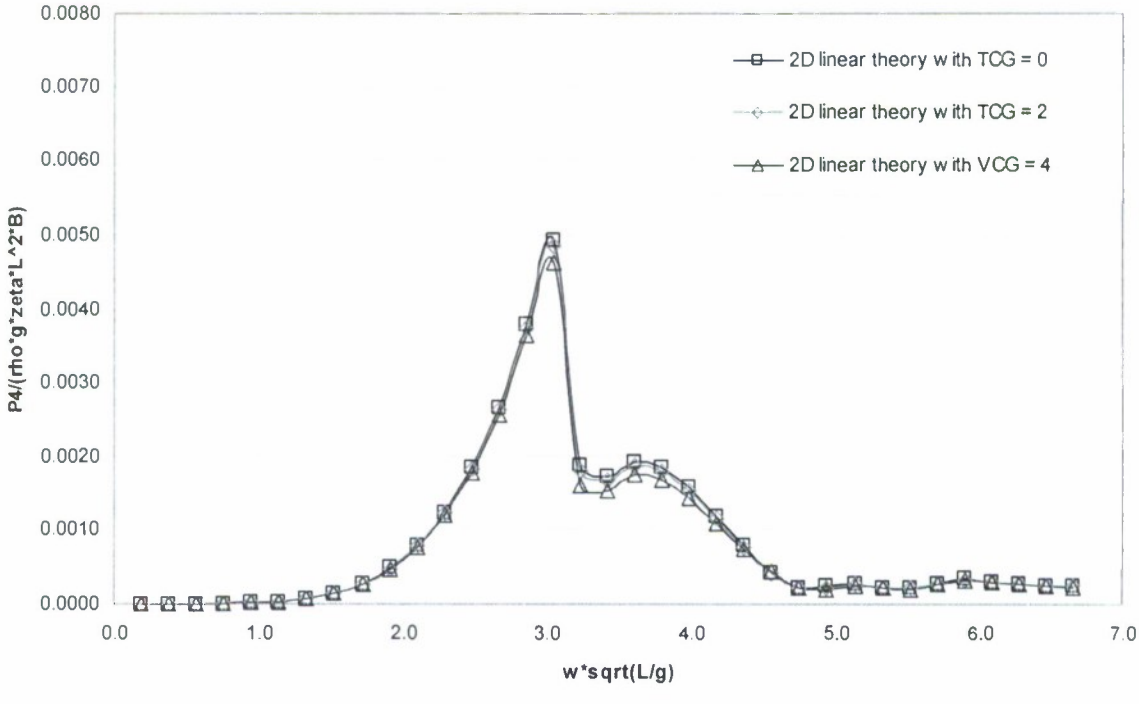

Figure 5.2.1-4: Torsion moment RAO in DS2 at stern quartering waves (heading 315)

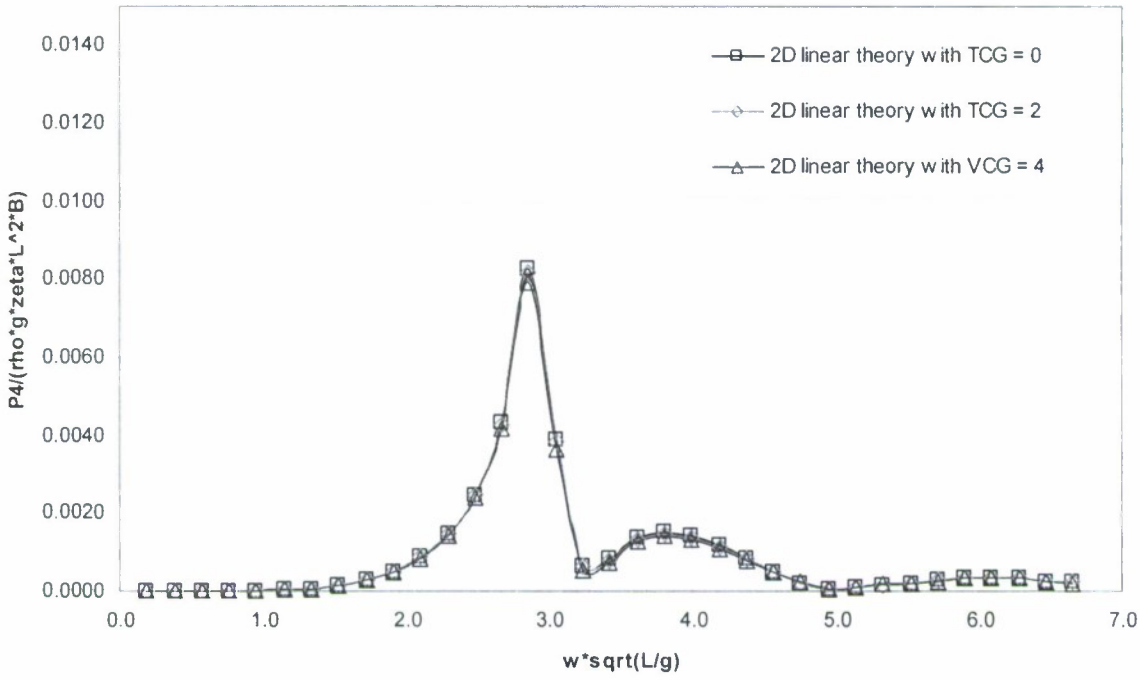

Figure 5.2.1-5: Torsion moment RAO in DS3 at stern quartering waves

These figures indicate that TCG has marginal effects on torsion moment. The maximum difference tends to occur around the resonant regions, while the difference in other frequencies is noticeably smaller. The maximum difference at various conditions is summarised as follows:

- In intact condition stern quartering seas, the maximum difference is 10%.
- In intact condition stern quartering seas, the maximum difference is 12.9%.
- In damage scenario 2 stern quartering seas (heading 45°), the maximum difference is 14.5%.
- In damage scenario 2 stern quartering seas (heading 315°), the maximum difference is 11%.
- In damage scenario 3 stern quartering seas, the maximum difference is 18.5%.

Therefore the actual TCG of each transverse section has been estimated and used in the following calculations.

5.2.2 Results in intact condition

The global dynamic wave induced loads calculated by the 2D linear method and the experimental results in intact condition at 4 different wave headings are presented in the following figures.

- Figures 5.2.2-1 to 5.2.2-5 for intact condition in head waves.
- Figures 5.2.2-6 to 5.2.2-10 for intact condition in stern quartering waves.
- Figures 5.2.2-11 to 5.2.2-15 for intact condition in bow quartering waves.
- Figures 5.2.2-16 to 5.2.2-20 for intact condition in beam waves.

In intact condition, the most important load is the vertical bending moment in head seas, which is shown in Figure 5.2.2-4. The results of the 2D linear method agreed very well with the

experimental results. The test results of small wave amplitude, which were plotted by square dots in the figure, appeared being closer to the solid line, which was for the numerical results, than those of large wave amplitude, which were indicated by triangle and diamond dots. This means that the 2D linear method predicts the vertical bending moment more accurately at small wave amplitude than at large wave amplitude. This is understandable because the ship's responses to small wave amplitude are more likely to be in the linear range, so the results from a linear theory are expected to agree reasonably well with the experimental results. Non-linear responses would normally occur in large wave amplitude. More detailed calculations in section 5.4, in which model uncertainties of the 2D linear method were predicted, provide quantitative support to this observation. As defined in section 3.1.5, model uncertainty of a given method is a good measure of accuracy of the method. When the model uncertainty factor (X_m) is equal to one, it means that it is a 100% accurate result. The coefficient of variation (COV) of the model uncertainty factor measures how much dispersion there is in the calculations. So the nearer the mean of X_m is to one and the smaller the COV of X_m is, the more accurate the numerical method is. The results in Table B-1 in Appendix B clearly support the above observations. The vertical bending moment in head seas had a X_m of 0.890 at the peak response, and a mean of X_m of 0.89 and a COV of X_m of 19.3% in small wave amplitude. This accuracy is reasonably good. However the mean and COV of X_m become 0.773 and 24.5% for large wave amplitude, and 0.750 and 27.4% for very large wave amplitude. This demonstrates that the accuracy is deteriorating with the increase of wave amplitude.

Another interesting phenomenon shown in Figures 5.2.2-4, -9 and -14 about the vertical bending moment is that the measured RAO scattered in large range for different wave amplitudes in the resonant region, where wave length is close to the ship model length. This may suggest that the responses have high level of nonlinearity at this condition. Similar features could also be observed in the results in damage scenarios 2 and 3. This high nonlinearity may well be an inherent feature of this particular hull form, which is a typical destroyer with small block coefficient. In addition, the cut, where the loads were measured, was close to the stern region with sharp change of water-plane width. This is normally another major source of nonlinear responses. To further verify this, a second batch of experimental tests has been carried out, and the results will be presented in section 5.2.5.

The numerical predictions of vertical bending moment in quartering seas are also in good agreement with experimental results as shown in Figures 5.2.2-9 and -14. The mean and COV of X_m at small amplitude are 1.01 and 31.9% respectively in stern quartering seas, while they are 0.86 and 24.6% in bow quartering seas (see Table B1). As shown in Figure 5.2.19, the differences of the vertical bending moment between the numerical and experimental results in beam waves are significant. Nevertheless the magnitude of loads in beam waves is usually very small, so the large difference would not cause much concern in the strength assessment of hull girders.

Horizontal bending moment and torsion in quartering seas, which are shown in Figures 5.2.2-8, -10, -13 and -15, are also important force components. The curves of horizontal bending moment predicted by the 2D linear method have double peaks, while the peak of the test data is falling in between the peaks of the numerical results (see Figures 5.2.2-10 and 15). It is this shift of peaks that causes large difference between the numerical and experimental results. The mean and COV of X_m at small amplitude are 1.12 and 70.5% respectively in stern quartering seas, while they are 0.78 and 67.3% in bow quartering seas (see Table B1). Although the mean of X_m at small amplitude in stern quartering seas looks reasonably good, its COV is quite large. Further scrutiny on the individual figures of X_m has revealed that 5 out of 9 have more than 50% error, and only 2 of them have less than 20% error. Especially the X_m around the resonant

region have a value of 1.92 and 2.65, which are far away from 1. The accuracy of the prediction around the resonant region is more important than those in other frequencies because the current load combination method would use the load in this area for strength assessment. Similar features could be seen for X_m in bow quartering seas. Therefore the accuracy in predicting horizontal bending moment is not as good as that for vertical bending moment.

The disappointing accuracy in horizontal bending moment prediction might be caused partly by the mooring lines in the experimental tests. As described in section 3.1.4, the ship model was moored by four mooring lines, which were attached to the ends of the model, to keep the model from drifting too far away from its original position and orientation (see Figure 3.1-4). It is a very dedicate process to adjust the tensions in the mooring lines. On one hand, the tensions should be as small as possible to reduce its effects on the responses to waves. On the other hand, the model could not maintain its original position and direction if the tensions in the mooring lines were too small. So during the test, the mooring lines were initially fixed fairly loosely. A trial run was then carried out. If the model drifted too far away, the tension would be increased. However if the tension in the mooring lines were clearly interfering with the ship motions under waves, the tension would be reduced. Hence a dedicate compromise had to be achieved. Even so the tensions in the mooring lines were still noticeable in the resonant frequencies, in which responses were quite large, in the recorded test runs. The tensions in the mooring lines could contribute to the horizontal bending moment at the cut. Unfortunately the tensions were not recorded in the tests, so it was not possible to evaluate the extent of the effects of the tensions on the horizontal bending moment.

Figures 5.2.2-8 and -13 present torsion moment in quartering seas. It can be seen that the numerical results were very different from the experimental results. This large difference comes from two major issues, one of which was the shift of peaks in between the numerical and experimental results while the other was the difference in magnitude even if the peaks were achieved at the same frequency. The mean and COV of X_m at small amplitude are 0.96 and 135.9% respectively in stern quartering seas, while they are 0.56 and 60.3% in bow quartering seas (see Table B1). Although the mean of X_m at small amplitude in stern quartering seas looks very good, its COV is too large. Further investigation into the individual figures of X_m has revealed that the values vary from 0.18 to 4.25, and the nearest figure to 1 is 0.85 at the highest frequency. Similarly in bow quarter seas the mean and COV are equally bad. Therefore the predictions of torsion moment were considered being very poor.

One of the possible reasons for such a poor performance in torsion moment prediction might be the small scale of the ship model, which is 1/100. The maximum measured torsion is only about 0.3 Nm, so its measurement is very sensitive to any imperfections, such as the quality of installation of the cling film, which was used to seal the cut section of the model; calibration of the instruments; electrical noise in the records; etc. The other possible reason is the inherent difficulty in determining the radius of gyration about roll motion (k_{xx}) and damping coefficient for roll motion, which is a very important motion component influencing the accuracy of the prediction of torsion moment.

Head waves

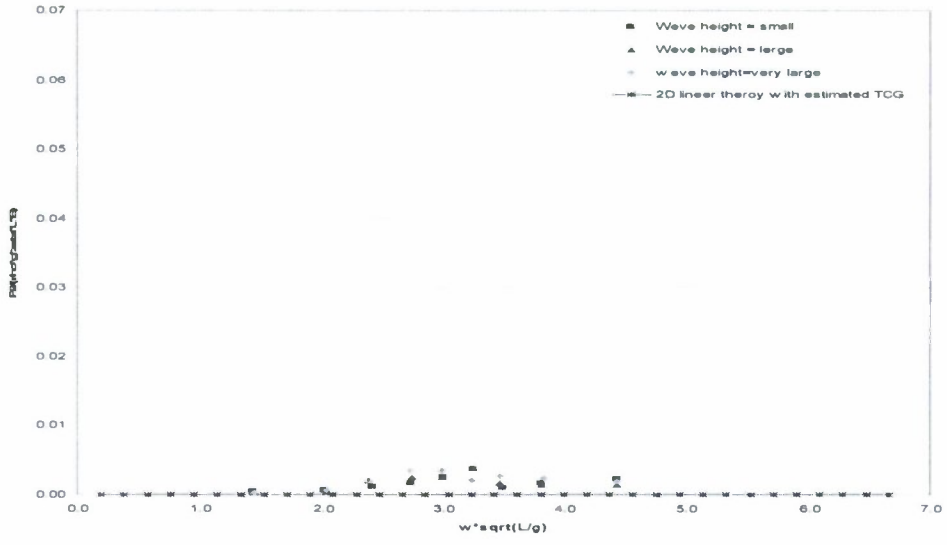

Figure 5.2.2-1: Horizontal shear force RAO in intact condition at head waves

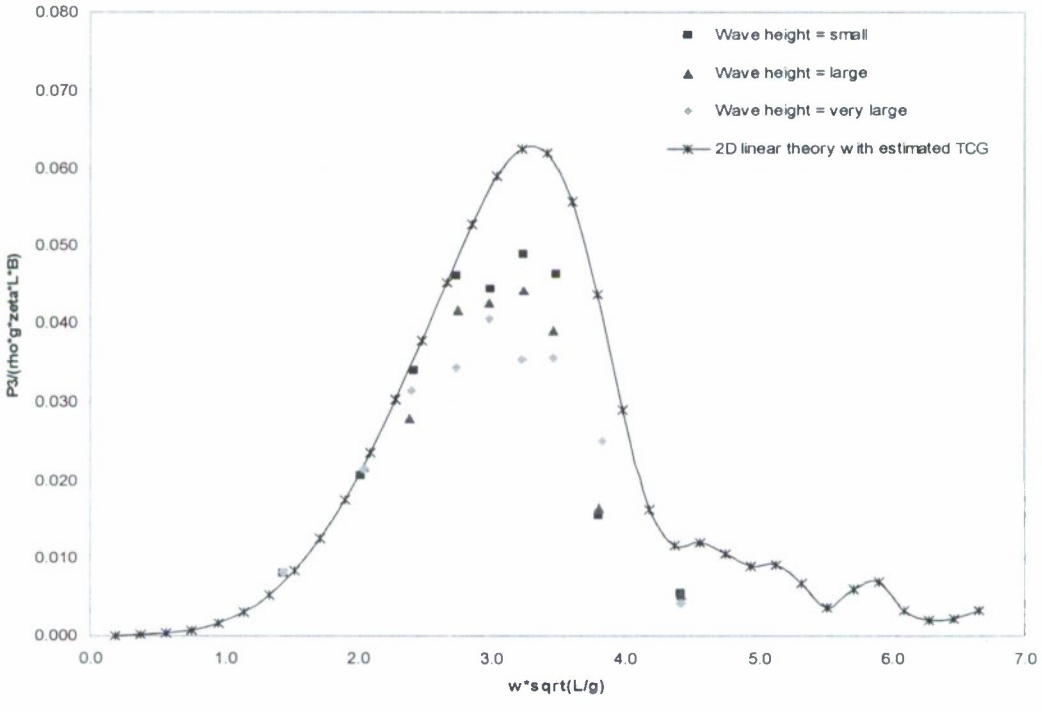

Figure 5.2.2-2: Vertical shear force RAO in intact condition at head waves

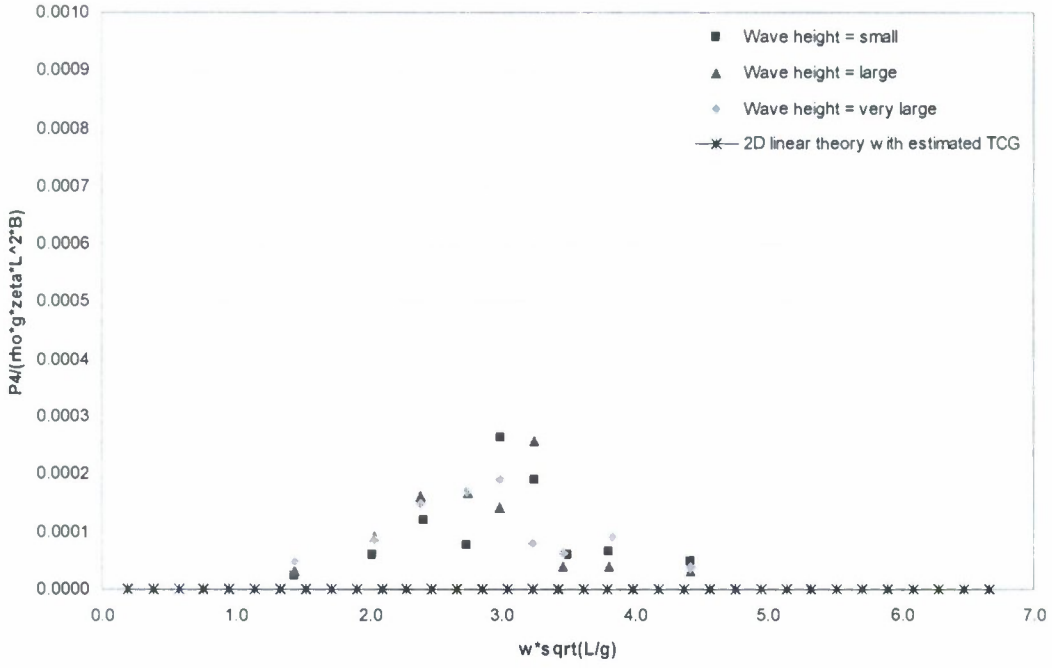

Figure 5.2.2-3: Torsion moment RAO in intact condition at head waves

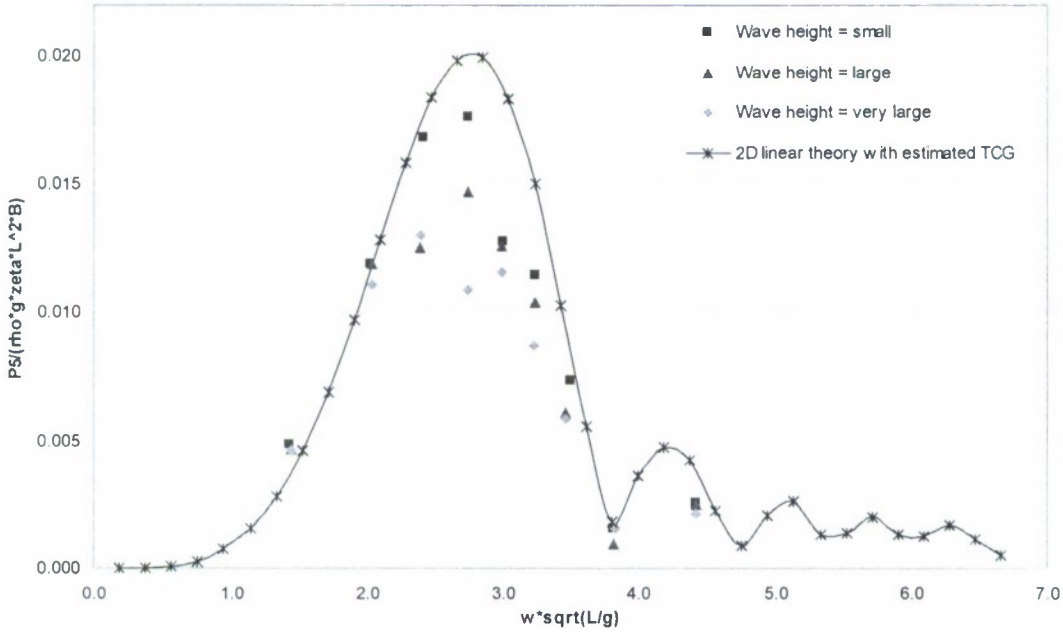

Figure 5.2.2-4: Vertical bending moment RAO in intact condition at head waves

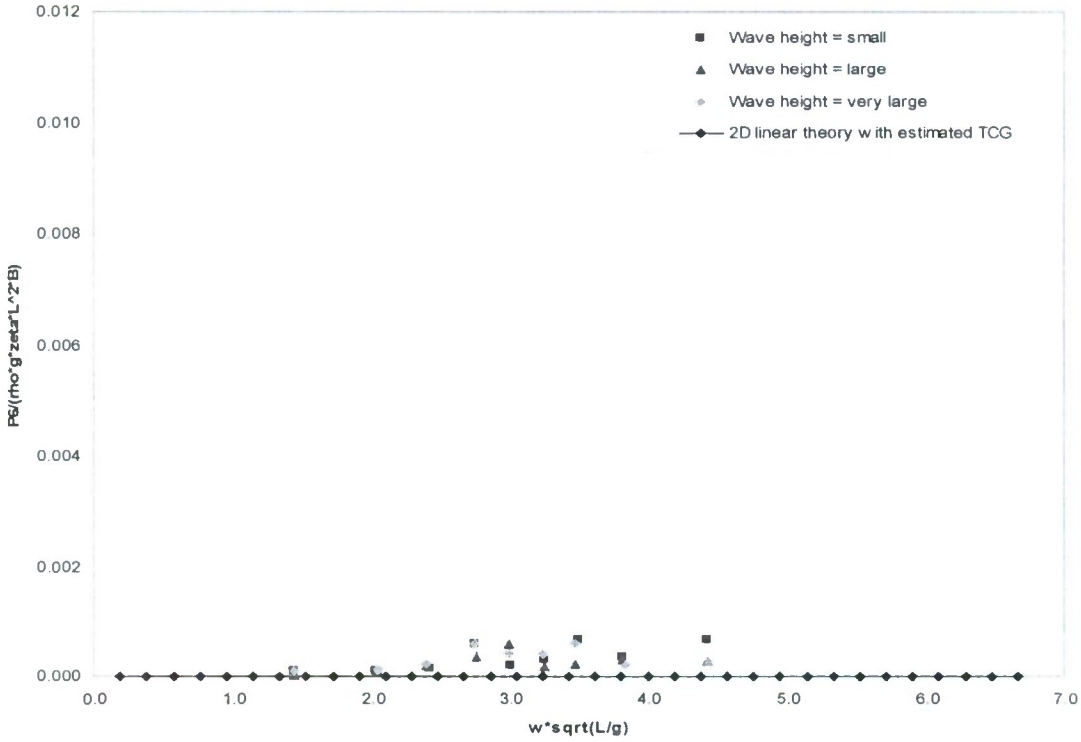

Figure 5.2.2-5: Horizontal bending moment RAO in intact condition at head waves

Stern quartering waves

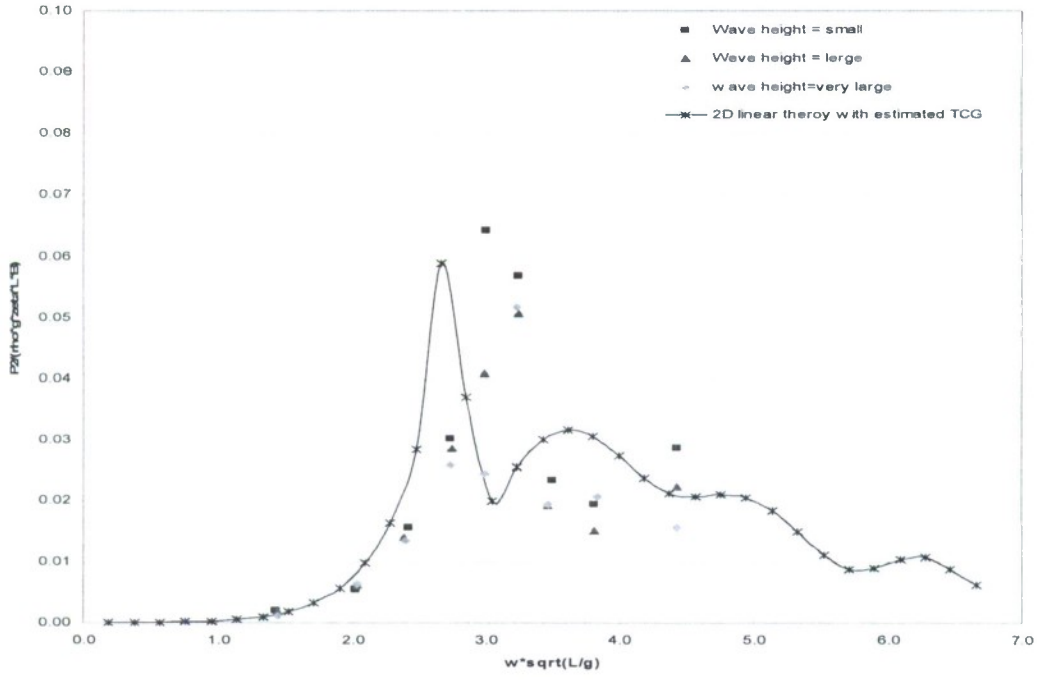

Figure 5.2.2-6: Horizontal shear force in intact condition at stern quartering waves

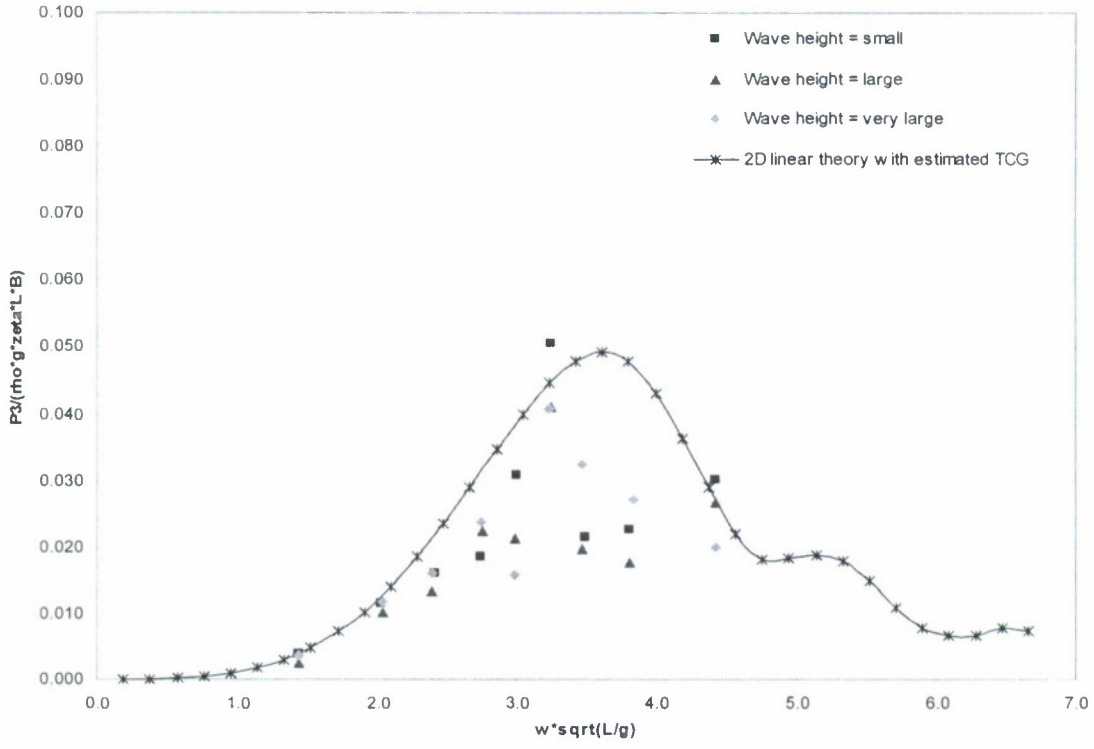

Figure 5.2.2-7: Vertical shear force RAO of intact condition at stern quartering waves

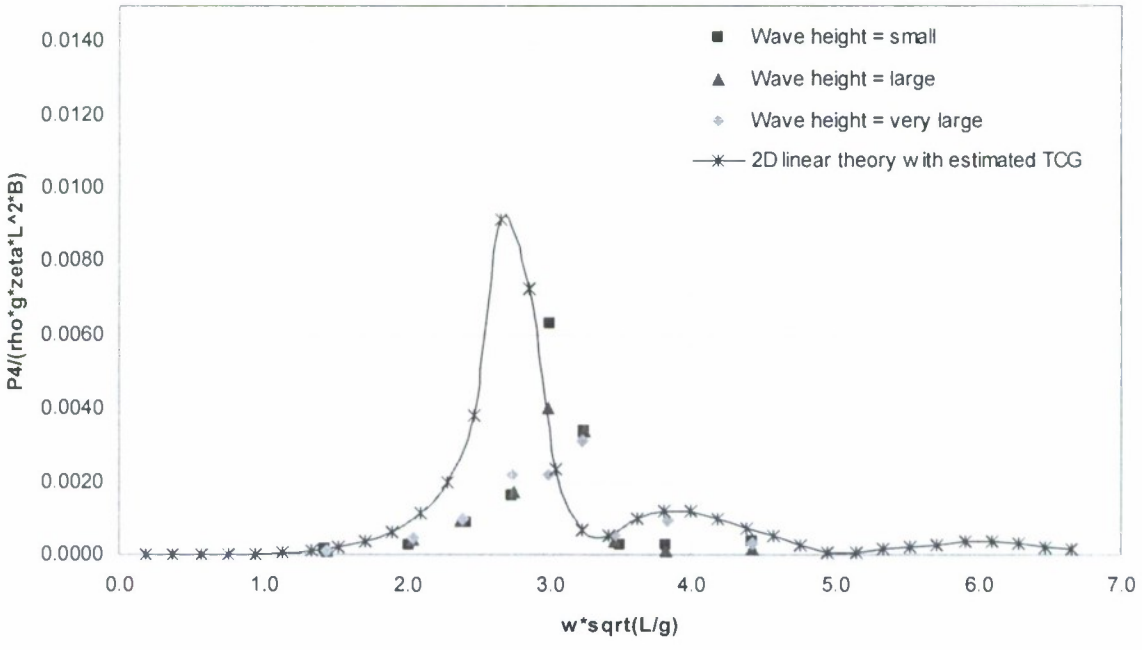

Figure 5.2.2-8: Torsion moment RAO in intact condition at stern quartering waves

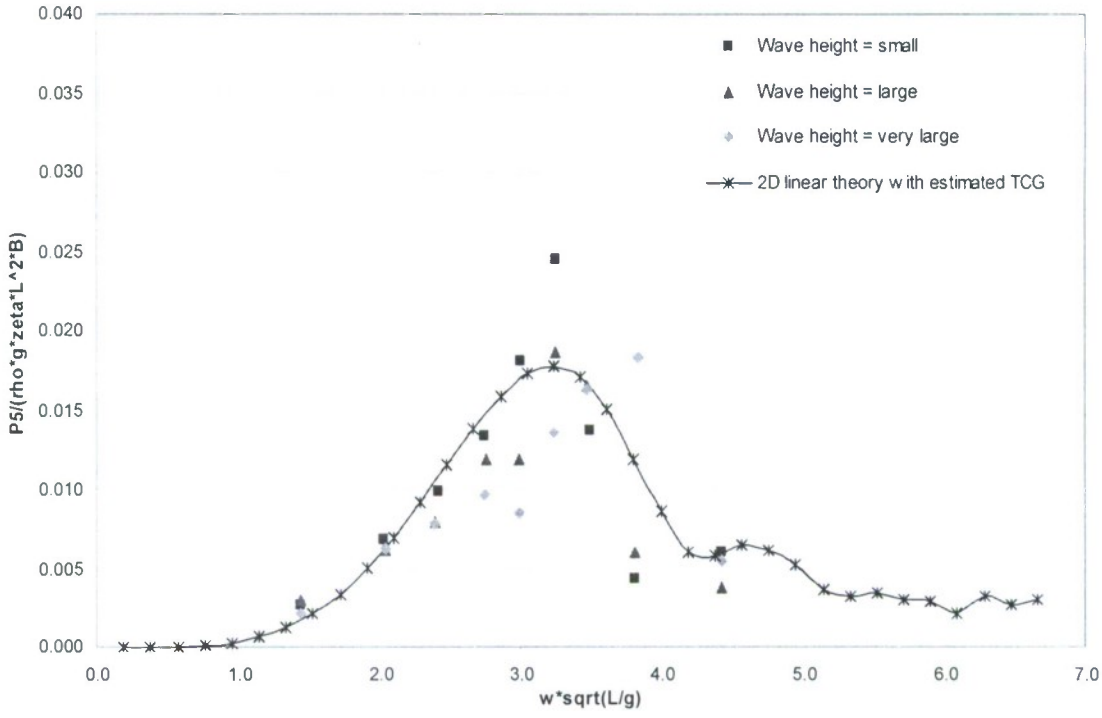

Figure 5.2.2-9: Vertical bending moment RAO in intact condition at stern quartering waves

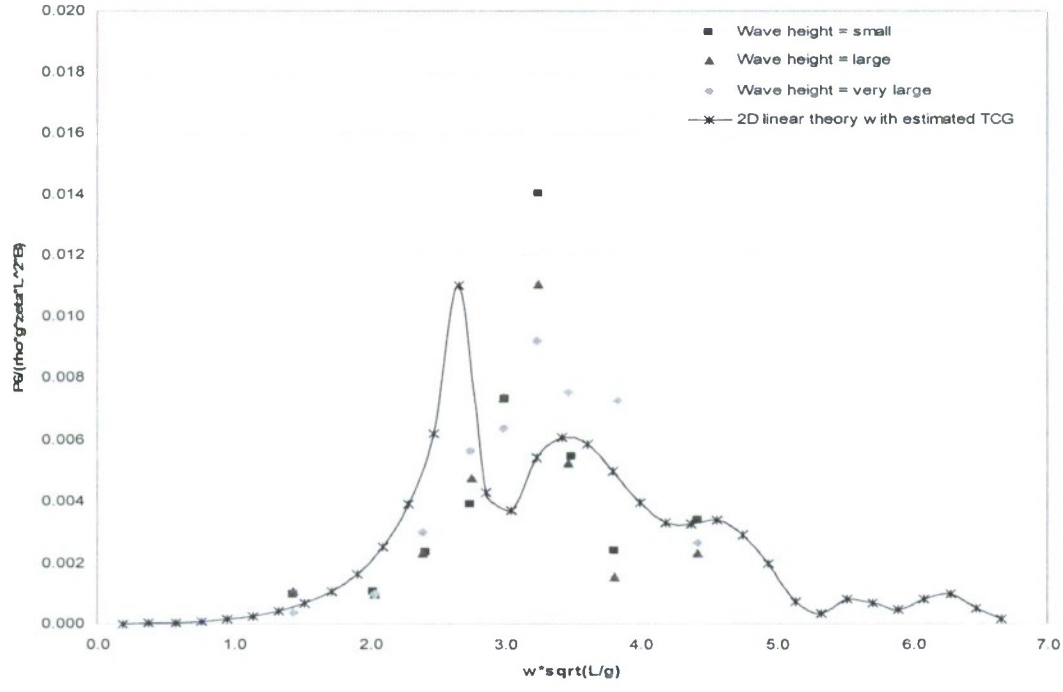

Figure 5.2.2-10: Horizontal bending moment RAO in intact condition at stern quartering waves

Bow quartering waves

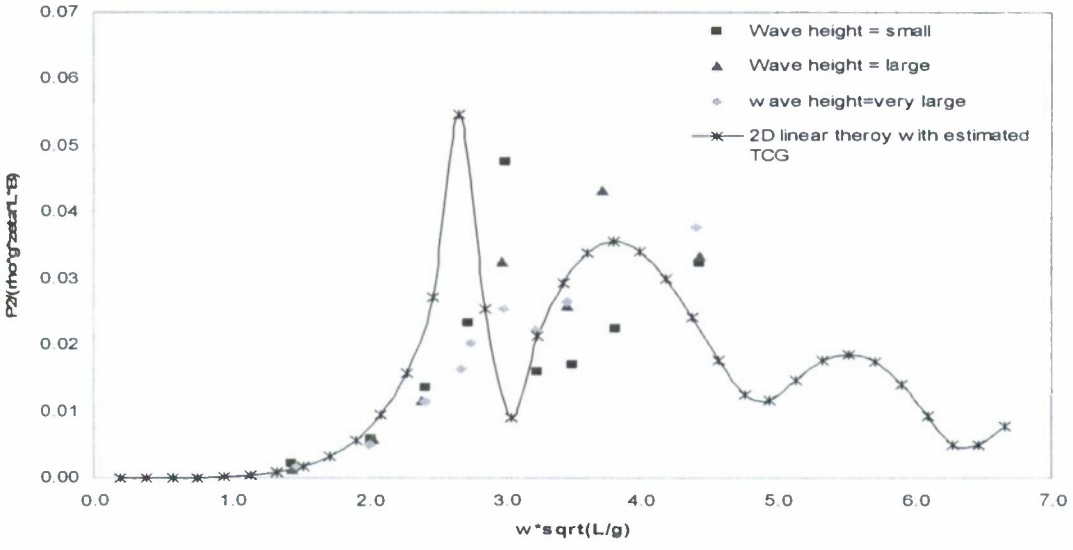

Figure 5.2.2-11: Horizontal shear force RAO in intact condition at bow quartering waves

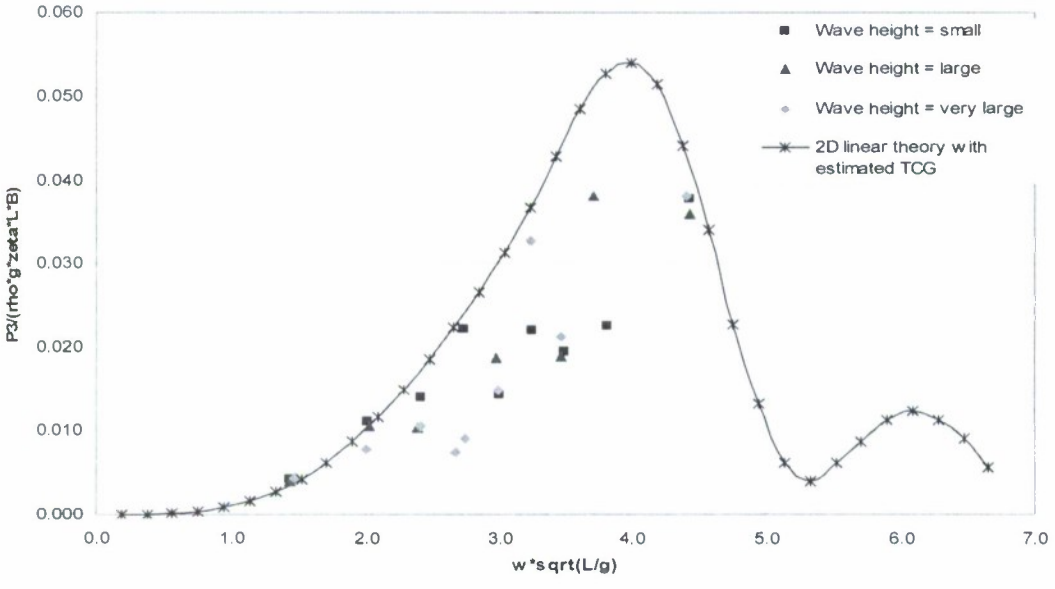

Figure 5.2.2-12: Vertical shear force RAO in intact condition at bow quartering waves

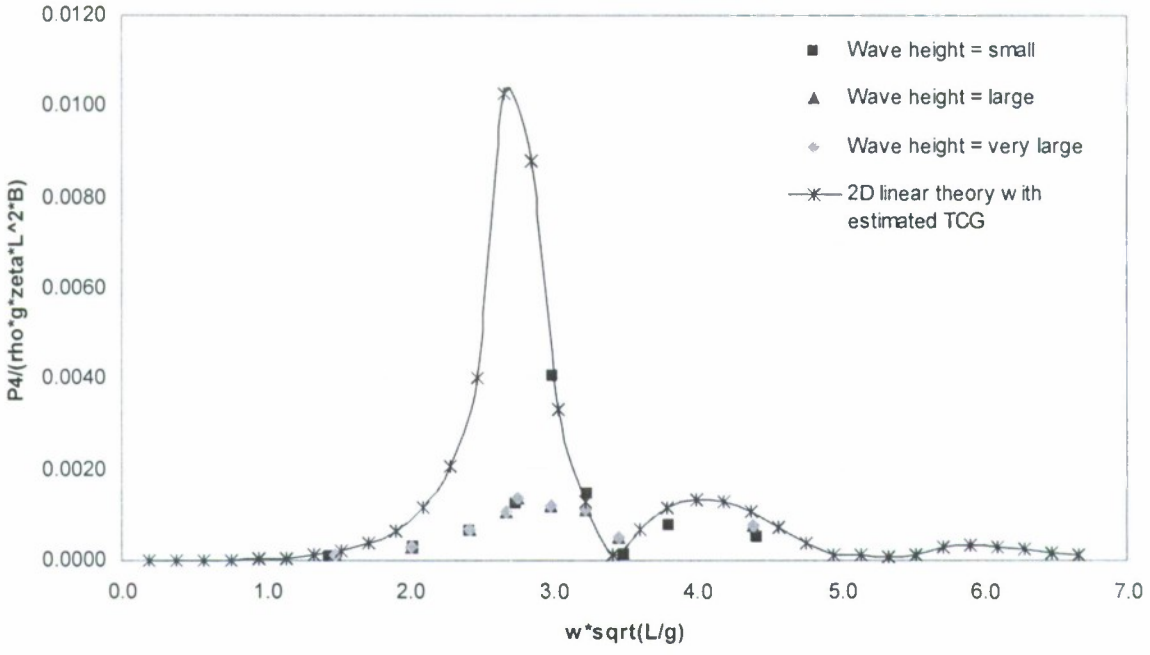

Figure 5.2.2-13: Torsion moment RAO in intact condition at bow quartering waves

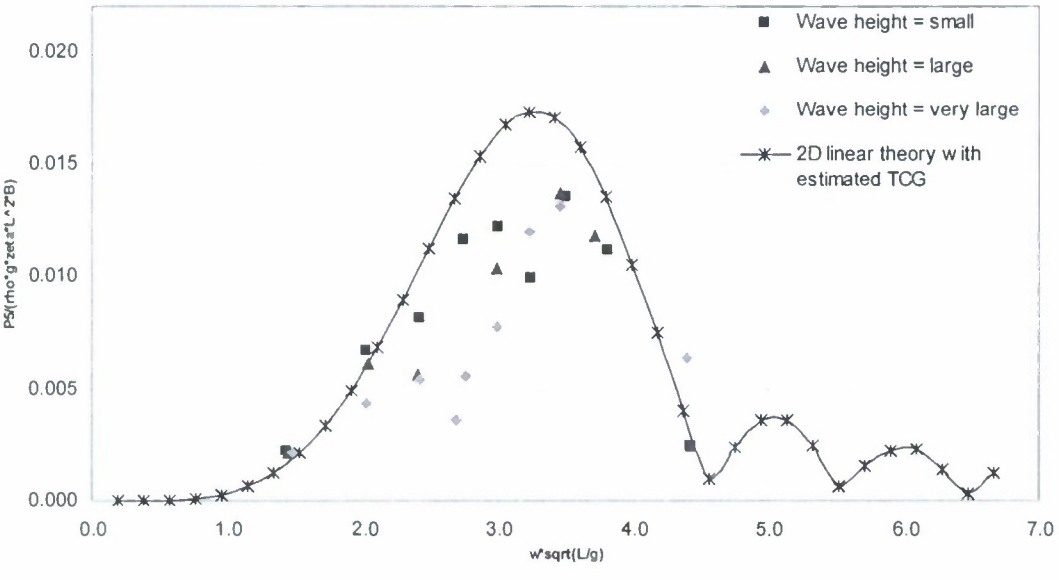

Figure 5.2.2-14: Vertical bending moment RAO in intact condition at bow quartering waves

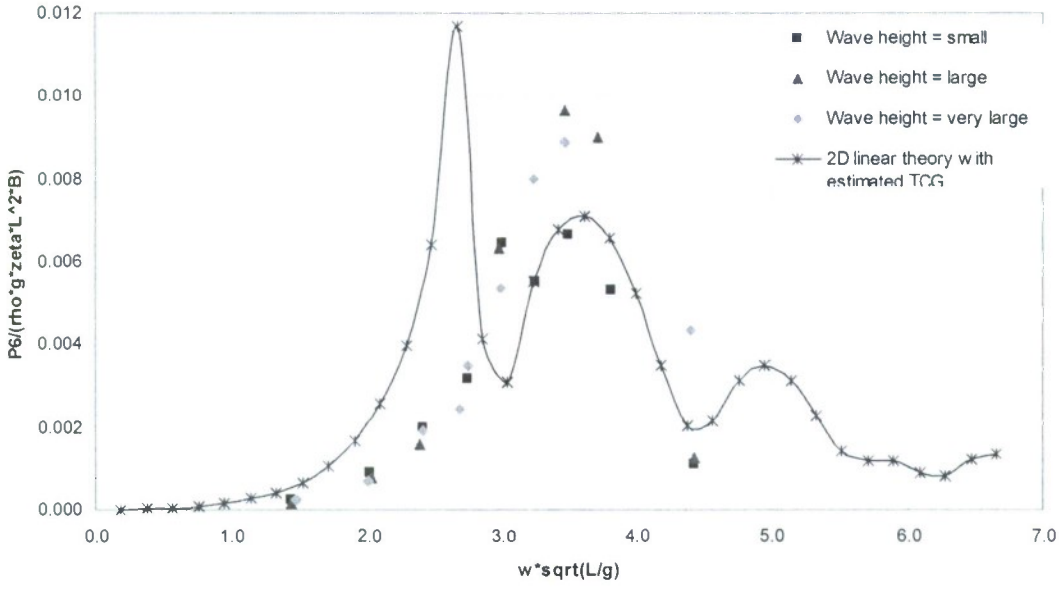

Figure 5.2.2-15: Horizontal bending moment RAO in intact condition at bow quartering waves

Beam waves

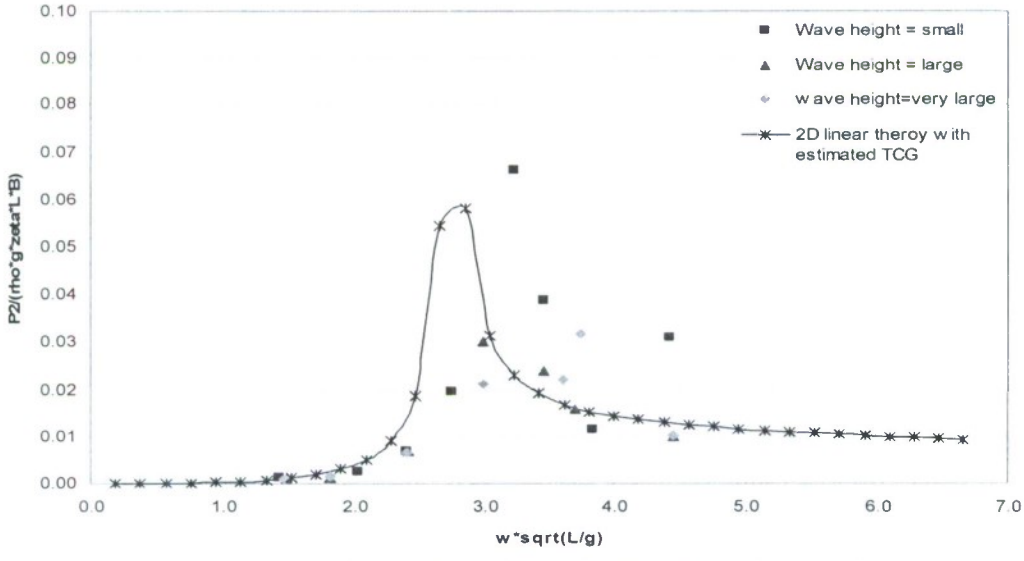

Figure 5.2.2-16: Horizontal shear force RAO in intact condition at beam waves

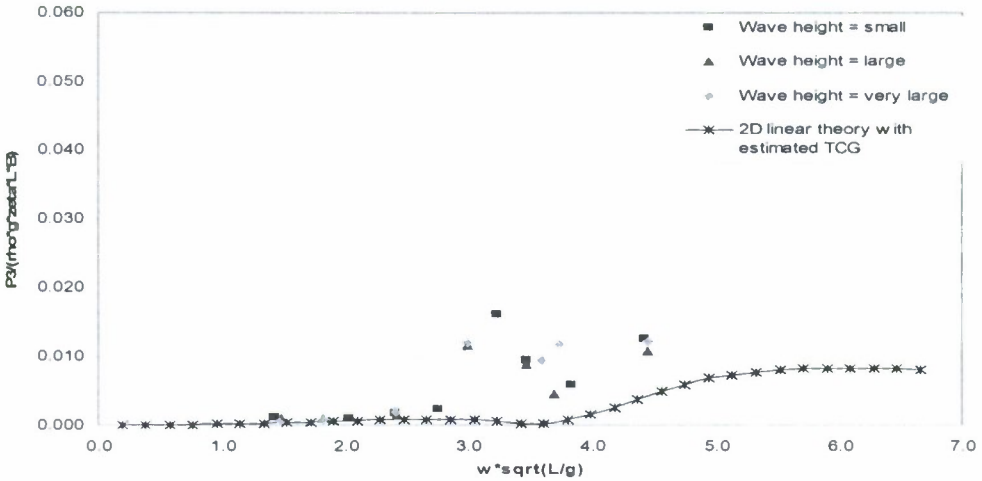

Figure 5.2.2-17: Vertical shear force RAO in intact condition at beam waves

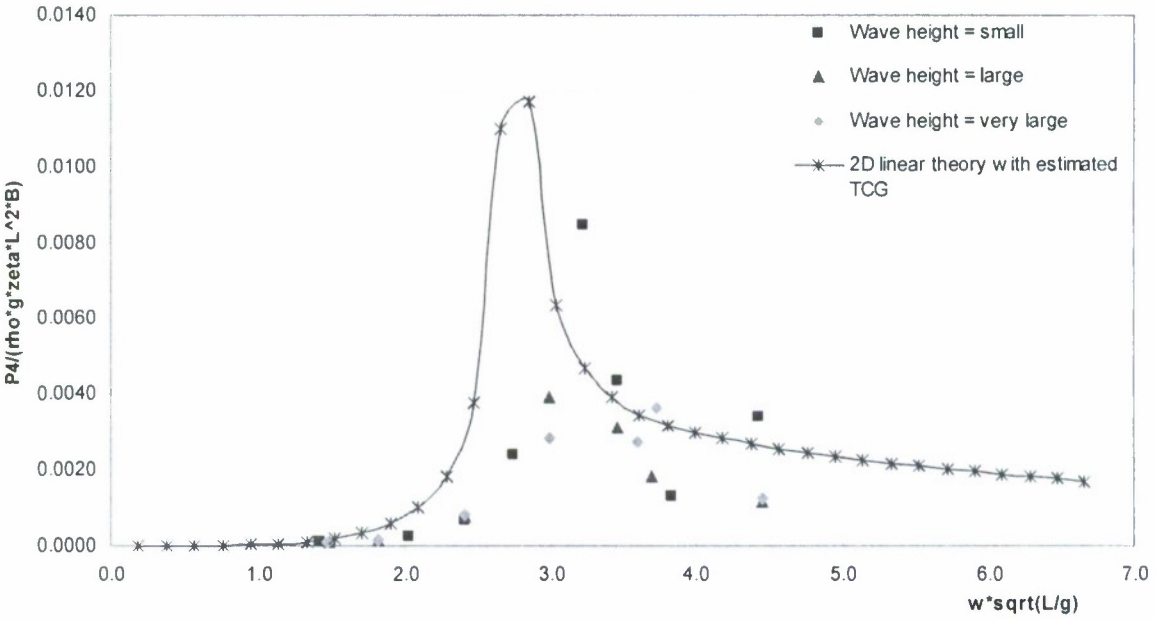

Figure 5.2.2-18: Torsion moment RAO in intact condition at beam waves

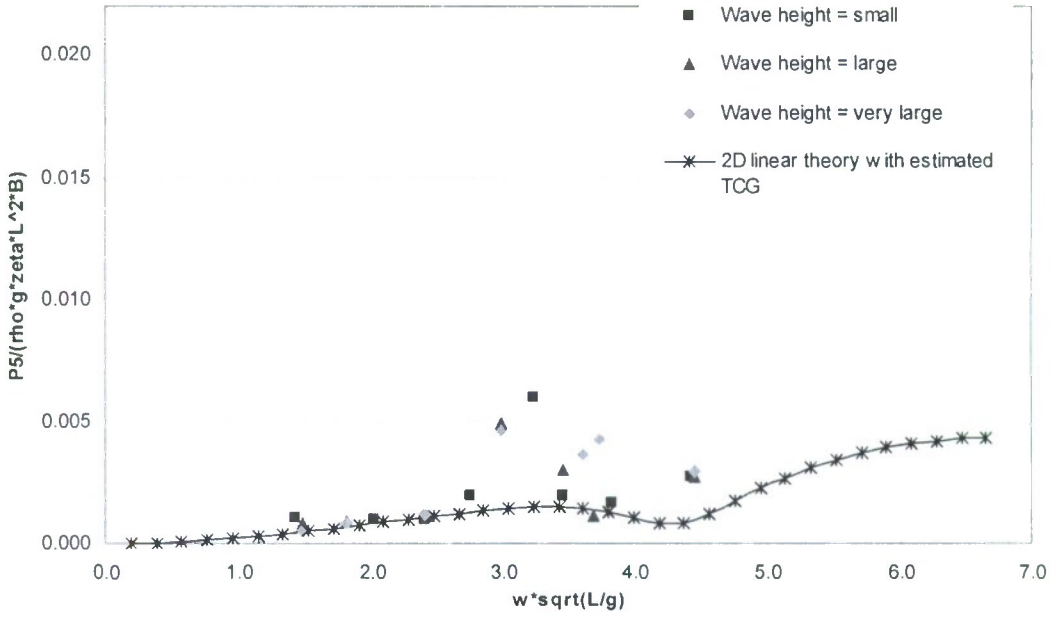

Figure 5.2.2-19: Vertical bending moment RAO in intact condition at beam waves

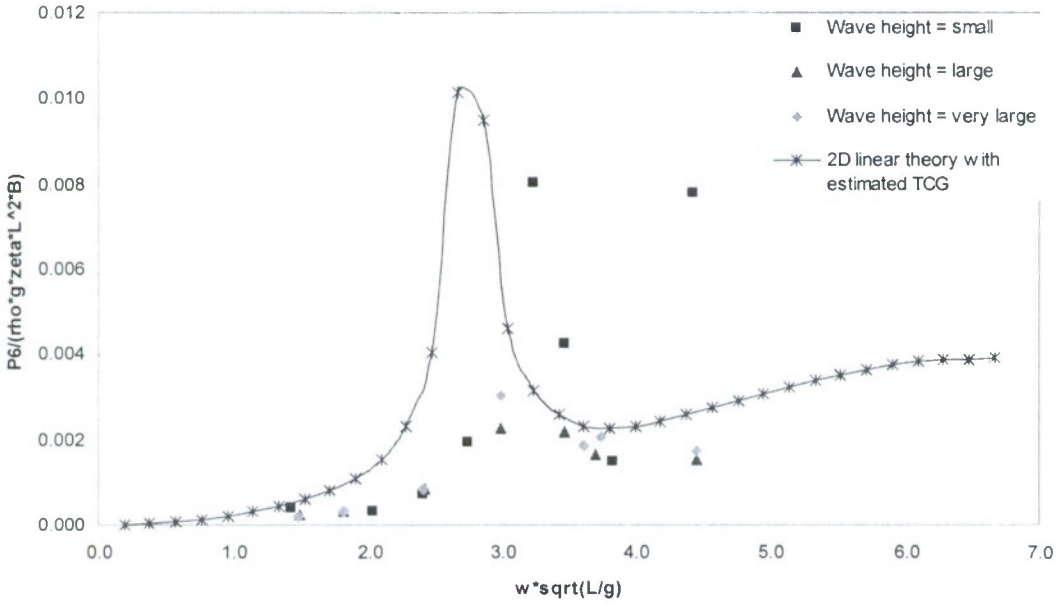

Figure 5.2.2-20: Horizontal bending moment RAO in intact condition at beam waves

5.2.3 Results in damage scenario 2

As mentioned in Chapter 4, in damage scenario 2 the ship model has an increase of draught by 1.09 centimetres (equivalent to 1.09 metres for the ship) and a heel angle of 1.1 degree towards starboard. The results in five different wave headings are presented in the following figures.

- Figures 5.2.3-1 to 5.2.3-5 for head waves.
- Figures 5.2.3-6 to 5.2.3-10 for stern quartering waves *(β=45)*.
- Figures 5.2.3-11 to 5.2.3-15 for stern quartering waves *(β=315)*.
- Figures 5.2.3-16 to 5.2.3-20 for beam waves *(β=90)*.
- Figures 5.2.3-21 to 5.2.3-25 for beam waves *(β=270)*.

The results of the vertical bending moment in head seas were shown in Figure 5.2.3-4. Generally speaking, the numerical results are in good agreement with the experimental results. In the resonant region, the numerical results agree better with the experimental results in small amplitude waves than in large amplitude waves. Quantitative comparisons have been presented in Table B.2 in Appendix B. It can be seen that the mean and COV of X_m are 0.789 and 27.0% for small wave amplitude, and 0.740 and 21.4% for large wave amplitude, and 0.783 and 18.3% for very large wave amplitude.

Because the damage is unsymmetrical transversely, it is expected that the wave-induced loads might be different when the wave is approaching the ship model from different sides due to the dynamic behaviour of the flooded water in the damaged compartment. Therefore two wave headings have been chosen for stern quartering seas, one is approaching from the starboard side (the damaged side), the other is from the port side. The 2D linear method have produced satisfactory results in both stern quartering seas in vertical bending moment predictions, as shown in Figures 5.2.3-9 and -14. The mean and COV of X_m are 1.063 and 28.2% in stern quartering seas from the starboard for small wave amplitude, and are 0.989 and 29.9% in stern quartering seas from the port for small wave amplitude. So the accuracy in both stern quartering seas is in the similar level. To clearly demonstrate the difference caused by different approaching angles, the vertical bending moment at 45° and 315° wave headings has been plotted together in Figure 5.2.3-26. Because the 2D linear method can't consider the effects of dynamic behaviour of flooded water and the heel angle is very small, the numerical results were nearly identical in both stern quartering seas. However, the test results have shown that the vertical bending moment at 45° wave heading at most of frequencies was slightly larger than that at 315° wave heading.

The vertical bending moment in beam seas, which were shown in Figures 5.2.3-19 and -24, was not significant, so there was no need for further discussions.

Figures 5.2.3-10 and -15 show the results of horizontal bending moment in both stern quartering seas. The agreement between the 2D linear method and experiment were reasonably good, although it was not as good as that in vertical bending moment predictions. The mean and COV of X_m are 1.164 and 67.2% in stern quartering seas from the starboard for small wave amplitude, and are 1.016 and 42.3% in stern quartering seas from the port for small wave amplitude. So the accuracy in stern quartering seas from the port side is slightly better than that from the starboard side. It is also true for large and very large wave amplitude (see Table B.2). The horizontal bending moment at 45° and 315° wave headings has been plotted together in Figure 5.2.3-27 to see how much difference was caused by these different approaching angles. There was no clear trend in this figure.

Horizontal bending moment in both beam seas (from the starboard and port side) has been shown Figures 5.2.3-20 and -25. The large difference between the numerical and experimental results was mainly occurring at either very low frequencies or very high frequencies. The mean and COV of X_m are 1.941 and 60.9% in beam seas from the starboard for small wave amplitude, and are 1.587 and 76.3% in beam seas from the port for small wave amplitude. The mean values in beam seas were not as good as in quartering seas. Similarly, the horizontal bending moment in beam seas at 90° and 270° wave headings has been plotted together in Figure 5.2.3-28. It is seen that the horizontal bending moment is slightly larger when the wave is approaching from the starboard side than that from the port side.

Figures 5.2.3-8 and -13 show the results of torsion moment in both stern quartering seas. The agreement between the 2D linear method and experiment were reasonably good. Its accuracy was not as good as that in vertical bending moment predictions, but surprisingly, was in a similar level to that in horizontal bending moment predictions. Unlike in intact conditions, the predicted frequency, where the maximum responses occur, matched reasonably well with measured frequency in the tests. The mean and COV of X_m are 0.633 and 64.1% in stern quartering seas from the starboard for small wave amplitude, and are 0.828 and 52.6% in stern quartering seas from the port for small wave amplitude. So the accuracy in stern quartering seas from the port side is slightly better than that from the starboard side. It is also true for large and very large wave amplitude (see Table B.2). The torsion moment at 45° and 315° wave headings has been plotted together in Figure 5.2.3-29. It is observed that the torsion moment at 315° wave headings is larger than that at 45° wave headings.

Again the numerical results tend to agree better with the experimental results at small amplitude waves in most cases than those at large amplitude waves.

Head waves

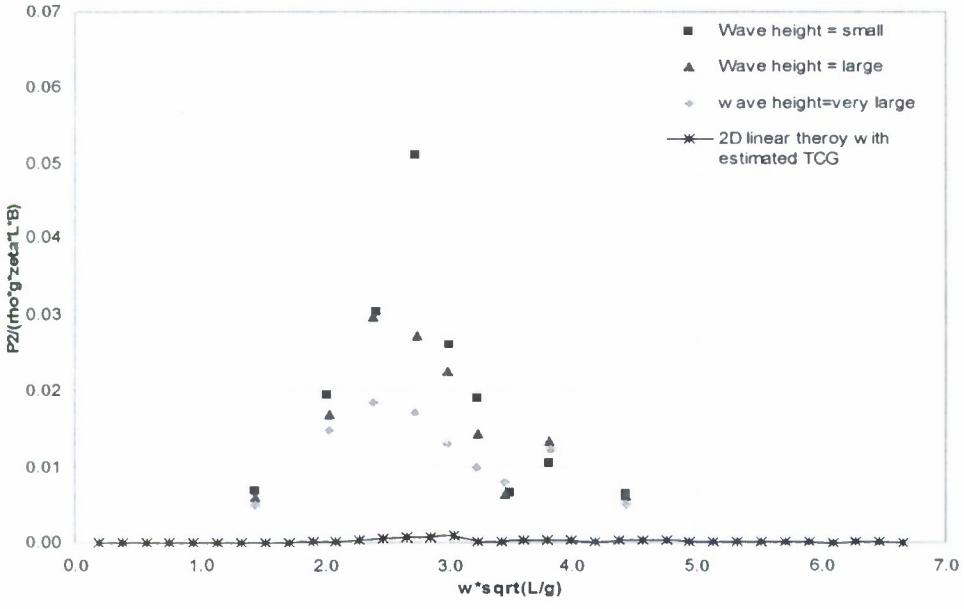

Figure 5.2.3-1: Horizontal shear force RAO in DS2 at head waves

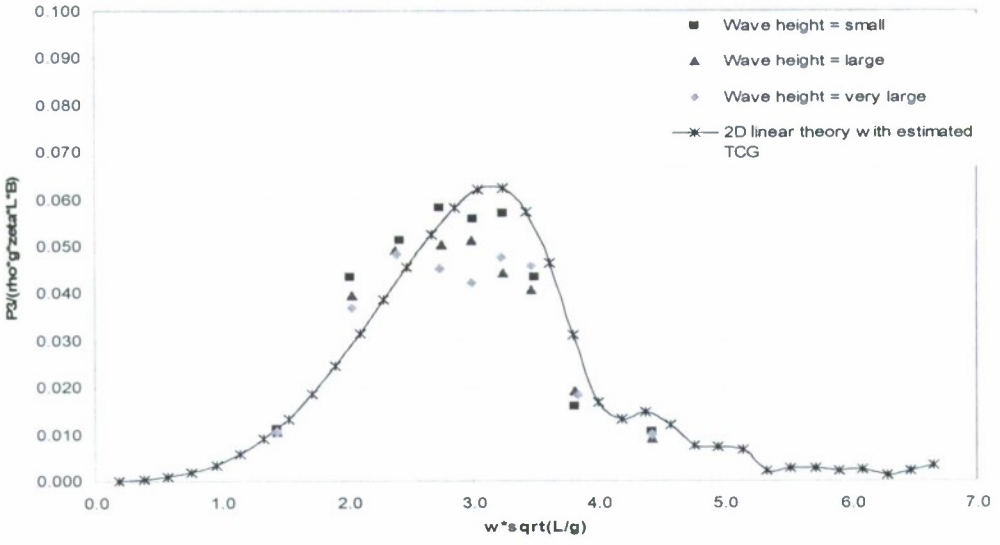

Figure 5.2.3-2: Vertical shear force RAO in DS2 at head waves

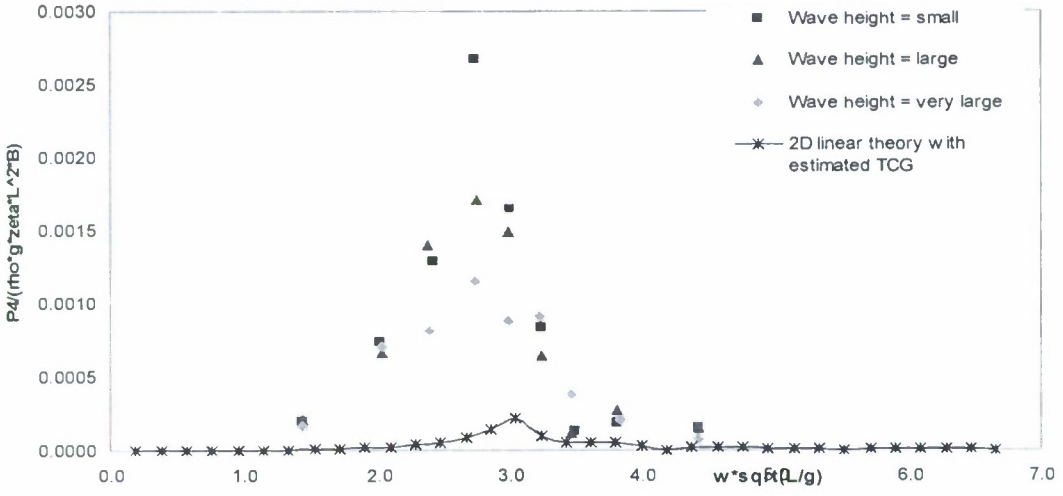

Figure 5.2.3-3: Torsion moment RAO in DS2 at head waves

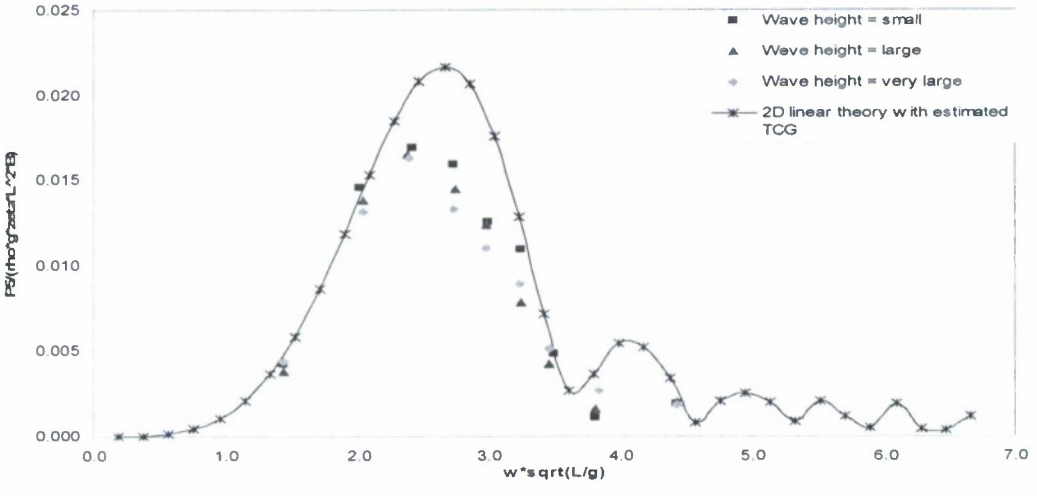

Figure 5.2.3-4: Vertical bending moment RAO in DS2 at head waves

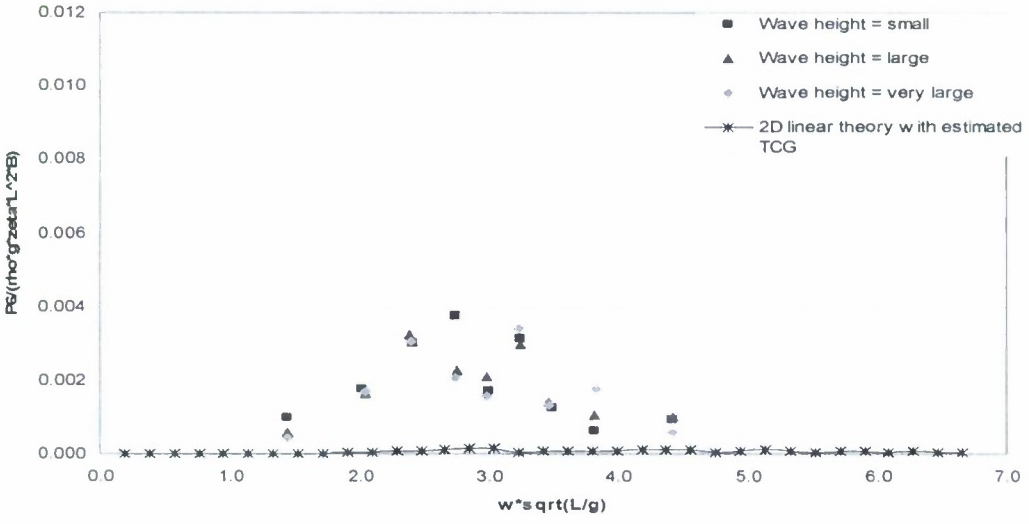

Figure 5.2.3-5: Horizontal bending moment RAO in DS2 at head waves

Stern quartering waves from starboard side (heading 45)

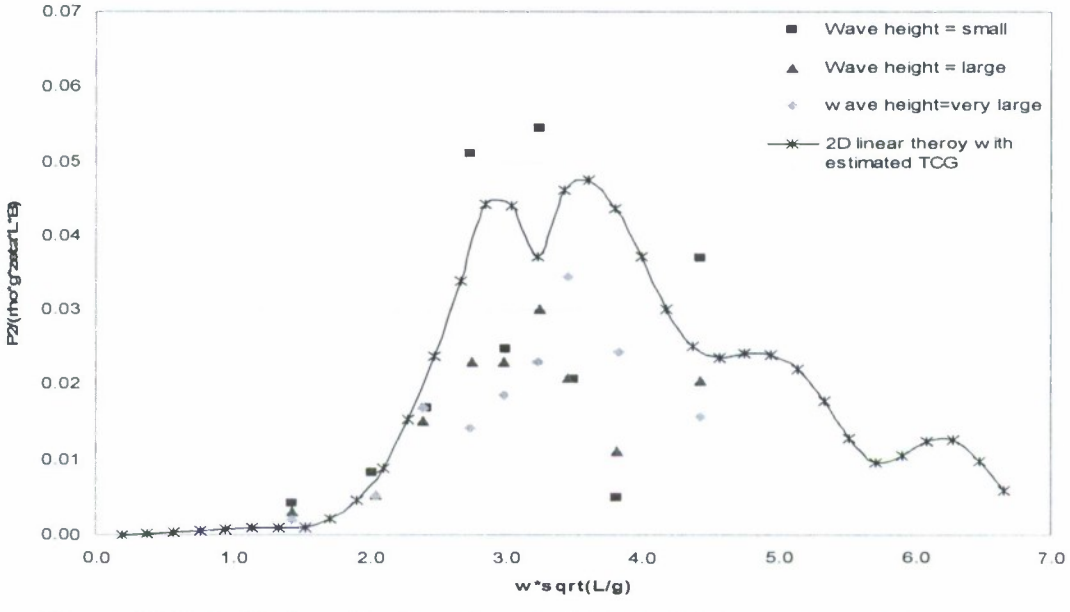

Figure 5.2.3-6: Horizontal shear force RAO in DS2 at stern quartering waves

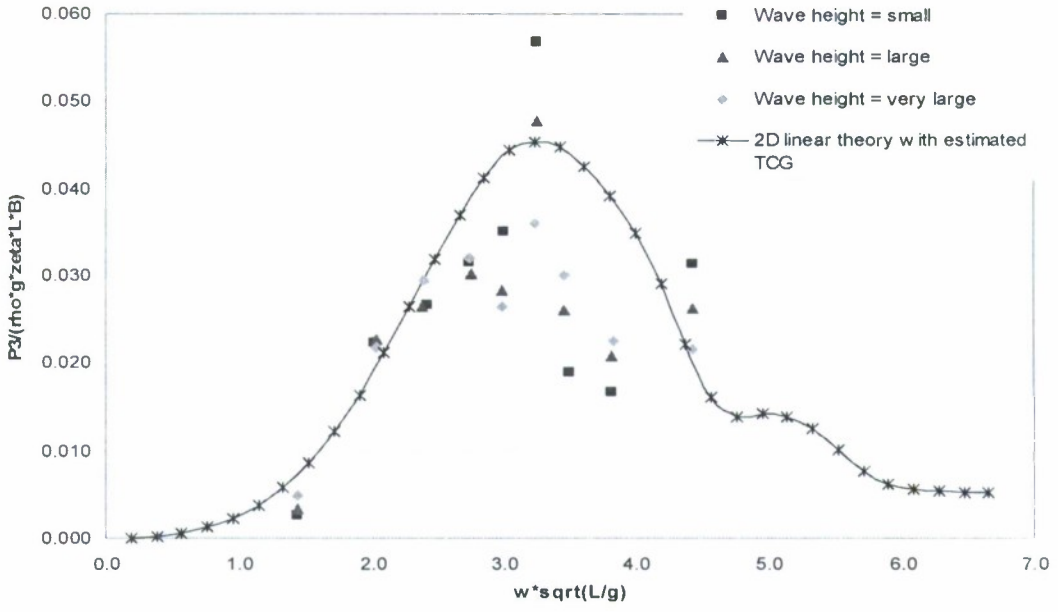

Figure 5.2.3-7: Vertical shear force RAO in DS2 at stern quartering waves

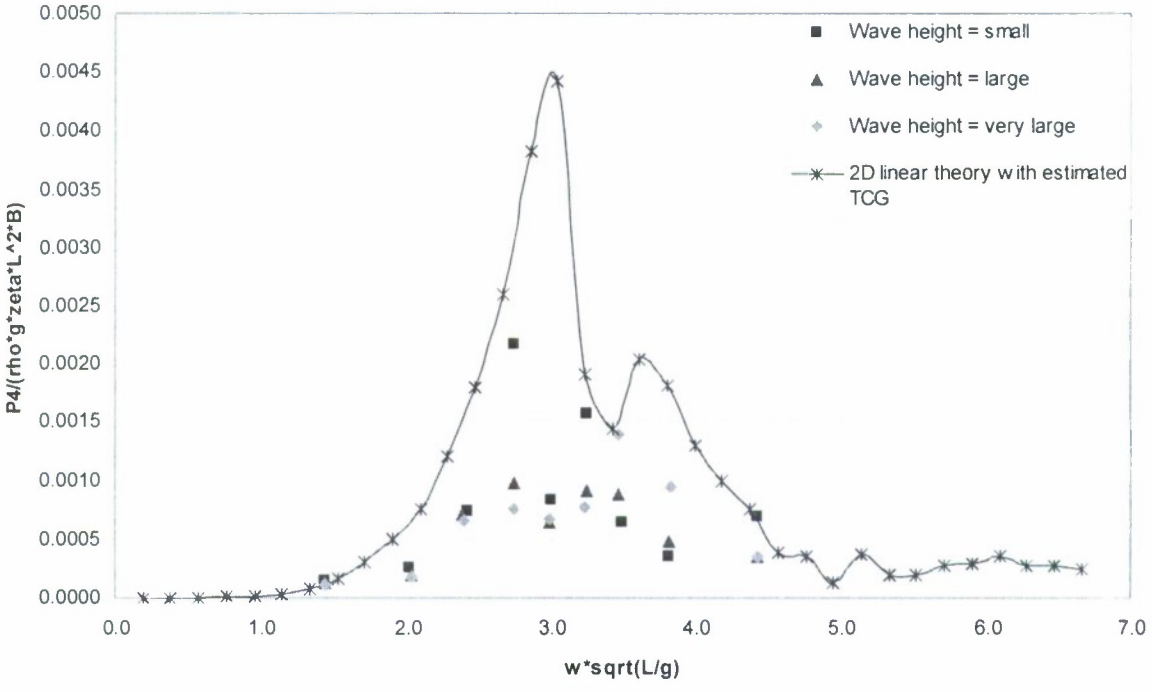

Figure 5.2.3-8: Torsion moment RAO in DS2 at stern quartering waves

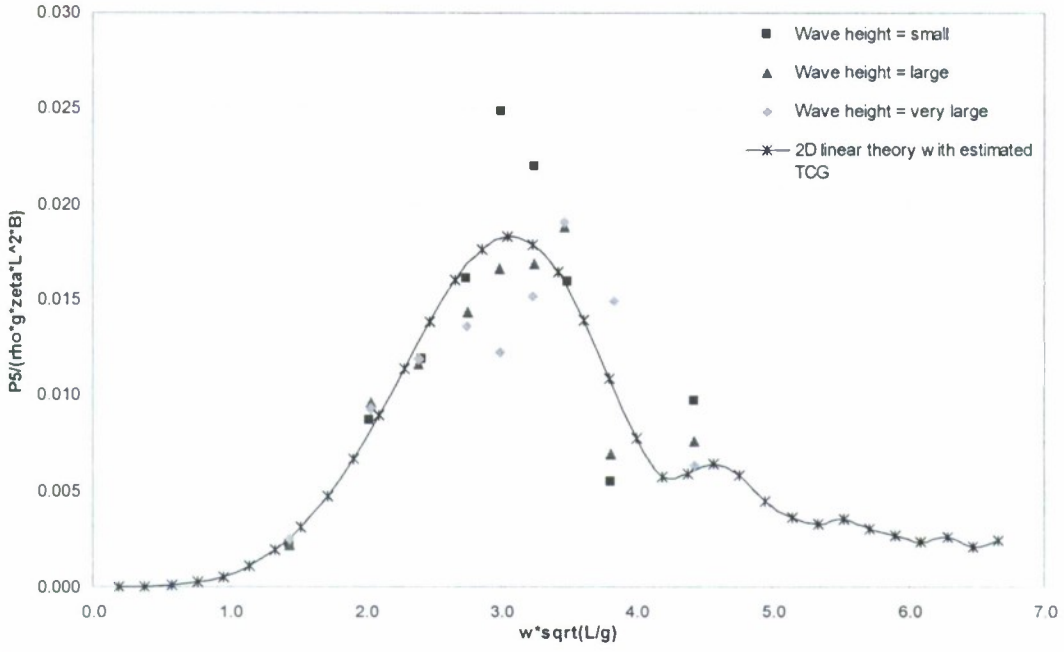

Figure 5.2.3-9: Vertical bending moment RAO in DS2 at stern quartering waves

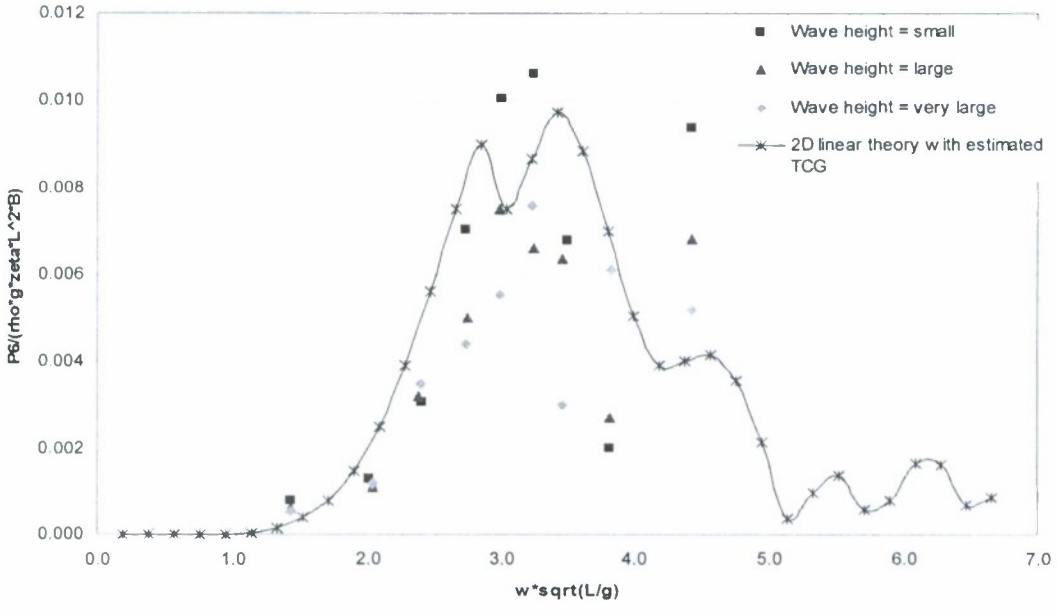

Figure 5.2.3-10: Horizontal bending moment RAO in DS2 at stern quartering waves

Stern quartering waves from the port side (heading 315)

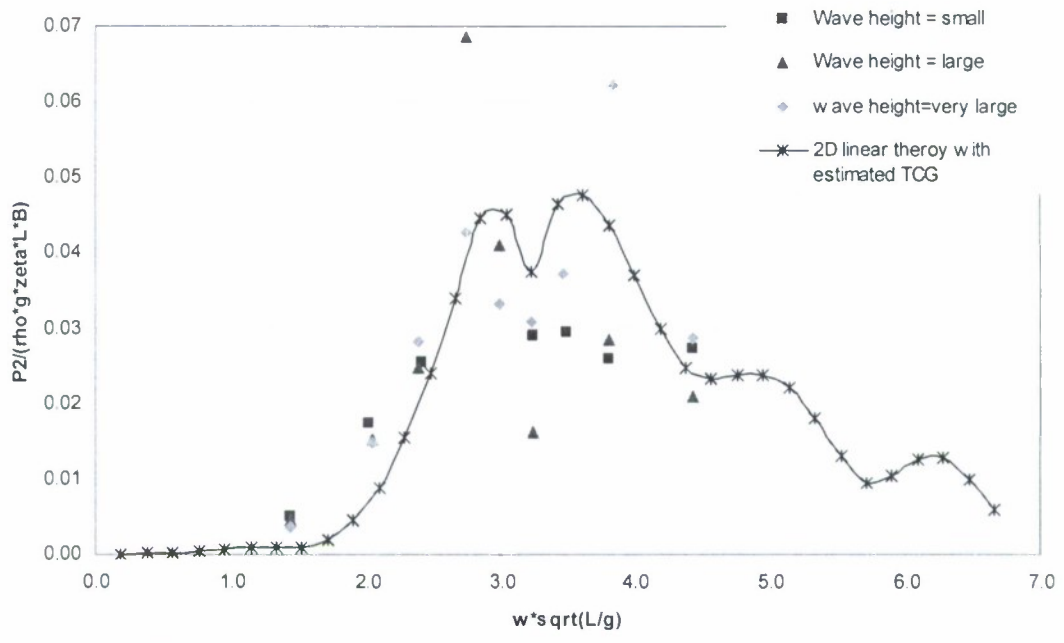

Figure 5.2.3-11: Horizontal shear force RAO in DS2 at stern quartering waves (heading 315)

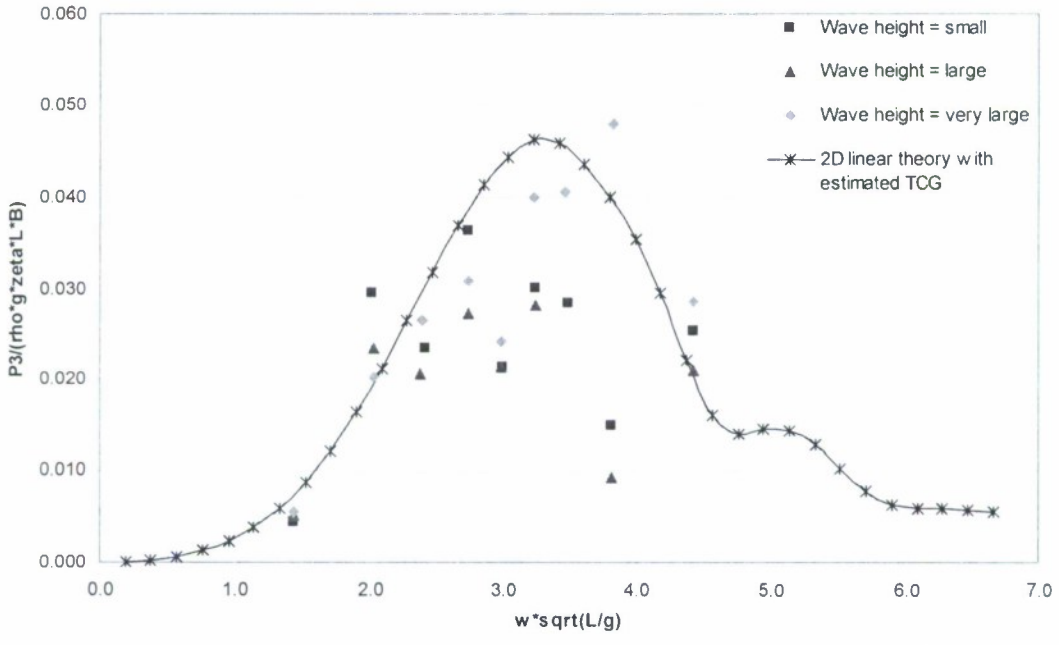

Figure 5.2.3-12: Vertical shear force RAO in DS2 at stern quartering waves (heading 315)

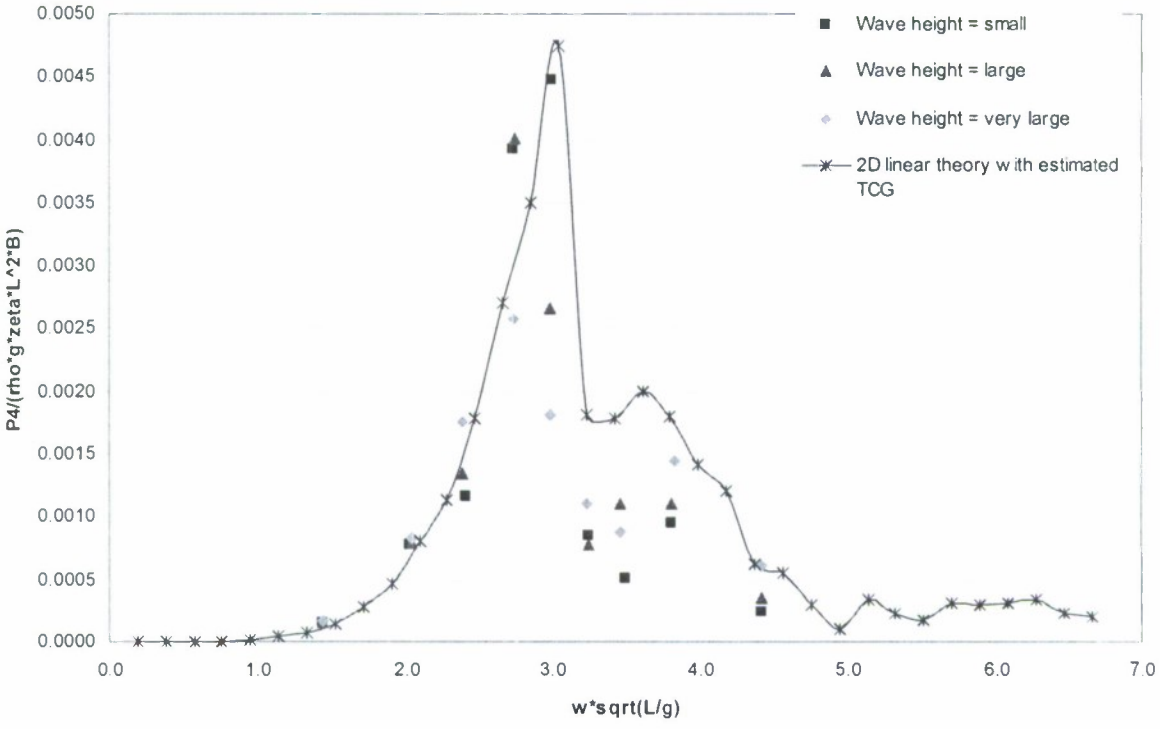

Figure 5.2.3-13: Torsion moment RAO in DS2 at stern quartering waves (heading 315)

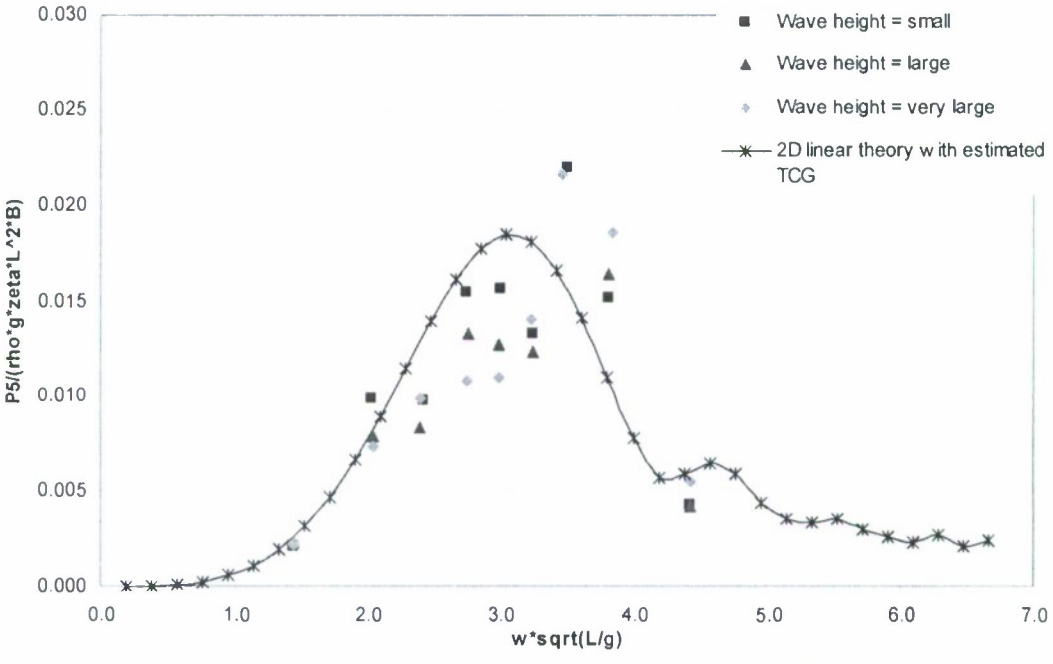

Figure 5.2.3-14: Vertical bending moment RAO in DS2
at stern quartering waves (heading 315)

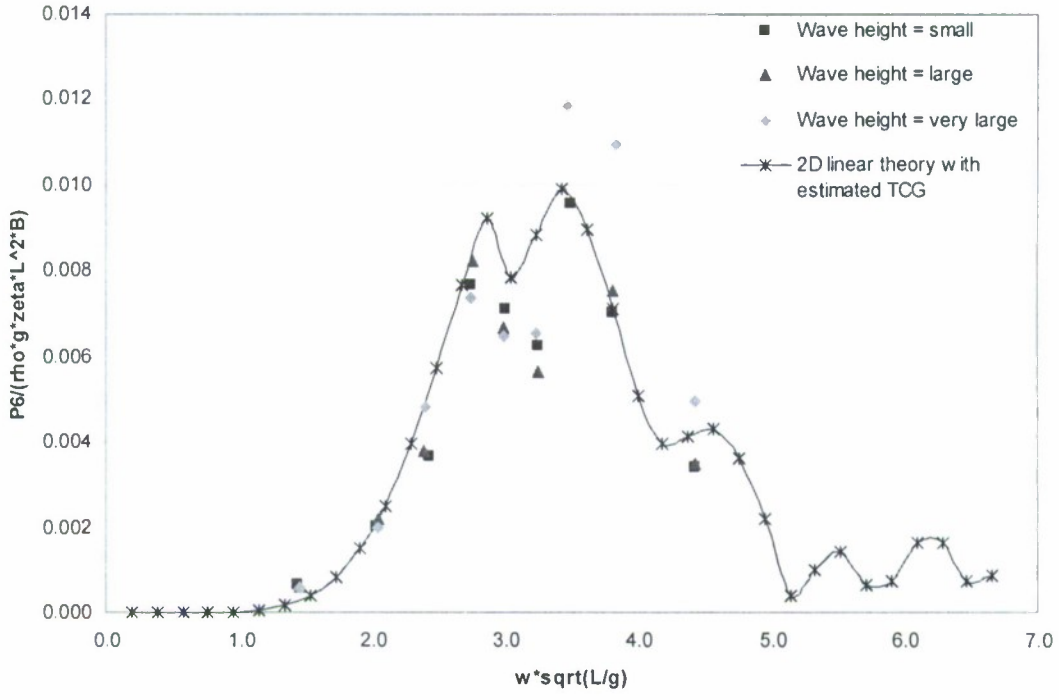

Figure 5.2.3-15: Horizontal bending moment RAO in DS2 at stern quartering waves (heading 315)

Beam waves from the starboard side (heading 90)

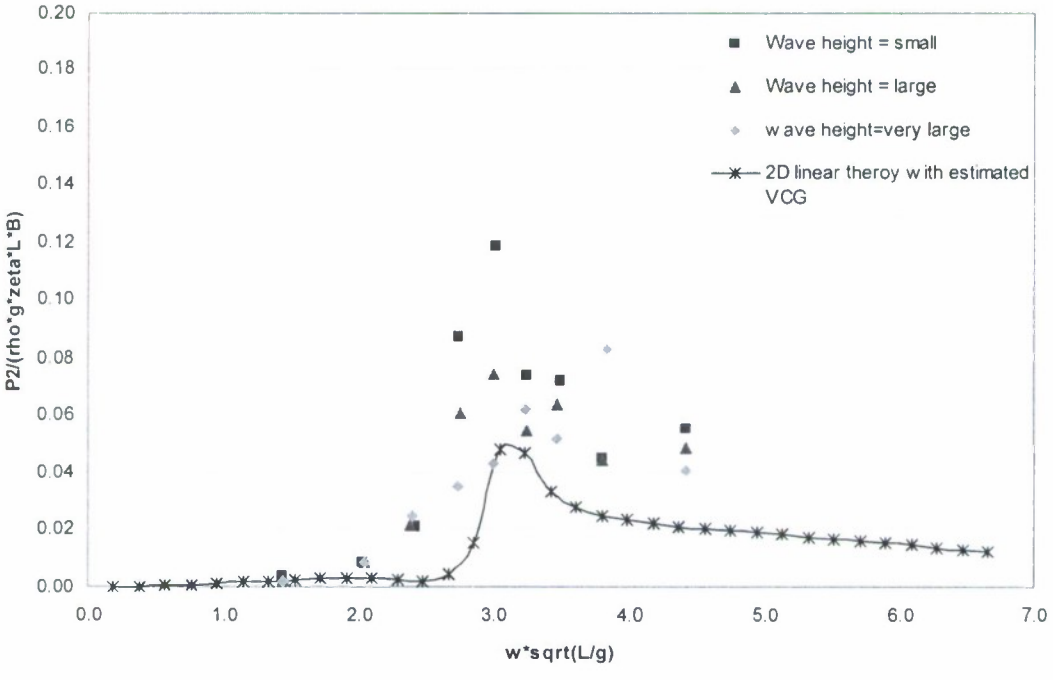

Figure 5.2.3-16: Horizontal shear force RAO in DS2 at beam waves (heading 90)

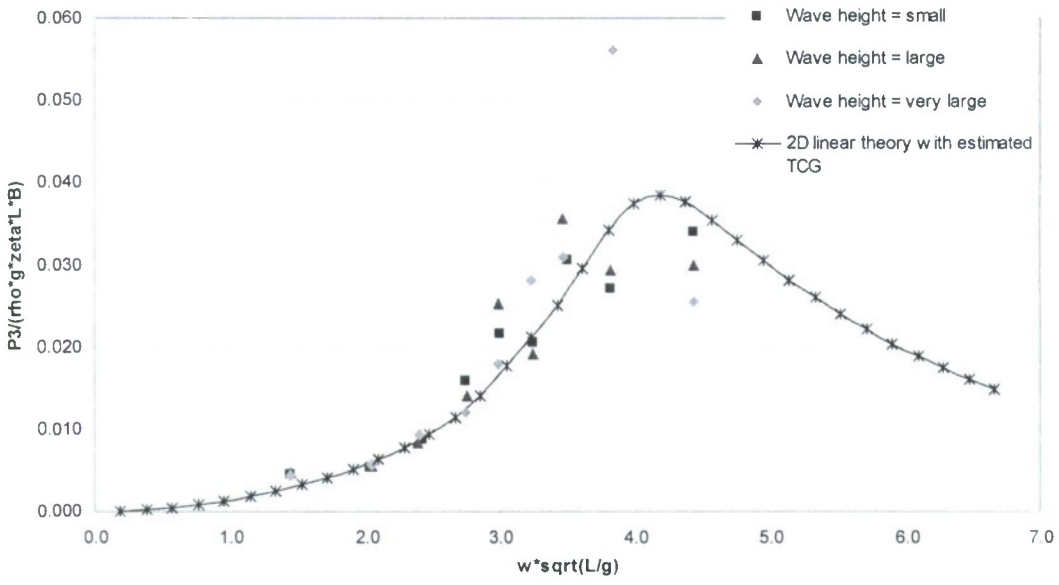

Figure 5.2.3-17: Vertical shear force RAO in DS2 at beam waves (heading 90)

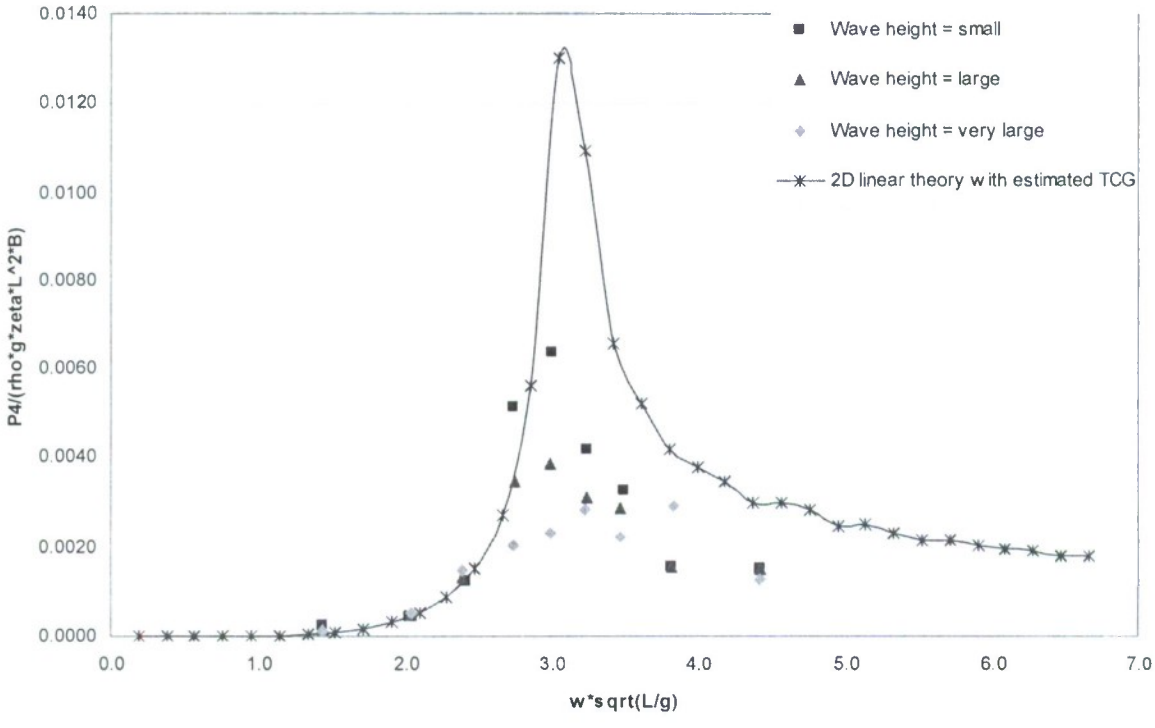

Figure 5.2.3-18: Torsion moment RAO in DS2 H5415 at beam waves (heading 90)

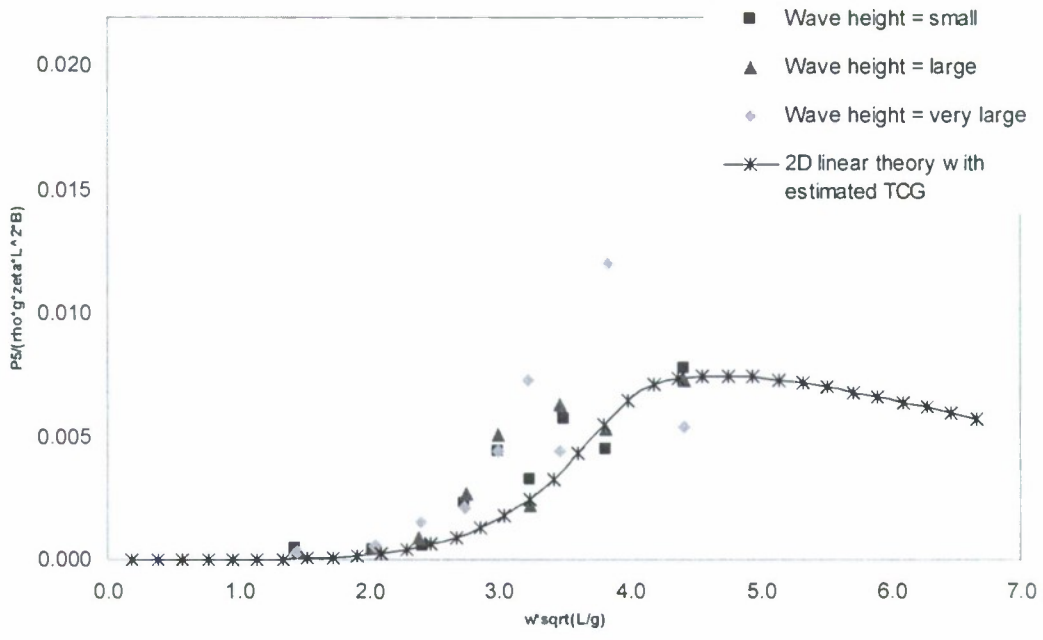

Figure 5.2.3-19: Vertical bending moment RAO in DS2 H5415 at beam waves (heading 90)

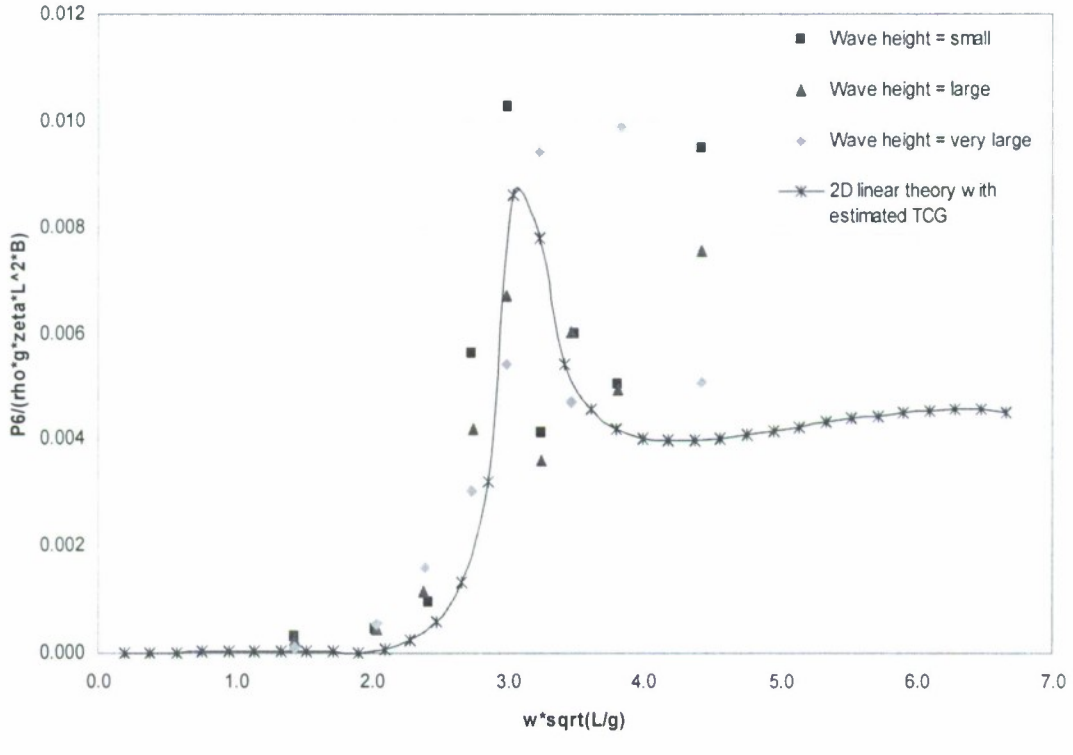

Figure 5.2.3-20: Horizontal bending moment RAO in DS2 at beam waves (heading 90)

Beam waves from the port side (heading 270)

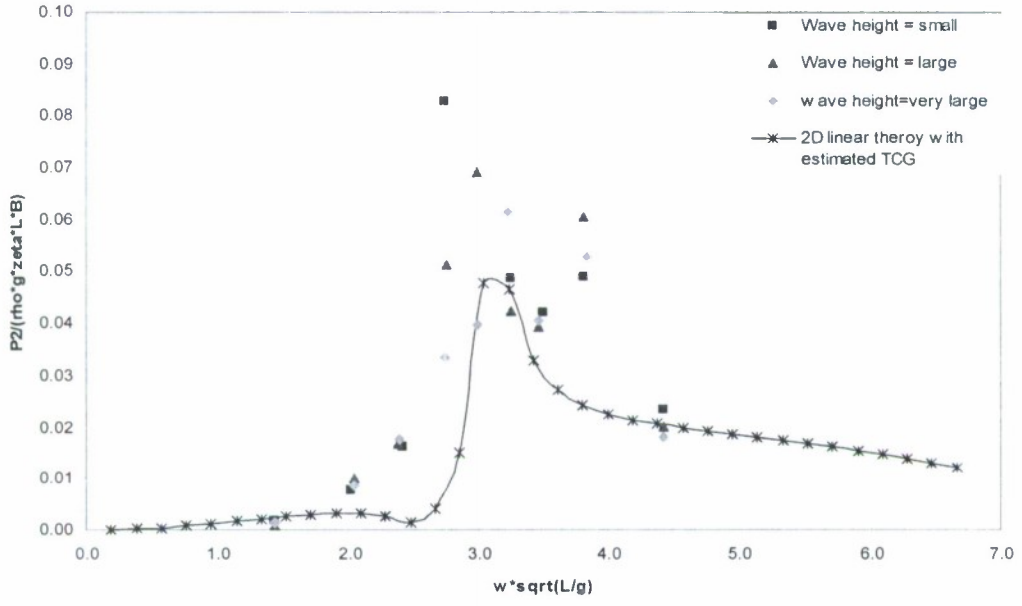

Figure 5.2.3-21: Horizontal shear force RAO in DS2 at beam waves (heading 270)

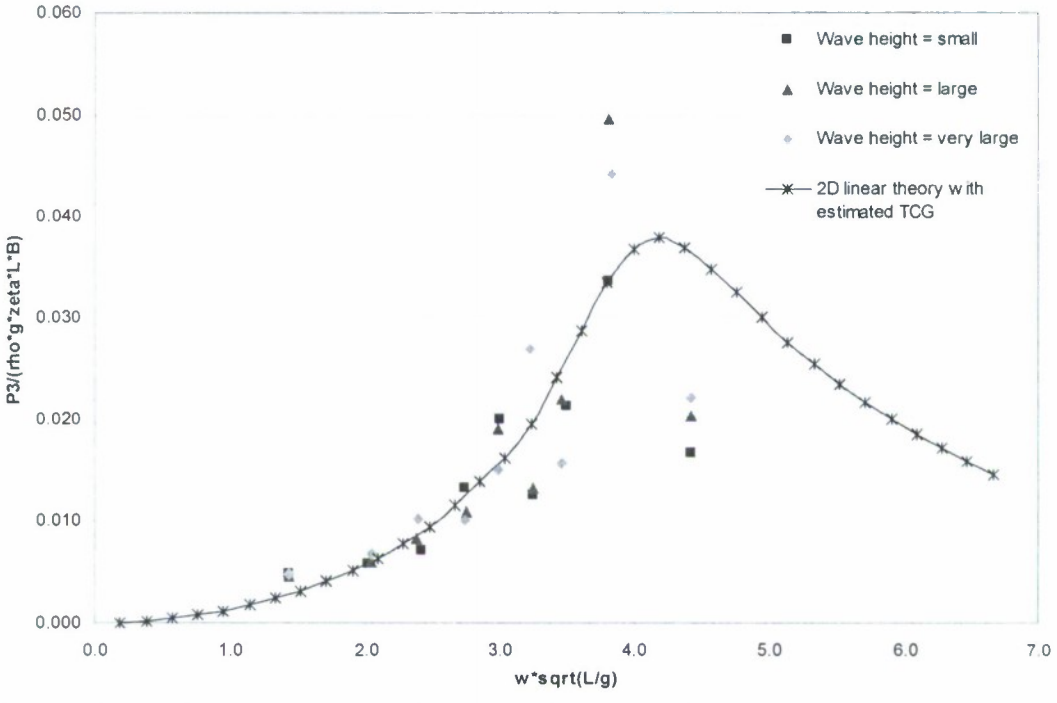

Figure 5.2.3-22: Vertical shear force RAO in DS2 at beam waves (heading 270)

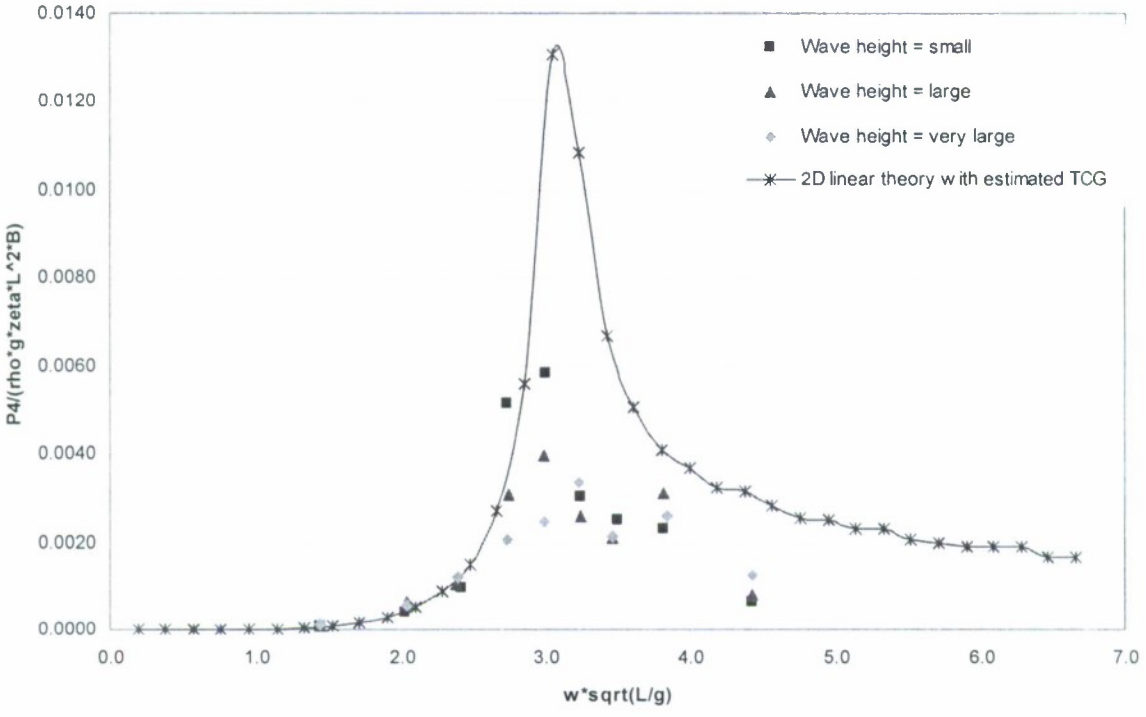

Figure 5.2.3-23: Torsion moment RAO in DS2 at beam waves (heading 270)

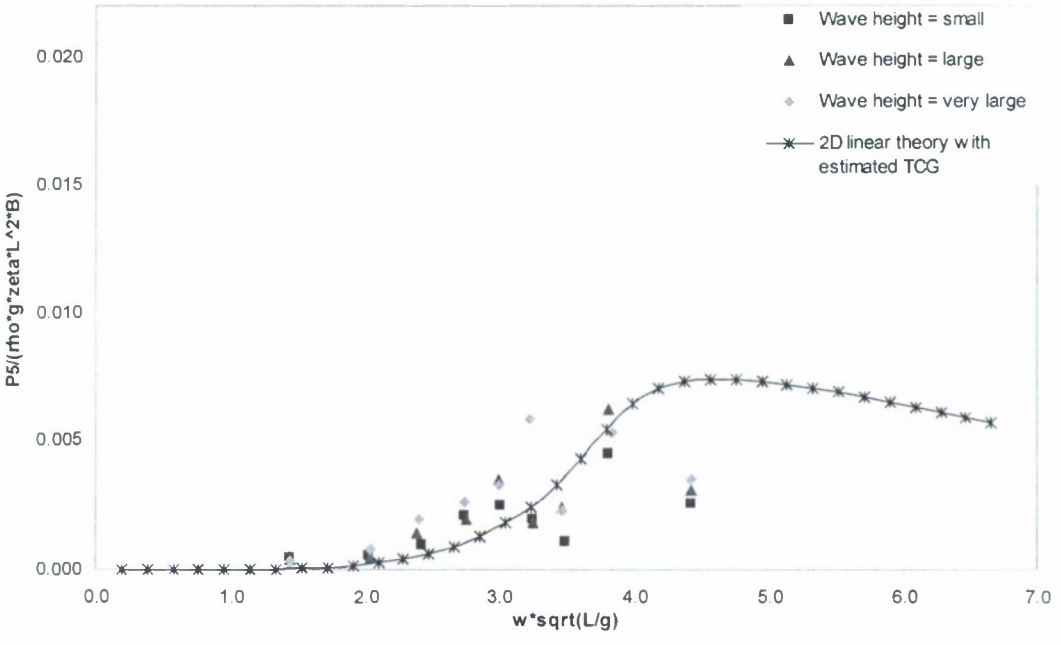

Figure 5.2.3-24: Vertical bending moment RAO in DS2 at beam waves (heading 270)

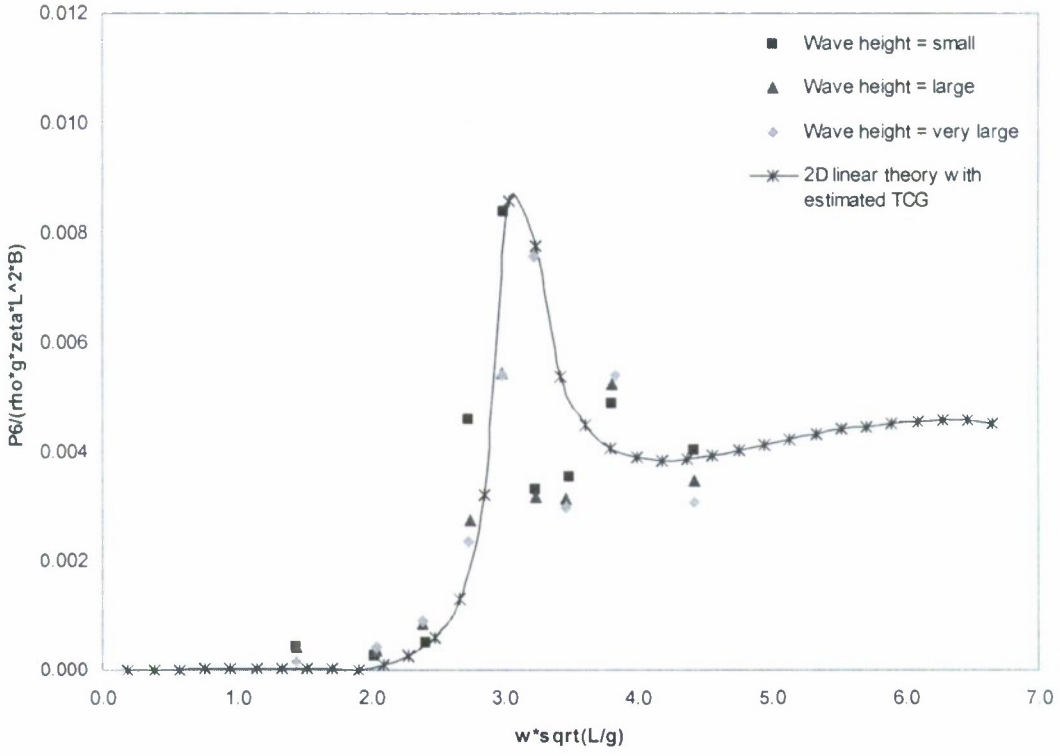

Figure 5.2.3-25: Horizontal bending moment RAO in DS2 at beam waves (heading 270)

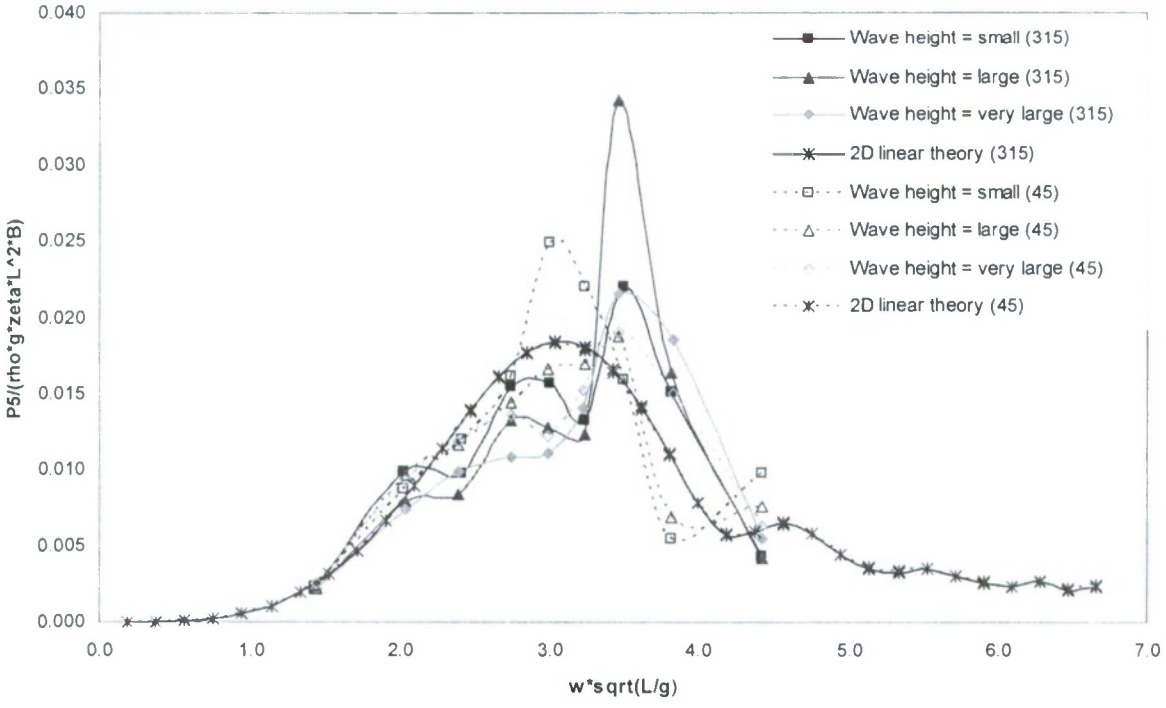

Figure 5.2.3-26: Comparison of vertical bending moment between different wave angles in stern quartering seas

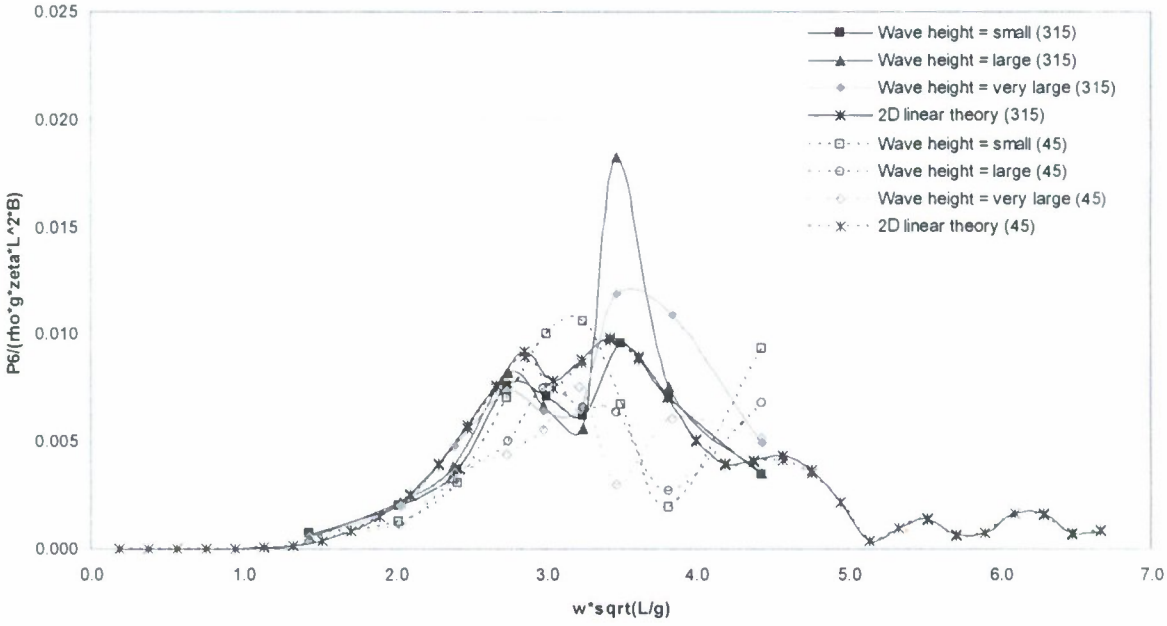

Figure 5.2.3-27: Comparison of horizontal bending moment between different wave angles in stern quartering seas

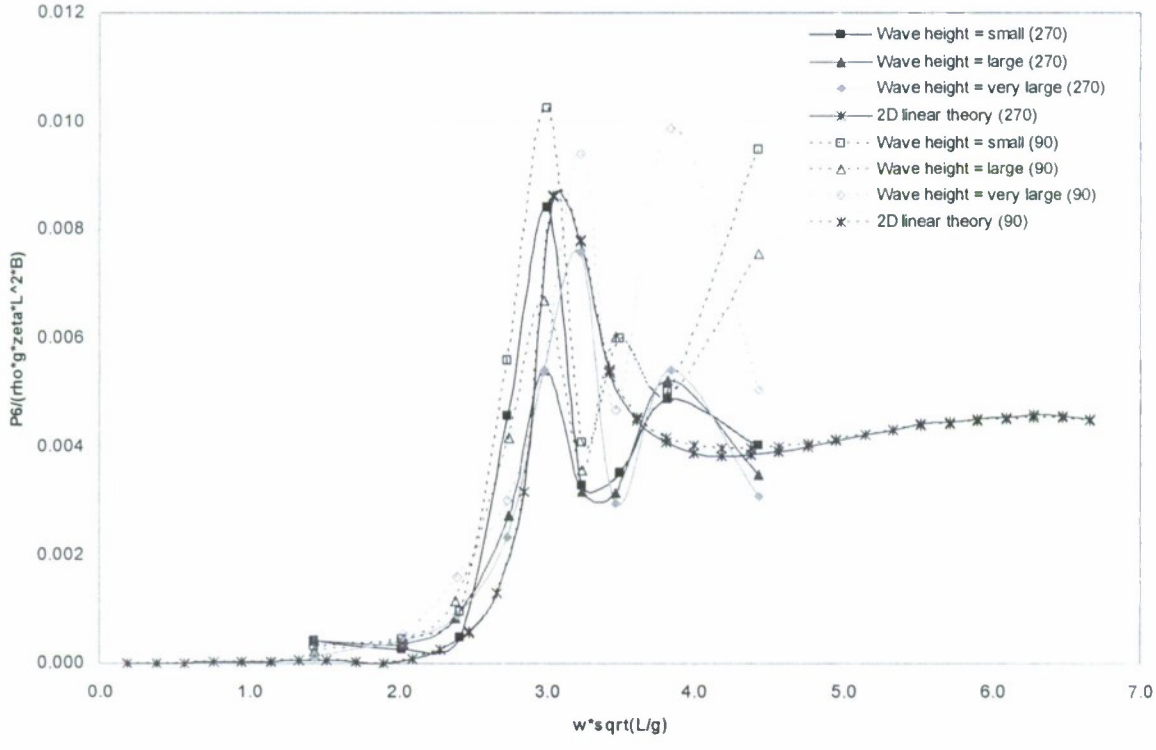

Figure 5.2.3-28: Comparison of horizontal bending moment between different wave angles in beam seas

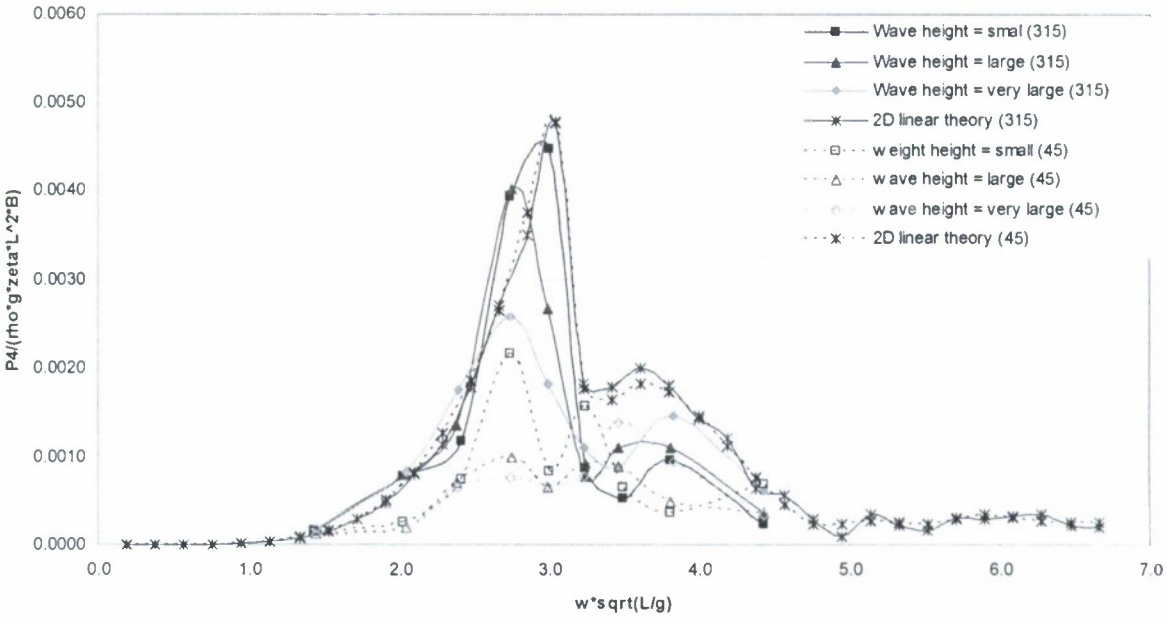

Figure 5.2.3-29: Comparison of torsion moment between different wave angles in stern quartering seas

5.2.4 Results in damage scenario 3

The calculated global dynamic wave induced loads and measuremcnts of DS3 in three different wave angles are shown in the following figures.

- Figures 5.2.4-1 to 5.2.4-5 for DS3 in head waves.
- Figures 5.2.4-6 to 5.2.4-10 for DS3 in stern quartering waves.
- Figures 5.2.4-11 to 5.2.4-15 for DS3 in beam waves.

Figures 5.2.4-4, -9 and -14 show the vertical bending moment in head seas, stern quartering seas and beams. As in intact condition, thc numerical results agree well with the experimental results, especially at small wave amplitude. In head seas, the vertical bending moment had a mean of X_m of 0.762 and a COV of X_m of 31.0% in small wave amplitude, and 0.711 and 31.7% for large wave amplitude (see Table B.3 in Appendix B). This accuracy is reasonably good. However the mean and COV of X_m become 1.362 and 106.8% for very large wave amplitude. This demonstrates that the accuracy is deteriorating with the increase of wave amplitude. It was observed that the accuracy in calculating vertical bending moment in stern quartering seas was better than in head seas with a mean of X_m of 0.945 and a COV of X_m of 19.5% in small wave amplitude, and 0.909 and 20.1% for large wave amplitude, and 0.850 and 18.1% for large wave amplitude.

Horizontal bending moment has been presented in Figures 5.2.4-5, -10 and -15. Thc fcatures of horizontal bending moment in this scenario were quite similar to those in intact condition. The accuracy was slightly worse than that for vertical bending moment. The mean and COV of X_m were 0.732 and 59.8% for small wave amplitude, and 0.735 and 49.7% for large wave amplitude, and 0.894 and 41.1% for large wave amplitude.

Torsion moment has been shown in Figures 5.2.4-3, -8 and -13. Torsion moment in head scas was insignificant, while the features of torsion moment in stern quartering seas and beam seas

in this scenario were quite similar to those in intact condition. The mean and COV of X_m in stern quartering seas were 1.145 and 133.0% for small wave amplitude, and 0.925 and 130.0% for large wave amplitude, and 0.790 and 110.9% for large wave amplitude. So the accuracy in torsion moment prediction was poor, especially in the resonant region.

Head waves

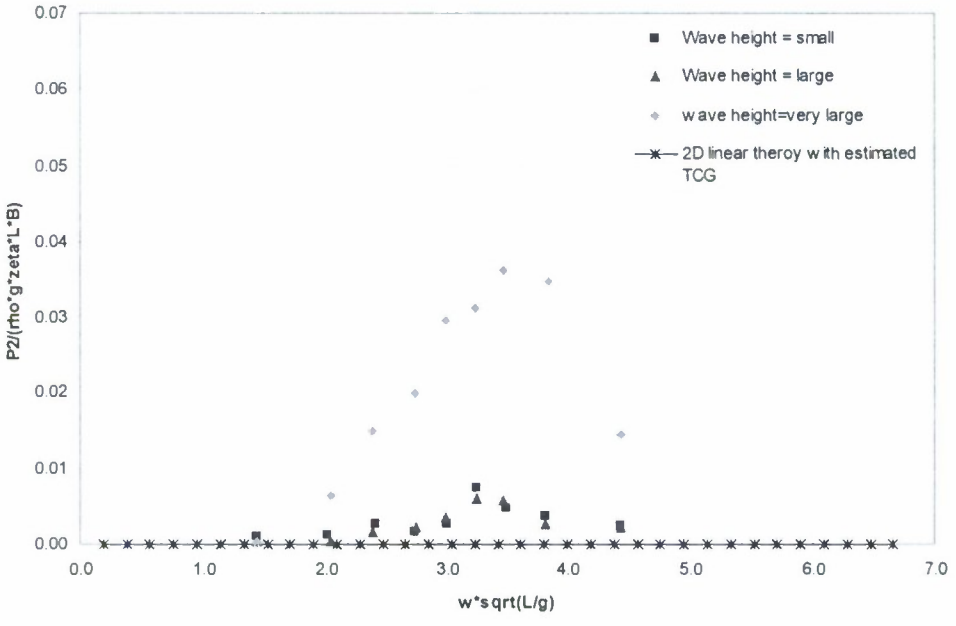

Figure 5.2.4-1: Horizontal shear force RAO in DS3 at head waves

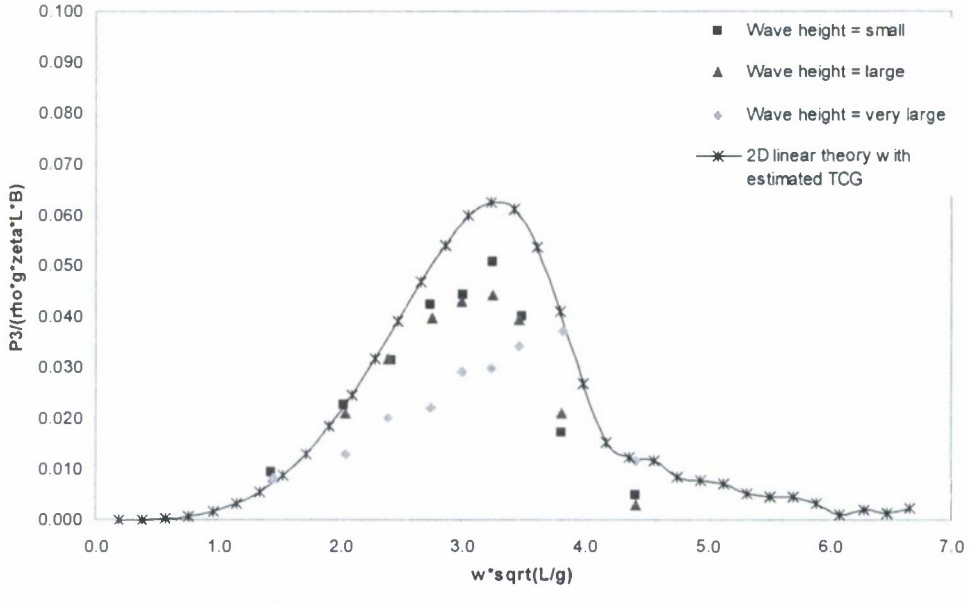

Figure 5.2.4-2: Vertical shear force RAO in DS3 at head waves

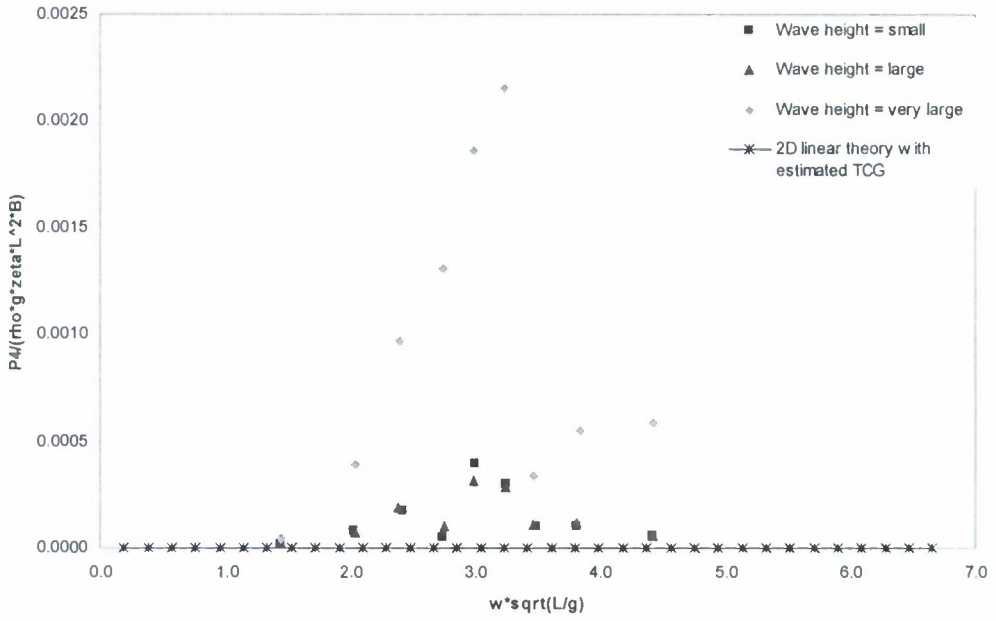

Figure 5.2.4-3: Torsion moment RAO in DS3 at head waves

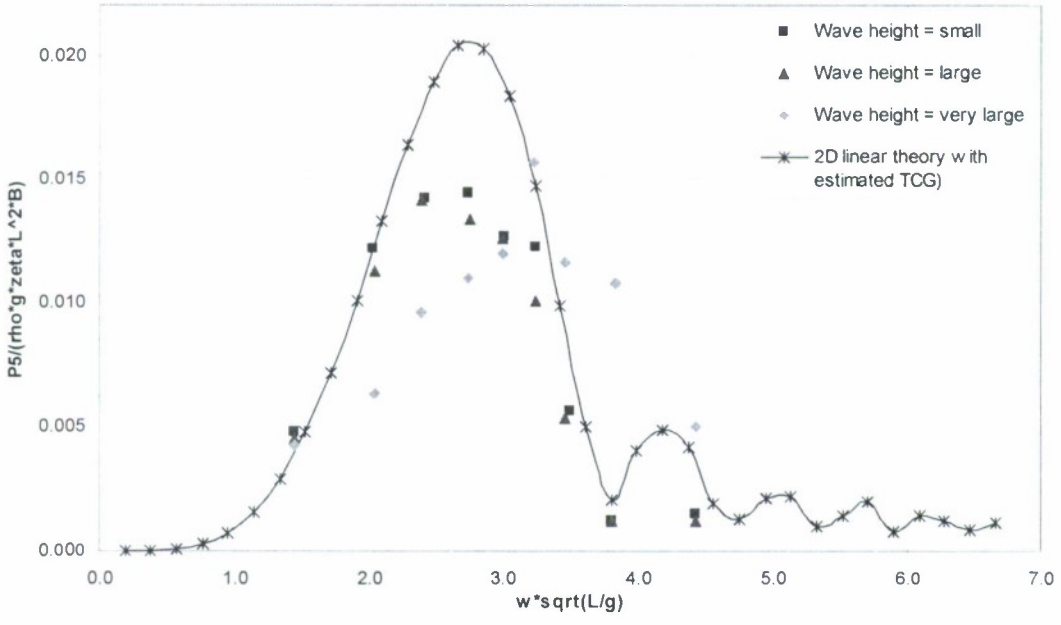

Figure 5.2.4-4: Vertical bending moment RAO in DS3 at head waves

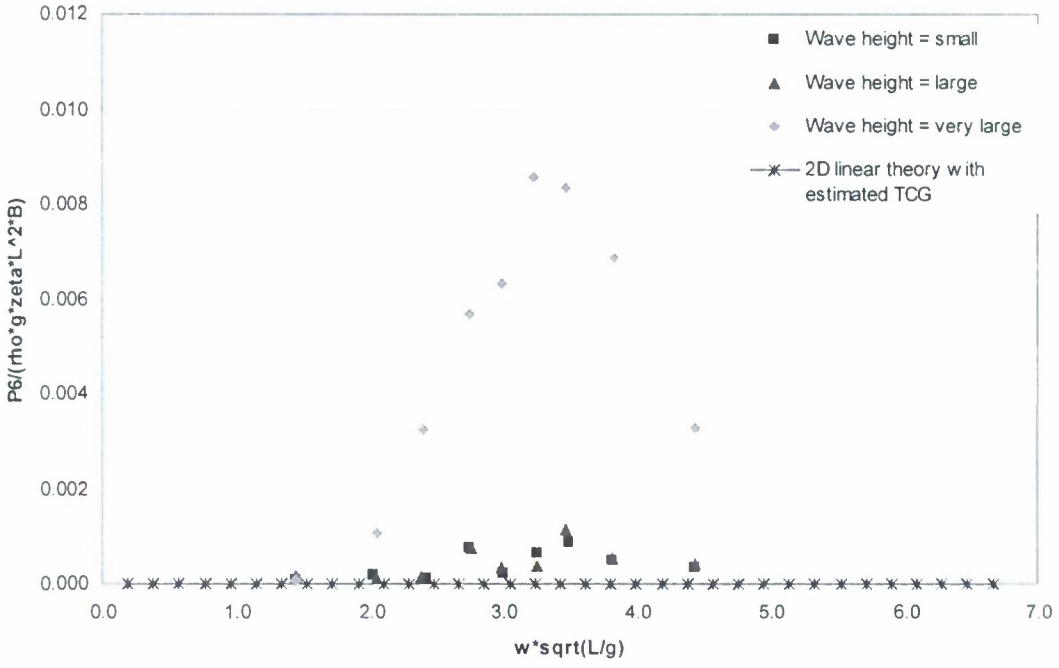

Figure 5.2.4-5: Horizontal bending moment RAO in DS3 at head waves

Stern quartering waves

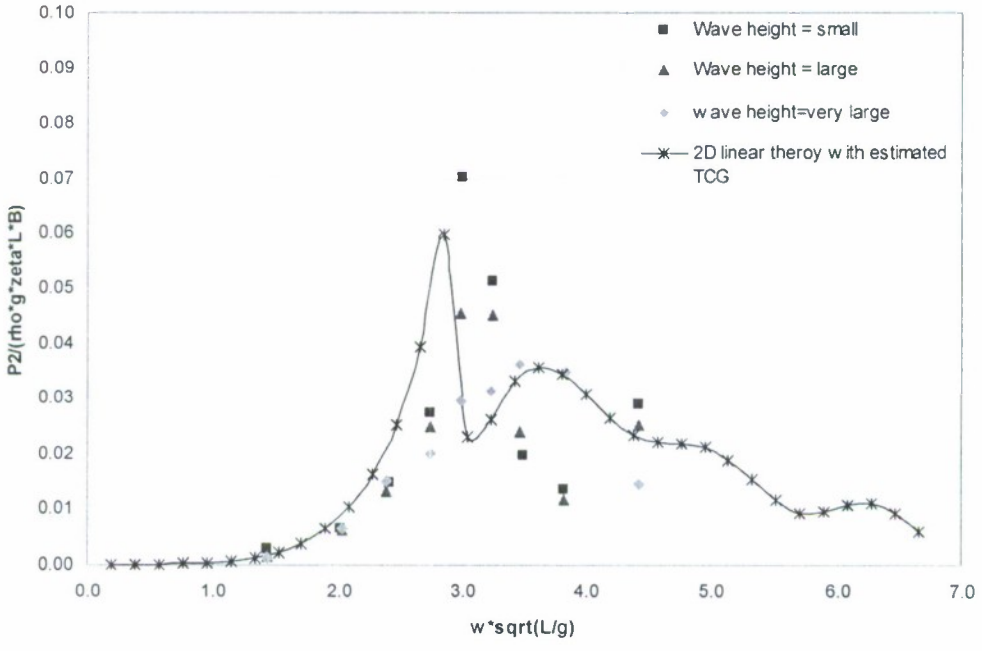

Figure 5.2.4-6: Horizontal shear force RAO in DS3 at stern quartering waves

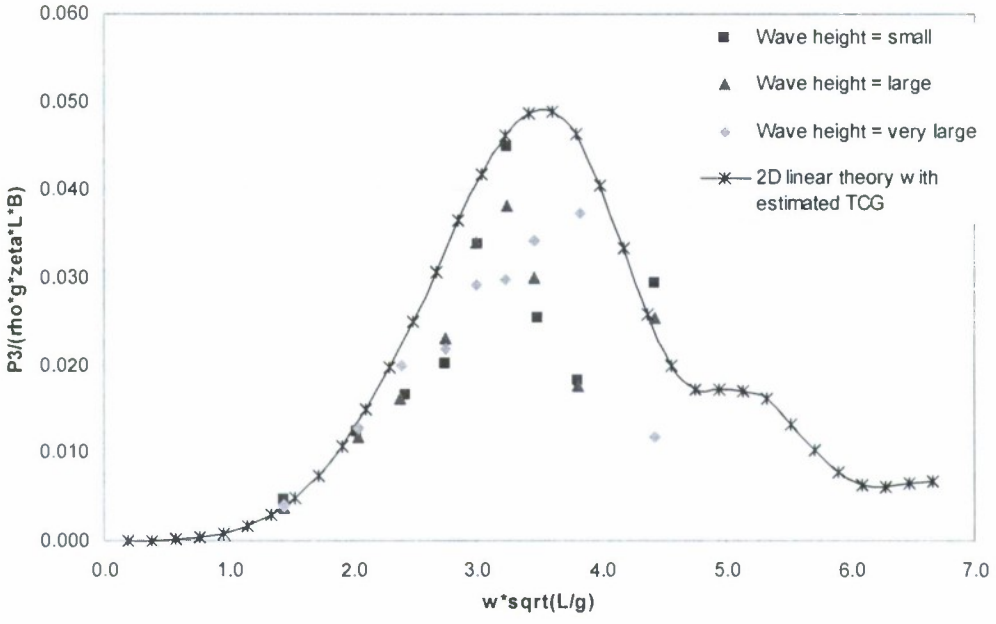

Figure 5.2.4-7: Vertical shear force RAO in DS3 at stern quartering waves

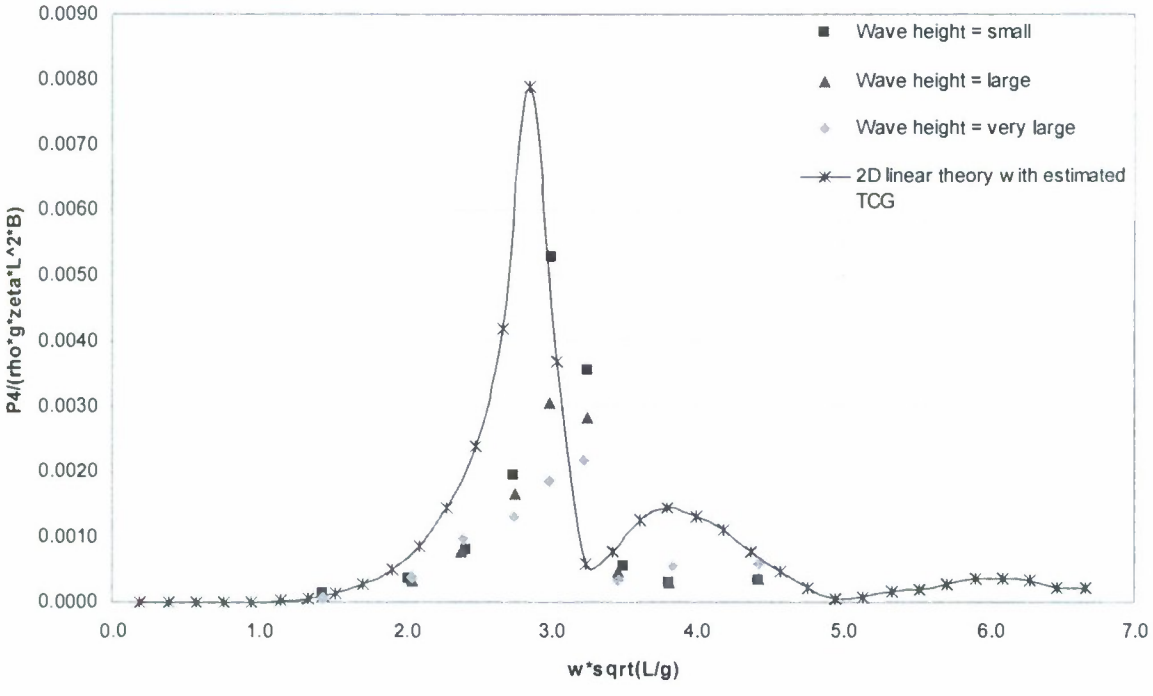

Figure 5.2.4-8: Torsion moment RAO in DS3 at stern quartering waves

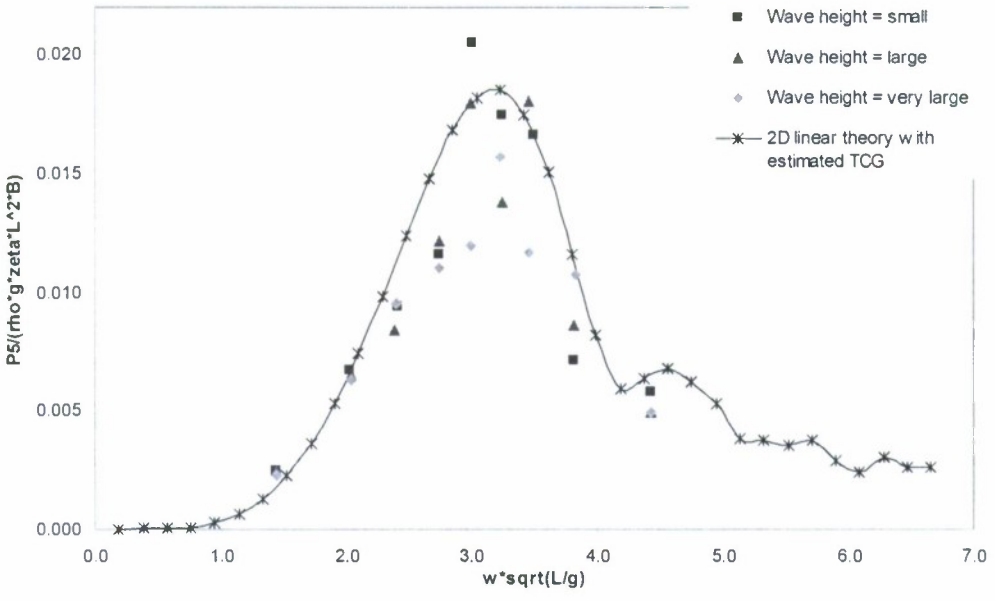

Figure 5.2.4-9: Vertical bending moment RAO in DS3 at stern quartering waves

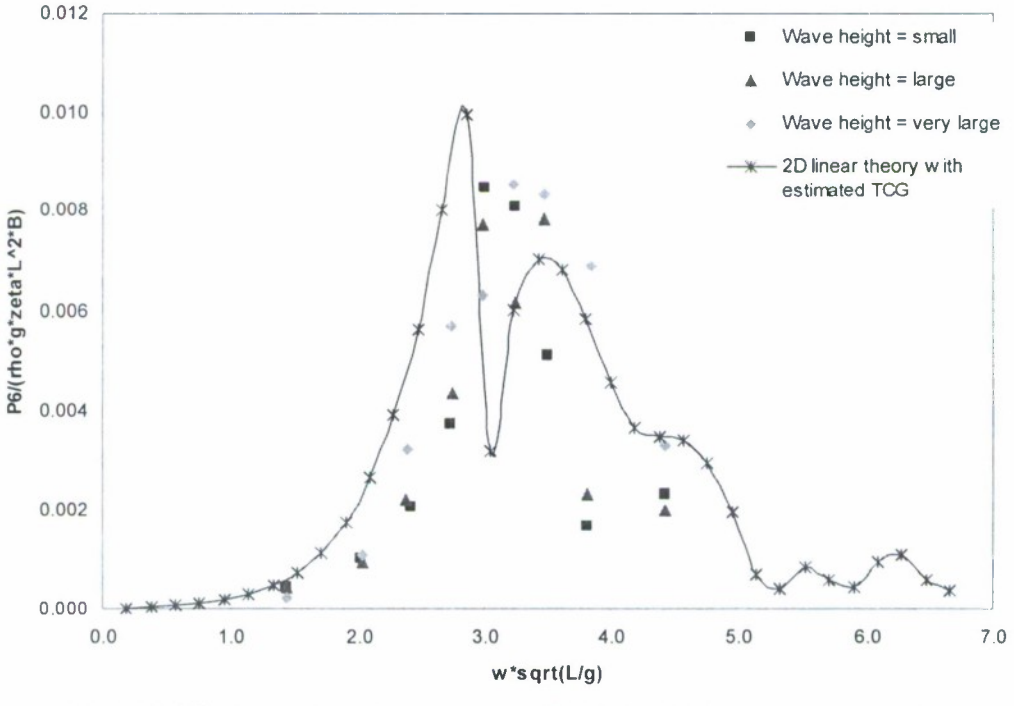

Figure 5.2.4-10: Horizontal bending moment RAO in DS3 at stern quartering waves

Beam waves

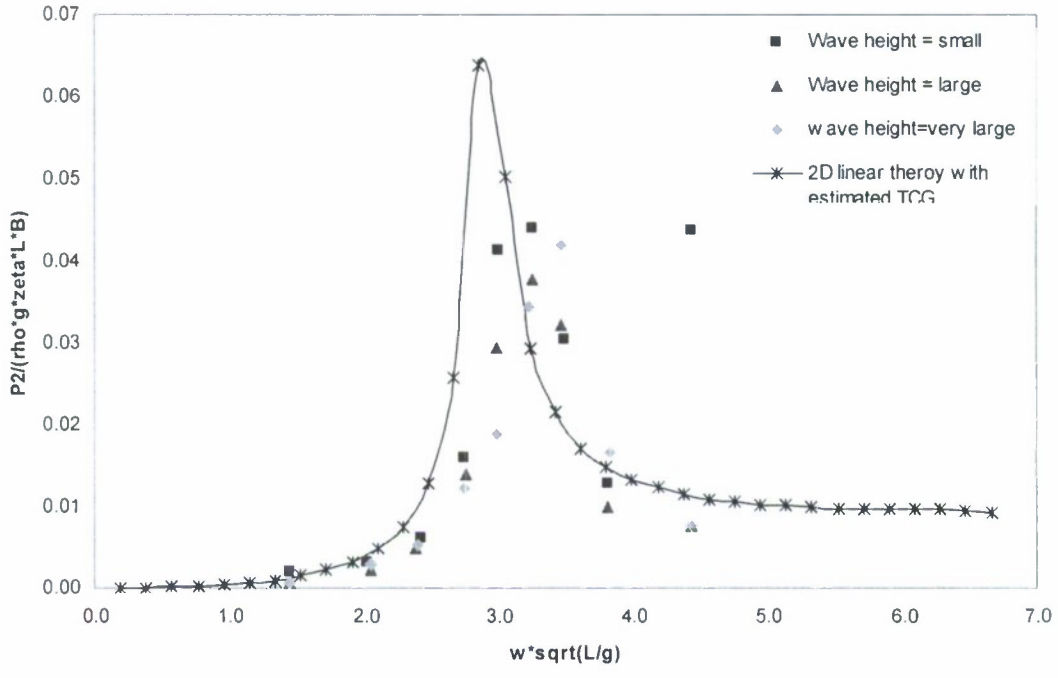

Figure 5.2.4-11: Horizontal shear force RAO in DS3 at beam waves

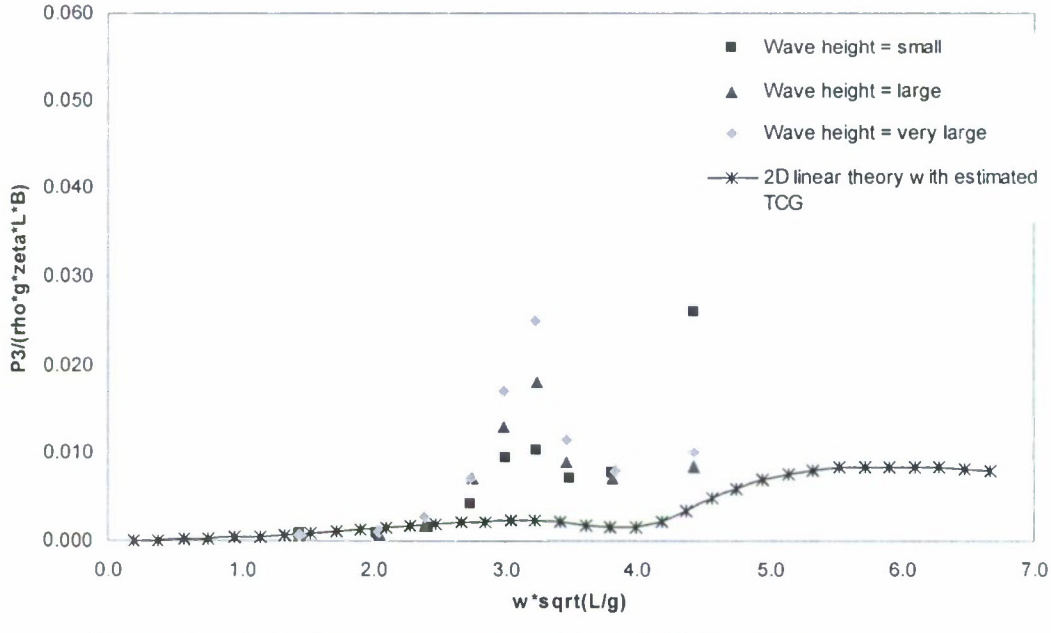

Figure 5.2.4-12: Vertical shear force RAO in DS3 at beam waves

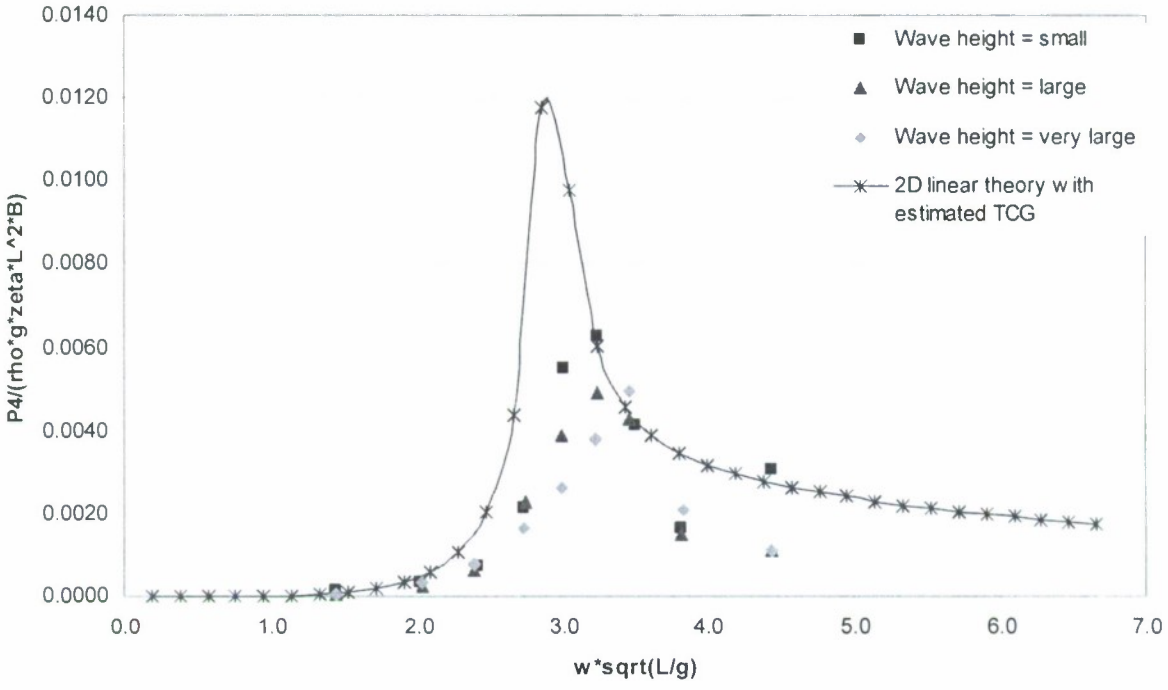

Figure 5.2.4-13: Torsion moment RAO in DS3 at beam waves

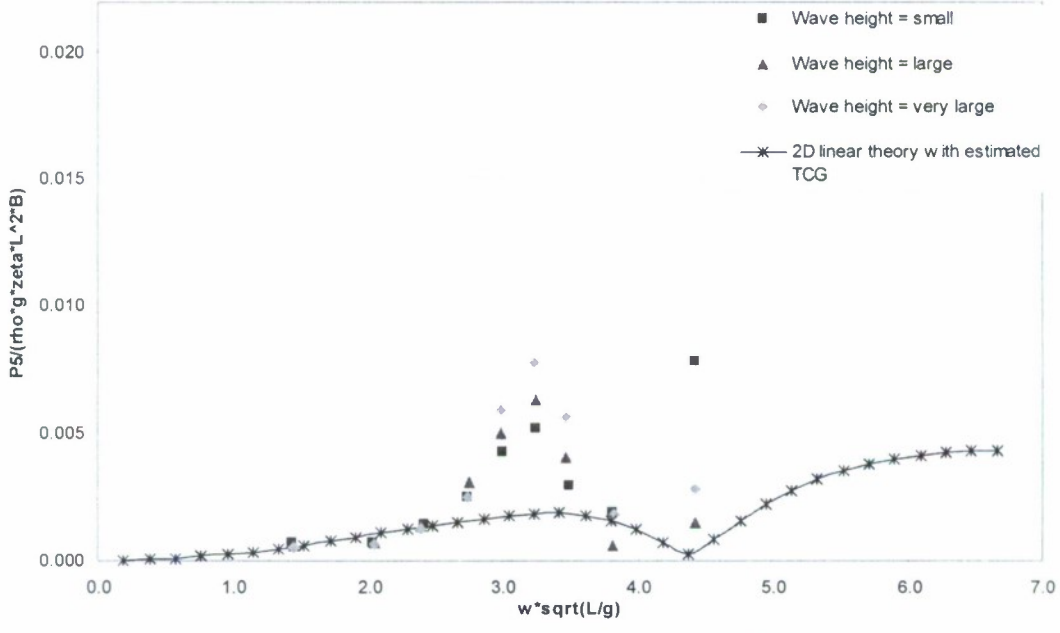

Figure 5.2.4-14: Vertical bending moment RAO in DS3 at beam waves

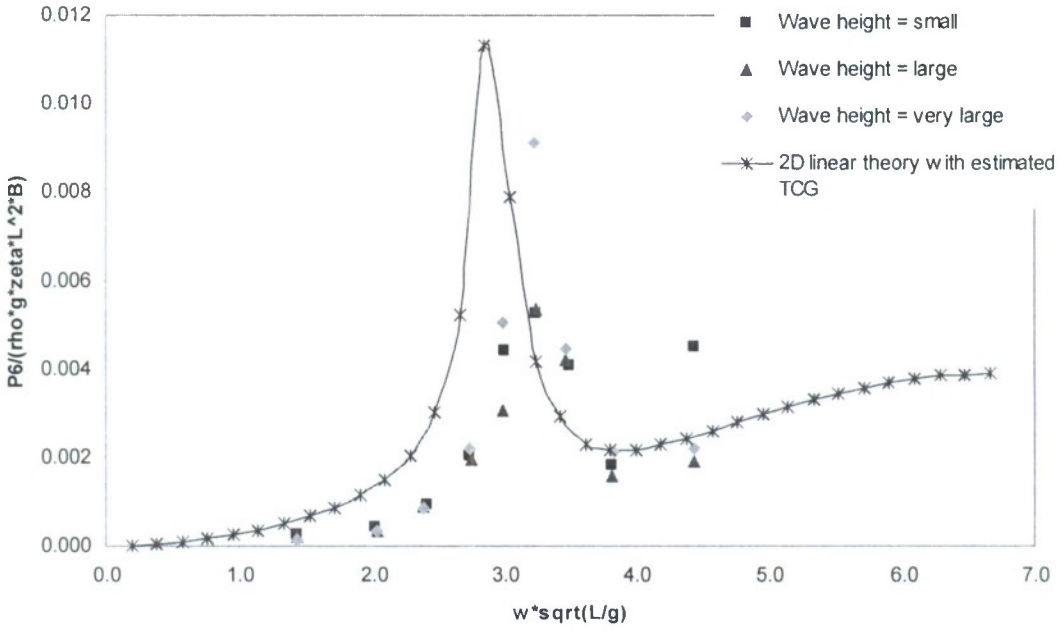

Figure 5.2.4-15: Horizontal bending moment RAO in DS3 at beam waves

5.2.5 Non-linearity of the wave-induced dynamic loads

As expressed in the foregoing sections, it was observed in the experimental results that the wave-induced dynamic loads at different wave amplitudes scatter in large range at some frequencies especially around resonant regions. In some cases, the RAO at small wave amplitude is as twice large as that in large wave amplitude. To further investigate this non-linear phenomenon, another batch of experiment has been carried out. In this set of tests, the frequencies are mainly selected around resonant regions. Four different wave amplitudes have been chosen for each frequency. The results are presented in Figures 5.2.5-1 to -27, in which horizontal axis is wave amplitude in mm while vertical axis is non-dimensional RAO of load components.

It could be seen that majority of the response RAOs show non-linear trend, in which the non-dimensional response is decreasing as wave amplitude increases in most of frequency range, especially at the frequency where the response achieves the maximum. For vertical bending moment this trend is very remarkable as shown in Figures 5.2.5-4, -9, -14, -19 and -24. There are only a few cases in which linear responses are observed (see Figure 5.2.5-27 at λ / L = 1.348 and 1.044). It may be said that the high non-linearity is an inherent feature of this unique hullform. This also supports the view that a non-linear method should be used to predict the wave-induced loads of this type of vessels.

Intact condition heading 45

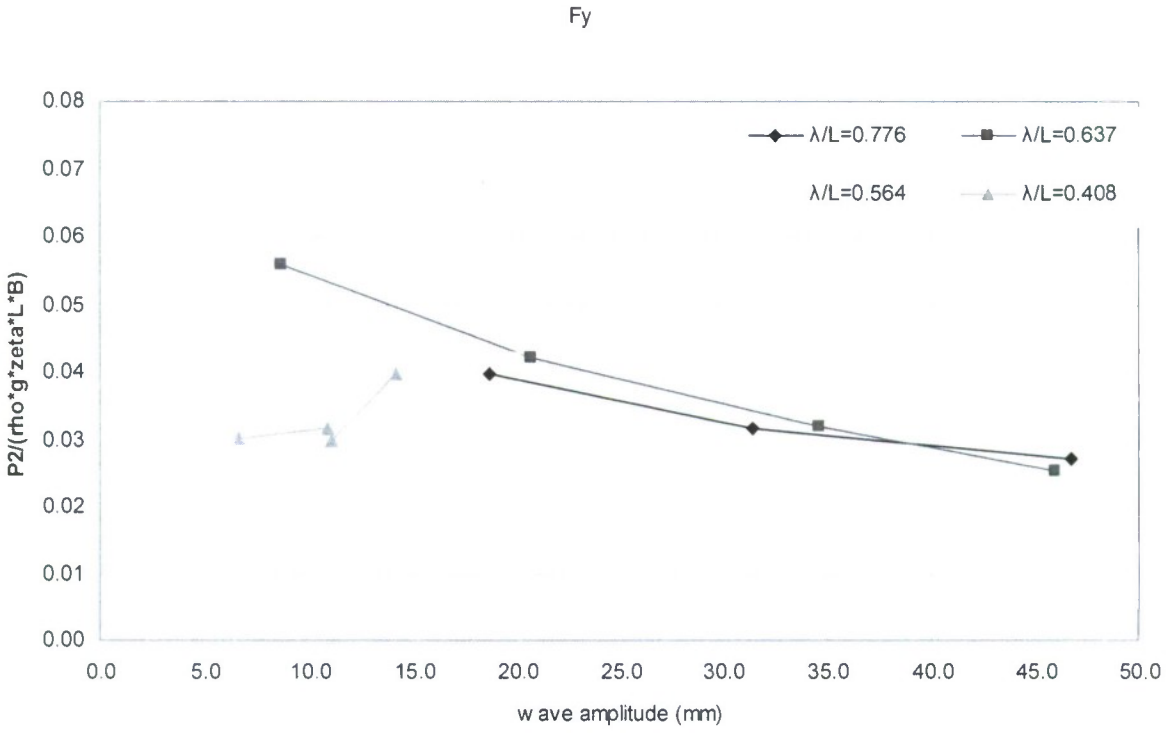

Figure 5.2.5-1: Horizontal shear force RAO at stern quartering waves

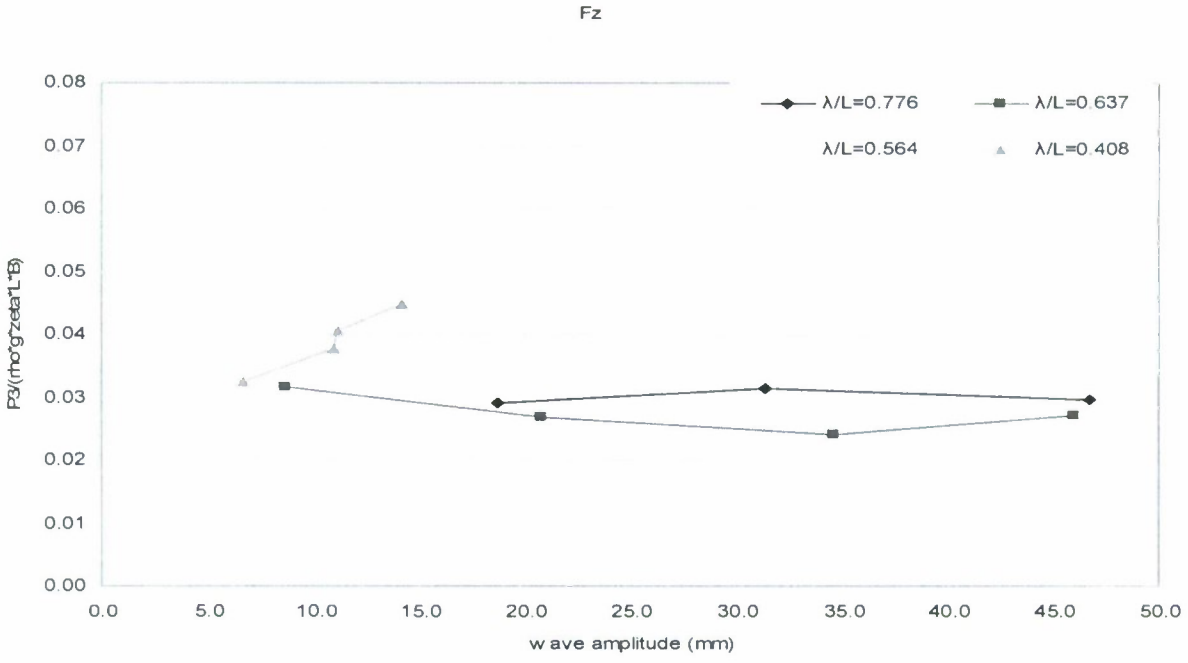

Figure 5.2.5-2: Vertical shear force RAO at stern quartering waves

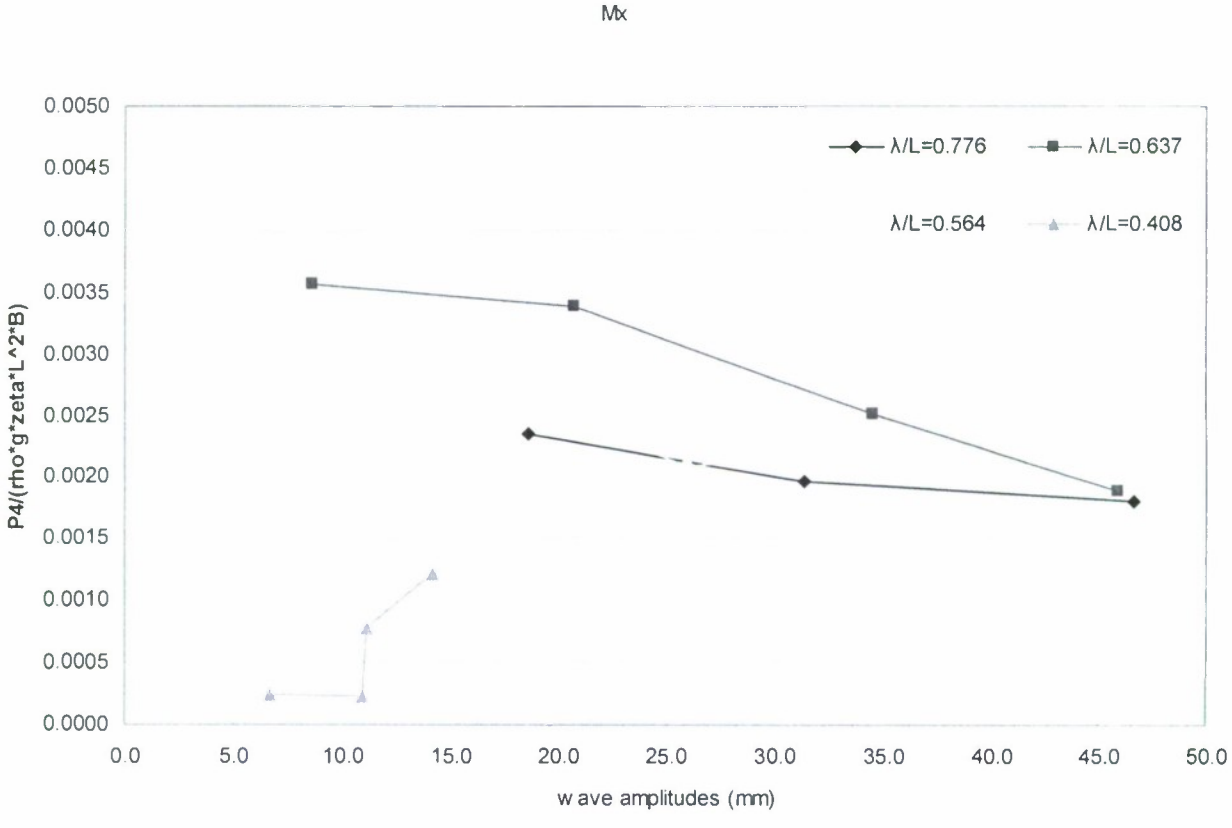

Figure 5.2.5-3: Torsion moment RAO at stern quartering waves

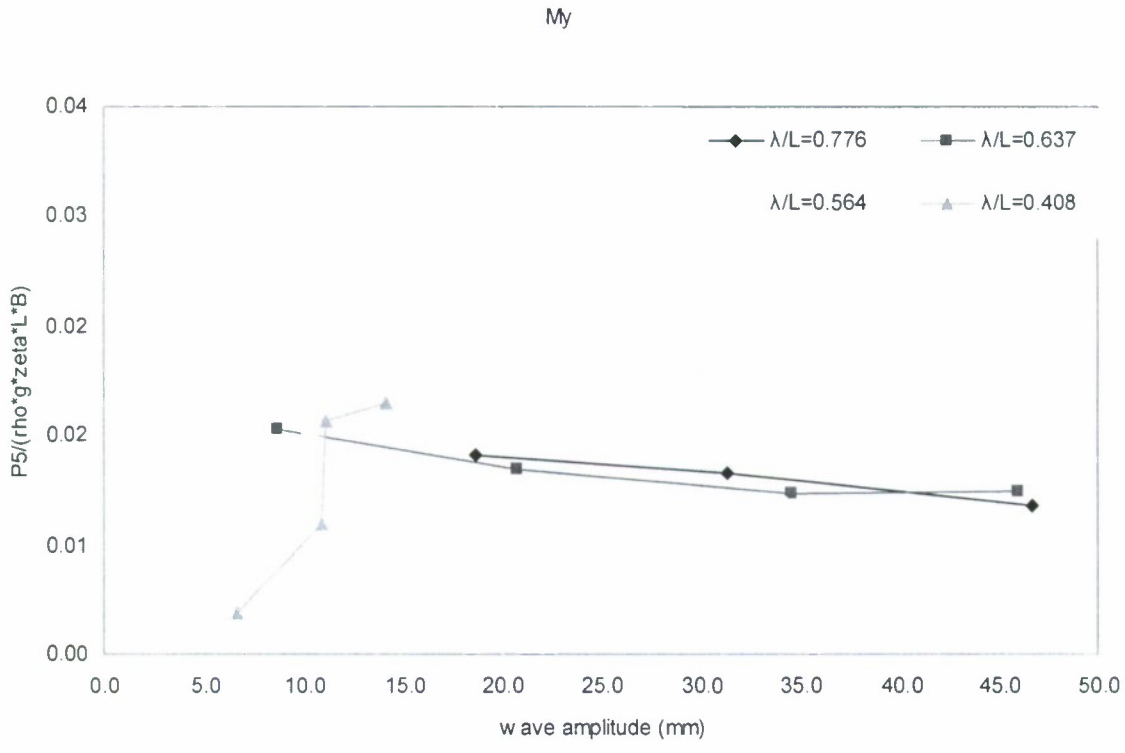

Figure 5.2.5-4: Vertical bending moment RAO at stern quartering waves

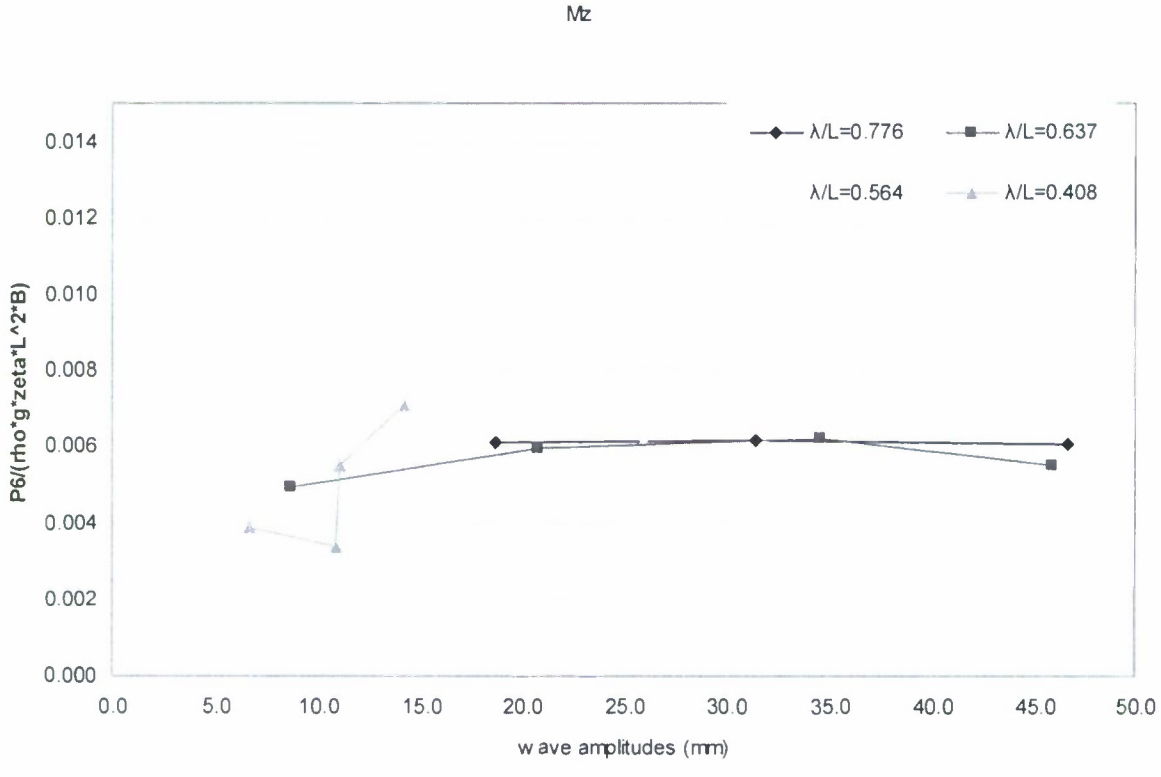

Figure 5.2.5-5: Horizontal bending moment RAO at stern quartering waves

Intact condition heading 135

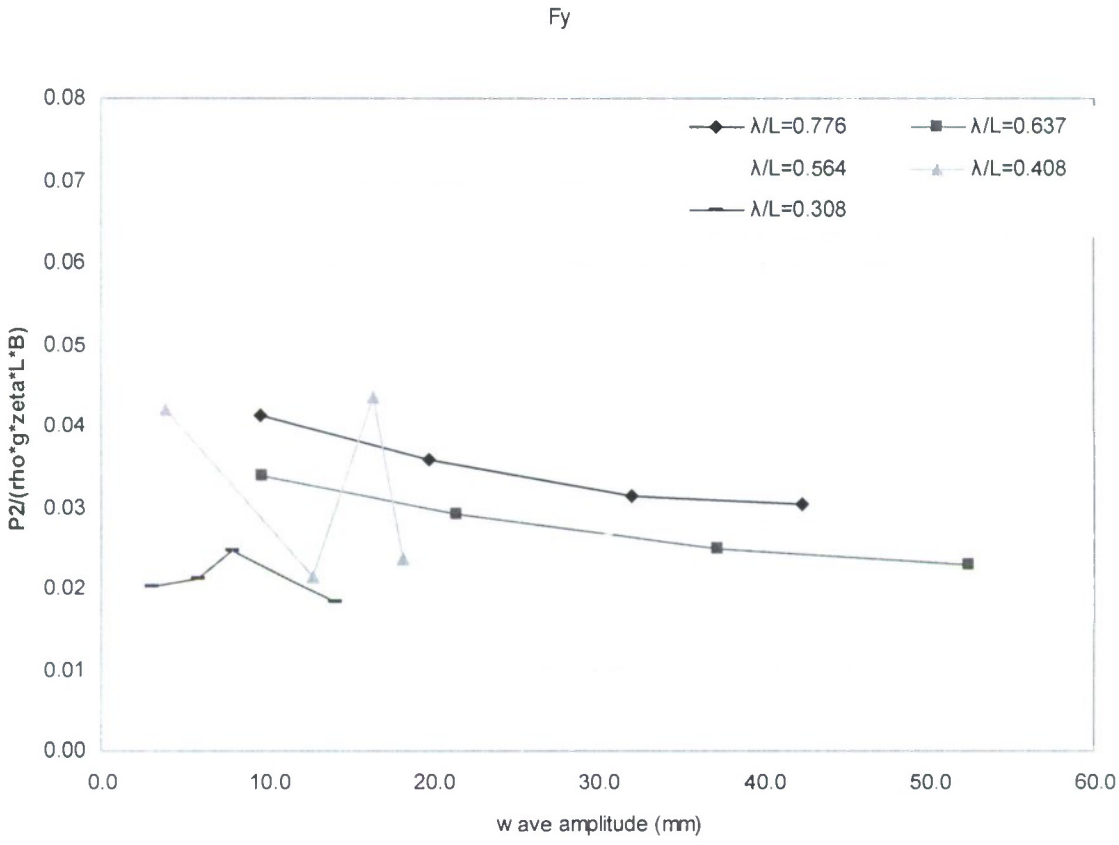

Figure 5.2.5-6: Horizontal shear force RAO at bow quartering waves

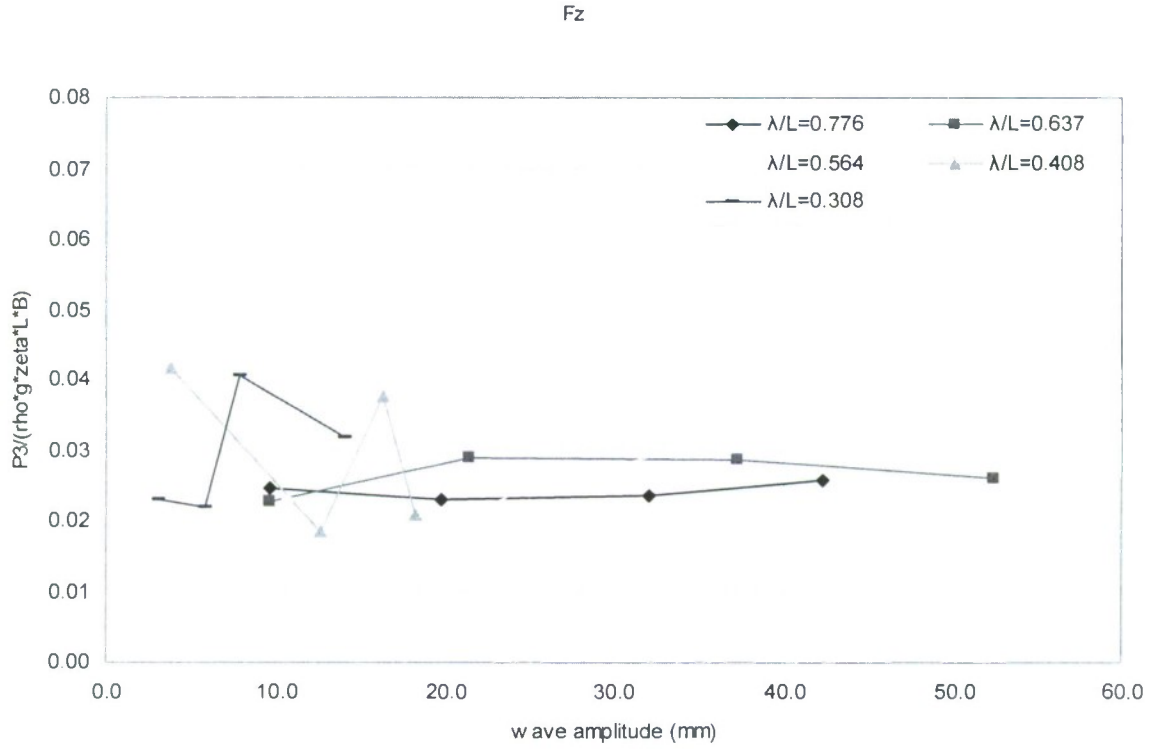

Figure 5.2.5-7: Vertical shear force RAO at bow quartering waves

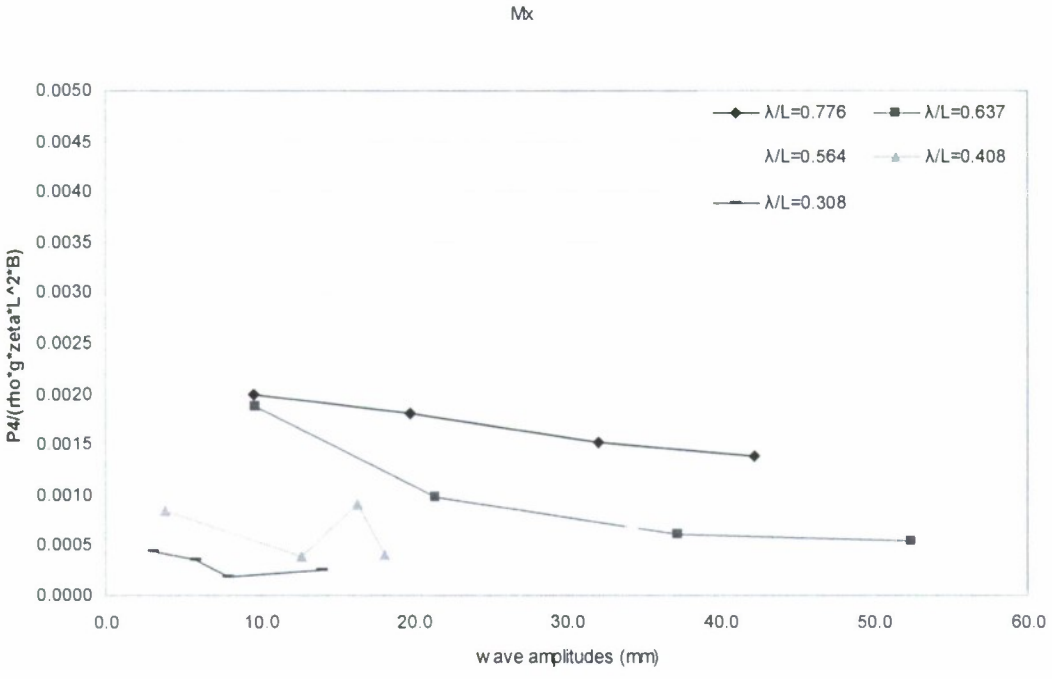

Figure 5.2.5-8: Torsion moment RAO at bow quartering waves

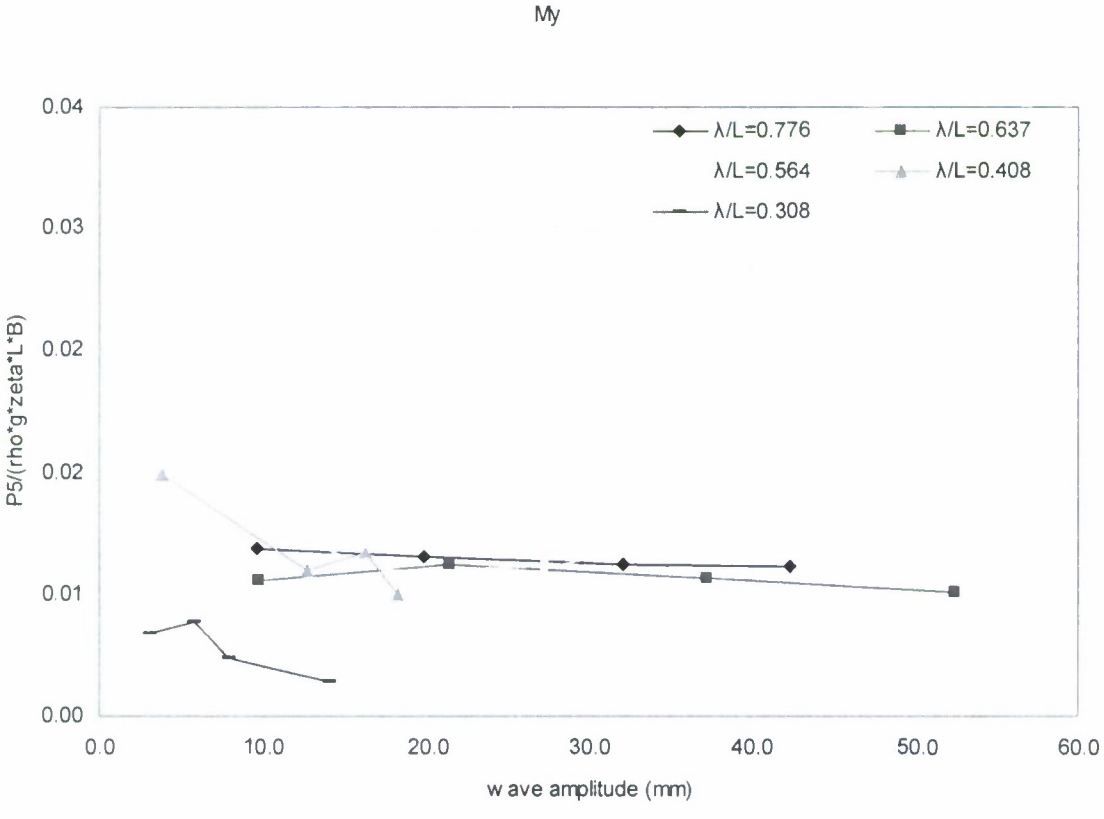

Figure 5.2.5-9: Vertical bending moment RAO at bow quartering waves

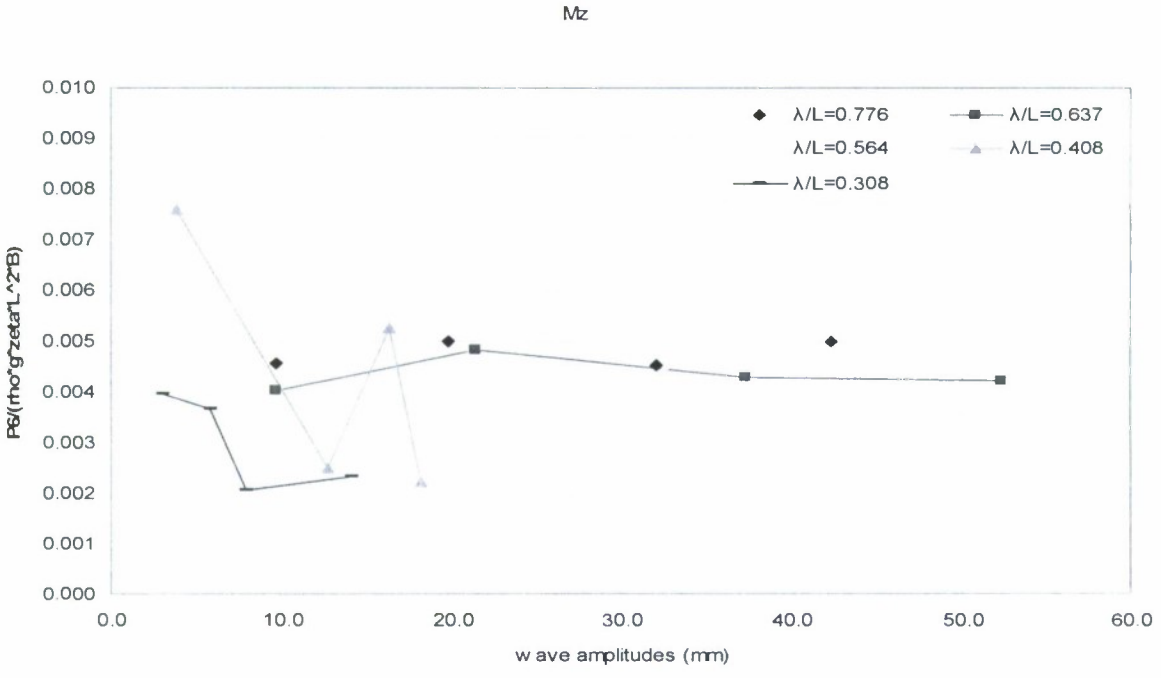

Figure 5.2.5-10: Horizontal bending moment RAO at bow quartering waves

Damage scenario 2 heading 45

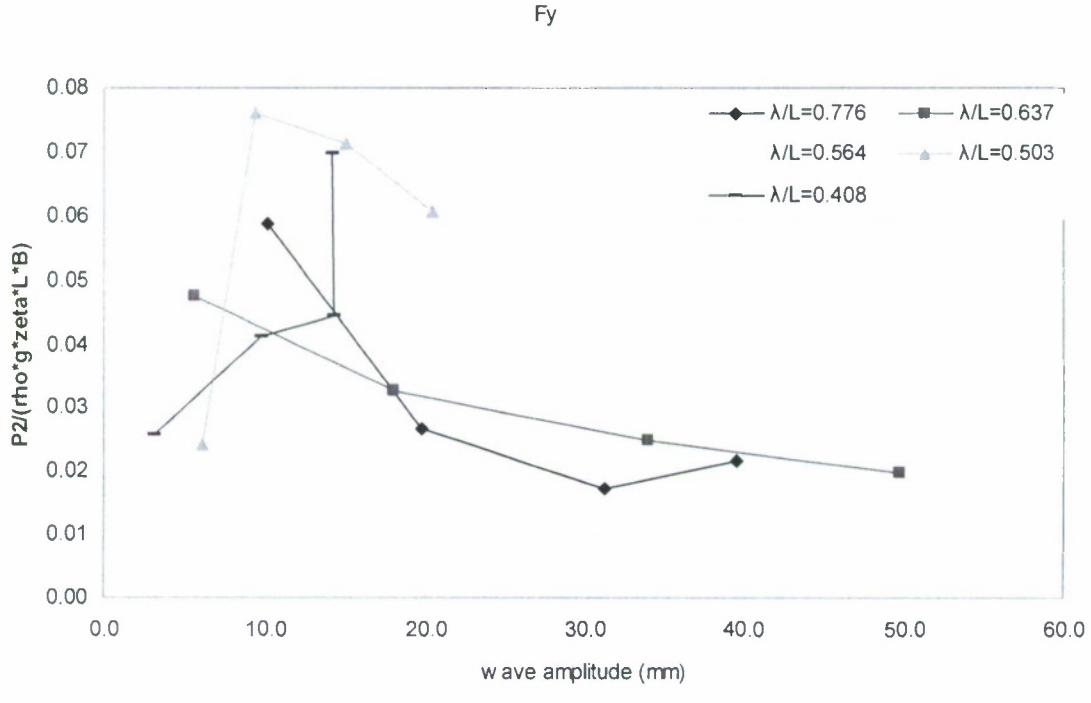

Figure 5.2.5-11: Horizontal shear force RAO at stern quartering waves (heading 45)

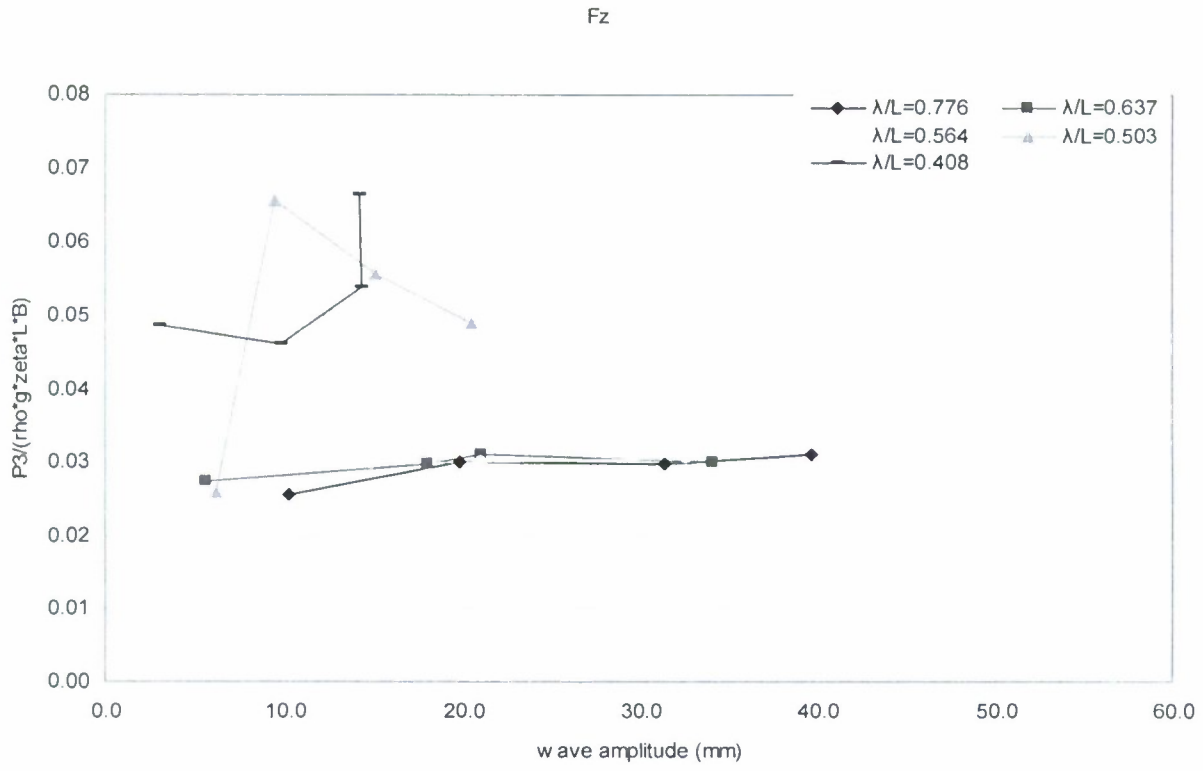

Figure 5.2.5-12: Vertical shear force RAO at stern quartering waves (heading 45)

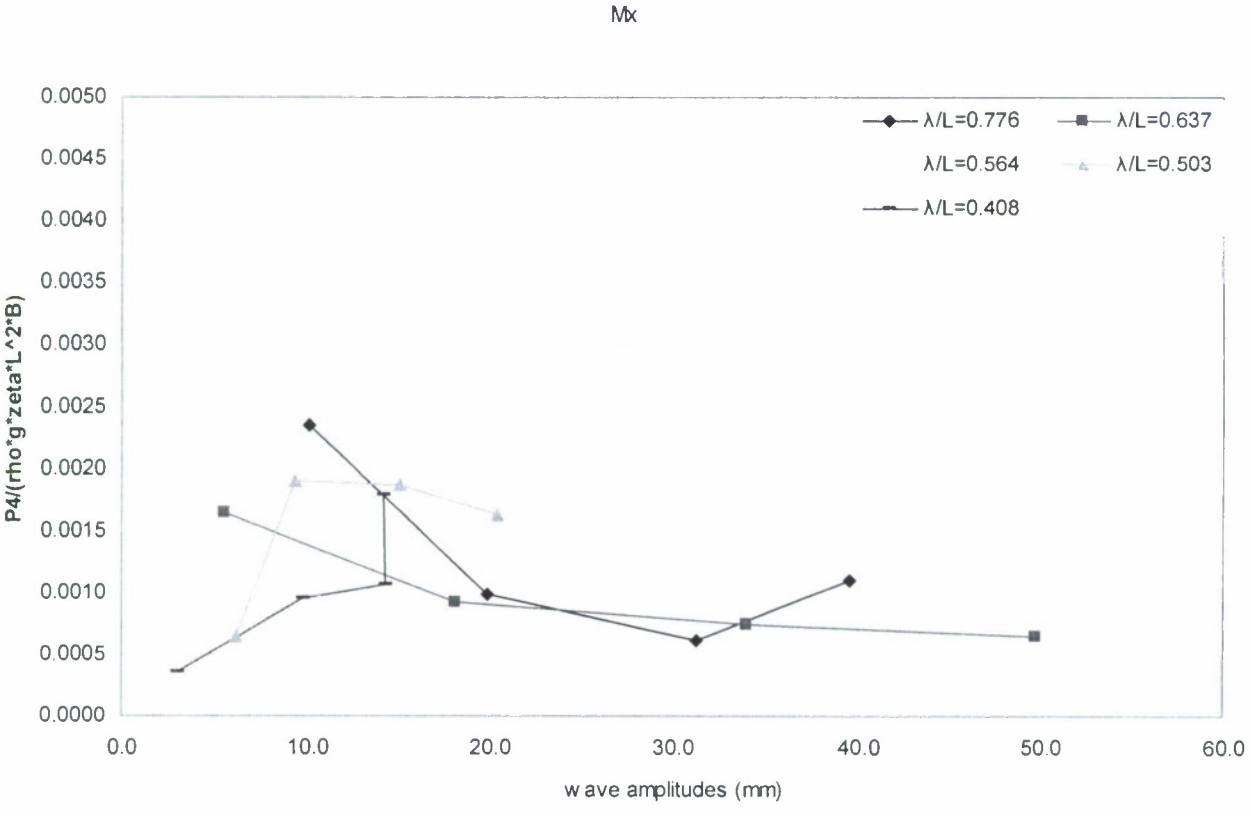

Figure 5.2.5-13: Torsion RAO at stern quartering waves (heading 45)

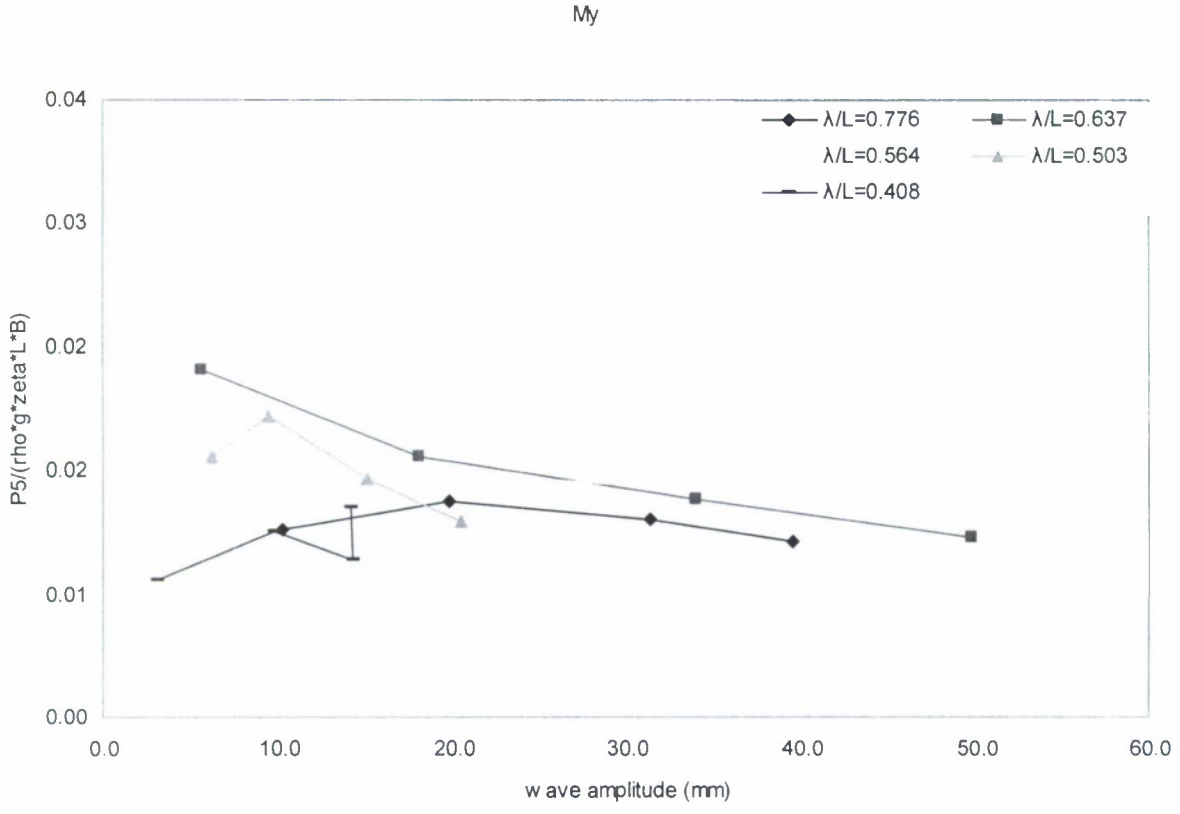

Figure 5.2.5-14: Vertical bending moment RAO at stern quartering waves (heading 45)

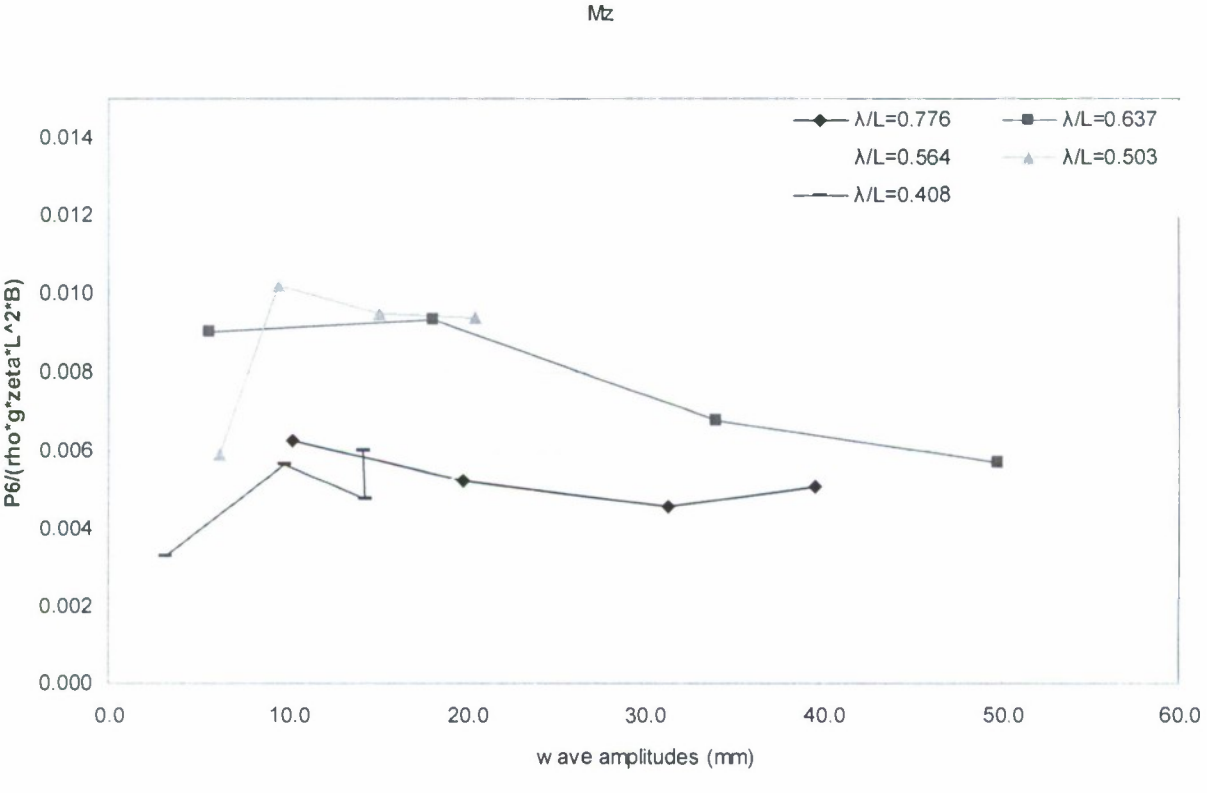

Figure 5.2.5-15: Horizontal bending moment RAO at stern quartering waves (heading 45)

Damage scenario 2 heading 315

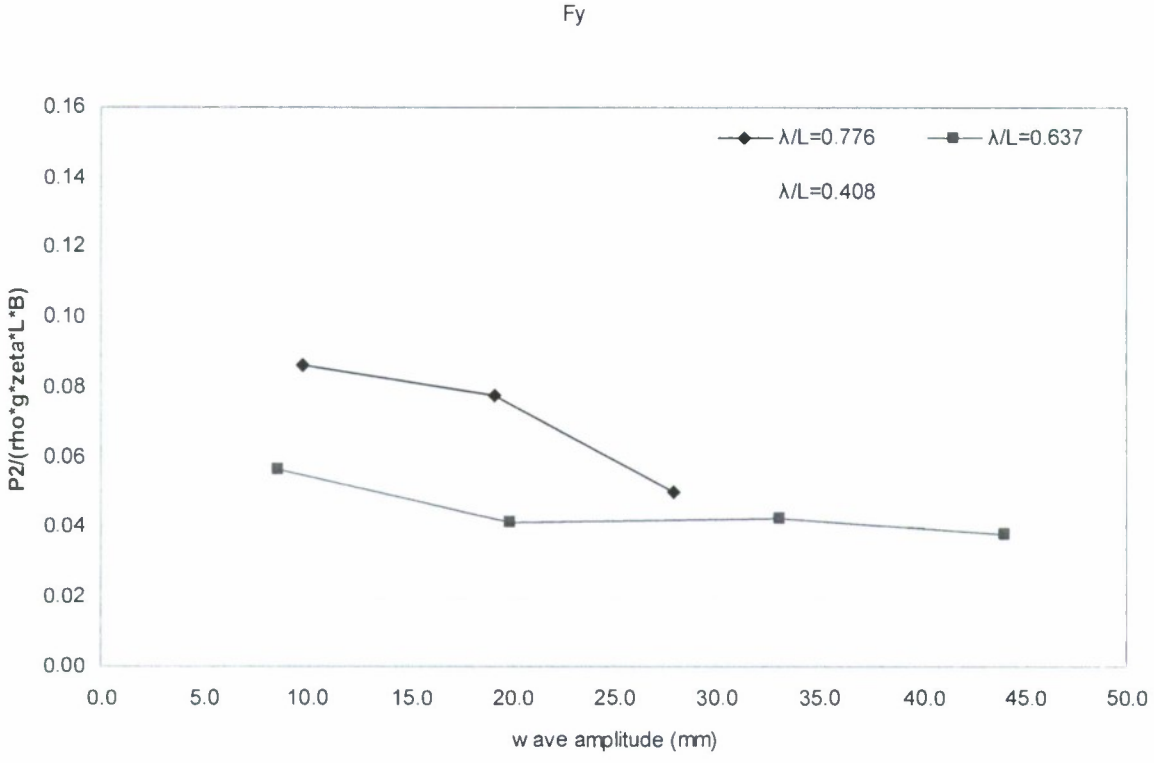

Figure 5.2.5-16: Horizontal shear force RAO at stern quartering waves (heading 315)

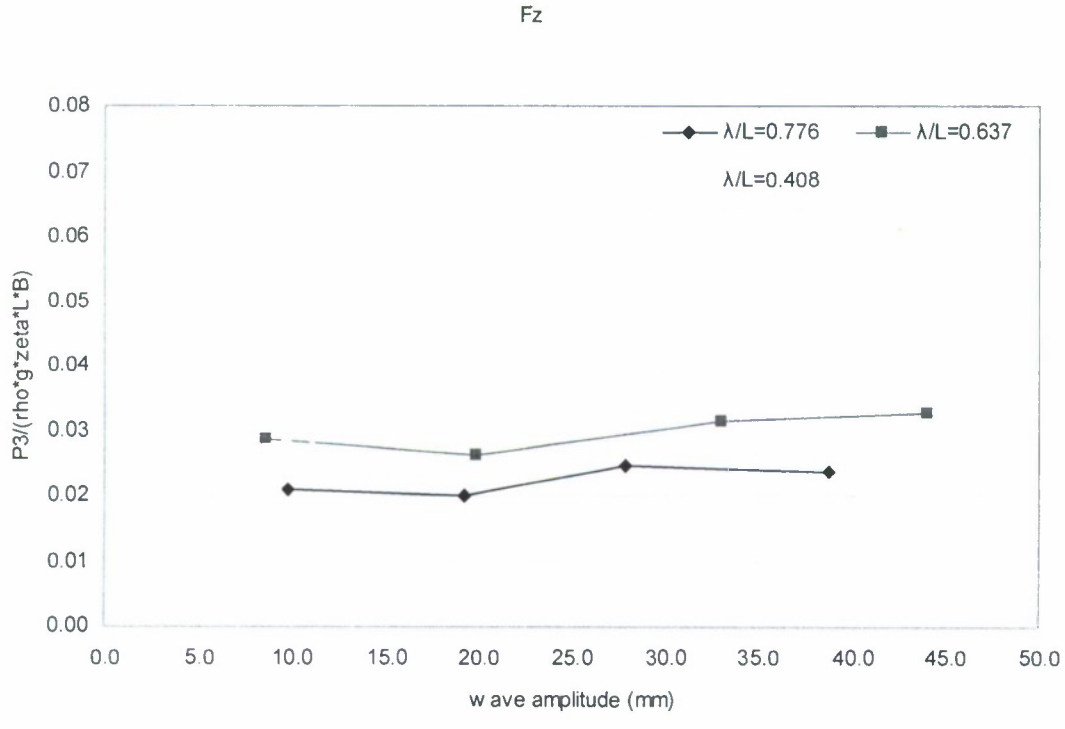

Figure 5.2.5-17: Vertical shear force RAO at stern quartering waves (heading 315)

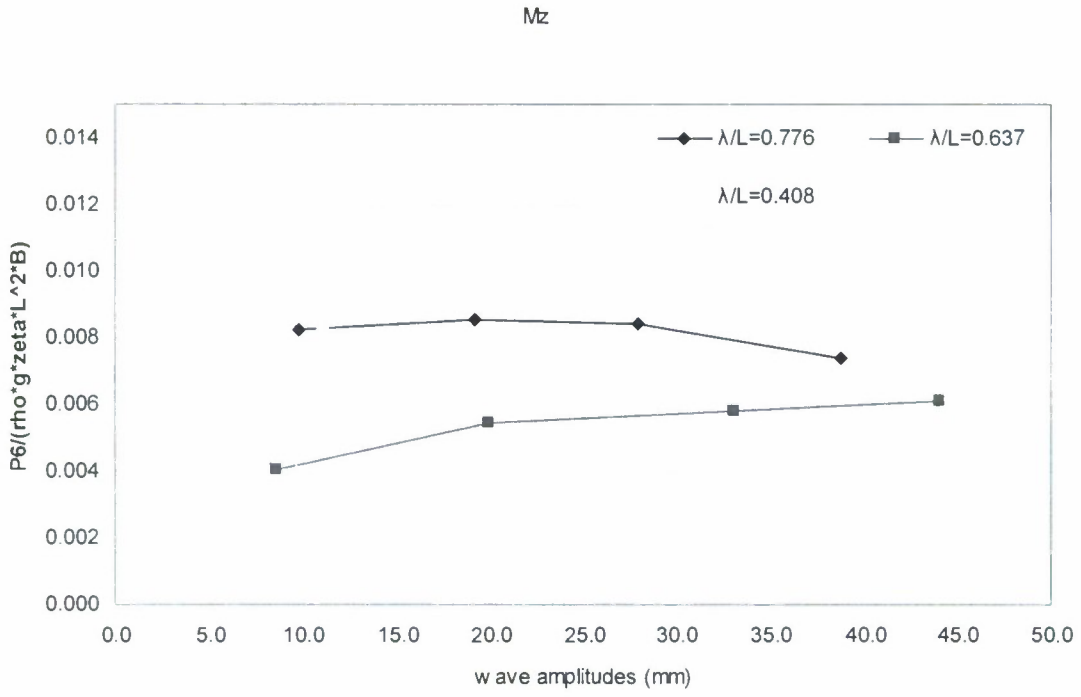

Figure 5.2.5-18: Torsion moment RAO at stern quartering waves (heading 315)

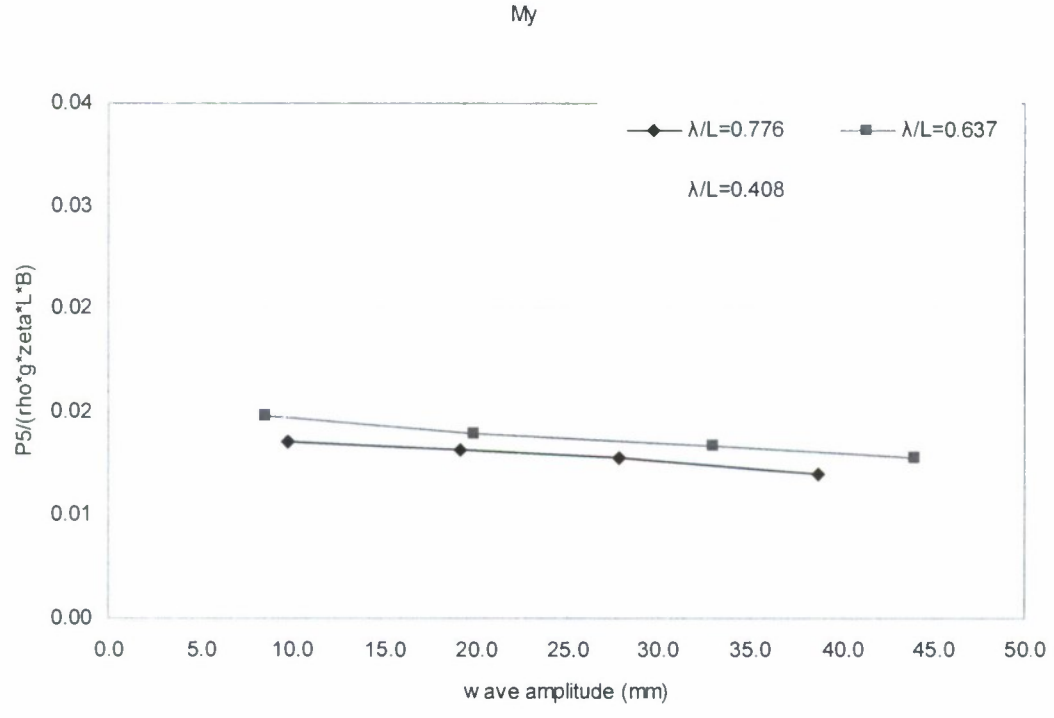

Figure 5.2.5-19: Vertical bending moment RAO at stern quartering waves (heading 315)

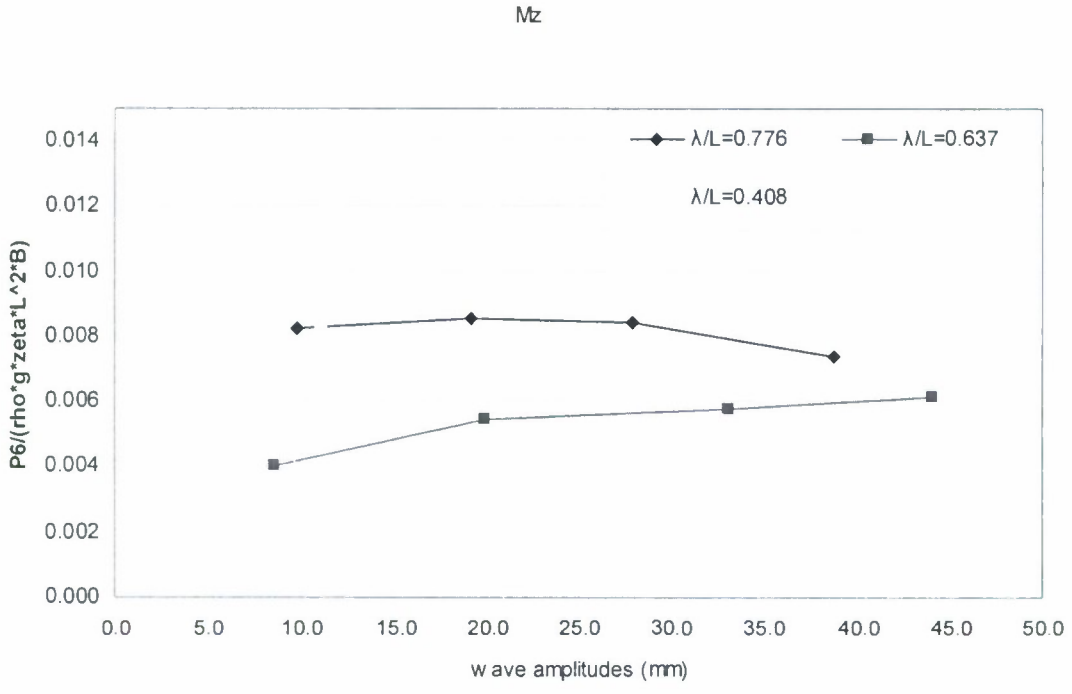

Figure 5.2.5-20: Horizontal bending moment RAO at stern quartering waves (heading 315)

Damage scenario 3 heading 45

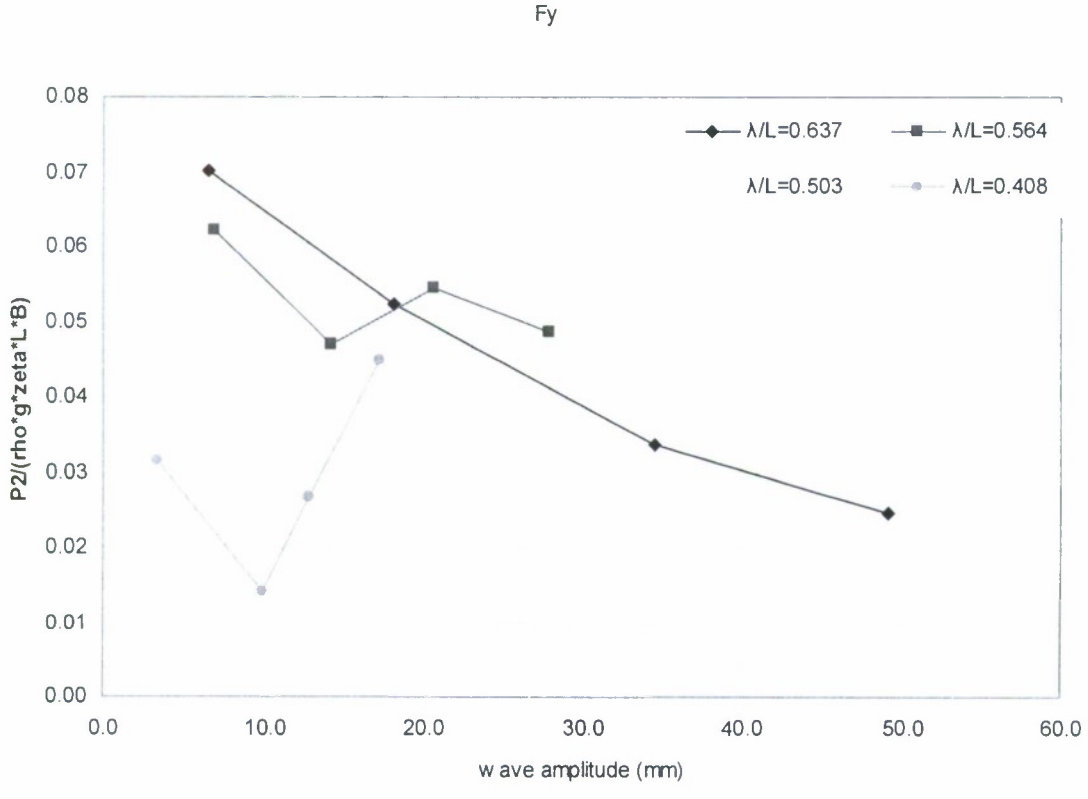

Figure 5.2.5-21: Horizontal shear force RAO at stern quartering waves

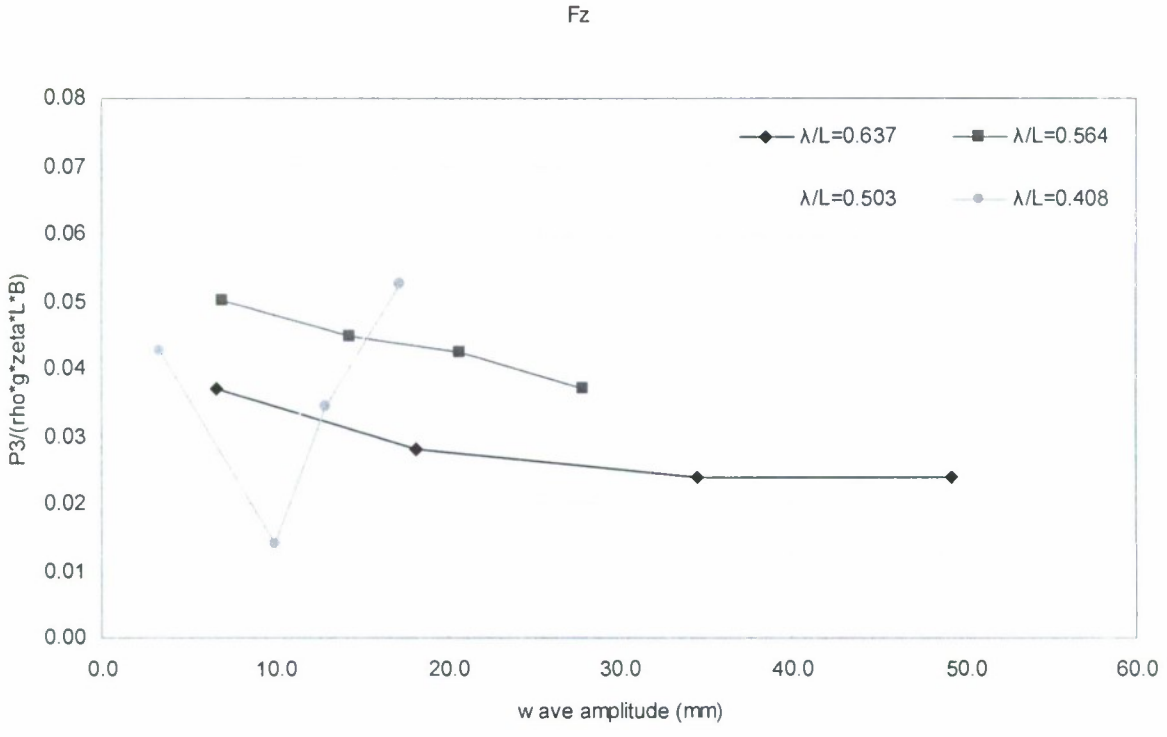

Figure 5.2.5-22: Vertical shear force RAO at stern quartering waves

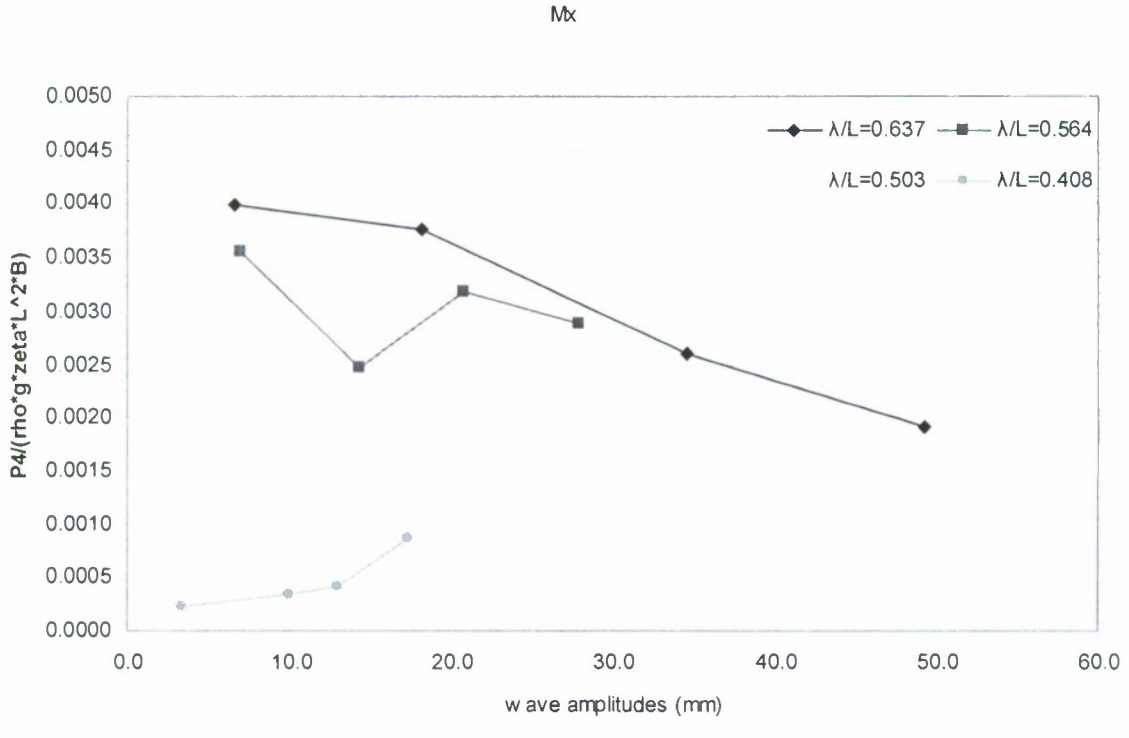

Figure 5.2.5-23: Torsion moment RAO at stern quartering waves

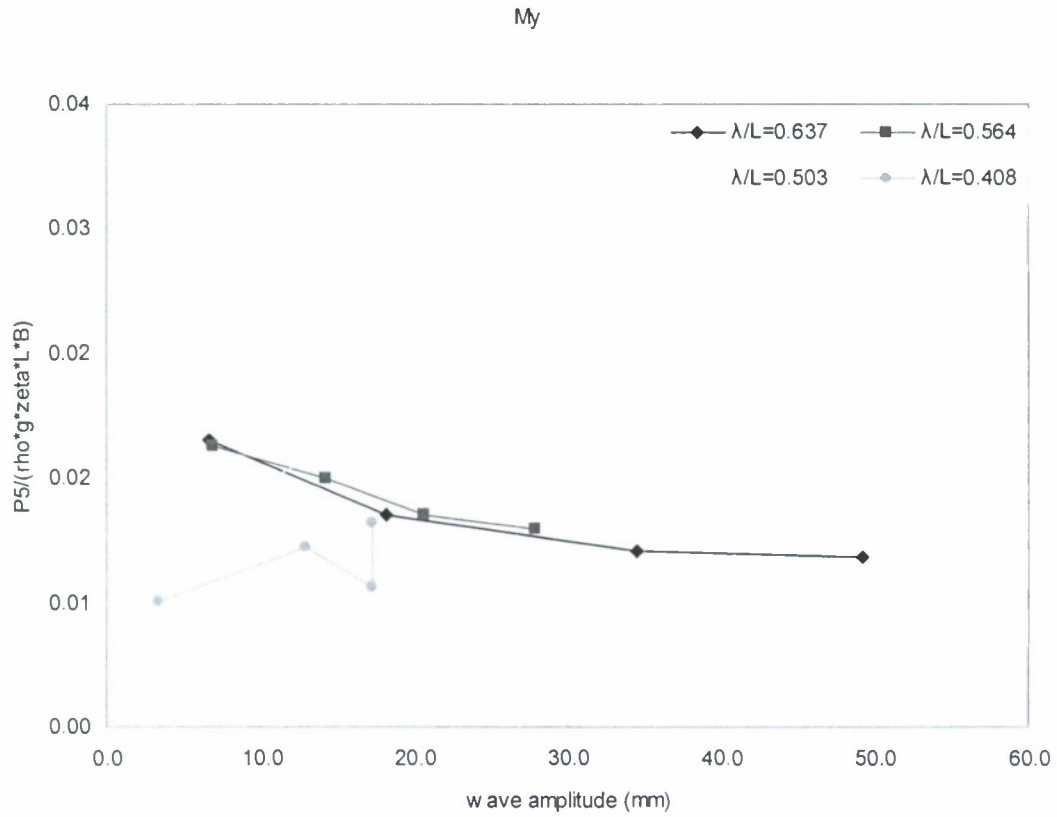

Figure 5.2.5-24: Vertical bending moment RAO at stern quartering waves

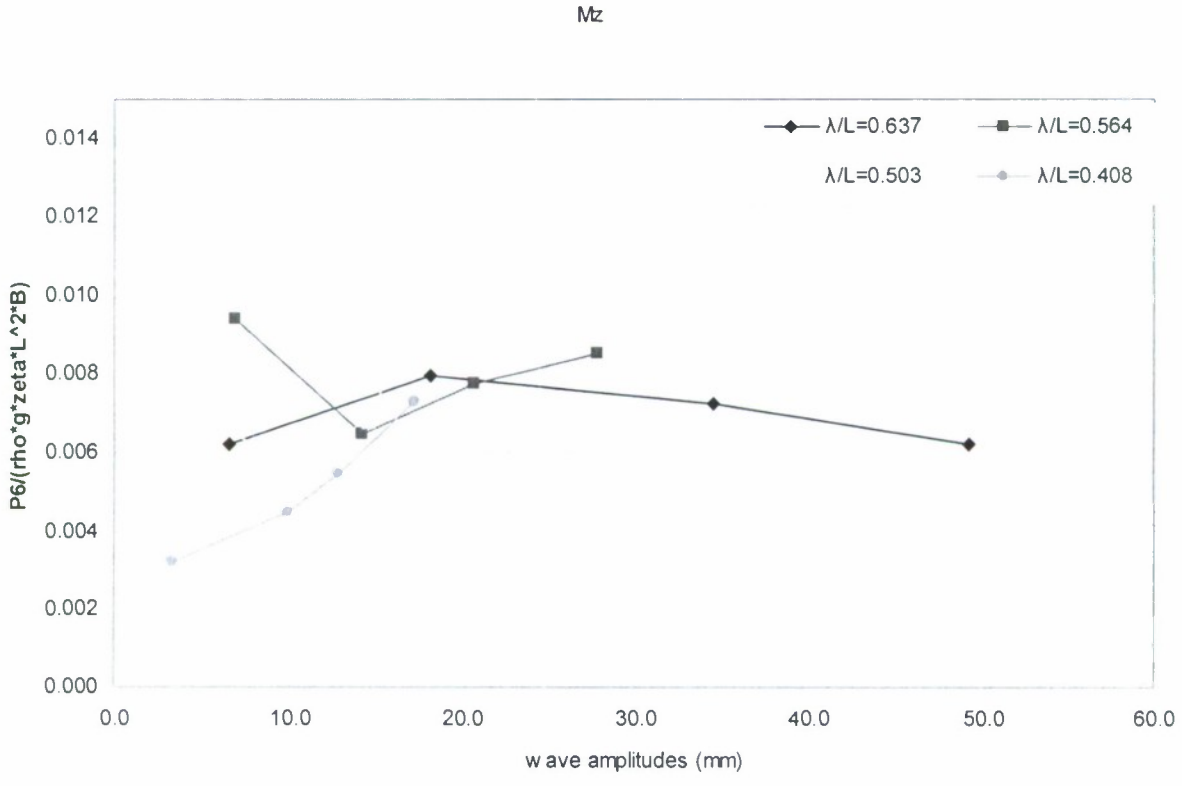

Figure 5.2.5-25: Horizontal bending moment RAO at stern quartering waves

Damage scenario 3 heading 180

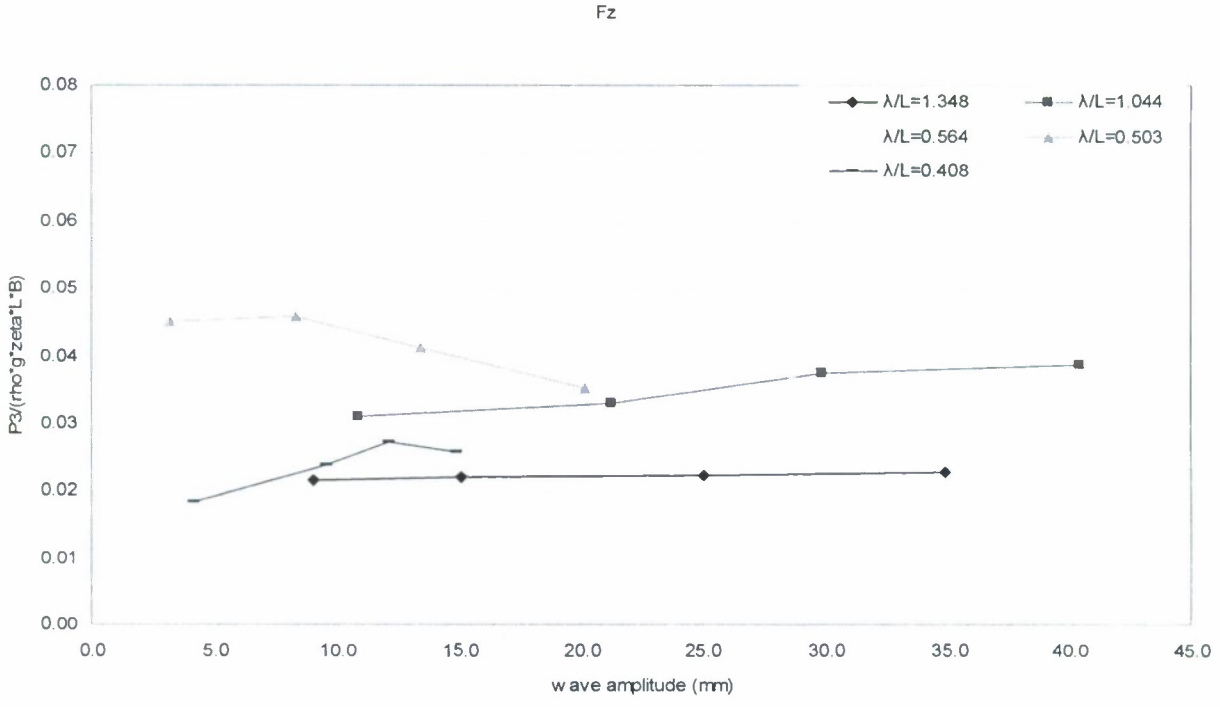

Figure 5.2.5-26: Vertical shear force RAO at head waves

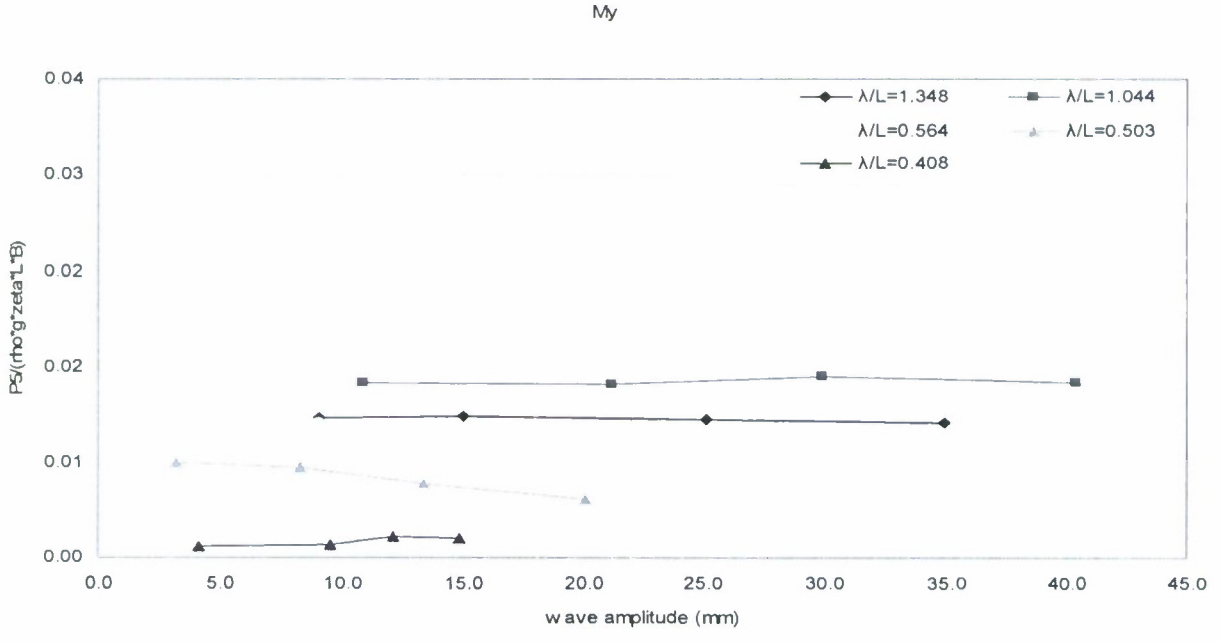

Figure 5.2.5-27: Vertical bending moment RAO of at head waves

5.3 Prediction of dynamic global wave loads using the 2D non-linear theory

An in-house program, which is based on the 2D nonlinear method presented in Chapter 3, has been used to calculate wave-induced loads in regular waves in this section in order to validate

the nonlinear method and compare it with the 2D linear method presented in the previous sections. For a given wave profile this method can calculate the dynamic responses in time domain. The time series are then filtered and the responses in frequency domain are obtained. Due to the nonlinearity in the responses, it is expected that the calculated RAO by different wave amplitudes would be different, so 2 wave amplitudes, namely 2 and 2.5 metres, have been chosen to calculate the RAOs of wave-induced loads on the ship model at the cut. One of the advantages of using a nonlinear method is its ability to distinguish the difference in positive and negative amplitude of the responses, while the positive and negative amplitude in a linear method would be the same. For ships, for instance, the sagging bending moment is normally greater than the hogging bending moment, especially for destroyers. Therefore positive and negative responses are presented separately to show their difference in the following figures.

Figures 5.3-1 to 5.3-34 have compared the 2D nonlinear results with the experimental results in intact condition and damage scenario 2. Due to the limited capability of the wave maker, the waves generated in the towing tank can't exactly match the wave amplitudes which were used in the theoretical calculations. Hence the "large" wave amplitudes in the experiment have been used to compare with the wave amplitude of 2m in theory, and "very large" wave amplitudes in the experiment have been used to compare with wave amplitude of 2.5m in theory. Only head seas and stern quartering seas are considered in this section because they are the critical headings for strength assessment. Horizontal bending moment and torsion moment in intact condition were not discussed in this comparison as they were almost zero in the numerical predictions. The sign conventions of dynamic force and moment on the transverse section of aft portion of the cut concerned are:

- Horizontal shear force is positive from starboard to port.
- Upward vertical shear force is positive.
- Anti-clockwise torsion moment is positive.
- Positive vertical bending moment is hogging.
- Horizontal bending moment is positive when its vector points upward.

Figures 5.3-3 shows the results of vertical bending moment in intact condition in head waves with a wave height of 2 metres in the numerical calculations. Also presented in this figure were the results of the 2D linear method, so the relative accuracy of both linear and nonlinear methods can be observed. More details of the quantitative comparison of the 2D nonlinear method with the experimental results can be seen in Table C.1 in Appendix C, in which the model uncertainties of the nonlinear method were presented. Close attention will be paid to the results at the frequencies of 2.37, 2.74 and 2.97 because the wave height in the tests at those frequencies was very near to 2.0 metres. The 2D nonlinear results of the vertical bending moment agree reasonably well with the experimental results at some cases, such as positive amplitude at frequency 2.97 and negative amplitude at frequency 2.37. The values of X_m in those cases were 0.779 and 0.791 respectively. However the agreement was poor in some other cases, such as positive amplitude at frequency 2.37. The value of X_m in that case was 0.598. The mean and COV of X_m were 0.910 and 63.3% for positive amplitude, and 1.280 and 102.6% for negative amplitude. Further investigation into the constituents of X_m has shown that there is a large value of 2.342 for positive amplitude and 4.771 for negative amplitude at low frequency. This large value could distort the mean and COV especially when the total number of data is only 9. In addition the wave height in the test at this frequency was less than 0.7 metres, which was far away from 2.0 metres used in the numerical calculation. Hence caution needs to be applied if the model uncertainty factor is to be used.

The results of the 2D linear method fail in between the positive and negative amplitudes predicted by the 2D nonlinear method in the resonant region. So the linear and nonlinear methods correlate fairly well in this condition. Overall the performance of the 2D nonlinear method was not satisfactory in this case.

Figures 5.3-4 shows the results of vertical bending moment in intact condition in head waves with a wave height of 2.5 metres in the numerical calculations. The features of this figure were quite similar to those of Figure 5.3-3. It should be pointed out that the majority of the experimental wave heights were not near the corresponding numerical wave height in this case. The mean and COV of X_m were 1.038 and 100.4% for positive amplitude, and 0.671 and 30.1% for negative amplitude. Again the agreement between the 2D nonlinear method and the tests was not desirable.

Figures 5.3-9 shows the results of vertical bending moment in intact condition in stern quartering seas with a wave height of 2.0 metres in the numerical calculations. Again more attention will be paid to the results at the frequencies of 2.37, 2.74 and 2.97. Generally the 2D nonlinear results of the vertical bending moment do not agree well with the experimental results except for one case, which was the negative amplitude at frequency 2.97 with a value of X_m of 0.862. The values of X_m in the two bad cases were 0.497 and 0.509 respectively. The mean and COV of X_m were 0.941 and 95.6% for positive amplitude, and 0.737 and 40.3% for negative amplitude.

Figures 5.3-19 shows the results of vertical bending moment in damage scenario 2 in head waves with a wave height of 2 metres in the numerical calculations. For the same reason more attention will be paid to the results at the frequencies of 2.37, 2.74 and 2.97 The 2D nonlinear results of the vertical bending moment agree reasonably well with the experimental results at some cases, such as positive amplitude at frequency 2.74 and negative amplitude at frequency 2.37. The values of X_m in those cases were 0.832 and 0.838 respectively as shown in Table C.2 in Appendix C. However the agreement was not satisfactory in some other cases, such as negative amplitude at frequencies 2.74 and 2.97, and positive amplitude at frequency 2.37. The values of X_m in those three cases were 0.599, 0.606 and 0.620 respectively. The mean and COV of X_m were 1.084 and 75.4% for positive amplitude, and 0.596 and 43.9% for negative amplitude. Further investigation into the constituents of X_m has shown that there is a very large value of 22.107 for positive amplitude and 17.572 for negative amplitude at a very low frequency of 1.435. This large value could distort the mean and COV especially when the total number of data is only 9. In addition the wave height in the test was 1.148 metres, which was far away from 2.0 metres used in the numerical calculation, at this low frequency. Hence caution needs to be applied if the model uncertainty factor is to be used.

The results of vertical bending moment in damage scenario 2 in stern quartering seas with a wave height of 2 metres in the numerical calculations have been presented in Figure 5.3-29 and Table C.2 in Appendix C. As before the results at the frequencies of 2.37, 2.74 and 2.97 were under close scrutiny. The 2D nonlinear results of the vertical bending moment agree reasonably well with the experimental results at some cases, such as positive amplitude at frequency 2.37 and 2.97 and negative amplitude at frequency 2.97. The values of X_m in those cases were 0.862 and 0.914 respectively as shown in Table C.2 in Appendix C. However the agreement was poor in some other cases, such as negative amplitude at frequencies 2.37, and positive amplitude at frequency 2.74. The values of X_m in those three cases were 0.606 and 0.668 respectively. The mean and COV of X_m were 0.719 and 43.9% for positive amplitude, and 0.866 and 41.1% for negative amplitude. This is the best performance for vertical bending moment prediction.

The horizontal bending moment in intact condition in stern quartering seas with a wave height of 2 metres in the numerical calculations has been presented in Figure 5.3-11 and Table C.1 in Appendix C. As before the results at the frequencies of 2.37, 2.74 and 2.97 were the main focus. The 2D nonlinear results of the horizontal bending moment do not agree well with the experimental results at these frequencies. The values of X_m in those cases vary in a large range from 0.227 to 2.906 as shown in Table C.1 in Appendix C. The mean and COV of X_m were 1.357 and 110% for positive amplitude, and 0.528 and 60.9% for negative amplitude. It is interesting to note that both linear and nonlinear methods produce two peaks, but the predicted peaks did not match the peak, which was measured in the tests. This seems the main reason for such a bad performance in the numerical predictions.

Figures 5.3-31 shows the results of horizontal bending moment in damage scenario 2 in stern quartering seas with a wave height of 2 metres in the numerical calculations. For the same reason the results at the frequencies of 2.37, 2.74 and 2.97 were the focus. The 2D nonlinear results of the horizontal bending moment agree reasonably well with the experimental results at some cases, such as positive amplitude at frequency 2.37 and 2.74. The values of X_m in those cases were 0.842 and 1.147 respectively as shown in Table C.2 in Appendix C. However the agreement was not satisfactory in some other cases, such as negative amplitude at all frequencies, and positive amplitude at frequency 2.97. The values of X_m in those three cases were 0.208, 0.342, 0.428 and 1.897 respectively. The mean and COV of X_m were 1.109 and 60.3% for positive amplitude, and 0.602 and 91.9% for negative amplitude.

The torsion moment in intact condition in stern quartering seas with a wave height of 2 metres in the numerical calculations has been presented in Figure 5.3-13 and Table C.1 in Appendix C. As before the results at the frequencies of 2.37, 2.74 and 2.97 were the main focus. The 2D nonlinear results of the torsion moment agree well with the experimental results at some frequencies but not the others. The mean and COV of X_m were 0.4955 and 105.5% for positive amplitude, and 0.489 and 47.2% for negative amplitude. It is interesting to note that the nonlinear method correctly predicted the peak responses, but the agreement at other frequencies were so bad so that the mean and COV of X_m were quite unsatisfactory.

Figures 5.3-33 shows the results of the torsion moment in damage scenario 2 in stern quartering seas with a wave height of 2 metres in the numerical calculations. The 2D nonlinear results of the torsion moment do not agree well with the experimental results at almost all the frequencies. As shown in Table C.2 in Appendix C the mean and COV of X_m were 0.130 and 85.1% for positive amplitude, and 0.343 and 82.8% for negative amplitude. Basically the experimental results were much smaller than the predicted responses.

In summary, the 2D nonlinear method does not produce satisfactory results for vertical bending moment, horizontal bending moment and torsion moment. Although this conclusion was largely based on the analysis of the results of 2 metres wave height, it was equally applicable to the results of 2.5 metres wave height as shown in the corresponding figures and Table C.1 and C.2 in Appendix C. Again the predictions of torsion moment are the worst among the three components of the wave-induced loads, while the predictions of vertical bending moment have similar level of accuracy to those of horizontal bending moment. The nonlinear method tends to produce better results at the resonant frequencies than at the other frequencies. However it should be pointed out that the measured wave heights were not equal to 2.0 metres, which was used in the numerical calculations, at most frequencies so that caution has to be applied when the mean and COV of X_m are used to judge the accuracy of the method.

Intact Condition

Head seas

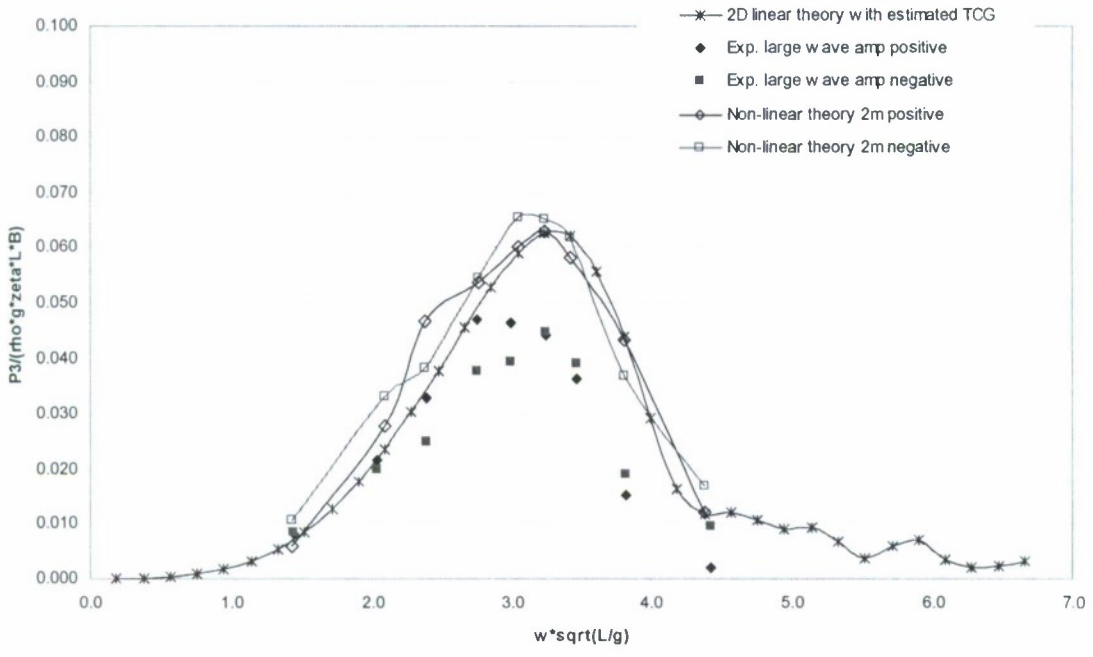

Figure 5.3-1: Dynamic vertical shear force RAO
at head seas (heading 180), theory ζ = 2m

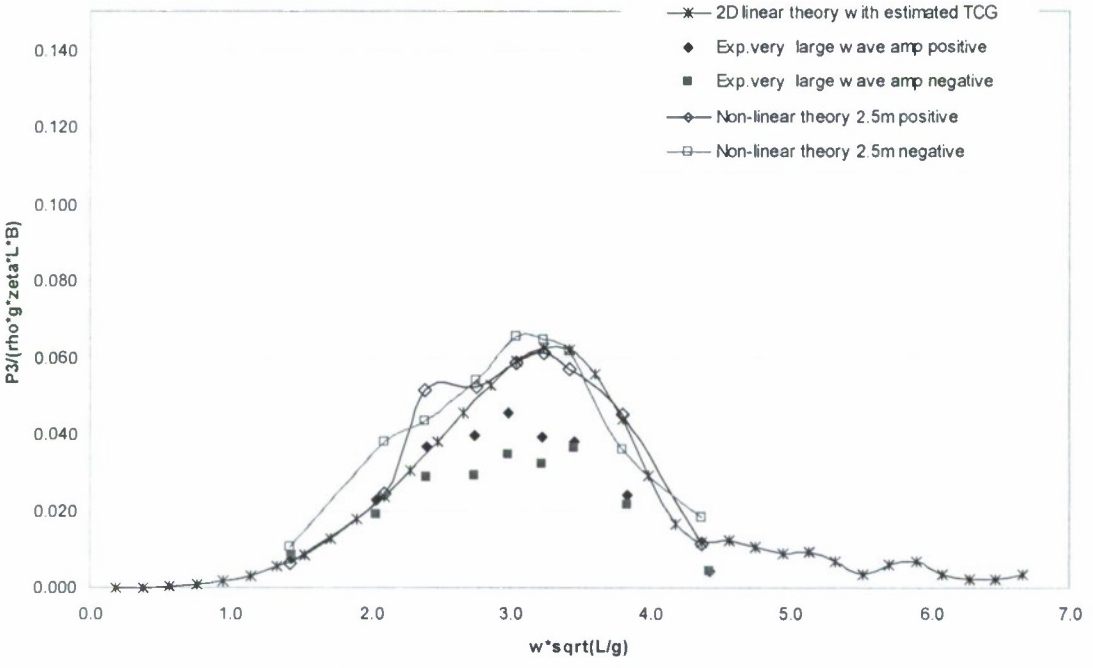

Figure 5.3-2: Dynamic vertical shear force RAO
at head seas (heading 180), theory ζ = 2.5m

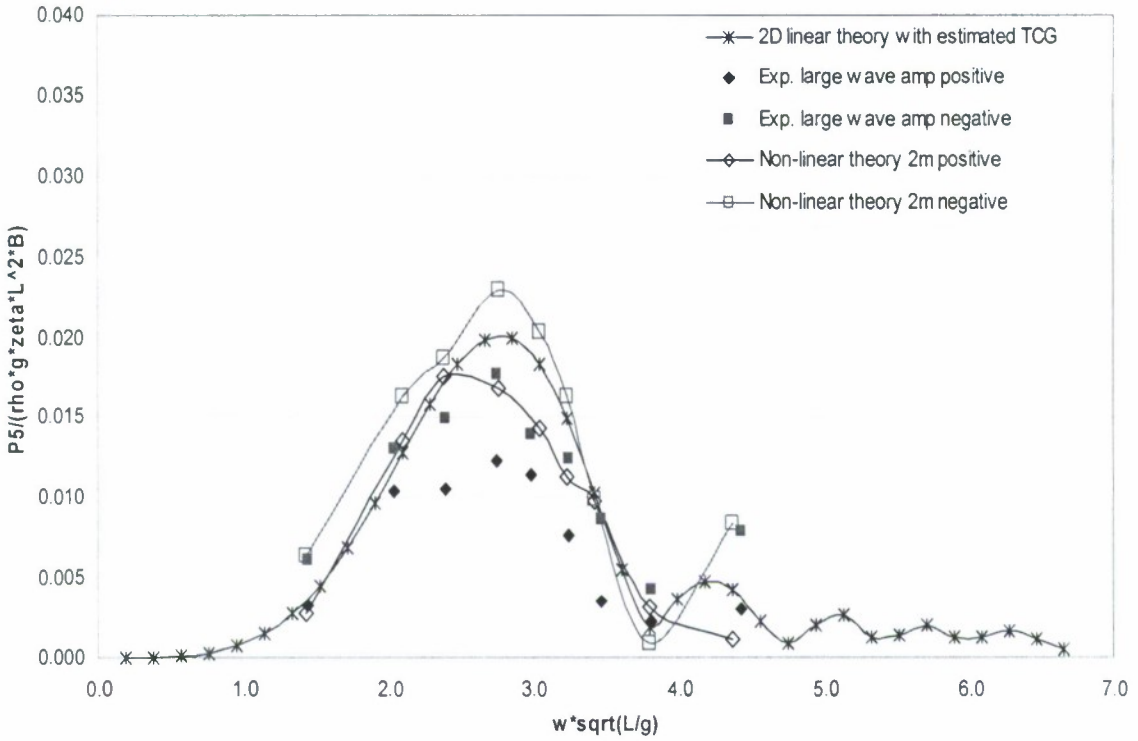

Figure 5.3-3: Dynamic vertical bending moment RAO
at head seas (heading 180), theory $\zeta = 2$m

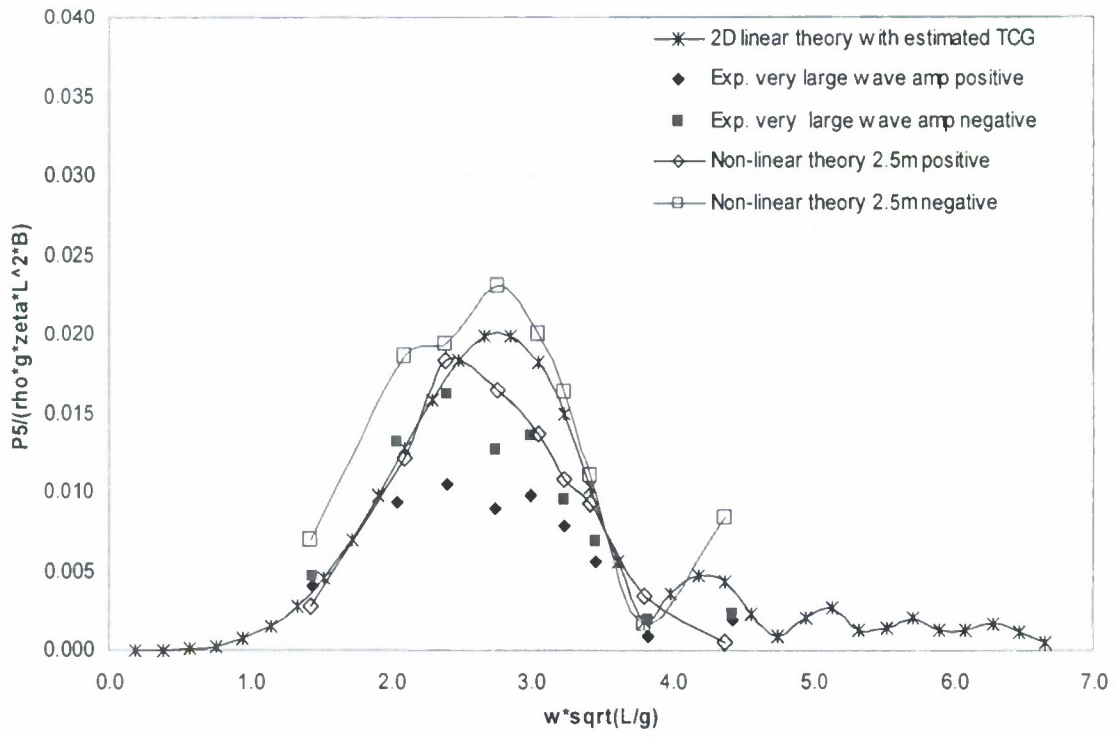

Figure 5.3-4: Dynamic vertical bending moment RAO
at head seas (heading 180), theory $\zeta = 2.5$m

Stern quartering seas

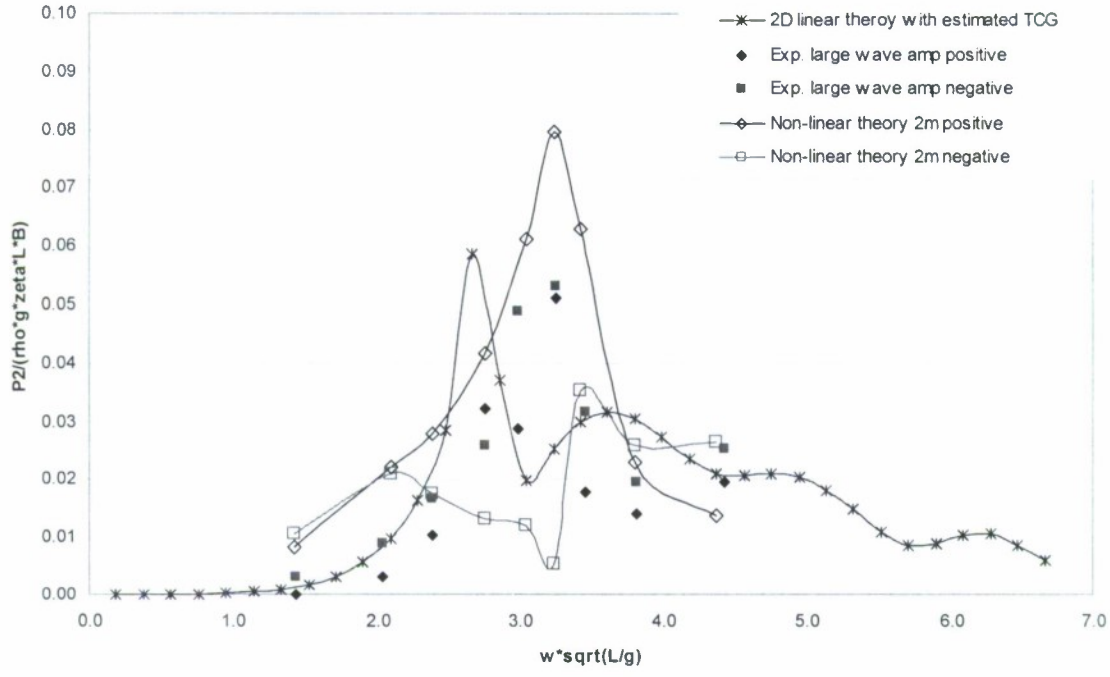

Figure 5.3-5: Dynamic horizontal shear force RAO
at stern quartering seas (heading 45), theory ζ = 2m

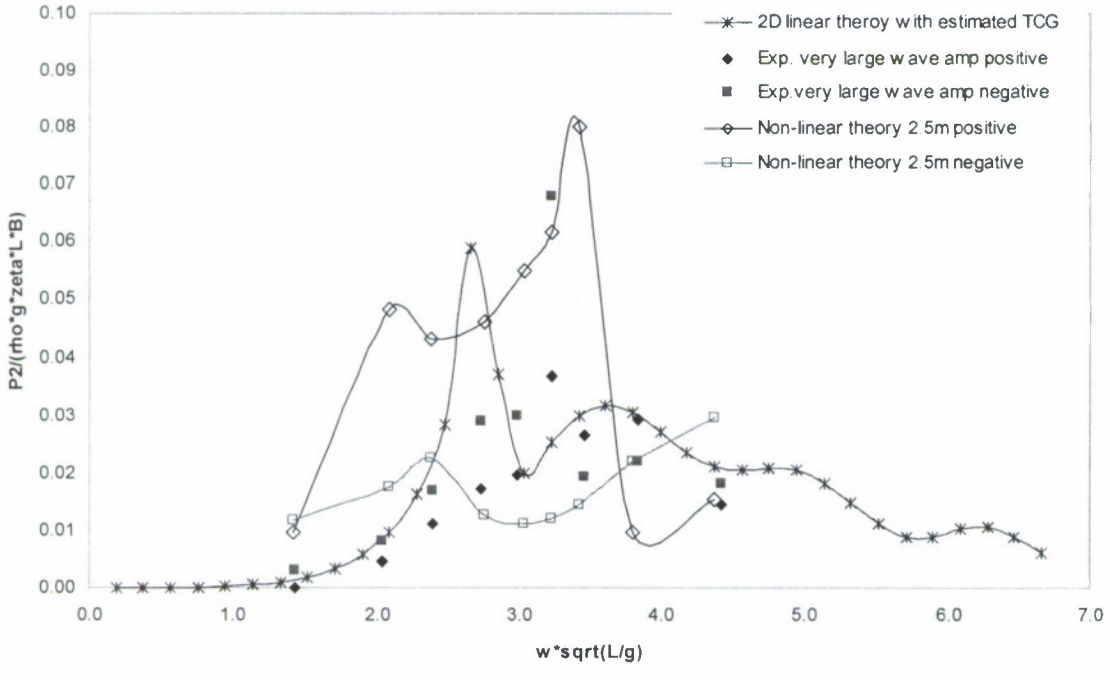

Figure 5.3-6: Dynamic horizontal shear force RAO
at stern quartering seas (heading 45), theory ζ = 2.5m

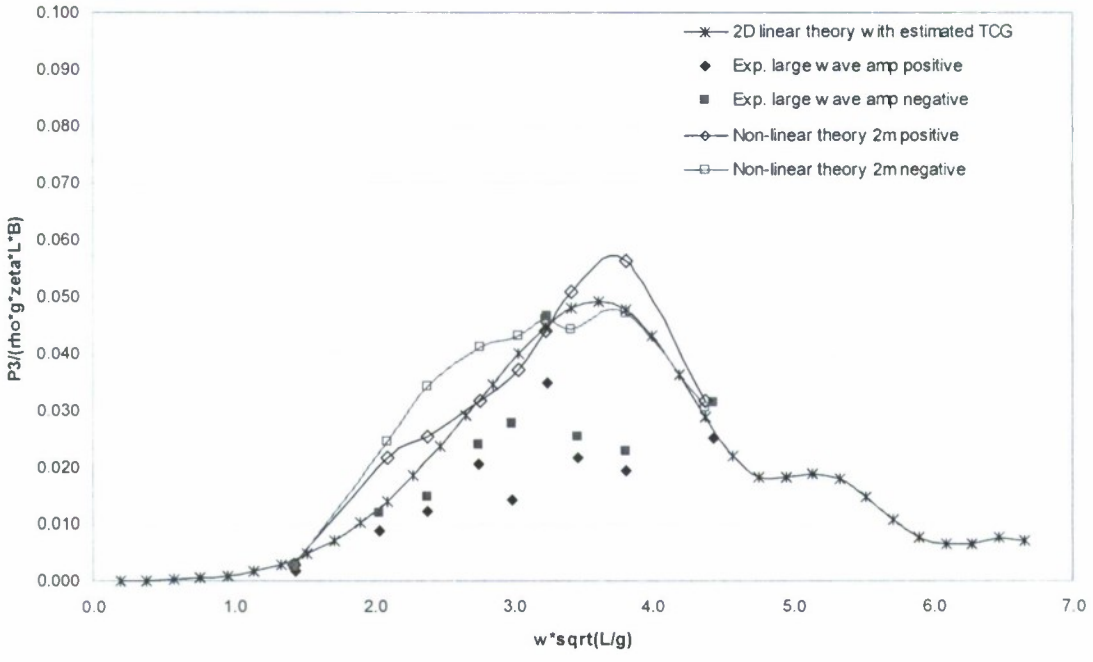

Figure 5.3-7: Dynamic vertical shear force RAO
at stern quartering seas (heading 45), theory ζ = 2m

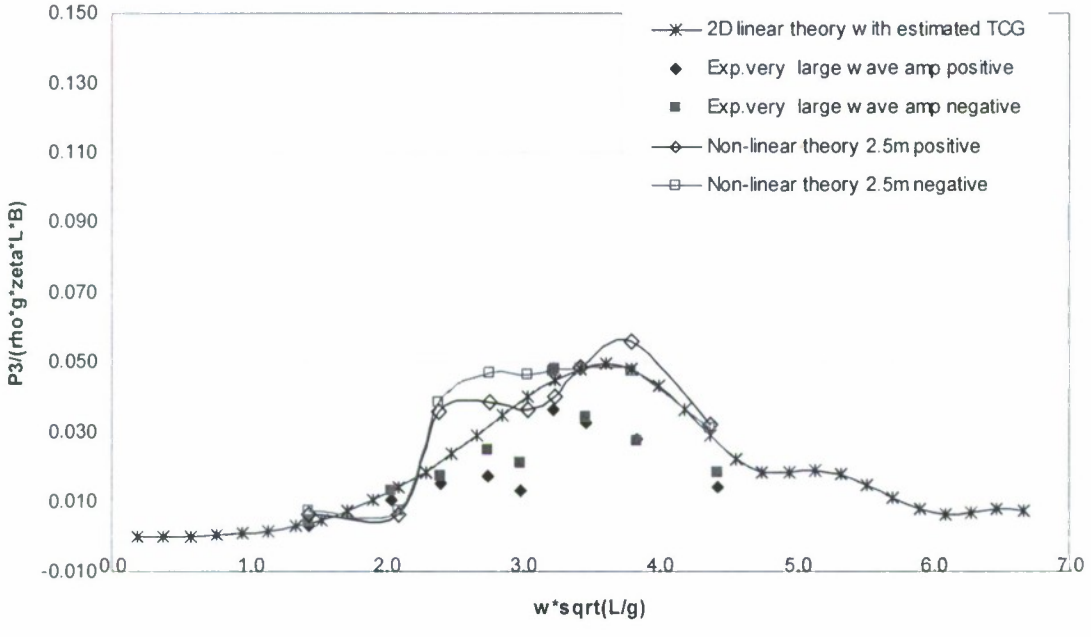

Figure 5.3-8: Dynamic vertical shear force RAO
at stern quartering seas (heading 45), theory ζ = 2.5m

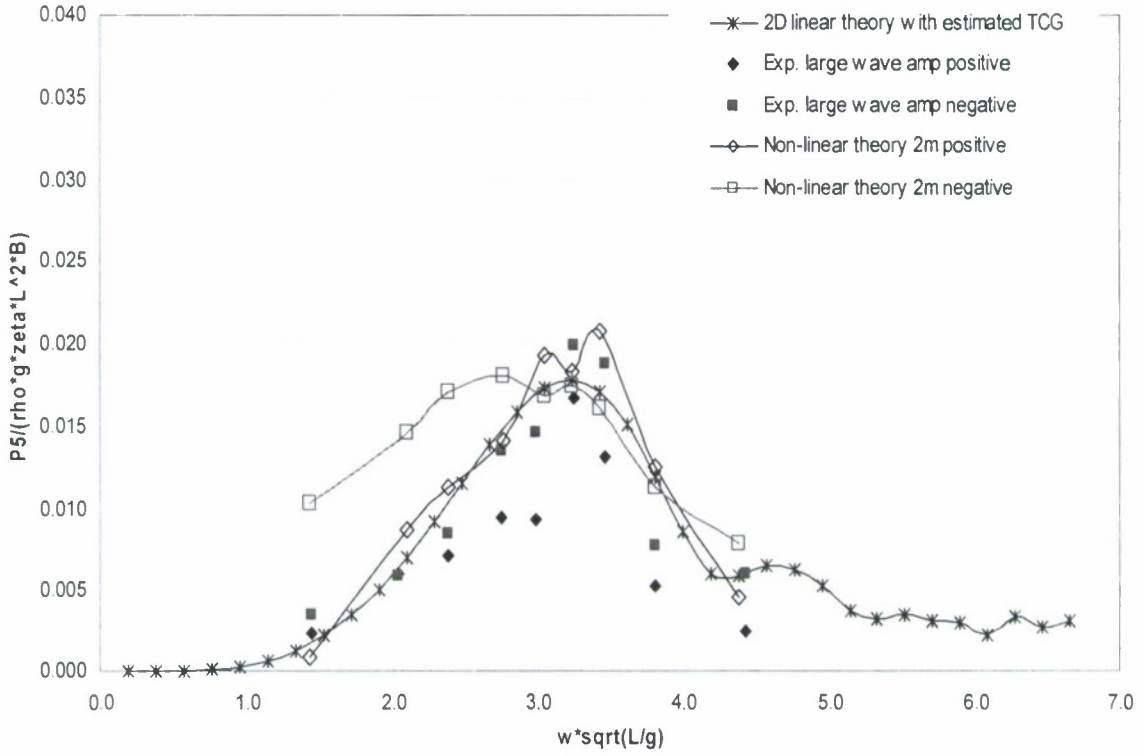

Figure 5.3-9: Dynamic vertical bending moment RAO
at stern quartering seas (heading 45), theory ζ = 2m

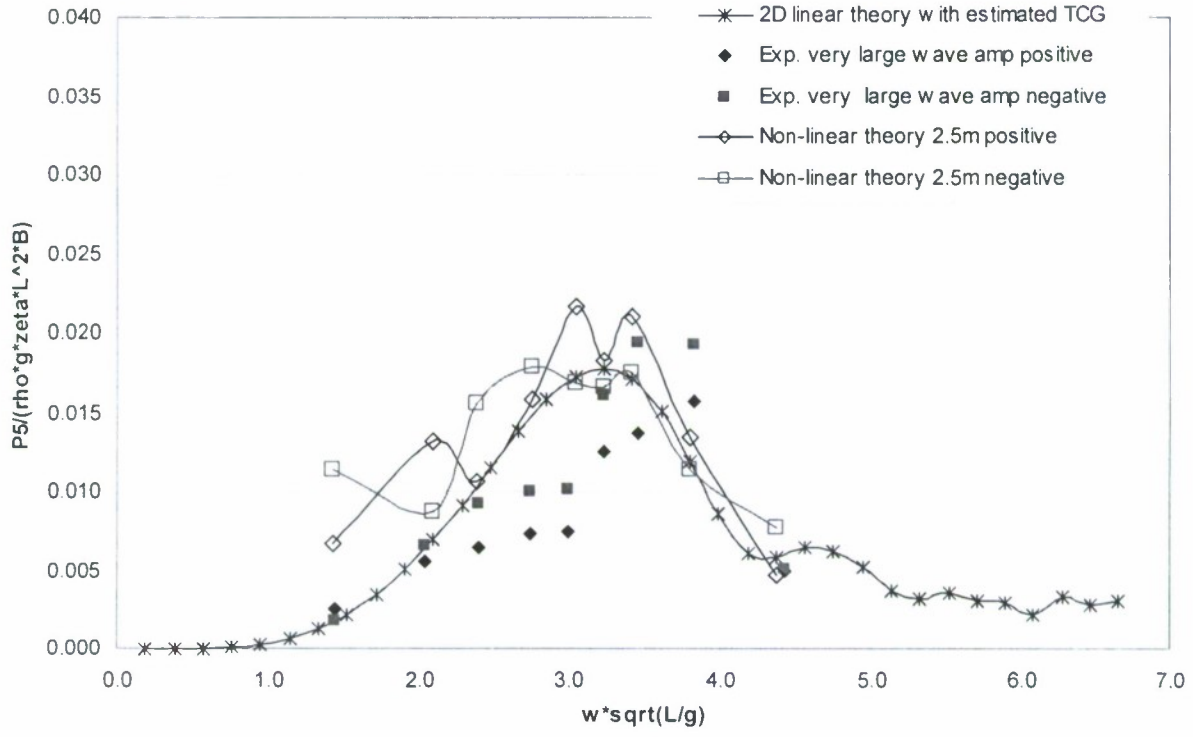

Figure 5.3-10: Dynamic vertical bending moment RAO
at stern quartering seas (heading 45), theory ζ = 2.5m

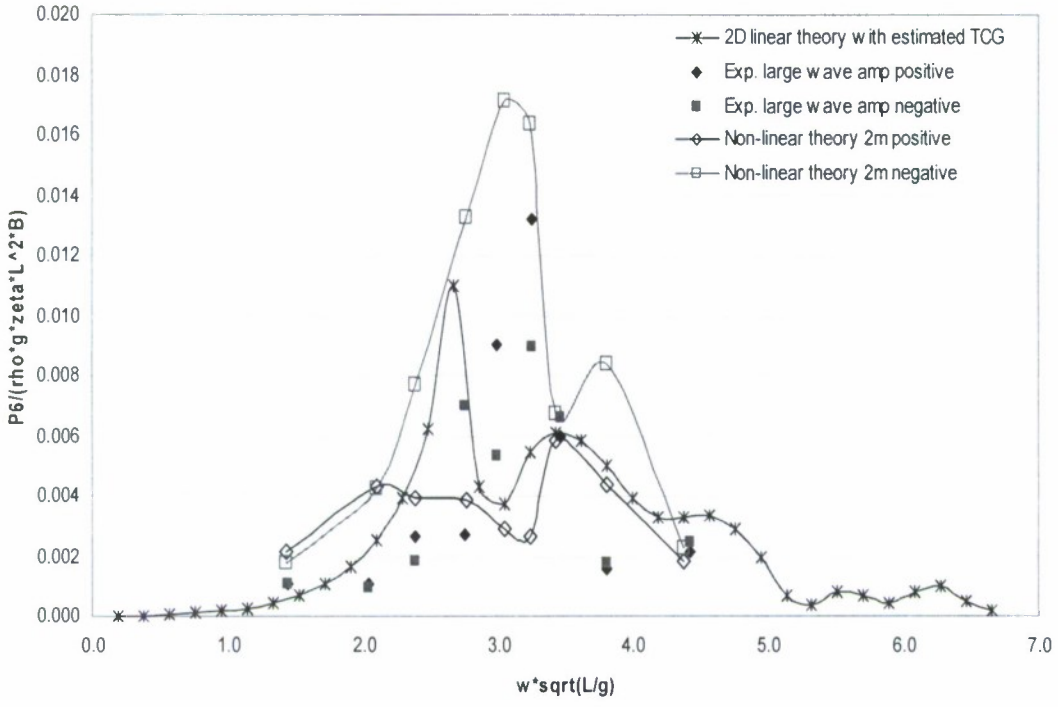

Figure 5.3-11: Dynamic horizontal bending moment RAO
at stern quartering seas (heading 45), theory ζ = 2m

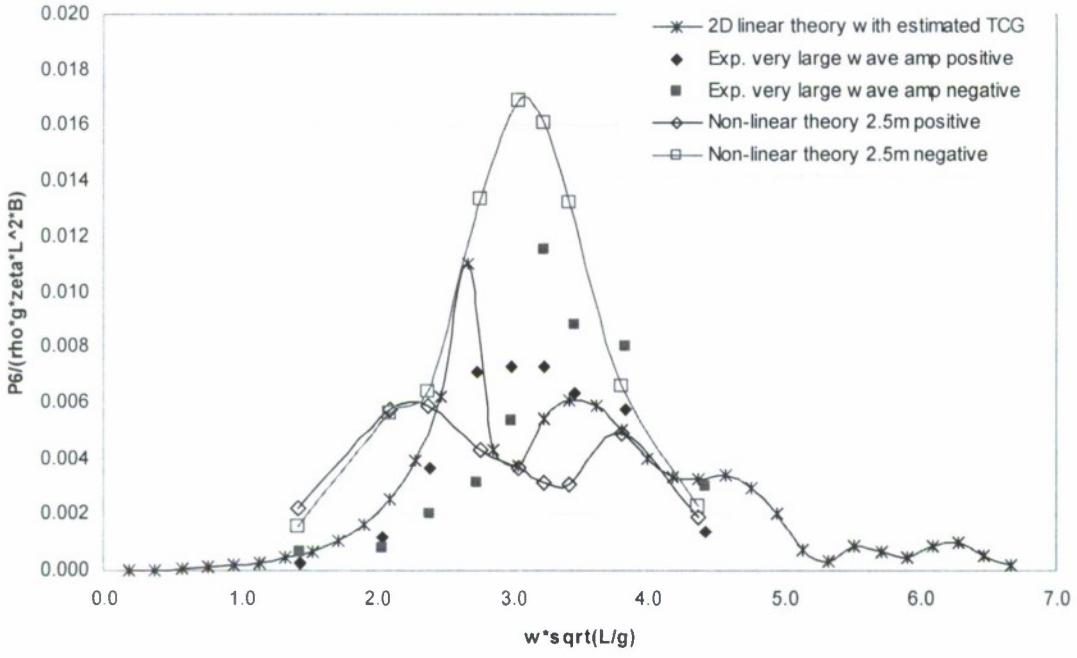

Figure 5.3-12: Dynamic horizontal bending moment RAO
at stern quartering seas (heading 45), theory ζ = 2.5m

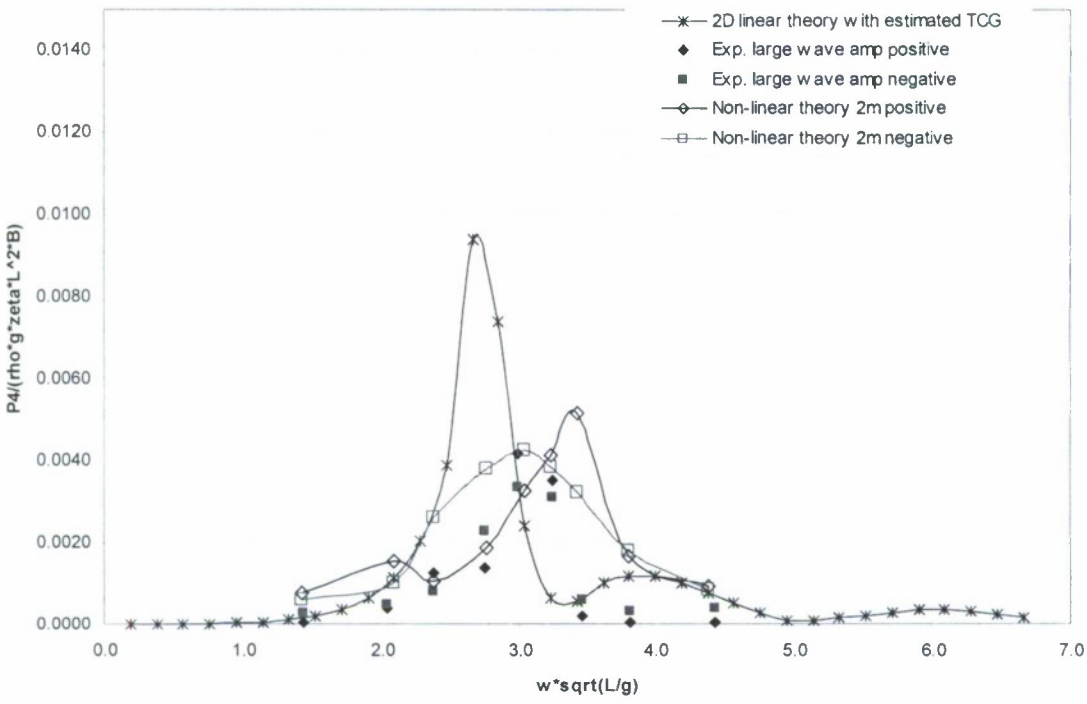

Figure 5.3-13: Dynamic torsion moment RAO
at stern quartering seas (heading 45), theory ζ = 2m

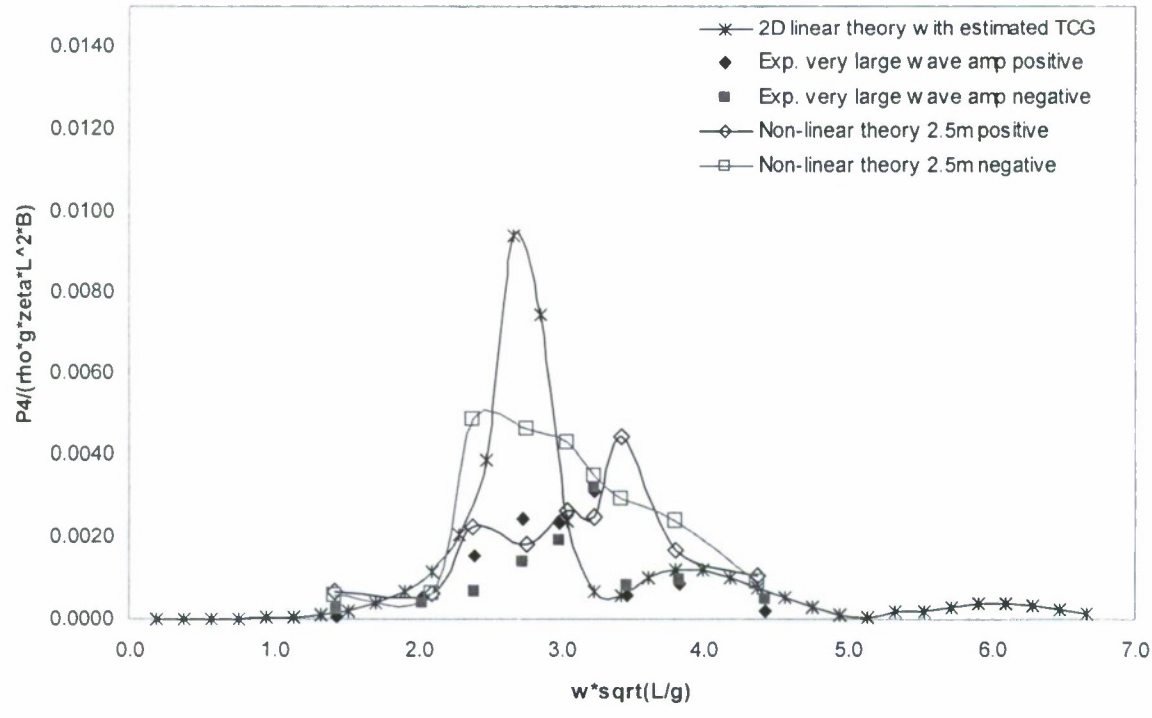

Figure 5.3-14: Dynamic torsion moment RAO
at stern quartering seas (heading 45), theory ζ = 2.5m

Damage Scenario 2

Head Seas

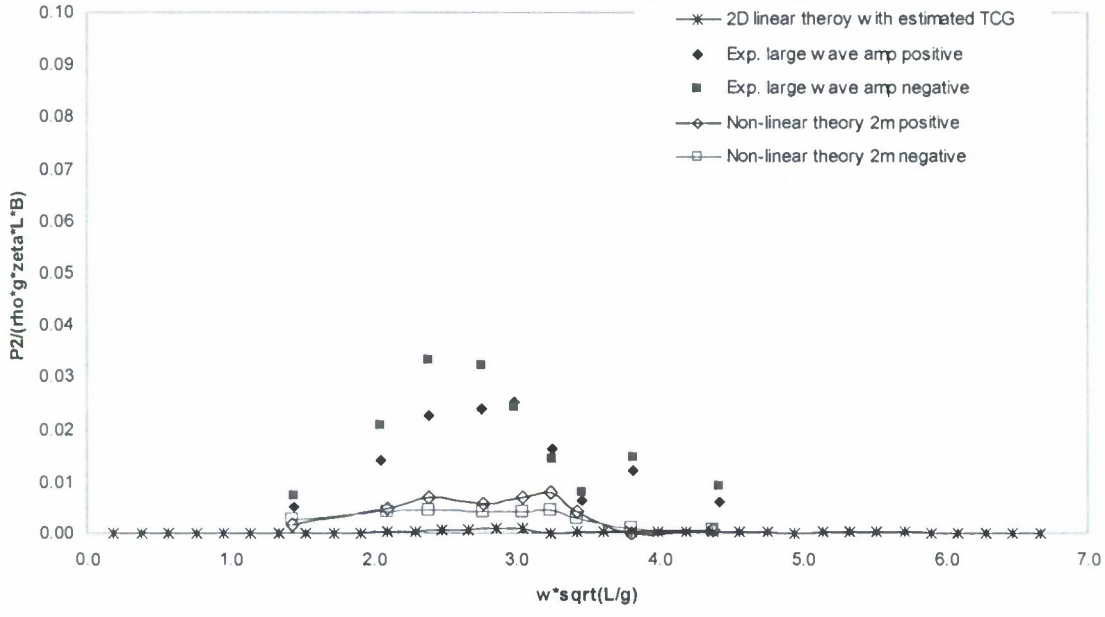

Figure 5.3-15: Dynamic horizontal shear force RAO at head seas (heading 180), theory ζ = 2m

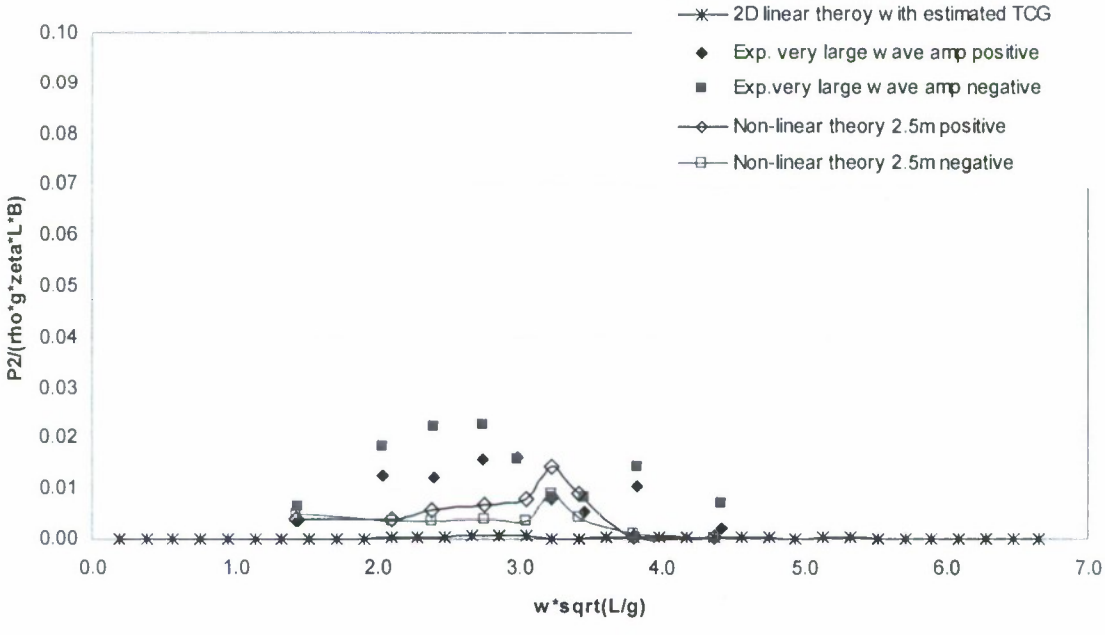

Figure 5.3-16: Dynamic horizontal shear force RAO at head seas (heading 180), theory ζ = 2.5m

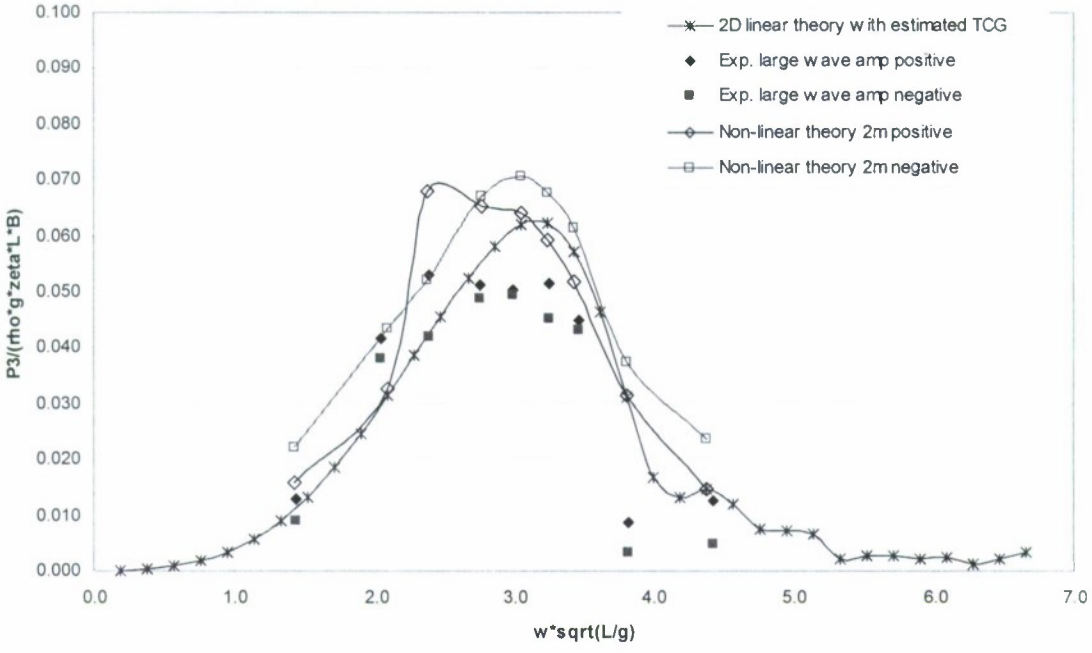

Figure 5.3-17: Dynamic vertical shear force RAO
at head seas (heading 180), theory ζ = 2m

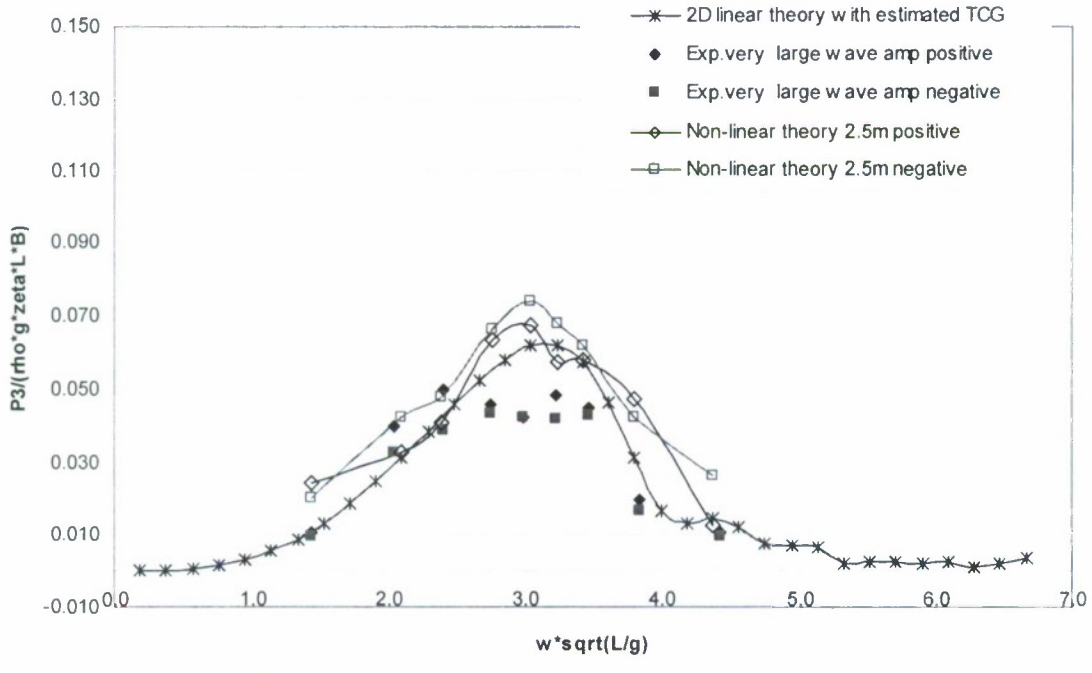

Figure 5.3-18: Dynamic vertical shear force RAO
at head seas (heading 180), theory ζ = 2.5m

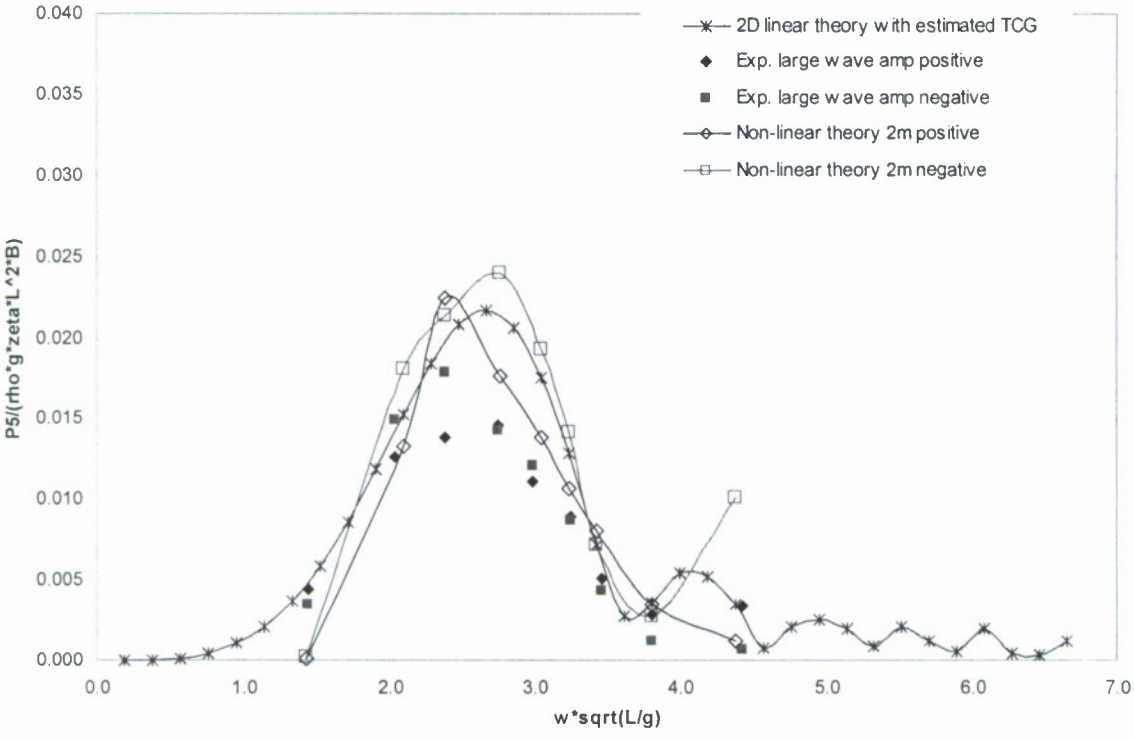

Figure 5.3-19: Dynamic vertical bending moment RAO at head seas (heading 180), theory ζ = 2m

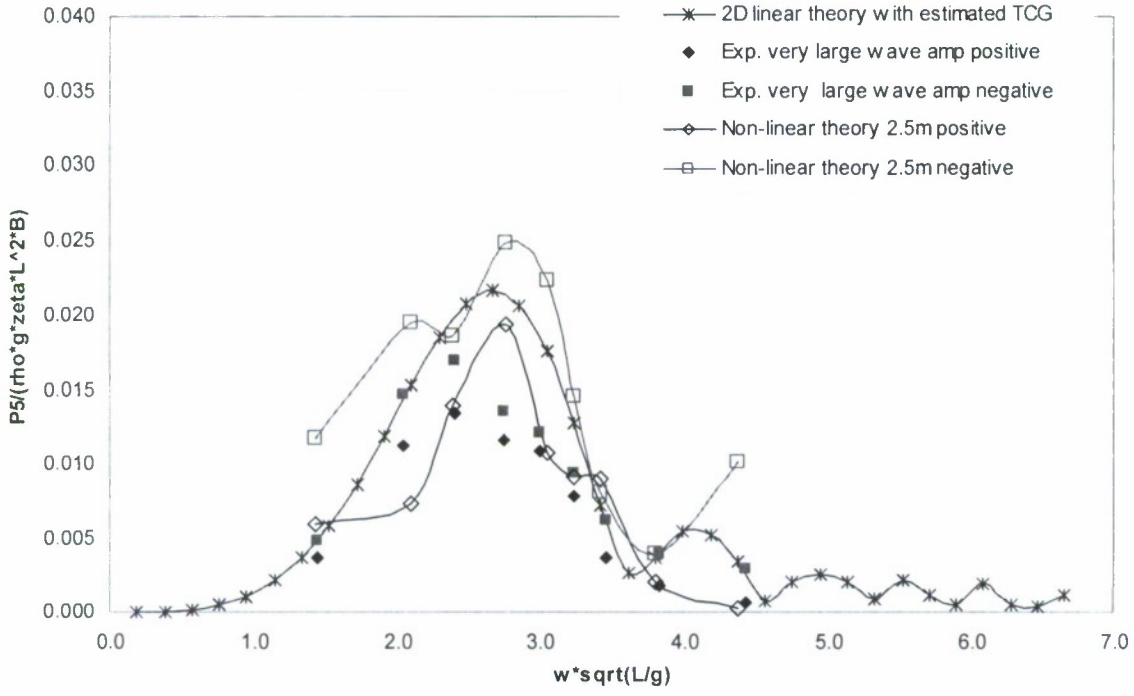

Figure 5.3-20: Dynamic vertical bending moment RAO at head seas (heading 180), theory ζ = 2.5m

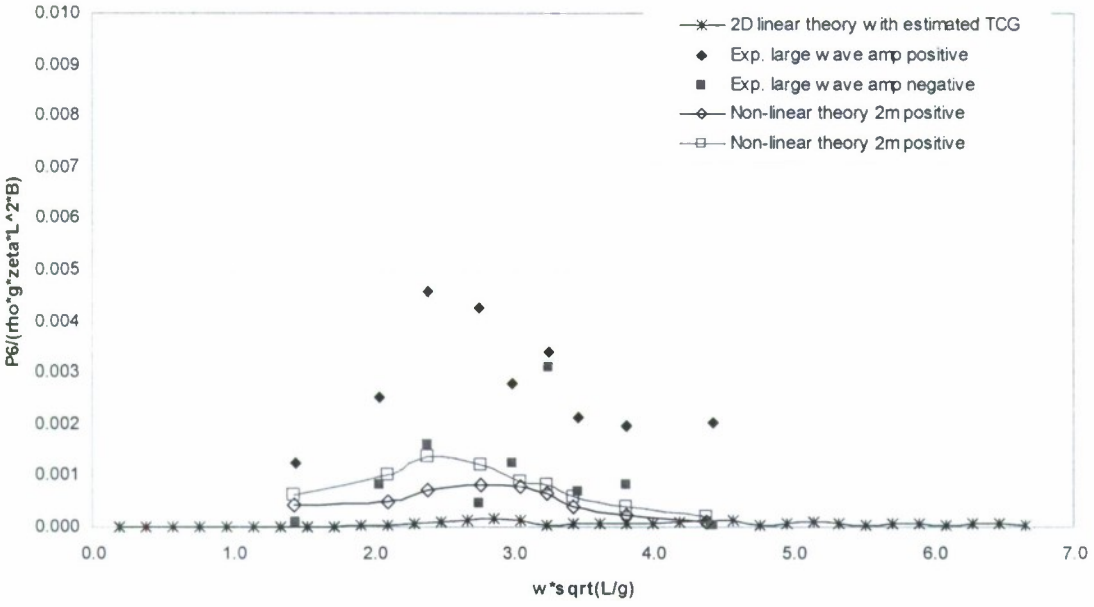

Figure 5.3-21: Dynamic horizontal bending moment RAO at head seas (heading 180), theory ζ = 2m

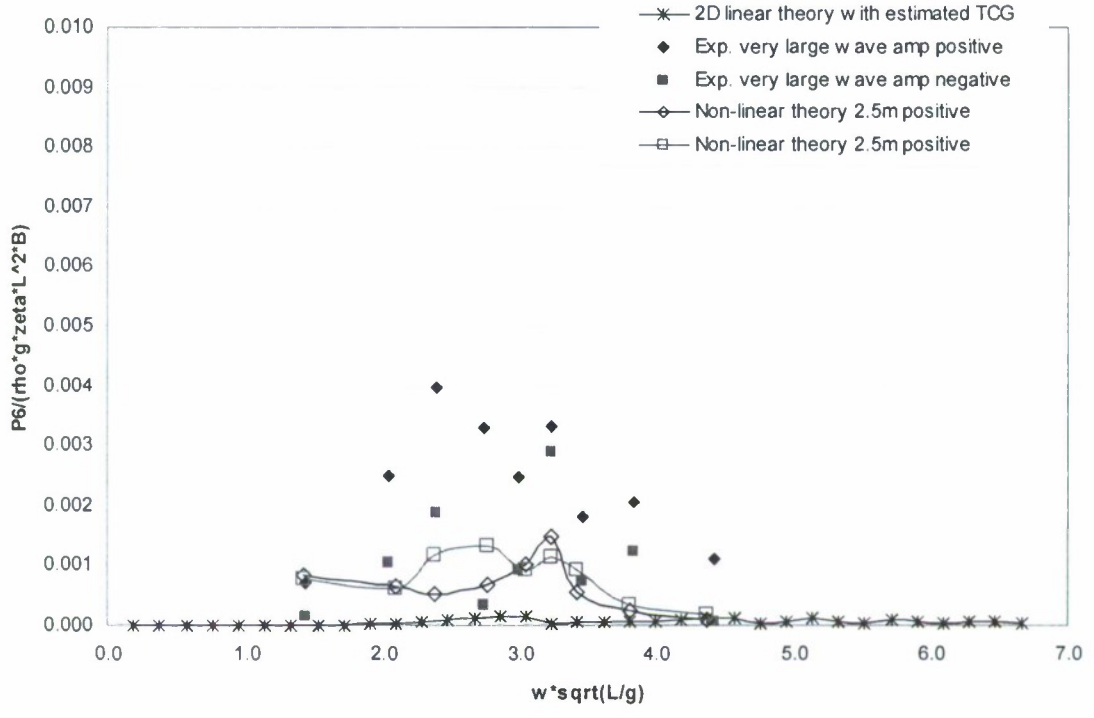

Figure 5.3-22: Dynamic horizontal bending moment RAO at head seas (heading 180), theory ζ = 2.5m

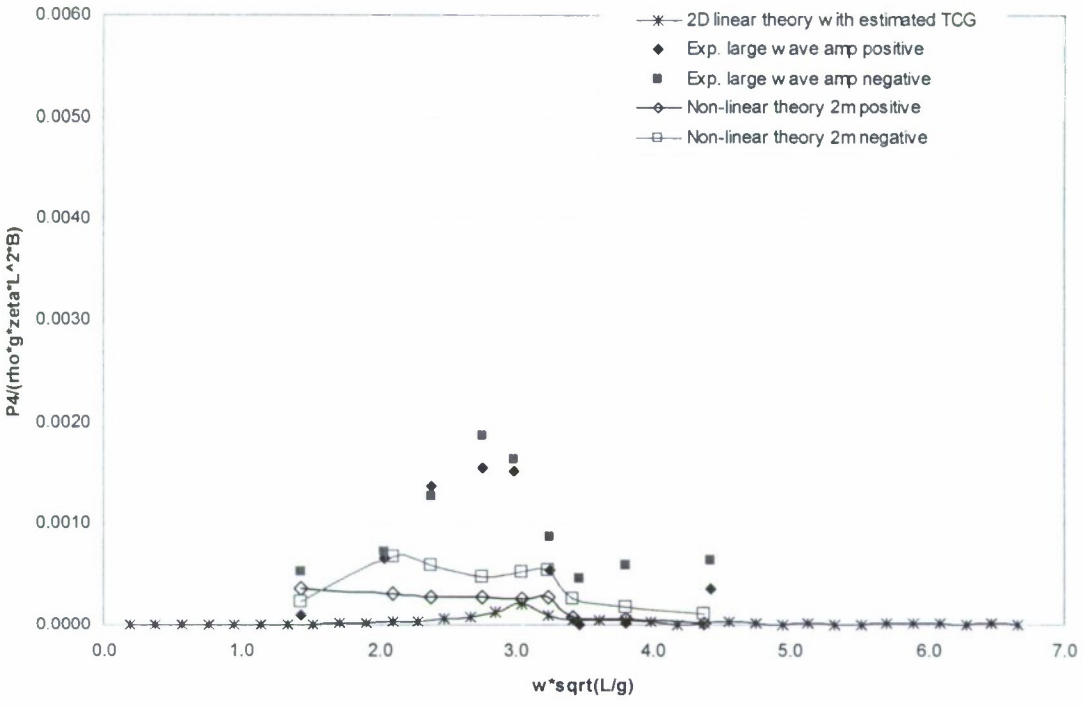

Figure 5.3-23: Dynamic torsion moment RAO
at head seas (heading 180), theory ζ = 2m

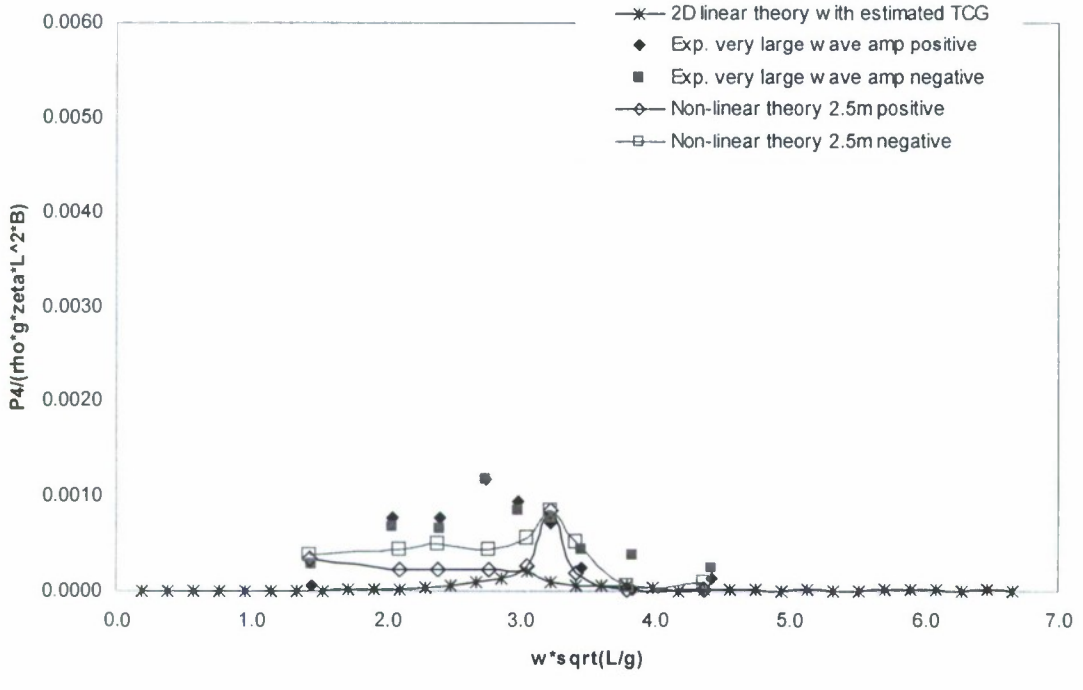

Figure 5.3-24: Dynamic torsion moment RAO
at head seas (heading 180), theory ζ = 2.5m

Stern quartering seas

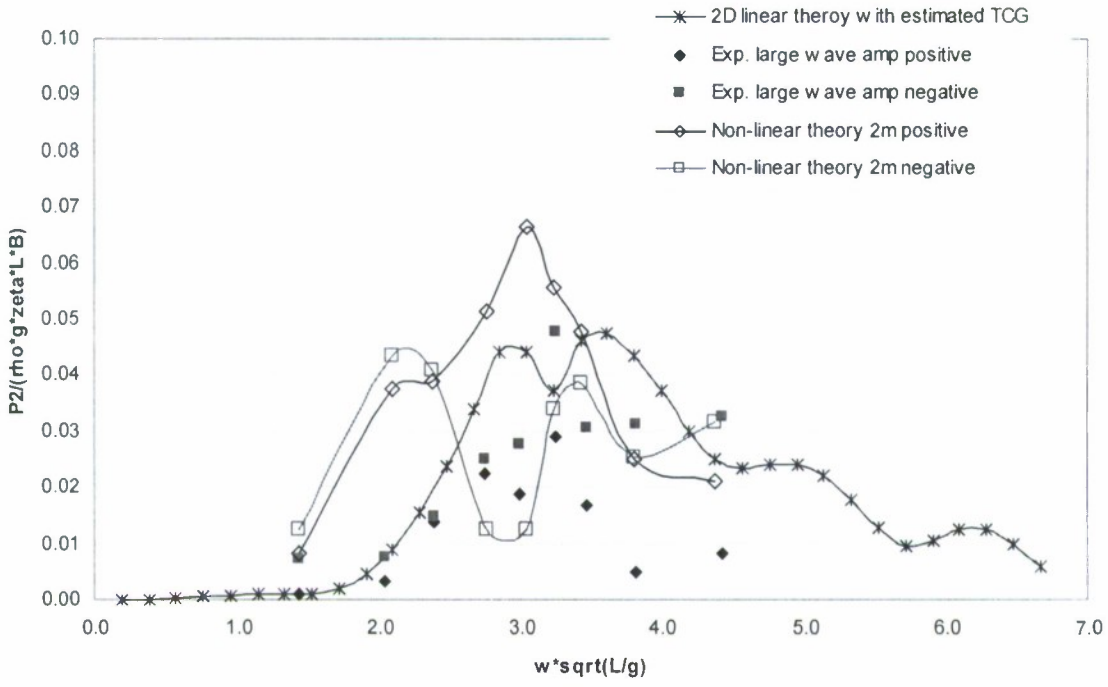

Figure 5.3-25: Dynamic horizontal shear force RAO at stern quartering seas (heading 45), theory ζ = 2m

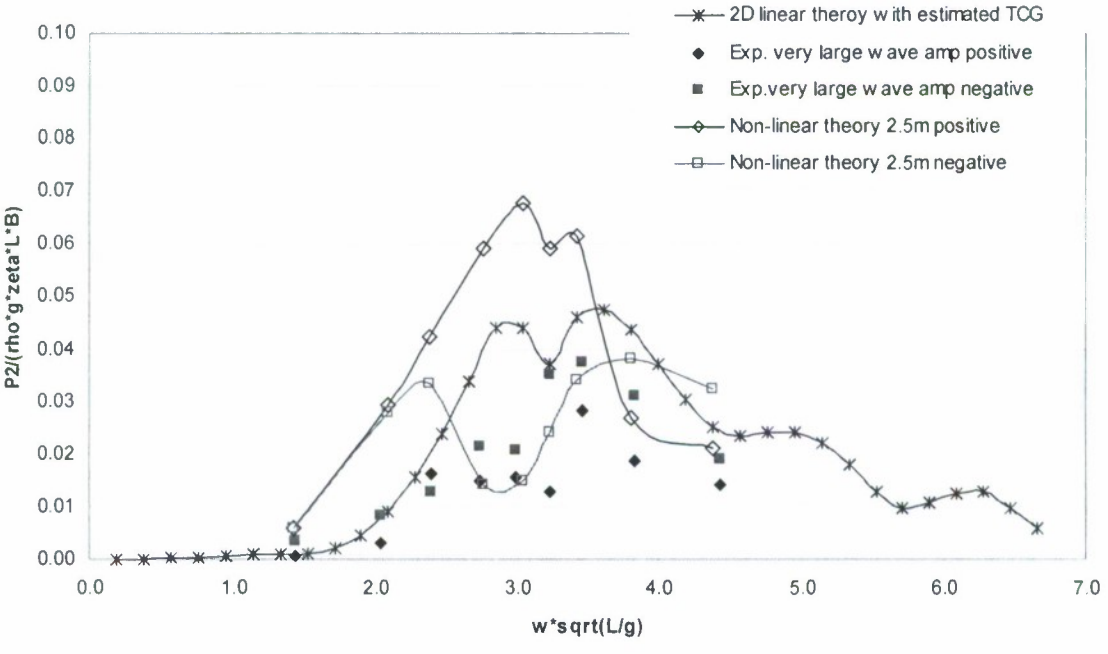

Figure 5.3-26: Dynamic horizontal shear force RAO at stern quartering seas (heading 45), theory ζ = 2.5m

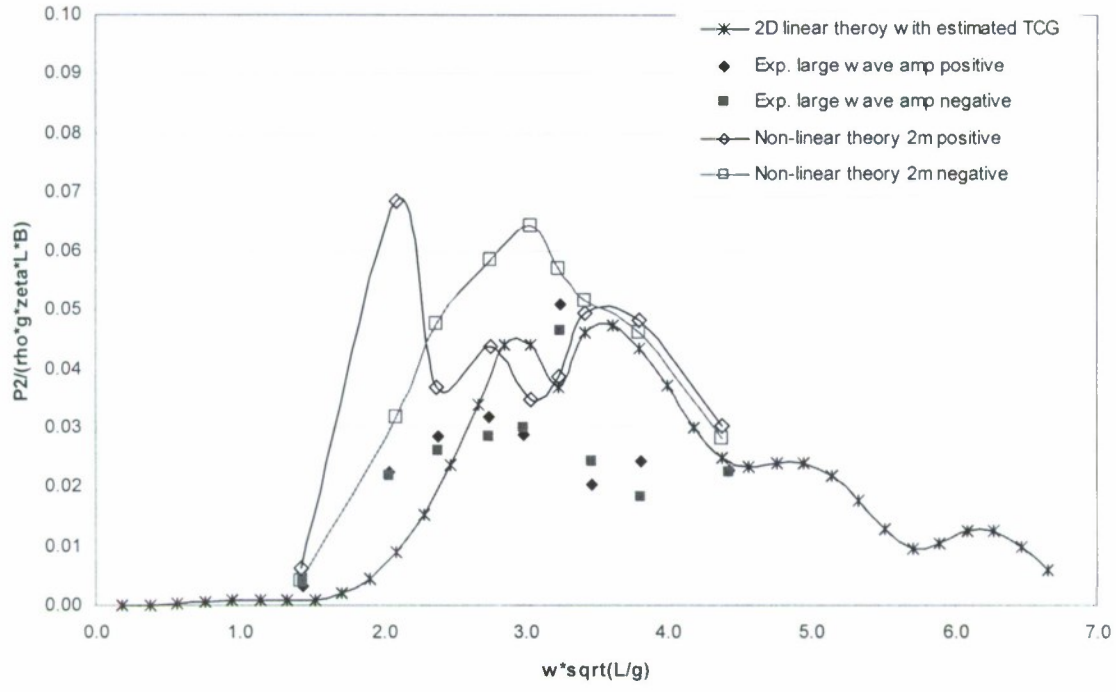

Figure 5.3-27: Dynamic vertical shear force RAO
at stern quartering seas (heading 45), theory ζ = 2m

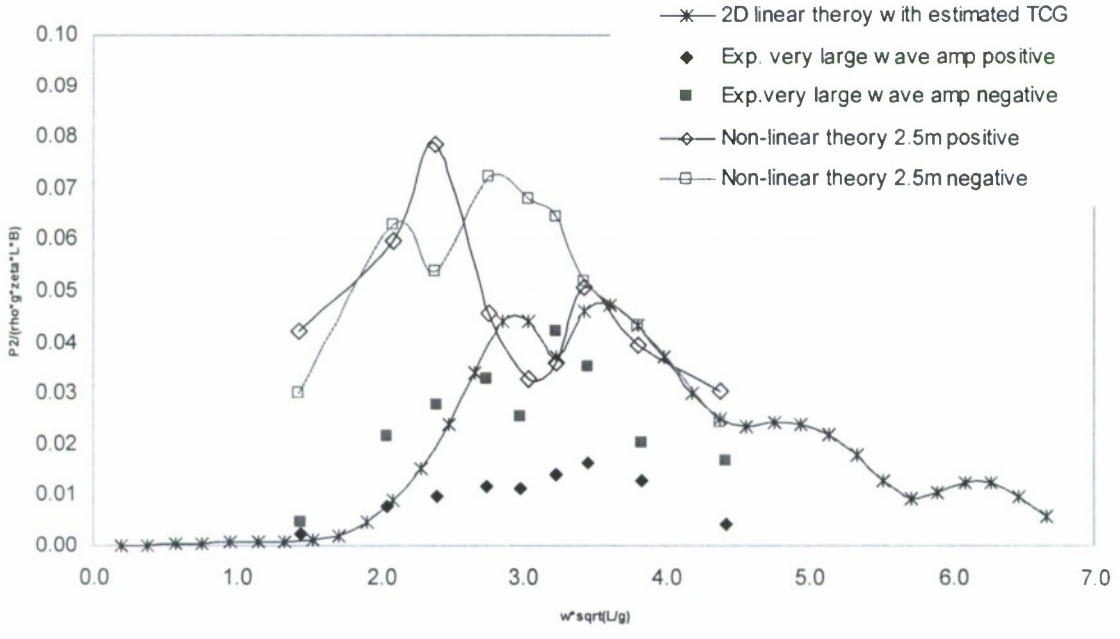

Figure 5.3-28: Dynamic vertical shear force RAO
at stern quartering seas (heading 45), theory ζ = 2.5m

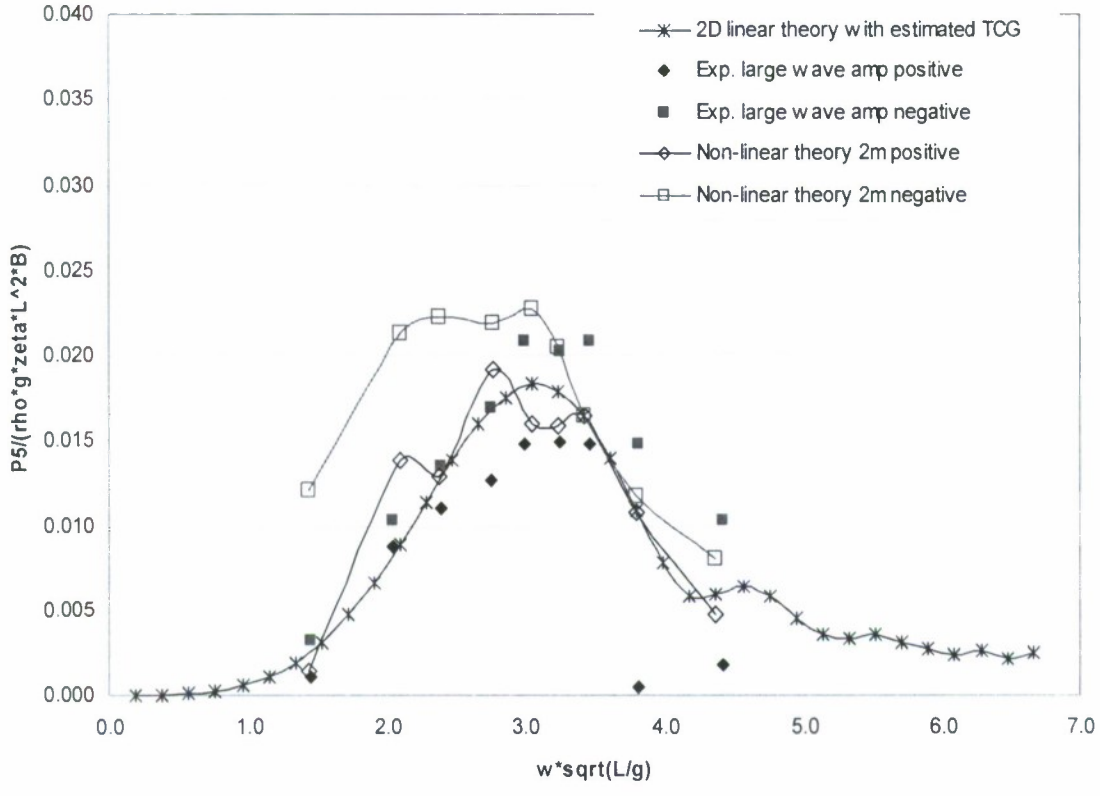

Figure 5.3-29: Dynamic vertical bending moment RAO at stern quartering seas (heading 45), theory ζ = 2m

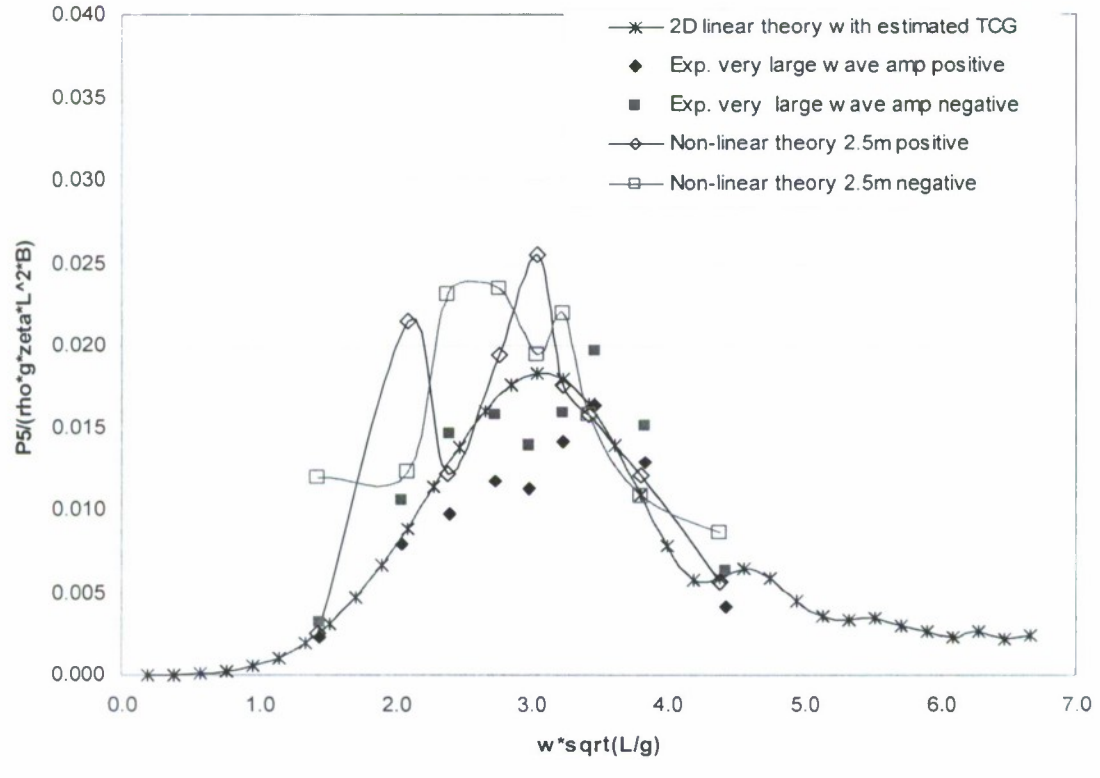

Figure 5.3-30: Dynamic vertical bending moment RAO at stern quartering seas (heading 45), theory ζ = 2.5m

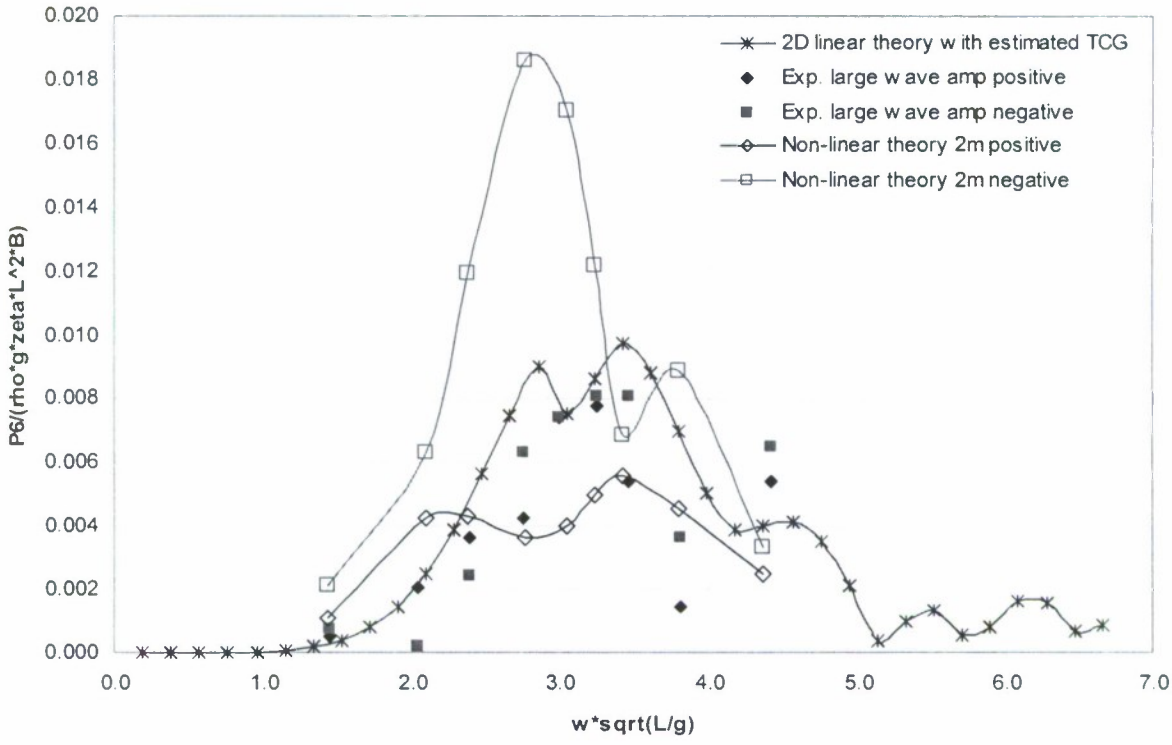

Figure 5.3-31: Dynamic horizontal bending moment RAO at stern quartering seas (heading 45), theory ζ = 2m

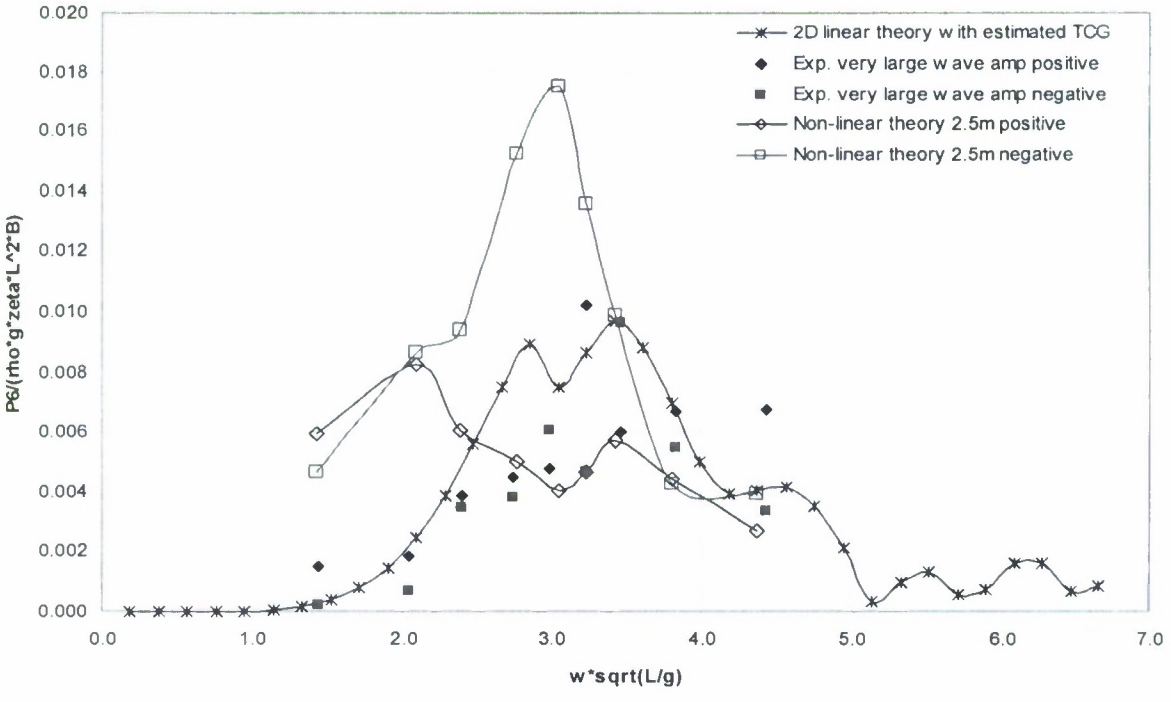

Figure 5.3-32: Dynamic horizontal bending moment RAO at stern quartering seas (heading 45), theory ζ = 2.5m

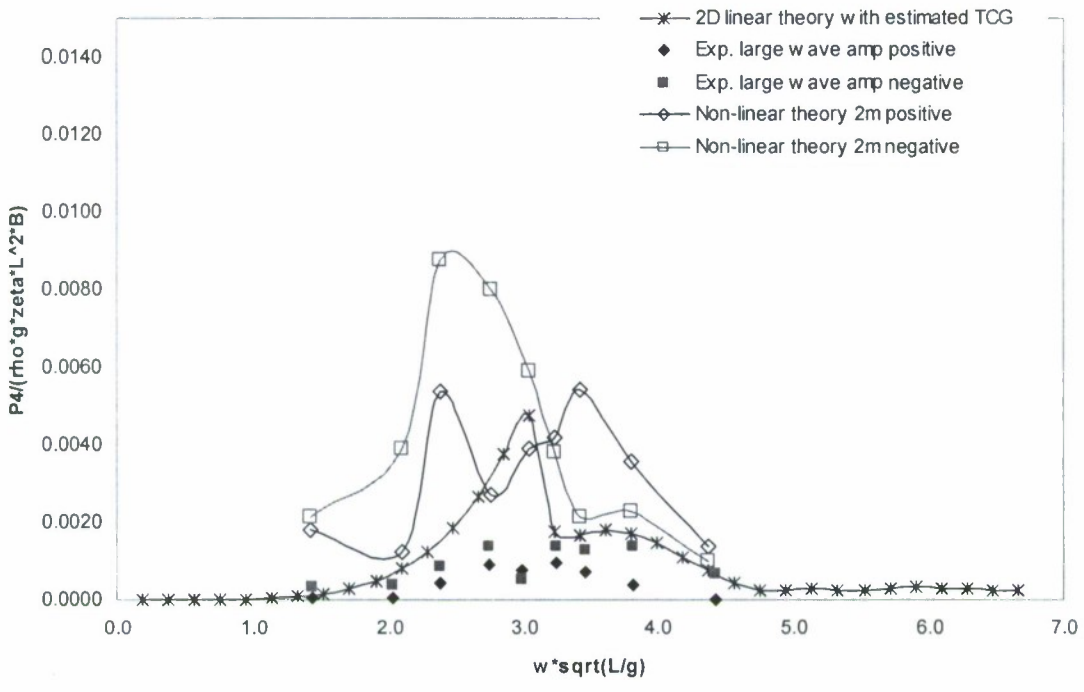

Figure 5.3-33: Dynamic torsion moment RAO
at stern quartering seas (heading 45), theory ζ = 2m

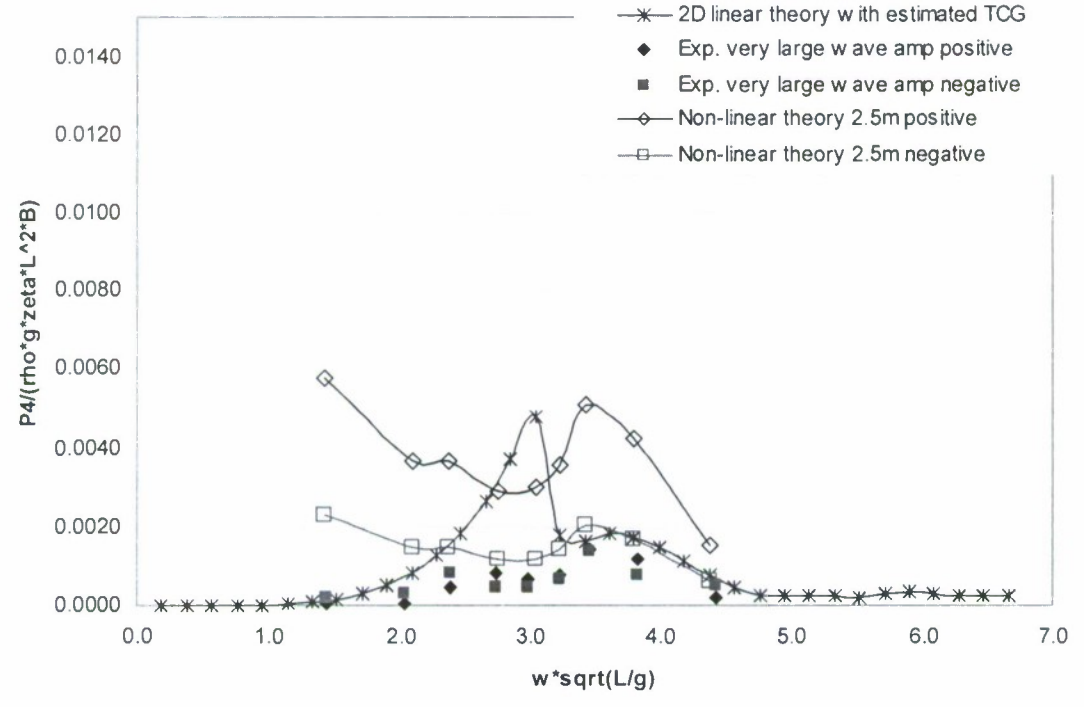

Figure 5.3-34: Dynamic torsion moment RAO
at stern quartering seas (heading 45), theory ζ = 2.5m

5.4 Model Uncertainties of the 2D Linear and Nonlinear Method

As mentioned in section 3.1.5 model uncertainty is a very important source of uncertainties in structural design process. Since a coefficient of variation (COV) of a typical strength prediction could be about 10 to 15% while a COV of wave-induced load prediction could be well above 30%, model uncertainties of wave-induced load prediction is a major uncertainty in structural strength assessment.

Table 5.4-1: Model uncertainties (X_{ml}) of the 2D linear method

design condition	load	heading	mean (S)	COV (S)	mean (L)	COV (L)	mean (V)	COV (V)
Intact	VBM	180	0.8879	0.1926	0.2446	0.2446	0.8879	0.2743
		45	1.0458	0.8879	0.9062	0.3760	0.9230	0.3374
		135	0.8647	0.2462	0.8443	0.2714	0.8053	0.6931
	HBM	180	small values ≈ 0		small values ≈ 0		small values ≈ 0	
		45	1.1190	0.7045	1.0192	0.6962	1.0458	0.4842
		135	0.7832	0.6414	0.5978	0.7393	0.9249	0.7063
	TM	180	small values ≈ 0		small values ≈ 0		small values ≈ 0	
		45	0.9638	1.3586	0.8660	1.4997	1.0264	1.2835
		135	0.5978	0.6027	0.9187	1.4778	1.0481	1.6661
DS2	VBM	180	0.9638	0.2698	0.7393	0.2145	0.7832	0.1834
		45	0.9638	0.2818	0.9744	0.1644	0.6404	0.2284
		315	0.9792	0.2991	1.0049	0.5182	0.9488	0.3998
	HBM	180	small values ≈ 0		small values ≈ 0		small values ≈ 0	
		45	1.1644	0.6721	0.9192	0.8660	0.2743	0.5020
		315	1.0190	0.4230	1.1236	0.5182	1.1247	0.3217
	TM	180	small values ≈ 0		small values ≈ 0		small values ≈ 0	
		45	0.2743	0.6414	0.8669	0.6754	0.6434	0.6093
		315	0.8277	0.5260	0.8734	0.4568	0.9341	0.4567
DS3	VBM	180	0.9638	0.1834	0.9187	0.3173	0.1834	1.0684
		45	0.9452	1.3586	0.8660	0.2446	0.8502	0.1812
	HBM	180	small values ≈ 0		small values ≈ 0		small values ≈ 0	
		45	0.7320	0.5978	0.7347	1.0949	0.2743	0.1926
	TM	180	small values ≈ 0		small values ≈ 0		small values ≈ 0	
		45	1.1452	1.3305	0.9247	1.2999	0.7901	1.1095

Hence the model uncertainties of the 2D linear method and 2D nonlinear method were calculated by using Eq. (3.1-33) in this section. Based on the observations in the previous sections, the accuracies of both linear and nonlinear methods are different for different load components. It would be interesting to quantitatively demonstrate this difference. So the model uncertainties are calculated separately for different load components. Conventionally model uncertainties were only predicted for intact condition, so it would be interesting to see how different the accuracy could be between the intact condition and the damaged conditions. A summary of model uncertainties (X_{ml}) of the 2D linear method and nonlinear method for vertical bending moment, horizontal bending moment as well as torsion moment are shown in

Tables 5.4-1 and -2, while the details of the model uncertainty calculations are presented in Appendices B and C.

In Table 5.4-1 Mean (S) and COV (S) stand for mean and COV for each load component in small wave amplitude; Mean (L) and COV (L) stand for mean and COV for each load component in large wave amplitude; Mean (V) and COV (V) stand for mean and COV for each load component in very large wave amplitude; VBM is vertical bending moment; HBM is horizontal bending moment; TM is torsion moment.

From Table 5.4-1 it is observed that the accuracy of vertical bending moment is generally better than that of horizontal bending moment and torsion moment, and the accuracy for loads in head seas is much better than those in stern quartering seas and beam seas. This could be mainly caused by the underwater hullform of the ship model with a small C_b compared with conventional ships. The COV of horizontal bending moment is almost as twice as that of vertical bending moment. The COV of torsion moment is the largest of the three. Because of the large difference in COV for different force components it is more rational to consider the model uncertainties for vertical bending moment, horizontal bending moment and torsion moment separately in reliability analysis rather than using one combined model uncertainty for all the components.

When the model uncertainties were calculated, the experimental results were assumed as the 'real response'. However there were also uncertainties in the tests, but unfortunately it was very difficult to quantify them although much effort has been made to reduce these uncertainties. One of the uncertainties in the current experiment was the way to measure the wave profile in terms of wave height and wave period. Two wave probes were placed in the front of the ship model to measure wave profile. Due to the effects of deflection of incident wave and radiation of the model's motion, the recorded wave in the second wave probe, which was nearer to the model, was subject to the interference, so could not be used. Therefore the wave profile measured by the first wave probe, which was further away from the model, was used to calculate RAO. It was possible that the wave profile at the first wave probe was slightly different from the wave profile at the ship model. Due to the limited availability of the towing tank, it was not possible to fully correlate the wave profile at these two locations so that this difference could be considered in the calculations.

The second uncertainty is caused by the mooring lines, which were attached to the fore and stern ends of the model, as mentioned in the previous sections. The mooring line could affect the model's motion, although more on the low frequency motions less on the wave frequency motions, and then wave-induced loads, especially the horizontal bending moment. However the forces in the mooring lines were not measured so that it was not possible to quantify the influence of the mooring lines on the horizontal bending moment.

The third uncertainty was the measurement of radius of gyration about x-axis (i.e. for roll motion). The roll radius of gyration of the model was measured by the method presented in Bhattacharyya (1978). In this method, a bar with circular cross-section was attached to the deck panel in the longitudinal direction (i.e. along the x-axis). Although the deck was strong enough to seal the model and to keep the model waterproof during the tests in the towing tank, it was not stiff enough so that it deformed noticeably when the whole model was hanging beneath the attached bar during the swing test. Therefore the accuracy in the measured roll radius of gyration may not be very good. This may cause the inaccuracy in the calculations of the natural frequency of roll and torsion moment. The large COV in torsion moment might be partly caused by this uncertainty.

Table 5.4-2 presents the model uncertainties of the 2D nonlinear method. In this table 'mean (2m)+' is mean value of model uncertainty under 2m wave weight from the positive responses; 'mean (2m)-' is mean value of model uncertainty under 2m wave weight from the negative responses; 'COV (2m)+' is coefficient of variation of model uncertainty under 2m wave weight from the positive responses; 'COV (2m)-' is coefficient of variation of model uncertainty under 2m wave weight from the negative responses; 'mean (2.5m)+' is mean value of model uncertainty under 2.5m wave weight from the positive responses; 'mean (2.5m)-' is mean value of model uncertainty under 2.5m wave weight from the negative responses; 'COV (2.5m)+' is coefficient of variation of model uncertainty under 2.5m wave weight from the positive responses; 'COV (2.5m)-' is coefficient of variation of model uncertainty under 2.5m wave weight from the negative responses; 'mean +' is mean value of model uncertainty under both 2m and 2.5m wave weight from the positive responses; 'mean -' is mean value of model uncertainty under both 2m and 2.5m wave weight from the negative responses; 'COV +' is coefficient of variation of model uncertainty under both 2m and 2.5m wave weight from the positive responses; 'COV -' is coefficient of variation of model uncertainty under both 2m and 2.5m wave weight from the negative responses. Comparing the results in Tables 5.4-1 and 5.4-2, it can be seen that the 2D linear method has better mean and COV of X_m in the predictions of vertical bending moment and horizontal bending moment in both intact condition and damage scenario 2 than the 2D nonlinear method, and both 2D linear and nonlinear methods have produced unsatisfactory results in torsion moment. Based on the current results, it may be said that the 2D linear method is more accurate than the nonlinear method. However the nonlinear method can distinguish the difference between the positive and negative responses, but linear methods can't. This advantage of the nonlinear method is especially important for ships with small block coefficient, such as frigate etc. For a frigate the ratio of sagging bending moment to hogging bending moment could be as large as 1.78 (Clarke, 1986). In addition, hull girder strength in hogging is normally different from that in sagging. Therefore the nonlinear method is preferred. This slight preference of the nonlinear method was also based on another fact that the nonlinear method tends to produce better results in the resonant region than at other frequencies. Based on the current method for combining different load components, the accuracy in resonant region is more important than that at other frequencies.

Table 5.4-2: Model uncertainties (X_{ml}) of the 2D non-linear method

design condition	load	heading	mean (2m) +	mean (2m) -	COV (2m) +	COV (2m) -	mean (2.5m) +	mean (2.5m) -	COV (2.5m) +	COV (2.5m) -	mean +	mean -	COV +	COV -
Intact	VBM	180	0.9365	1.2802	0.6332	1.0255	1.0382	0.6711	1.0040	0.3009	0.9743	0.9757	0.8413	0.9876
		45	0.9416	0.7365	0.9562	0.4032	0.8668	0.7926	0.4354	0.5354	0.7912	0.7646	0.8403	0.4662
	HBM	45	1.3567	0.5282	1.0998	0.6088	1.2072	0.5960	0.6585	0.7275	1.2820	0.5621	0.9067	0.6617
	TM	45	0.4955	0.4893	1.0838	0.4721	0.6664	0.4748	0.7152	0.5393	0.5810	0.4821	0.8483	0.4910
DS2	VBM	180	1.0838	0.5955	0.7537	0.4385	1.0307	0.8661	0.5186	0.3490	1.0557	0.6247	0.6280	0.3802
		45	0.7765	0.8661	0.8307	0.4113	0.7765	0.8661	0.3288	0.4025	0.7475	0.8372	0.3744	0.3969
	HBM	45	1.1085	0.8660	0.6034	0.9186	1.1479	0.5114	0.6758	0.8428	1.1282	0.5567	0.6231	0.8680
	TM	45	0.1295	0.3429	0.8507	0.8275	0.1706	0.3429	0.6280	0.5335	0.1500	0.3937	0.7165	0.6579

5.5 Prediction of Extreme Design Loads and Load Combinations

5.5.1 Prediction of extreme design loads using the results from the 2D linear method

The extreme design loads in irregular waves have been calculated by short term prediction, which was presented in Chapter 3, for the sample vessel at amidships, which is 70.5 m from AP, in intact condition and 3 damage scenarios. The 2D linear method has been used to predict RAOs of wave-induced dynamic loads in regular waves. For the clarity, only the extreme design loads, which will be used to assess the structural strength, are included here, while RAOs are presented in Appendix A.

Sea Condition

In order to predict the extreme design loads, environment conditions need to be specified. It is assumed that this vessel is to be operated in North Atlantic Ocean. Sea state specifications of the North Atlantic are presented in Table 5.5.1-1

Table 5.5.1-1 Annual sea state occurrences in the North Atlantic and North Pacific (Lee et al., 1985)

					North Atlantic			North Pacific		
Sea state no.	Significant wave height (m)		Sustained wind speed (knots)[a]		Percentage probability of sea state	Modal wave period (s)		Percentage probability of sea state	Modal wave period (s)	
	Range	Mean	Range	Mean		Range[b]	Most probable[c]		Range[b]	Most probable[c]
0–1	0–0.1	0.05	0–6	3	0.70	—	—	1.30	—	—
2	0.1–0.5	0.3	7–10	8.5	6.80	3.3–12.8	7.5	6.40	5.1–14.9	6.3
3	0.5–1.25	0.88	11–16	13.5	23.70	5.0–14.8	7.5	15.50	5.3–16.1	7.5
4	1.25–2.5	1.88	17–21	19	27.80	6.1–15.2	8.8	31.60	6.1–17.2	8.8
5	2.5–4	3.25	22–27	24.5	20.64	8.3–15.5	9.7	20.94	7.7–17.8	9.7
6	4–6	5	28–47	37.5	13.15	9.8–16.2	12.4	15.03	10.0–18.7	12.4
7	6–9	7.5	48–55	51.5	6.05	11.8–18.5	15.0	7.00	11.7–19.8	15.0
8	9–14	11.5	56–63	59.5	1.11	14.2–18.6	16.4	1.56	14.5–21.5	16.4
>8	>14	>14	>63	>63	0.05	18.0–23.7	20.0	0.07	16.4–22.5	20.0

As the purpose of this task is to evaluate vessel's survivability in damage conditions, the most severe sea condition has been chosen. Comparisons have been made among several sea areas provided by BMT global wave statistics data. Sea area 16 as illustrated in Figure 5.5.1-1 is the most severe sea condition in the North Atlantic. Table 5.5.1-2 shows the wave scatter diagram of sea area 16 under 12 months with 100000 observations.

Fig 5.5.1-1 Location of Sea area 16 (source: BMT)

Table 5.5.1-2 Wave scatter diagram of sea area 16 in the North Atlantic

Sig Hgt (m)	54	2601	28268	[illegible]	[illegible]	[illegible]	[illegible]	90322	33641	10283	2709	100000
> 14				1	11	66	176	259	242	159	79	994
13 to 14				1	11	57	134	174	143	84	37	640
12 to 13				2	23	109	240	293	229	127	54	1077
11 to 12				4	48	214	438	500	368	192	77	1842
10 to 11				9	106	429	811	863	594	292	111	3215
9 to 10			1	23	239	884	1532	1506	963	443	158	5748
8 to 9			2	61	562	1869	2941	2648	1562	666	222	10532
7 to 8			5	169	1366	4035	5699	4645	2500	980	302	19703
6 to 7			17	490	3404	8774	10946	7964	3860	1374	387	37217
5 to 6			64	1463	8609	18693	20173	12854	5514	1755	445	69470
4 to 5		2	242	4368	20522	37215	33739	18333	6796	1891	424	[illegible]
3 to 4		10	933	12415	44682	63727	46481	20711	6406	1510	290	[illegible]
2 to 3		60	3472	30724	77361	80193	43878	15070	3682	700	110	[illegible]
1 to 2	1	404	11000	52578	77910	50775	18425	4390	772	109	13	[illegible]
0 to 1	53	2124	12532	21782	14432	4587	858	110	11	1		56491
	< 4	4 ~ 5	5 ~ 6	6 ~ 7	7 ~ 8	8 ~ 9	9 ~ 10	10 ~ 11	11 ~ 12	12 ~ 13	> 13	
	Zero Crossing Period (s)											

Based on the information above, the significant wave height in each sea state and its corresponding zero crossing period in sea area 16 can be obtained as follows:

	Hs (m)	Zero crossing period (s)
sea state 3	1.25	7.5
sea state 4	2.5	8
sea state 5	4	8.5
sea state 6	6	9
sea state 7	9	10

ITTC SPECTRUM

The ITTC spectrum has been chosen for the extreme design load calculation, and can be expressed as

$$S(\omega) = \alpha g^2 \omega^{-5} \exp\left[-\frac{4\alpha g^2 \omega^{-4}}{H_s^2}\right] \quad [5.5.1\text{-}1]$$

Where, $\alpha = \frac{0.0081}{k^4}$ [5.5.1-2]

And, $k = \frac{\sqrt{g/\sigma}}{3.54\omega_z}$ [5.5.1-3]

in which $\sigma = \sqrt{m_0} = H_s/4$, the standard deviation (r.m.a. value) of the water surface elevation.

Tables 5.5.1-3 to -16 present the wave induced vertical, horizontal bending moment and torsion moment at sea states 3 - 7 for a duration of 96 hours. In those tables 'R_Max' is the most probable extreme design load, and 'R_design' is extreme design load with a probability of exceedance of 0.01 in N encounters. M_{wv} is vertical wave-induced bending moment, M_{wh} is horizontal wave-induced bending moment, TM is torsion moment, and M_S is stillwater bending moment.

Intact Condition

Table 5.5.1-3: Extreme design loads at stern quartering waves (heading 45)

	M_{wv} (Nm)	M_{wh} (Nm)	TM (Nm)	M_S (Nm)
Sea State 3				
R_Max	7.21E+07	3.61E+07	1.02E+07	
R_Design	8.63E+07	4.32E+07	1.22E+07	
Sea State 4				
R_Max	1.36E+08	6.79E+07	1.92E+07	1.65E+08
R_Design	1.63E+08	8.12E+07	2.29E+07	
Sea State 5				
R_Max	2.05E+08	1.01E+08	2.85E+07	
R_Design	2.45E+08	1.21E+08	3.42E+07	
Sea State 6				
R_Max	2.87E+08	1.41E+08	3.97E+07	
R_Design	3.44E+08	1.69E+08	4.75E+07	
Sea State 7				
R_Max	3.75E+08	1.82E+08	5.08E+07	
R_Design	4.49E+08	2.18E+08	6.09E+07	

Table 5.5.1-4: Extreme design loads at head waves (heading 180)

	M_{wv} (Nm)	M_{wh} (Nm)	TM (Nm)	M_S (Nm)
Sea State 3				
R_Max	8.92E+07	1.13E+02	4.18E+00	
R_Design	1.07E+08	1.35E+02	5.02E+00	
Sea State 4				
R_Max	1.74E+08	2.22E+02	8.21E+00	1.65E+08
R_Design	2.09E+08	2.66E+02	9.85E+00	
Sea State 5				
R_Max	2.69E+08	3.44E+02	1.28E+01	
R_Design	3.23E+08	4.13E+02	1.54E+01	
Sea State 6				
R_Max	3.86E+08	4.97E+02	1.87E+01	
R_Design	4.63E+08	5.96E+02	2.24E+01	
Sea State 7				
R_Max	5.22E+08	6.76E+02	2.65E+01	
R_Design	6.26E+08	8.12E+02	3.18E+01	

Table 5.5.1-5: Extreme design loads at beam waves (heading 90)

	M_{wv} (Nm)	M_{wh} (Nm)	TM (Nm)	M_S (Nm)
Sea State 3				
R_Max	1.01E+07	2.41E+07	1.52E+07	
R_Design	1.20E+07	2.88E+07	1.82E+07	
Sea State 4				
R_Max	1.90E+07	4.45E+07	2.81E+07	1.65E+08
R_Design	2.27E+07	5.32E+07	3.36E+07	
Sea State 5				
R_Max	2.86E+07	6.57E+07	4.14E+07	
R_Design	3.42E+07	7.85E+07	4.95E+07	
Sea State 6				
R_Max	4.05E+07	9.07E+07	5.69E+07	
R_Design	4.84E+07	1.08E+08	6.81E+07	
Sea State 7				
R_Max	5.39E+07	1.16E+08	7.18E+07	
R_Design	6.44E+07	1.38E+08	8.59E+07	

Damage Scenario 1

Table 5.5.1-6: Extreme design loads at stern quartering waves (heading 45)

	M_{wv} (Nm)	M_{wh} (Nm)	TM (Nm)	M_S (Nm)
Sea State 3				
R_Max	7.48E+07	3.82E+07	8.14E+06	
R_Design	8.95E+07	4.57E+07	9.74E+06	
Sea State 4				
R_Max	1.42E+08	7.12E+07	1.53E+07	5.51E+07
R_Design	1.70E+08	8.52E+07	1.83E+07	
Sea State 5				
R_Max	2.14E+08	1.06E+08	2.28E+07	
R_Design	2.57E+08	1.27E+08	2.72E+07	
Sea State 6				
R_Max	3.02E+08	1.47E+08	3.17E+07	
R_Design	3.62E+08	1.76E+08	3.79E+07	
Sea State 7				
R_Max	3.97E+08	1.88E+08	4.06E+07	
R_Design	4.75E+08	2.25E+08	4.87E+07	

Table 5.5.1-7: Extreme design loads at head waves (heading 180)

	M_{wv} (Nm)	M_{wh} (Nm)	TM (Nm)	M_S (Nm)
Sea State 3				
R_Max	9.26E+07	1.07E+02	1.05E+01	
R_Design	1.11E+08	1.28E+02	1.25E+01	
Sea State 4				
R_Max	1.82E+08	2.12E+02	2.08E+01	5.51E+07
R_Design	2.18E+08	2.54E+02	2.49E+01	
Sea State 5				
R_Max	2.82E+08	3.30E+02	3.30E+01	
R_Design	3.38E+08	3.95E+02	3.96E+01	
Sea State 6				
R_Max	4.06E+08	4.77E+02	4.91E+01	
R_Design	4.87E+08	5.72E+02	5.90E+01	
Sea State 7				
R_Max	5.51E+08	6.51E+02	7.22E+01	
R_Design	6.61E+08	7.82E+02	8.68E+01	

Table 5.5.1-8: Extreme design loads at beam waves

	M_{wv} (Nm)	M_{wh} (Nm)	TM (Nm)	M_S (Nm)
Sea State 3				
R_Max	9.09E+06	2.14E+07	1.39E+07	
R_Design	1.08E+07	2.56E+07	1.66E+07	
Sea State 4				
R_Max	1.62E+07	3.88E+07	2.54E+07	5.51E+07
R_Design	1.92E+07	4.63E+07	3.03E+07	
Sea State 5				
R_Max	2.32E+07	5.62E+07	3.70E+07	
R_Design	2.75E+07	6.71E+07	4.42E+07	
Sea State 6				
R_Max	3.13E+07	7.65E+07	5.06E+07	
R_Design	3.72E+07	9.13E+07	6.05E+07	
Sea State 7				
R_Max	3.87E+07	9.52E+07	6.33E+07	
R_Design	4.59E+07	1.14E+08	7.57E+07	

Damage Scenario 2

Table 5.5.1-9: Extreme design loads at stern quartering waves (heading 45)

	M_{wv} (Nm)	M_{wh} (Nm)	TM (Nm)	M_S (Nm)
Sea State 3				
R_Max	7.71E+07	3.59E+07	1.01E+07	
R_Design	9.23E+07	4.29E+07	1.21E+07	
Sea State 4				
R_Max	1.47E+08	6.65E+07	1.94E+07	3.75E+07
R_Design	1.76E+08	7.95E+07	2.32E+07	
Sea State 5				
R_Max	2.24E+08	9.82E+07	2.95E+07	
R_Design	2.68E+08	1.17E+08	3.53E+07	
Sea State 6				
R_Max	3.17E+08	1.36E+08	4.18E+07	
R_Design	3.79E+08	1.62E+08	5.01E+07	
Sea State 7				
R_Max	4.20E+08	1.72E+08	5.55E+07	
R_Design	5.03E+08	2.06E+08	6.65E+07	

Table 5.5.1-10: Extreme design loads at head waves

	M_{wv} (Nm)	M_{wh} (Nm)	TM (Nm)	M_S (Nm)
Sea State 3				
R_Max	9.79E+07	6.79E+05	1.85E+05	
R_Design	1.17E+08	8.12E+05	2.21E+05	
Sea State 4				
R_Max	1.93E+08	1.27E+06	3.56E+05	3.75E+07
R_Design	2.31E+08	1.52E+06	4.27E+05	
Sea State 5				
R_Max	3.00E+08	1.89E+06	5.45E+05	
R_Design	3.60E+08	2.25E+06	6.53E+05	
Sea State 6				
R_Max	4.33E+08	2.62E+06	7.78E+05	
R_Design	5.19E+08	3.14E+06	9.32E+05	
Sea State 7				
R_Max	5.90E+08	3.37E+06	1.04E+06	
R_Design	7.09E+08	4.03E+06	1.25E+06	

Table 5.5.1-11: Extreme design loads at beam waves (heading 90)

	M_{wv} (Nm)	M_{wh} (Nm)	TM (Nm)	M_S (Nm)
Sea State 3				
R_Max	2.53E+07	1.98E+07	1.64E+06	
R_Design	3.01E+07	2.35E+07	1.94E+06	
Sea State 4				
R_Max	4.54E+07	3.55E+07	2.90E+06	3.75E+07
R_Design	5.41E+07	4.23E+07	3.44E+06	
Sea State 5				
R_Max	6.56E+07	5.11E+07	4.13E+06	
R_Design	7.81E+07	6.09E+07	4.90E+06	
Sea State 6				
R_Max	8.91E+07	6.93E+07	5.55E+06	
R_Design	1.06E+08	8.26E+07	6.58E+06	
Sea State 7				
R_Max	1.11E+08	8.58E+07	6.78E+06	
R_Design	1.32E+08	1.02E+08	8.05E+06	

Table 5.5.1-12: Extreme design loads beam waves (heading 270)

	M_{wv} (Nm)	M_{wh} (Nm)	TM (Nm)	M_S (Nm)
Sea State 3				
R_Max	2.58E+07	1.91E+07	1.64E+06	
R_Design	3.07E+07	2.28E+07	1.94E+06	
Sea State 4				
R_Max	4.63E+07	3.44E+07	2.90E+06	3.75E+07
R_Design	5.52E+07	4.09E+07	3.44E+06	
Sea State 5				
R_Max	6.68E+07	4.95E+07	4.13E+06	
R_Design	7.96E+07	5.90E+07	4.90E+06	
Sea State 6				
R_Max	9.07E+07	6.72E+07	5.55E+06	
R_Design	1.08E+08	8.00E+07	6.58E+06	
Sea State 7				
R_Max	1.13E+08	8.32E+07	6.78E+06	
R_Design	1.34E+08	9.91E+07	8.05E+06	

Table 5.5.1-13: Extreme design loads at stern quartering waves (heading 315)

	M_{wv} (Nm)	M_{wh} (Nm)	TM (Nm)	M_S (Nm)
Sea State 3				
R_Max	7.71E+07	3.65E+07	1.01E+07	
R_Design	9.23E+07	4.36E+07	1.21E+07	
Sea State 4				
R_Max	1.47E+08	6.77E+07	1.94E+07	3.75E+07
R_Design	1.76E+08	8.09E+07	2.32E+07	
Sea State 5				
R_Max	2.24E+08	9.99E+07	2.95E+07	
R_Design	2.68E+08	1.20E+08	3.53E+07	
Sea State 6				
R_Max	3.17E+08	1.38E+08	4.18E+07	
R_Design	3.79E+08	1.65E+08	5.01E+07	
Sea State 7				
R_Max	4.20E+08	1.76E+08	5.55E+07	
R_Design	5.03E+08	2.10E+08	6.65E+07	

Damage Scenario 3

Table 5.5.1-14: Extreme design loads at stern quartering waves (heading 45)

	M_{wv} (Nm)	M_{wh} (Nm)	TM (Nm)	M_S (Nm)
Sea State 3				
R_Max	6.96E+07	3.37E+07	8.49E+06	
R_Design	8.33E+07	4.04E+07	1.02E+07	
Sea State 4				
R_Max	1.32E+08	6.33E+07	1.62E+07	-2.47E+08
R_Design	1.58E+08	7.57E+07	1.94E+07	
Sea State 5				
R_Max	1.98E+08	9.44E+07	2.44E+07	
R_Design	2.37E+08	1.13E+08	2.93E+07	
Sea State 6				
R_Max	2.77E+08	1.32E+08	3.44E+07	
R_Design	3.32E+08	1.57E+08	4.12E+07	
Sea State 7				
R_Max	3.62E+08	1.70E+08	4.52E+07	
R_Design	4.33E+08	2.04E+08	5.42E+07	

Table 5.5.1-15: Extreme design loads at head waves

	M_{wv} (Nm)	M_{wh} (Nm)	TM (Nm)	M_S (Nm)
Sea State 3				
R_Max	8.86E+07	6.19E-04	1.91E-05	
R_Design	1.06E+08	7.35E-04	2.27E-05	
Sea State 4				
R_Max	1.73E+08	1.09E-03	3.38E-05	-2.47E+08
R_Design	2.07E+08	1.30E-03	4.01E-05	
Sea State 5				
R_Max	2.67E+08	1.55E-03	4.80E-05	
R_Design	3.20E+08	1.84E-03	5.70E-05	
Sea State 6				
R_Max	3.82E+08	2.08E-03	6.44E-05	
R_Design	4.59E+08	2.47E-03	7.64E-05	
Sea State 7				
R_Max	5.16E+08	2.54E-03	7.85E-05	
R_Design	6.19E+08	3.02E-03	9.31E-05	

Table 5.5.1-16: Extreme design loads at beam waves

	M_{wv} (Nm)	M_{wh} (Nm)	TM (Nm)	M_S (Nm)
Sea State 3				
R_Max	1.09E+07	1.32E+07	9.41E+05	
R_Design	1.30E+07	1.58E+07	1.12E+06	
Sea State 4				
R_Max	2.04E+07	2.50E+07	1.68E+06	-2.47E+08
R_Design	2.44E+07	2.98E+07	1.99E+06	
Sea State 5				
R_Max	3.07E+07	3.77E+07	2.41E+06	
R_Design	3.67E+07	4.50E+07	2.86E+06	
Sea State 6				
R_Max	4.33E+07	5.32E+07	3.25E+06	
R_Design	5.18E+07	6.36E+07	3.86E+06	
Sea State 7				
R_Max	5.75E+07	7.11E+07	4.00E+06	
R_Design	6.88E+07	8.49E+07	4.75E+06	

5.5.2 Prediction of extreme design loads using the results from the 2D Non-linear method

In this section the short term prediction is used to predict extreme design loads in irregular waves by using the results of the 2D nonlinear method in regular waves. Strictly speaking the short term prediction is only valid in linear range, so it is not desirable to mix it with the 2D nonlinear method. However this method can produce results quickly and fairly accurately. The 2D nonlinear method has been used to calculate the wave-induced loads in time domain in regular waves, and the time series have then been converted to RAOs for each load components. Finally the RAOs have been used in short term prediction to calculate extreme design value for each load components. An immediate issue to be addressed in this context is what wave amplitude should be used to calculate RAOs because different wave amplitudes would lead to different values of RAOs due to the nonlinearity in the responses. 2 wave amplitudes, namely 2.0 m and 2.5 m, have been chosen to calculate RAOs of wave-induced loads in order to see how much difference would be in the predicted extreme design loads.

Firstly the 2D nonlinear method has been applied to predict extreme design value of hogging and sagging bending moment at the cut of the ship model in intact condition at head seas with duration of 96 hours under 2 different wave amplitudes, namely 2.0 m and 2.5 m. The results were presented in Table 5.5.2-1. Similarly the 2D nonlinear method has also been applied to predict extreme design value of hogging and sagging bending moment at the cut of the ship model in damage scenario 2 at head seas with duration of 12 hours under 2 different wave amplitudes. The results were shown in Table 5.5.2-2. It can be seen that the difference of extreme design loads (both hogging and sagging) between 2m and 2.5m wave height was increasing with the increase of sea roughness, but always less than 6.62% in intact condition and 6.60% in damage scenario 2. For hogging bending moment, the extreme design value based on 2m wave height is greater than that based on 2.5m wave height, but it was opposite for sagging bending moment.

Table 5.5.2-1: Extreme design loads by the 2D nonlinear method in intact condition

	M_{wv} (Nm) , Hogging			M_{wv} (Nm) , Sagging		
	(2m)	(2.5m)	% difference	(2m)	(2.5m)	% difference
Sea State 3						
R_Max	7.83E+07	7.66E+07	2.22E+00	9.60E+07	1.01E+08	-4.95E+00
R_Design	9.38E+07	9.18E+07	2.18E+00	1.15E+08	1.21E+08	-4.96E+00
Sea State 4						
R_Max	1.54E+08	1.51E+08	1.99E+00	1.88E+08	1.99E+08	-5.53E+00
R_Design	1.85E+08	1.81E+08	2.21E+00	2.26E+08	2.39E+08	-5.44E+00
Sea State 5						
R_Max	2.39E+08	2.33E+08	2.58E+00	2.91E+08	3.09E+08	-5.83E+00
R_Design	2.87E+08	2.80E+08	2.50E+00	3.49E+08	3.71E+08	-5.93E+00
Sea State 6						
R_Max	3.43E+08	3.34E+08	2.69E+00	4.18E+08	4.45E+08	-6.07E+00
R_Design	4.12E+08	4.00E+08	3.00E+00	5.01E+08	5.34E+08	-6.18E+00
Sea State 7						
R_Max	4.60E+08	4.46E+08	3.14E+00	5.64E+08	6.04E+08	-6.62E+00
R_Design	5.52E+08	5.35E+08	3.18E+00	6.77E+08	7.25E+08	-6.62E+00

Table 5.5.2-2: Extreme design loads by the 2D nonlinear method in DS2

	M_{wv} (Nm) Hogging			M_{wv} (Nm) Sagging		
	(2m)	(2.5m)	% difference	(2m)	(2.5m)	% difference
Sea State 3						
R_Max	6.31E+07	6.17E+07	2.27E+00	7.74E+07	8.13E+07	-4.80E+00
R_Design	7.84E+07	7.67E+07	2.22E+00	9.62E+07	1.01E+08	-4.75E+00
Sea State 4						
R_Max	1.24E+08	1.21E+08	2.48E+00	1.52E+08	1.61E+08	-5.59E+00
R_Design	1.55E+08	1.51E+08	2.65E+00	1.89E+08	2.00E+08	-5.50E+00
Sea State 5						
R_Max	1.93E+08	1.88E+08	2.66E+00	2.35E+08	2.49E+08	-5.62E+00
R_Design	2.40E+08	2.34E+08	2.56E+00	2.92E+08	3.10E+08	-5.81E+00
Sea State 6						
R_Max	2.77E+08	2.69E+08	2.97E+00	3.37E+08	3.59E+08	-6.13E+00
R_Design	3.44E+08	3.34E+08	2.99E+00	4.19E+08	4.47E+08	-6.26E+00
Sea State 7						
R_Max	3.71E+08	3.59E+08	3.34E+00	4.55E+08	4.87E+08	-6.57E+00
R_Design	4.61E+08	4.47E+08	3.13E+00	5.66E+08	6.06E+08	-6.60E+00

In order to further evaluate the results from the 2D nonlinear method, RAOs obtained in the experimental tests have also been used to predict extreme design loads. Similarly 2 different sets of wave amplitudes, namely large amplitude waves and very large amplitude waves, have been used separately to calculate extreme design loads. Because the experimental data were available only at the cut (the section where the force gauge was installed) of the ship model, the extreme design loads presented in this section were for the ship model at the cut, which was 54.5cm apart from AP. The sea area 16 at the Atlantic Ocean under sea state 3 to sea state 7 was used in short term predictions. A duration of 96 hours was used in the short term prediction for the intact condition while a reduced duration of 12 hours, which was recommended in Lloyds Register's Navy Vessel Rule (Lloyds Register of Shipping, 2002), was used for damage scenario 2. The results of the above calculations have been presented in Tables 5.5.2-3 and -4 for intact condition and damage scenario 2 respectively.

In addition, also presented in Tables 5.5.2-3 and -4 were the results obtained from the analytical formulae, which were recommended in Lloyds Register's Navy Vessel Rules (Lloyds Register of Shipping, 2002). The details of the formulae used in this study were presented in Appendix D.

Table 5.5.2-3: Extreme vertical bending moment in intact condition

	Extreme Design Load (Nm), Hogging	Extreme Design Load (Nm), Sagging	Sagging/Hogging Ratio
Nonlinear method[a]	5.52E+08	6.77E+08	1.23
Nonlinear method[b]	5.35E+08	7.25E+08	1.36
Rules[c]	5.58E+08	7.00E+08	1.25
Experiment[d]	4.01E+08	5.45E+08	1.36
Experiment[e]	3.67E+08	5.22E+08	1.42
Lincar method	5.52E+08	5.52E+08	1.00

Table 5.5.2-4: Extreme vertical bending moment in damage scenario 2

	Extreme Design Load (Nm), Hogging	Extreme Design Load (Nm), Sagging	Sagging/Hogging Ratio
Nonlinear method[a]	4.61E+08	5.66E+08	1.23
Nonlinear method[b]	4.47E+08	6.06E+08	1.36
Rules[c]	3.13E+08	3.92E+08	1.25
Experiment[d]	3.35E+08	4.55E+08	1.36
Experiment[e]	3.07E+08	4.36E+08	1.42
Linear method	5.38E+08	5.38E+08	1.00

The footnotes in Tables 5.5.2-3 and -4 are as follows:

a: Using RAOs from the 2D non-linear method under constant wave amplitude 2m.
b: Using RAOs from the 2D non-linear method under constant wave amplitude 2.5m.
c: Using the formulae in Lloyds Register's Navy Vessel Rules.
d: Using RAOs obtained from the experiment with large wave amplitude.
e: Using RAOs obtained from the experiment with very large wave amplitude.

From Table 5.5.2-3 it can be seen that the 2D nonlinear method overestimates extreme design hogging bending moment by 37.7% and 45.8% for 2.0m and 2.5m wave height respectively. Similarly it overestimates extreme design sagging bending moment by 24.2% and 38.9%. However the 2D linear method overestimates extreme design hogging bending moment by 37.7% and 50.4% for 2.0m and 2.5m wave height respectively, and overestimates extreme design sagging bending moment by 1.3% and 5.8% for 2.0m and 2.5m wave height respectively. Hence the results in intact condition are slightly in favour of the 2D linear method.

Similar comparison has also been applied to the results in Table 5.5.2-4. The 2D nonlinear method overestimates extreme design hogging bending moment by 37.6% and 45.6% for 2.0m and 2.5m wave height respectively, and overestimates extreme design sagging bending moment by 24.4% and 39.0%. However the 2D linear method overestimates extreme design hogging bending moment by 60.6% and 75.2% for 2.0m and 2.5m wave height respectively, and overestimates extreme design sagging bending moment by 18.2% and 23.4% for 2.0m and 2.5m wave height respectively. Therefore the accuracy of the 2D linear method is almost as good as that of the 2D nonlinear method in damage scenario 2.

In Table 5.5.2-3, both hogging and sagging bending moments of the 2D nonlinear method agree well with those of LR Rules' formulae. However hogging bending moment of the 2D linear method agrees well with that of LR Rules' formulae, but agreement in sagging bending moment is not as good as in hogging bending moment because in the 2D linear method the sagging bending moment is the same as hogging bending moment. It should be pointed out that the extreme design value predicted by LR Rules is the maximum value for the ship model. In another word, the extreme design value at the cut is the same as that of the sections at the amidships because the cut is not far away from amidships. However the extreme design value predicted by the 2D nonlinear method at the cut could potentially be quite different from that of the sections at amidships, where the maximum vertical bending moment would occur. This might, at least partly, explain that LR Rules produces the largest extreme design hogging and sagging moments in intact condition.

The ratio of sagging bending moment to hogging bending moment of the 2D nonlinear method is in good agreement with that of the experimental tests. This is an advantage of the 2D nonlinear method over the 2D linear method.

5.5.3 Load combinations for strength assessment

The load components are combined for both intact condition and damage scenario 1 using the methods described in section 3.2, based on the results predicted by the 2D linear method. The loads are for the cross-section, which is 70.5 meters from AP. The details are presented in Tables 5.5.3-1 and 5.5.3-2.

Table 5.5.3-1 Load combinations in intact condition at 45 heading

Ms	1.65E+08				
RAO^{My}_{max}	7.68E+07	RAO^{Mz}_{max}	4.25E+07	RAO^{Mx}_{max}	1.74E+07
ω_1	0.85	ω_2	0.75	ω_3	0.75
		RAO_1^{Mz}	3.48E+07	RAO_1^{Mx}	3.76E+06
RAO_2^{My}	6.92E+07			RAO_2^{Mx}	1.74E+07
RAO_3^{My}	6.92E+07	RAO_3^{Mz}	4.25E+07		
Sea state 3					
M_y^{max}	8.63E+07	M_z^{max}	4.32E+07	M_x^{max}	1.22E+07
H_{eq1}	1.12E+00	H_{eq2}	1.02E+00	H_{eq3}	7.01E-01
Load combination without Ms					
		M_y	M_z	M_x	

		component	component	component	
LC1		8.63E+07	3.91E+07	4.23E+06	
LC2		7.03E+07	4.32E+07	1.77E+07	
LC3		4.85E+07	2.98E+07	1.22E+07	
Sea state 4					
M_y^{max}	1.63E+08	M_z^{max}	8.12E+07	M_x^{max}	2.29E+07
H_{eq1}	2.12E+00	H_{eq2}	1.91E+00	H_{eq3}	1.32E+00
Load combination without Ms					
		M_y component	M_z component	M_x component	
LC1		1.63E+08	7.39E+07	7.98E+06	
LC2		1.32E+08	8.12E+07	3.32E+07	
LC3		9.11E+07	5.59E+07	2.29E+07	
Sea state 5					
M_y^{max}	2.45E+08	M_z^{max}	1.21E+08	M_x^{max}	3.42E+07
H_{eq1}	3.19E+00	H_{eq2}	2.85E+00	H_{eq3}	1.97E+00
Load combination without Ms					
		M_y component	M_z component	M_x component	
LC1		2.45E+08	1.11E+08	1.20E+07	
LC2		1.97E+08	1.21E+08	4.95E+07	
LC3		1.36E+08	8.35E+07	3.42E+07	
Sea state 6					
M_y^{max}	3.44E+08	M_z^{max}	1.69E+08	M_x^{max}	4.75E+07
H_{eq1}	4.48E+00	H_{eq2}	3.98E+00	H_{eq3}	2.73E+00
Load combination without Ms					
		M_y component	M_z component	M_x component	
LC1		3.44E+08	1.56E+08	1.68E+07	

LC2		2.75E+08	1.69E+08	6.92E+07	
LC3		1.89E+08	1.16E+08	4.75E+07	
Sea state 7					
M_y^{max}	4.49E+08	M_z^{max}	2.18E+08	M_x^{max}	6.09E+07
H_{eq1}	5.85E+00	H_{eq2}	5.13E+00	H_{eq3}	3.50E+00
Load combination without Ms					
		M_y component	M_z component	M_x component	
LC1		4.49E+08	2.03E+08	2.20E+07	
LC2		3.55E+08	2.18E+08	8.93E+07	
LC3		2.42E+08	1.49E+08	6.09E+07	

Table 5.5.3-2 Load combinations in damage scenario 1 at 45 heading

Ms	5.51E+07				
RAO_{max}^{My}	7.65E+07	RAO_{max}^{Mz}	3.99E+07	RAO_{max}^{Mx}	1.27E+07
ω_1	0.85	ω_2	0.8	ω_3	0.8
		RAO_1^{Mz}	3.59E+07	RAO_1^{Mx}	7.05E+06
RAO_2^{My}	7.65E+07			RAO_2^{Mx}	1.27E+07
RAO_3^{My}	7.65E+07	RAO_3^{Mz}	3.99E+07		
Sea state 3					
M_y^{max}	8.95E+07	M_z^{max}	4.57E+07	M_x^{max}	9.74E+06
H_{eq1}	1.17E+00	H_{eq2}	1.15E+00	H_{eq3}	7.67E-01
Load combination without Ms					
		M_y component	M_z component	M_x component	
LC1		8.95E+07	4.20E+07	8.25E+06	
LC2		8.76E+07	4.57E+07	1.45E+07	
LC3		5.87E+07	3.06E+07	9.74E+06	

Sea state 4					
M_y^{max}	1.70E+08	M_z^{max}	8.52E+07	M_x^{max}	1.83E+07
H_{eq1}	2.22E+00	H_{eq2}	2.14E+00	H_{eq3}	1.44E+00
Load combination without Ms					
		M_y component	M_z component	M_x component	
LC1		1.70E+08	7.98E+07	1.57E+07	
LC2		1.63E+08	8.52E+07	2.71E+07	
LC3		1.10E+08	5.75E+07	1.83E+07	
Sea state 5					
M_y^{max}	2.57E+08	M_z^{max}	1.27E+08	M_x^{max}	2.72E+07
H_{eq1}	3.36E+00	H_{eq2}	3.18E+00	H_{eq3}	2.14E+00
Load combination without Ms					
		M_y component	M_z component	M_x component	
LC1		2.57E+08	1.21E+08	2.37E+07	
LC2		2.43E+08	1.27E+08	4.04E+07	
LC3		1.64E+08	8.55E+07	2.72E+07	
Sea state 6					
M_y^{max}	3.62E+08	M_z^{max}	1.76E+08	M_x^{max}	3.79E+07
H_{eq1}	4.73E+00	H_{eq2}	4.41E+00	H_{eq3}	2.98E+00
Load combination without Ms					
		M_y component	M_z component	M_x component	
LC1		3.62E+08	1.70E+08	3.34E+07	
LC2		3.37E+08	1.76E+08	5.60E+07	
LC3		2.28E+08	1.19E+08	3.79E+07	
Sea state 7					

M_y^{max}	4.75E+08	M_z^{max}	2.25E+08	M_x^{max}	4.87E+07
H_{eq1}	6.21E+00	H_{eq2}	5.64E+00	H_{eq3}	3.83E+00
Load combination without Ms					
		M_y component	M_z component	M_x component	
LC1		5.30E+08	2.23E+08	4.38E+07	
LC2		4.86E+08	2.25E+08	7.16E+07	
LC3		3.48E+08	1.53E+08	4.87E+07	

5.6 Ultimate Strength of Hull Girders

5.6.1 Hull 5415 and Damaged Scenario

The studies on reliability based assessment of residual strength of damaged ship are performed for the Notional US Combatant ship, the hull form number 5415. The principal dimensions of the hull 5415 are given in Table 5.6.1-1.

Table 5.6.1-1: Principal dimension of USN Hull 5415

Principal Dimensions	Value
Length Between Perpendiculars	142.04 metres (466 ft)
Overall Length	151.18 metres (496 ft)
Maximum Beam	21.15 metres (69.4 ft)
Beam at Water Line	20.03 metres (65.7 ft)
Depth of Hull	12.74 metres (41.8 ft)
Design Draught (moulded)	6.31 metres (20.7 ft)
Displacement at Load Draught	9032.24 tonnes (8890 LTons)

The ships layout plan and damaged scenario for this study is shown in Figure 4-7. The collision damage scenario is based on Lloyd's Register Rules for naval ships that for collision damage of level A is given in Table 3.3-1. It is also graphically illustrated in Figure 5.6.2-2.

Table 5.6.1-2. Properties of steel materials

Material	Yield Strength
HY80	
σ_y (MN/m^2)	552
High Strength Steel	
σ_y (MN/m^2)	351

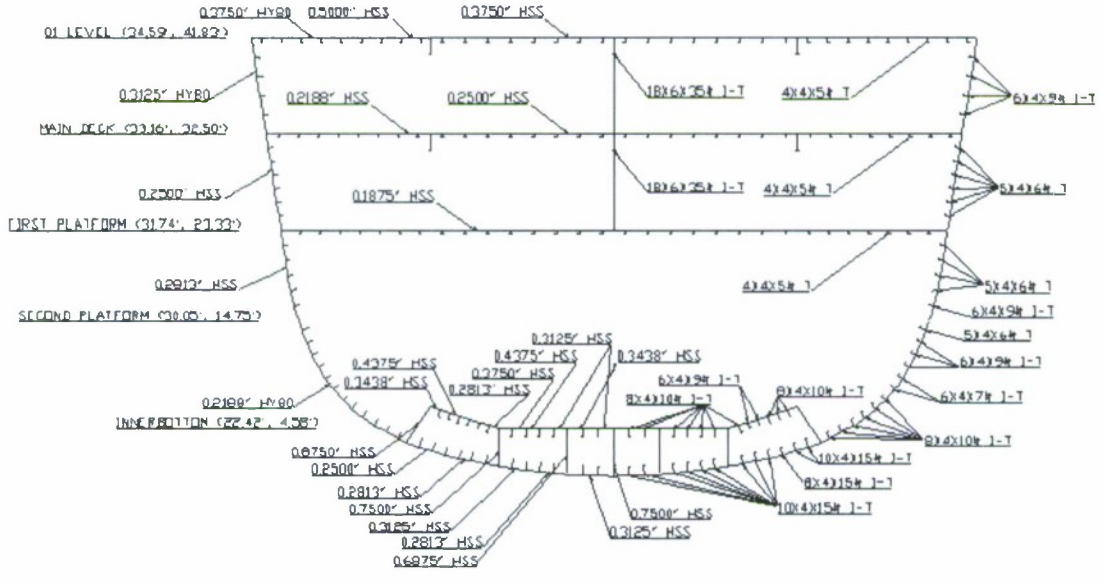

Figure 5.6.1-2: Midship scantling of Hull 5415

The structural design of the Hull 5415 is developed on two types of steel HY80 and HSS. The relevant properties of the steel materials are given in Table 5.6.1-2. The detail of midship section of the Hull 5415 is given in Figure 5.6.1-2. The relevant cross sectional properties are listed in Table 5.6.1-3 that includes the values as calculated using MARS (Bureau Veritas software for structural calculation) and ANSYS (FE analysis software) for comparison of structural model of each software.

Table 5.6.1-3: Cross section characteristics

Parameter	Value (MARS)	Value (ANSYS)
Total Section Area	1.2592 m^2	1.2576 m^2
Neutral axis above baseline	6.57486 m	6.5119 m
Vertical Moment of Inertia	28.968810 m^4	28.995 m^4
Horizontal Moment of Inertia	43.141570 m^4	43.11 m^4

In accordance to BV rule for ship with C_b less then 0.8, the requirement for section modulus is:

$$Z_{R\,MIN} = n_1\, C\, L^2\, B\, (C_B + 0.7)\, k\, 10^{-6} \qquad (5.6.1.1)$$

The comparison of required section modulus properties as per BV rules and that actual for Hull 5415 midship section are given in table 5.6.1-4.

Table 5.6.1-4: Section modulus required as per BV Rules and actual for MIDSHIP section.

Parameter	BV Rule	Hull 5415
Deck	3.2728 m^3	4.6912 m^3
Bottom	3.0655 m^3	4.4060 m^3
Vertical Moment of Inertia	21.1343 m^4	28.968810 m^4

5.6.2 Ultimate Hull Girder Strength – using MARS

The MARS software from Bureau Veritas is used to calculate ultimate hull girder strength using beam-column idealization as of Smith Method. The MARS software provides different failure mode algorithms for calculation of ultimate strength that include Elastic Ideally Plastic (EIP) failure mode and Beam-Column (BC) failure mode, apart from the others.

As already discussed in section 3.3, for EIP failure mode, material beyond elastic limit is considered fully plastic in both under tension and compression. Beam-Column method of MARS uses the following load-end shortening curves given in equation 3.3-1.

The MARS calculations are performed for both intact and damaged condition. The figure 5.6.2-1 shows intact ship section modelled for MARS calculation. The damaged cross section shown in figure 5.6.2-2 is modelled as per LR recommended damaged structure sizes as discussed section 4.3.

The figure 5.6.2-3 shows the MARS calculation results of ultimate strength in pure horizontal bending of Hull 5415 for elastic ideally plastic failure mode. The results for ultimate strength in pure vertical bending for beam-column failure mode are given in figure 5.6.2-4. The ultimate vertical moment capacity for elastic-plastic failure mode is 2.556 GNm where as ultimate moment capacity for beam-column failure mode is 1.561 GNm. The ultimate moment

capacity for beam-column mode is 38.92% lower than that of elastic-plastic failure mode since the beam-column method is based on load shortening curves that take into count the shear lag, residual stress, initial deformation along with other production related effects.

The ultimate bending moment capacity for combination of vertical and horizontal moments are given in figures 5.6.2-5 & 5.6.2-6 for elastic-plastic failure mode and in figures 5.6.2-7 & 5.6.2-8 for beam-column method. These results are for intact ship in hogging condition.

The M_V and M_H interaction formula of the form of equation 3.3-6 are as follows:

– For elastic ideally plastic failure mode (see figure 5.6.2-6 also).

$$\left(\frac{M_V}{M_{VU}}\right)^{1.62467} + \left(\frac{M_H}{M_{HU}}\right)^{2.04339} = 1 \qquad (5.6.2.1)$$

– For beam-column failure mode (see figure 5.6.2-8 also).

$$\left(\frac{M_V}{M_{VU}}\right)^{4.53198} + \left(\frac{M_H}{M_{HU}}\right)^{2.35511} = 1 \qquad (5.6.2.2)$$

The comparison ultimate moment capacity of intact and damaged condition (DS1) in term of vertical and horizontal moment interaction diagram is given in figure 5.6.2-9 for both hogging and sagging conditions. For damaged ship, the vertical and horizontal moment interaction formula derived from interaction terms as plotted in figure 5.6.2-9 are as follows:

– For damaged ship hogging condition

$$\left(\frac{M_V}{M_{VU}}\right)^{2.7489} + \left(\frac{M_H}{M_{HU}}\right)^{3.45775} = 1 \qquad (5.6.2.3)$$

– For damaged ship sagging condition

$$\left(\frac{M_V}{M_{VU}}\right)^{1.9713} + \left(\frac{M_H}{M_{HU}}\right)^{1.82155} = 1 \qquad (5.6.2.4)$$

The comparison of ultimate moment for various bending curvatures ratio (horizontal/vertical) in hogging condition for intact and damaged ship is shown in figure 5.6.2-10. It may be observed that for hogging condition when the bending curvature ratio is small and, consequently, predominantly curvature is in vertical direction depicting predominant vertical bending moment, the difference between ultimate moment for damaged and intact condition is small. As the curvature ratio increases, accordingly horizontal moment also increases and the difference between intact and damaged condition ultimate moment slowly increases until curvature ratio reaches around a value of 2 and almost remain steady for further increase in curvature ratio, where the dominant moment is horizontal in nature. The ultimate moment

capacity of damaged ship in hogging condition is higher than that in case of intact ship for same loading condition, which is about 1% higher for pure vertical bending curvature and increasing to about 11% for pure horizontal bending curvature as shown in figure 5.6.2-12. The increase of ultimate moment capacity of damaged ship in hogging condition is attributed to shift and change of orientation of neutral axis as shown in figure 5.6.2-16 and 5.6.2-17.

For sagging condition, the ultimate moment capacity of damaged ship decreases with increase in horizontal/vertical curvature ratio as shown in figure 5.6.2-11. For sagging ship condition, the curvature ratio around zero represents predominant vertical moment resulting in compression in damaged section of the ship. For dominant vertical moment, the ultimate moment capacity of damaged ship is reduced by 20% comparing to that of intact ship as shown in figure 5.6.2-11. For dominant horizontal moment i.e. for higher curvature ratio, the difference between ultimate moment capacity of intact and damaged ship is reduced to around 10%.

The ultimate moment capacity of damaged ship as a function of damaged depth for ultimate vertical moment in sagging condition, ultimate vertical moment in hogging condition and ultimate horizontal moment are shown in figure 5.6.2-13, 5.6.2-14 and 5.6.2-15, respectively. The results presented in these graph are obtained using beam-column method for ultimate strength calculation. Such functional representation of damage vs ultimate strength at various section across whole length of ship may be an appropriate tool for residual strength assessment of damaged ship and quick assessment of risk in case of damage incident.

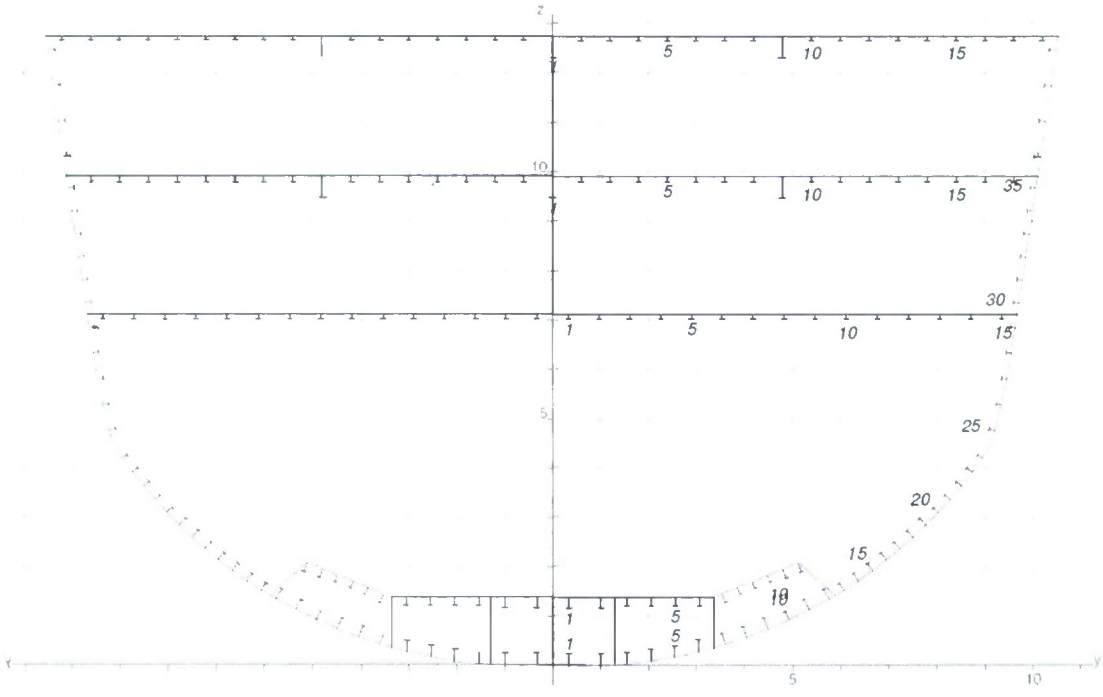

Figure 5.6.2-1 : Midship section, MARS model intact ship

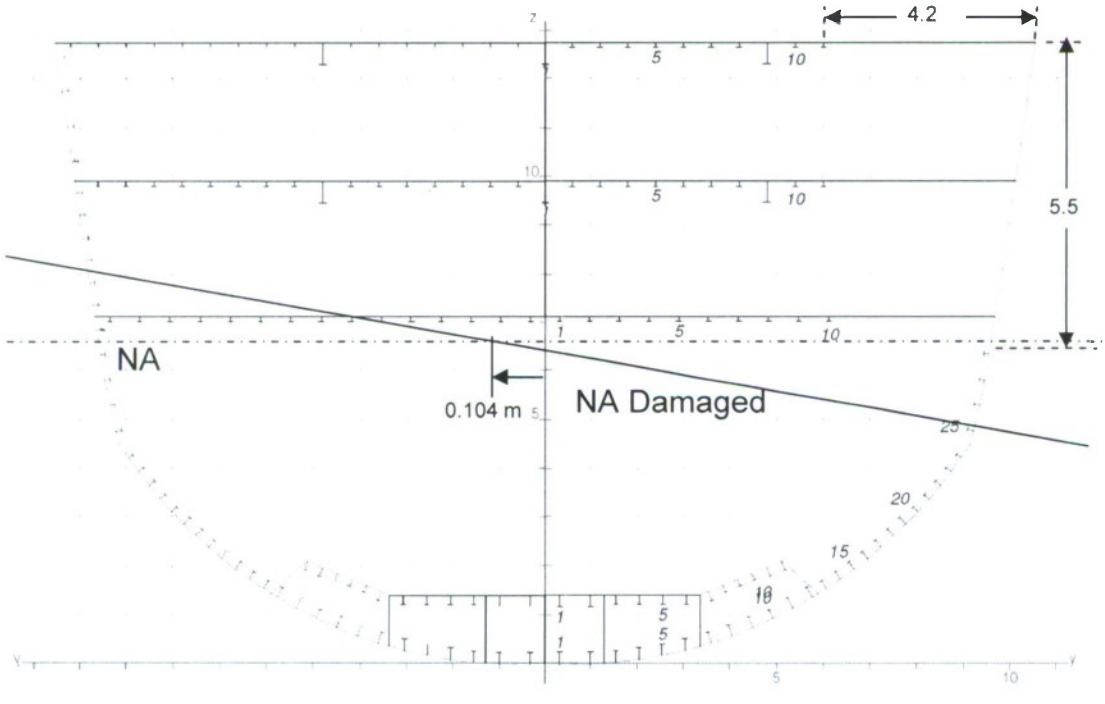

Figure 5.6.2-2 : Midship section, MARS model damaged condition

BV RULES - Mars Rule 2000 v2.2b
Section : MIDSHIP SECTION

Ship : BC2
x = 71 m
07/01/2008

Ultimate strength check

Calculation options

Scantling:	Gross
Solution:	Elastic ideally plastic behaviour
Moment:	Fixed vertical/horizontal bending moments ratio
Ratio:	0.00

Bending moment (kN.m)	Mu	Ultimate	Applied	%
Hogging	2 558 724.	2 558 724.	477 209.	18.65
Sagging	- 2 558 724.	- 2 558 724.	- 598 096.	23.37

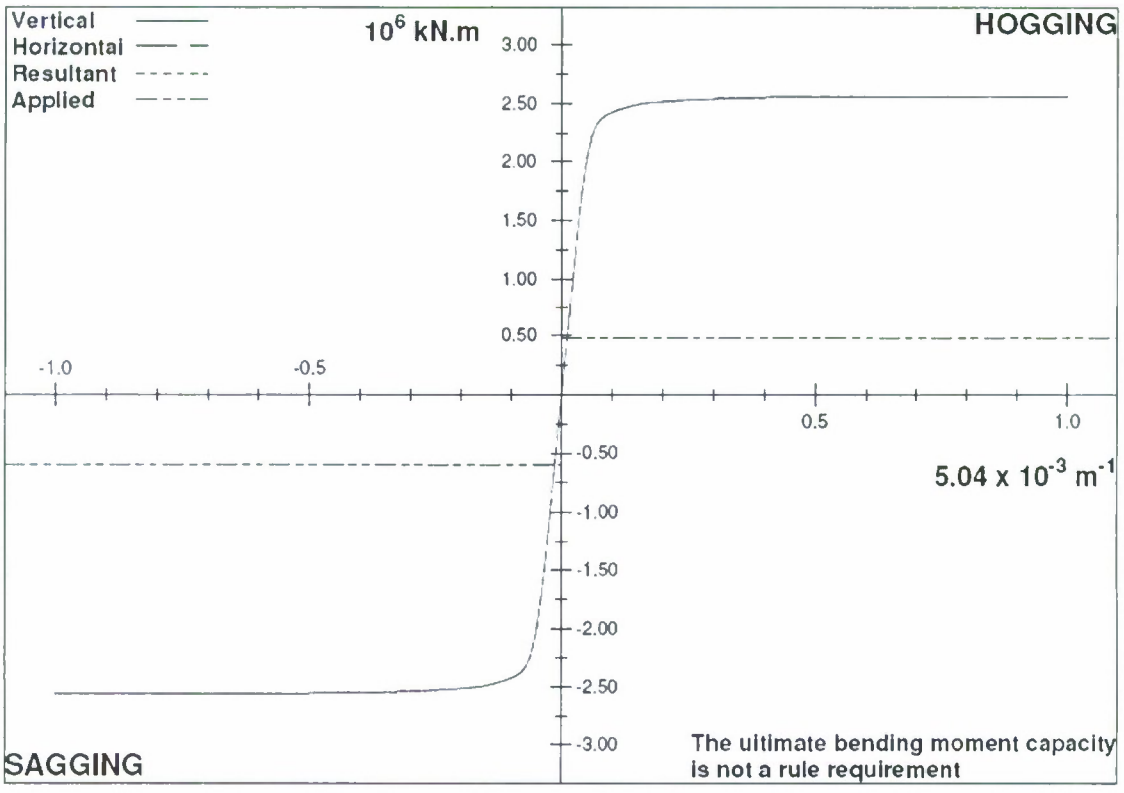

Figure 5.6.2-3: Elastic – Ideally Plastic ultimate strength of Hull 5415 in pure horizontal bending.

Ultimate strength check

Calculation options

Scantling: Gross
Solution: Beam-column failure mode
Moment: Fixed horizontal/vertical bending moments ratio
Ratio: 0.00

Bending moment (kN.m)	Mu	Ultimate	Applied	%
Hogging	1 560 943.	1 560 943.	479 209.	30.70
Sagging	- 1 327 268.	- 1 327 268.	- 600 096.	45.21

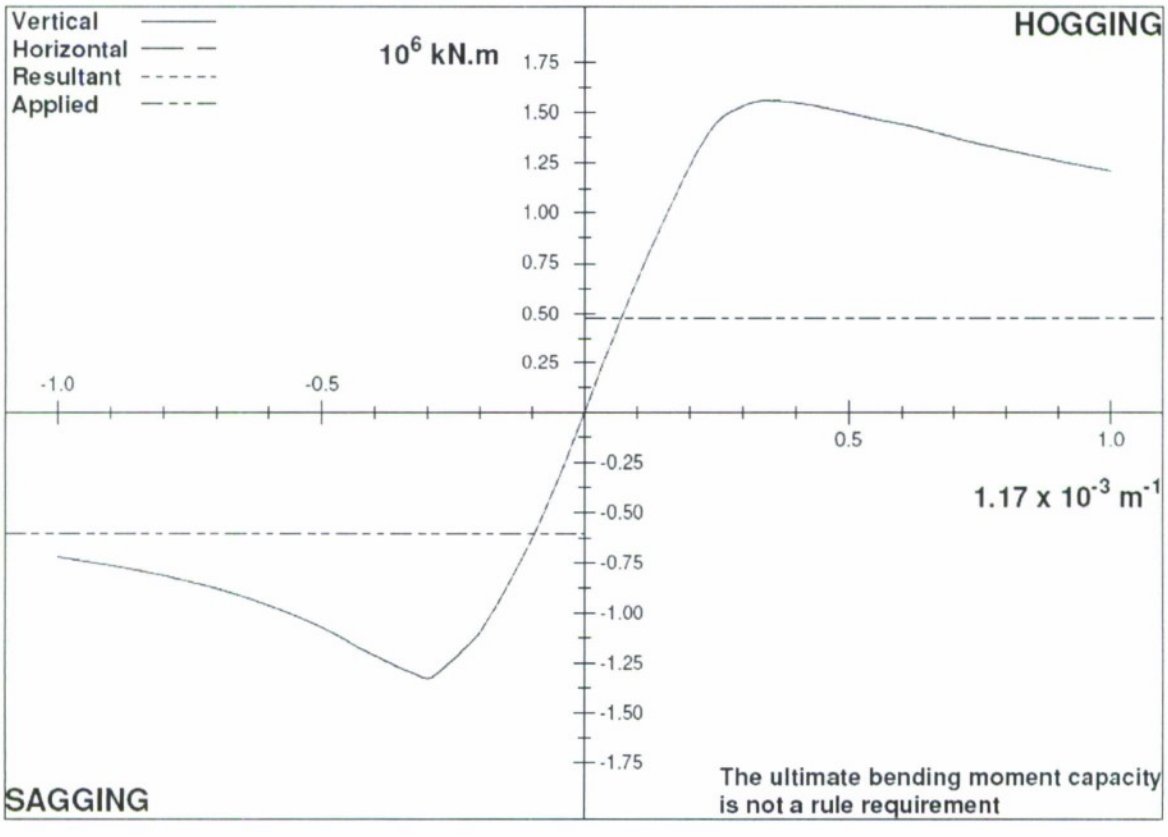

Figure 5.6.2-4: Beam-Column failure mode ultimate strength of Hull 5415 in pure vertical bending

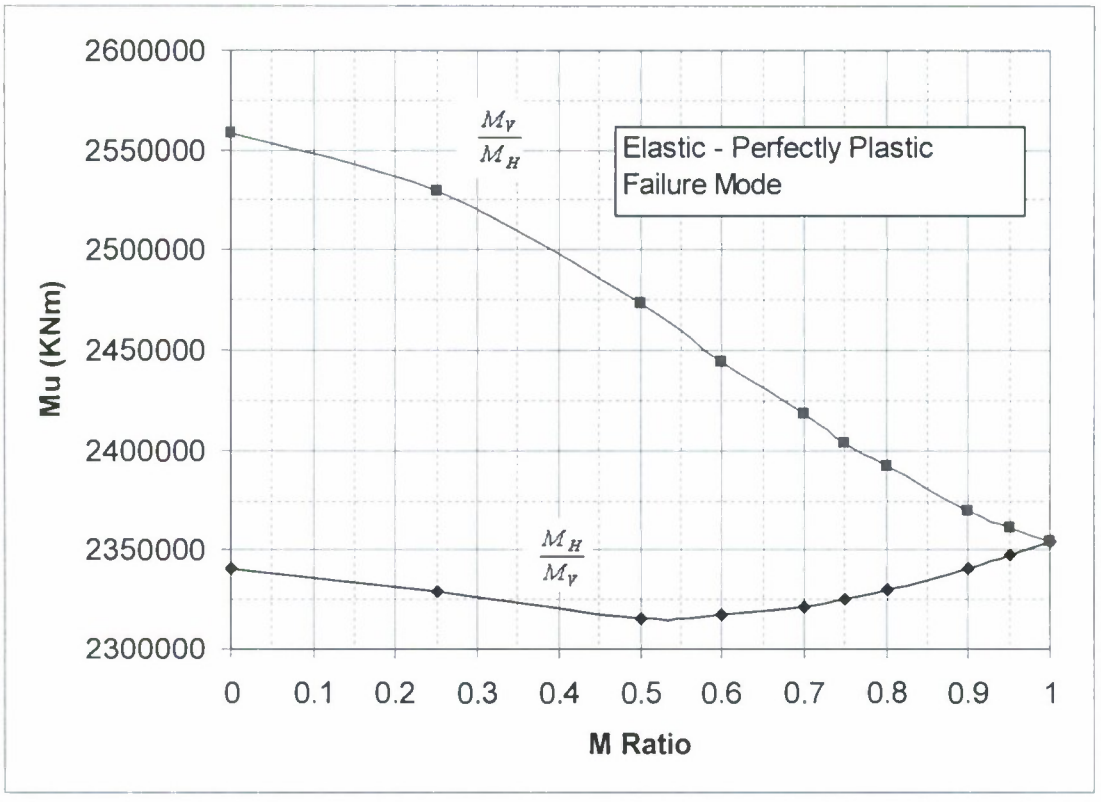

Figure 5.6.2-5: EIP ultimate strength of Hull 5415 for vertical & horizontal moments

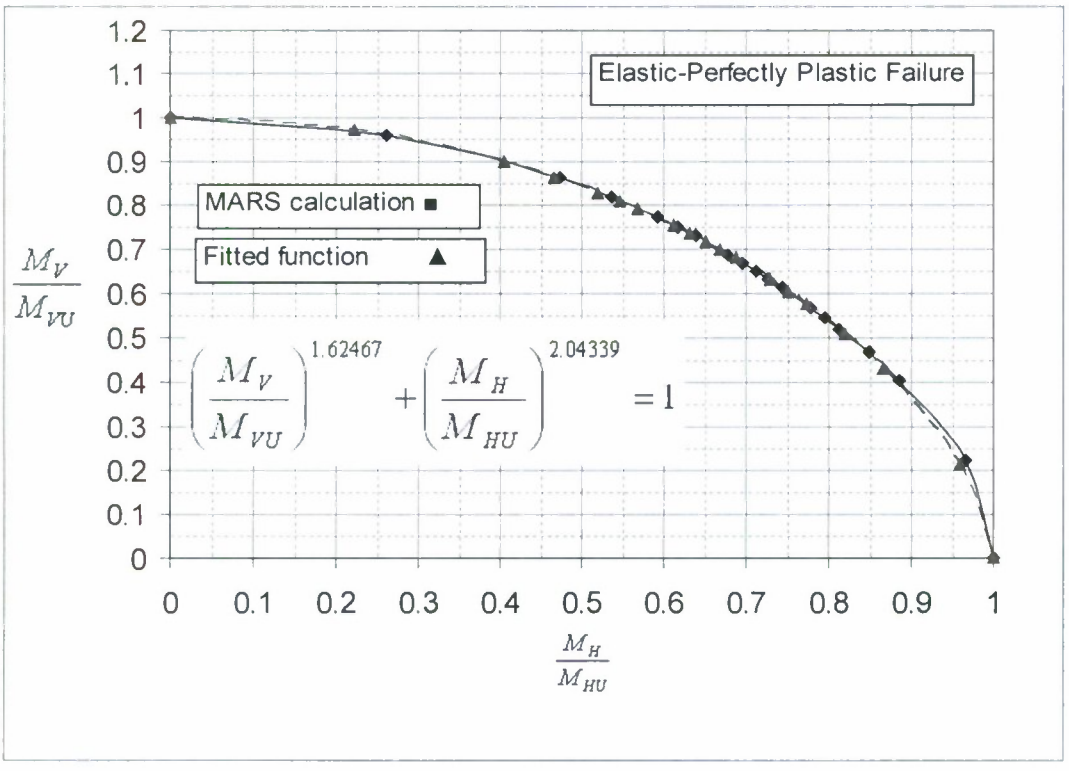

Figure 5.6.2-6: EIP ultimate strength for vertical & horizontal moments interaction

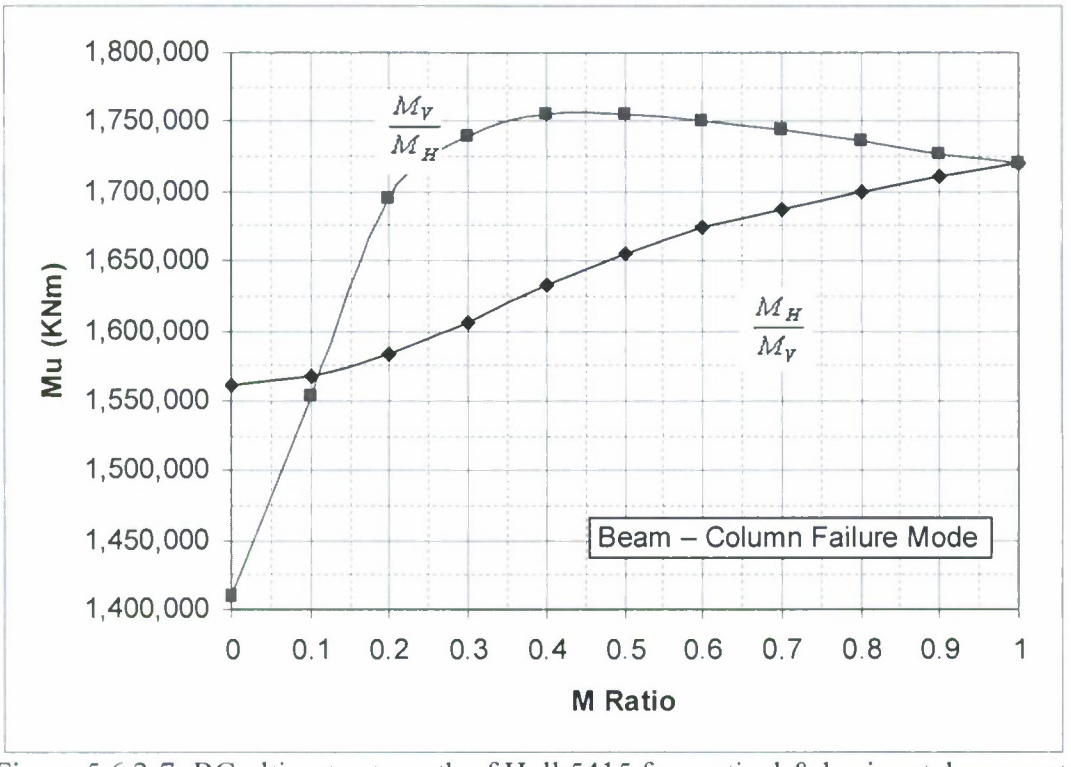

Figure 5.6.2-7: BC ultimate strength of Hull 5415 for vertical & horizontal moments

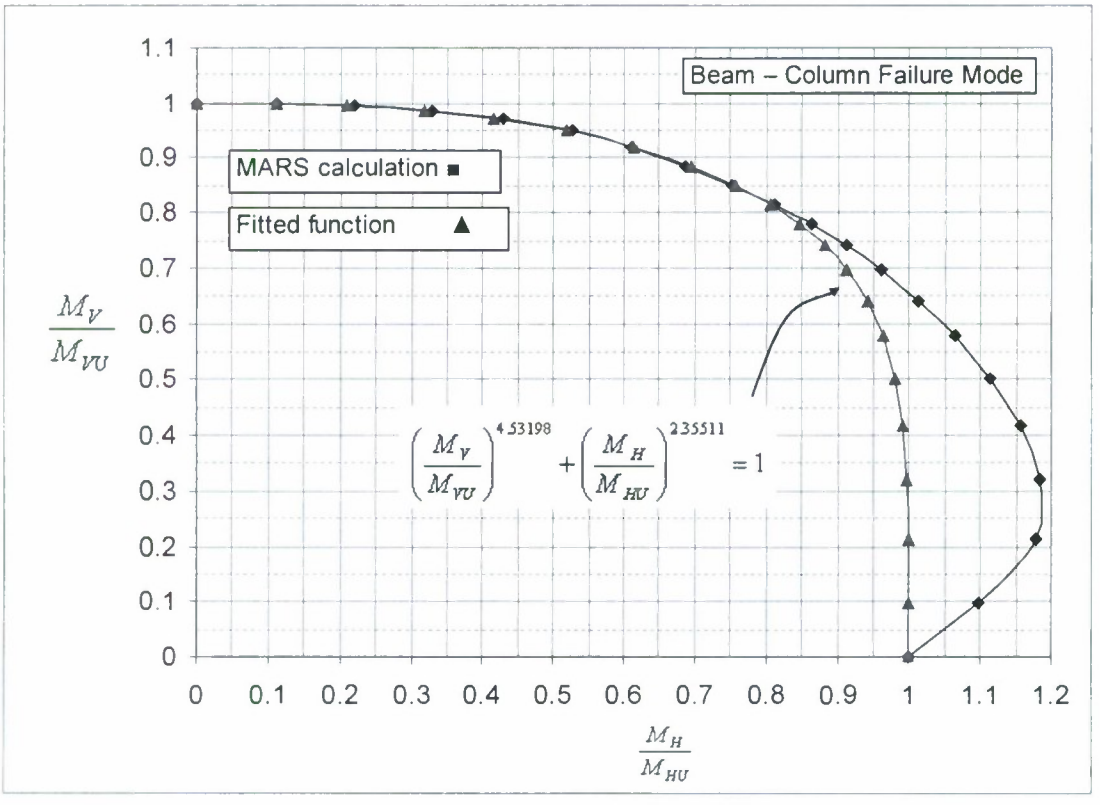

Figure 5.6.2-8: BC ultimate strength of Hull 5415 for vertical & horizontal interaction

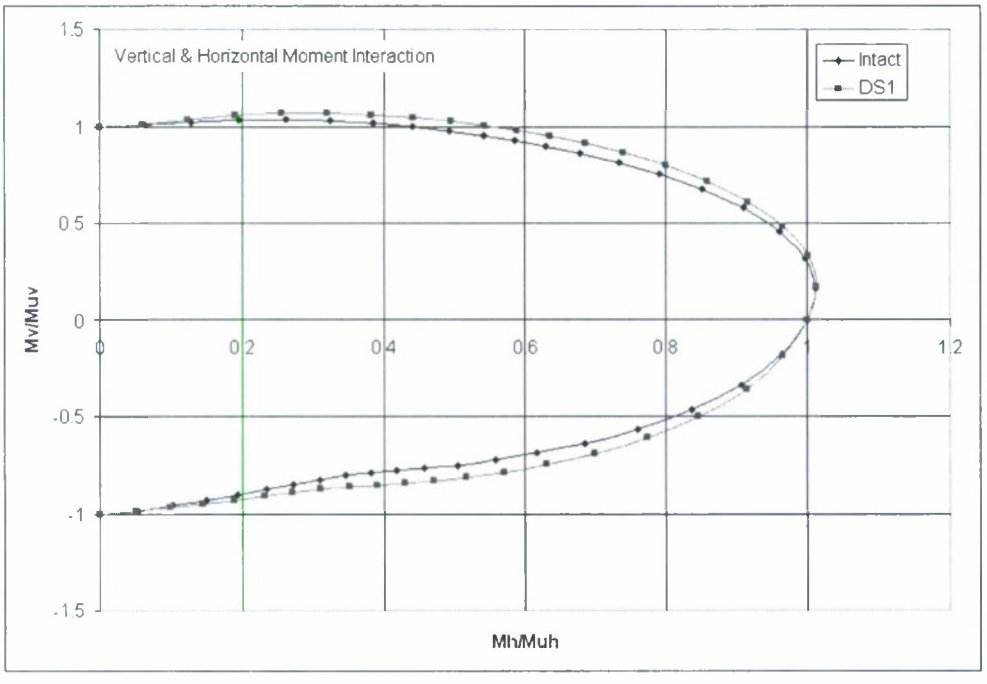

Figure 5.6.2-9: Comparison of M_v/M_{uv} and M_h/M_{uh} for intact and damaged condition

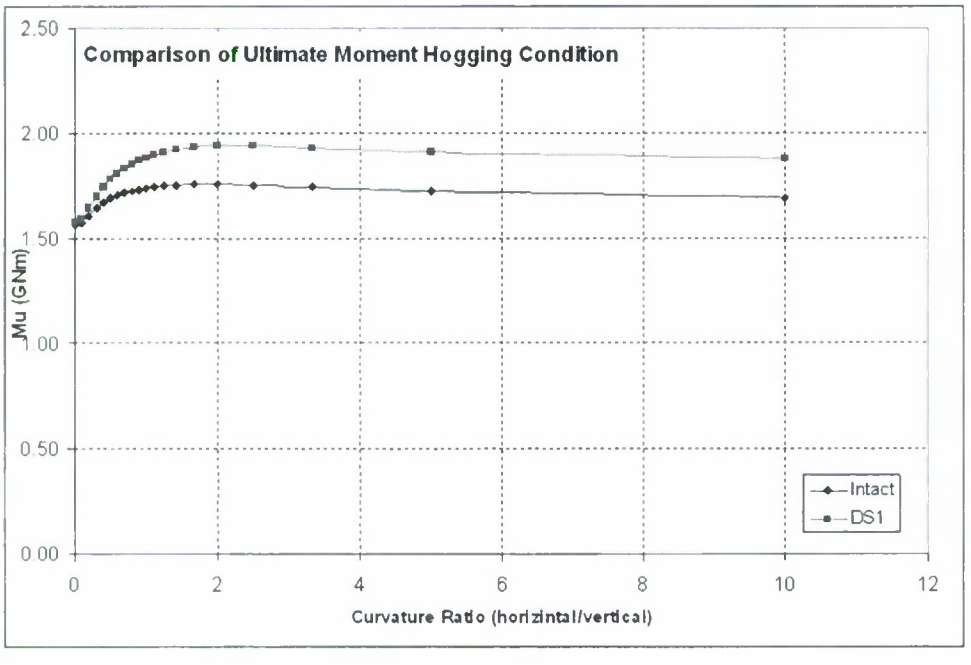

Figure 5.6.2-10: Ultimate hogging moment for intact and damaged condition

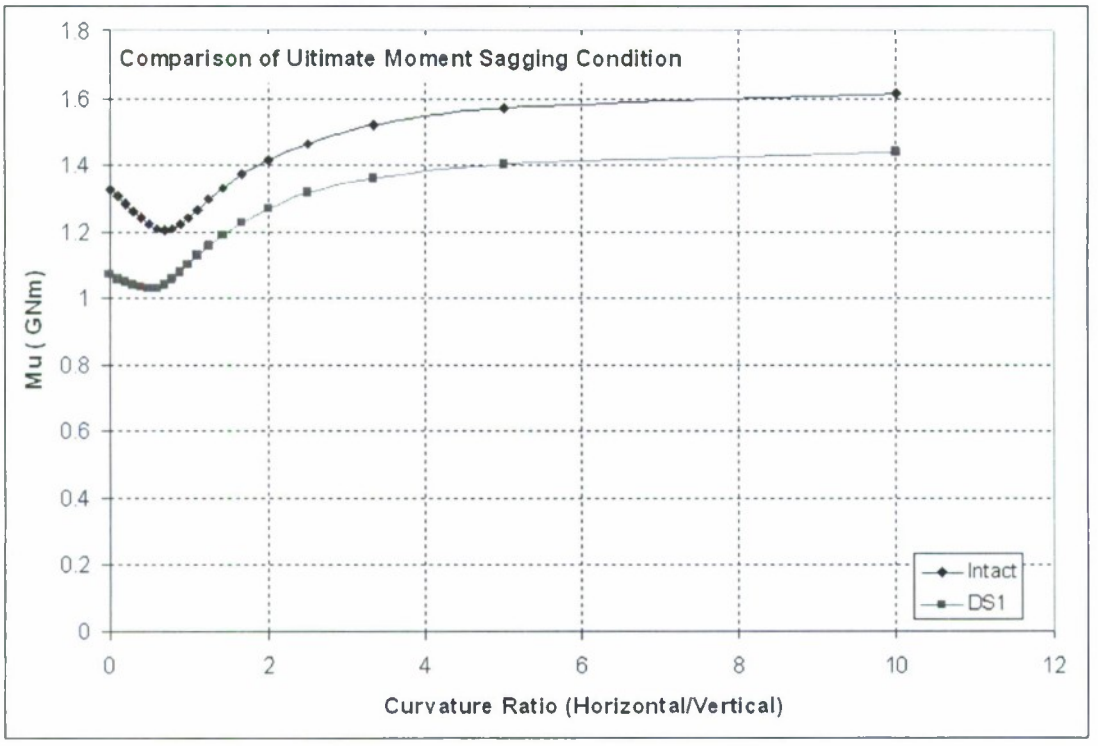

Figure 5.6.2-11: Comparison of ultimate moment for intact and damaged sagging condition

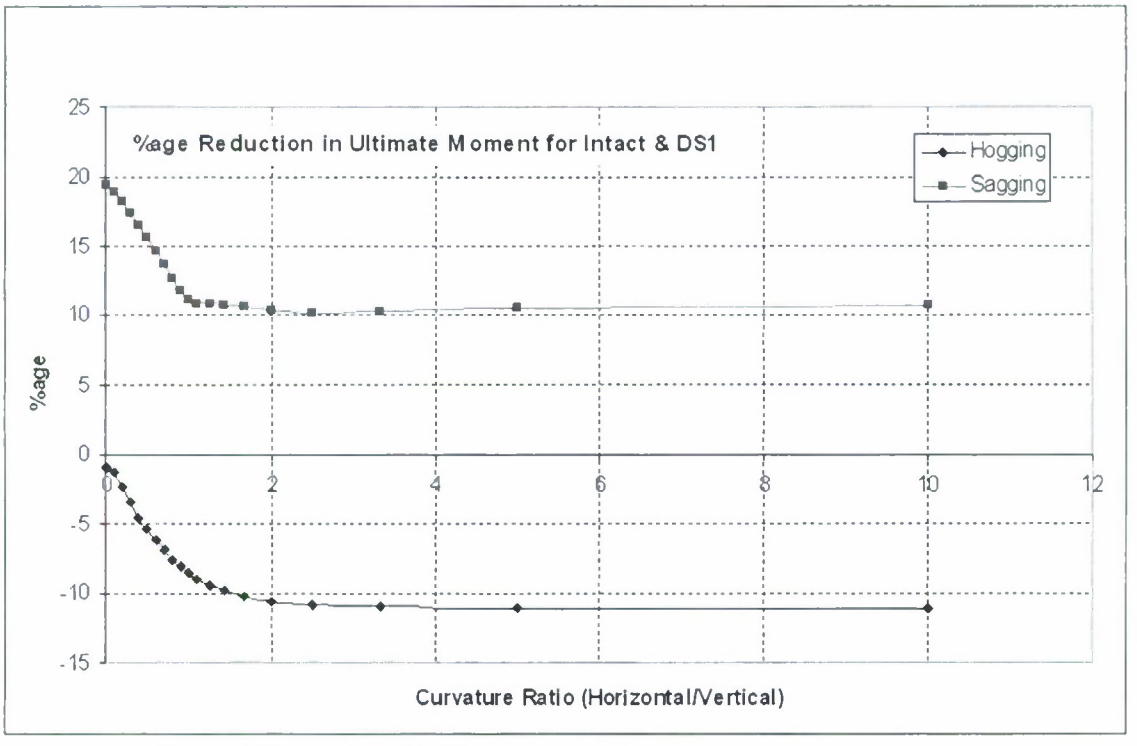

Figure 5.6.2-12: Percentage reduction in ultimate hogging and sagging moment for intact and damaged condition

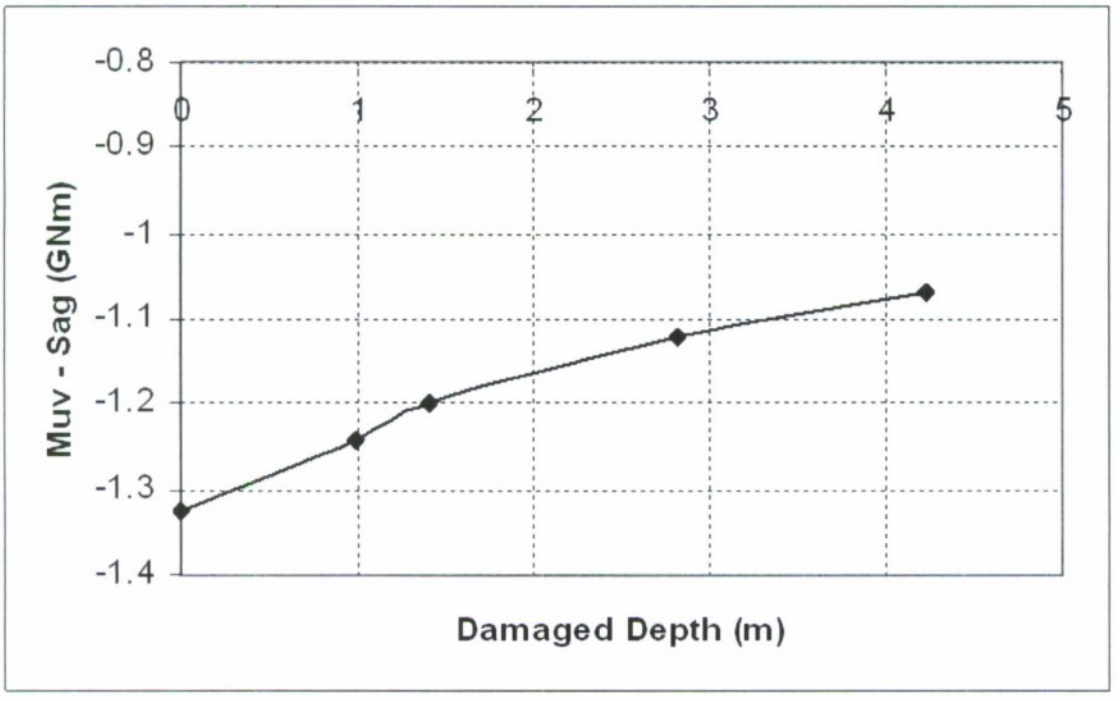

Figure 5.6.2-13: The ultimate sagging moment as function of damaged depth

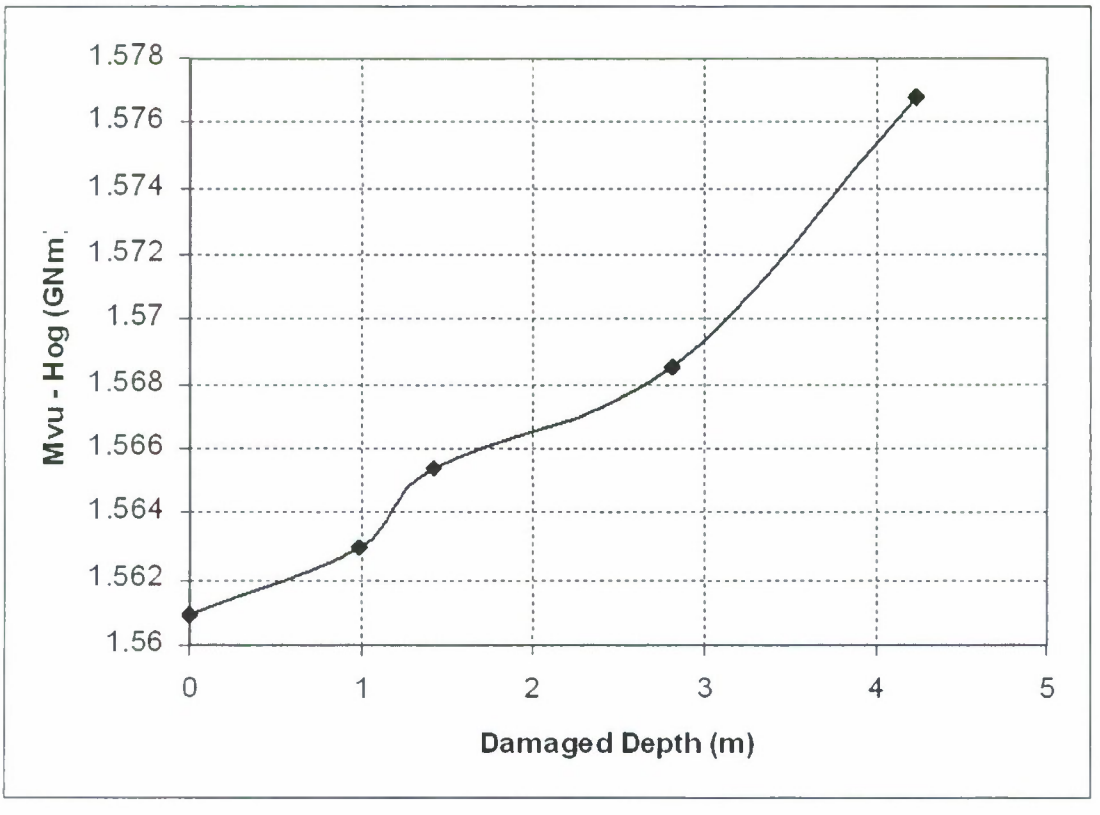

Figure 5.6.2-14: Ultimate hogging moment as a function of damaged depth

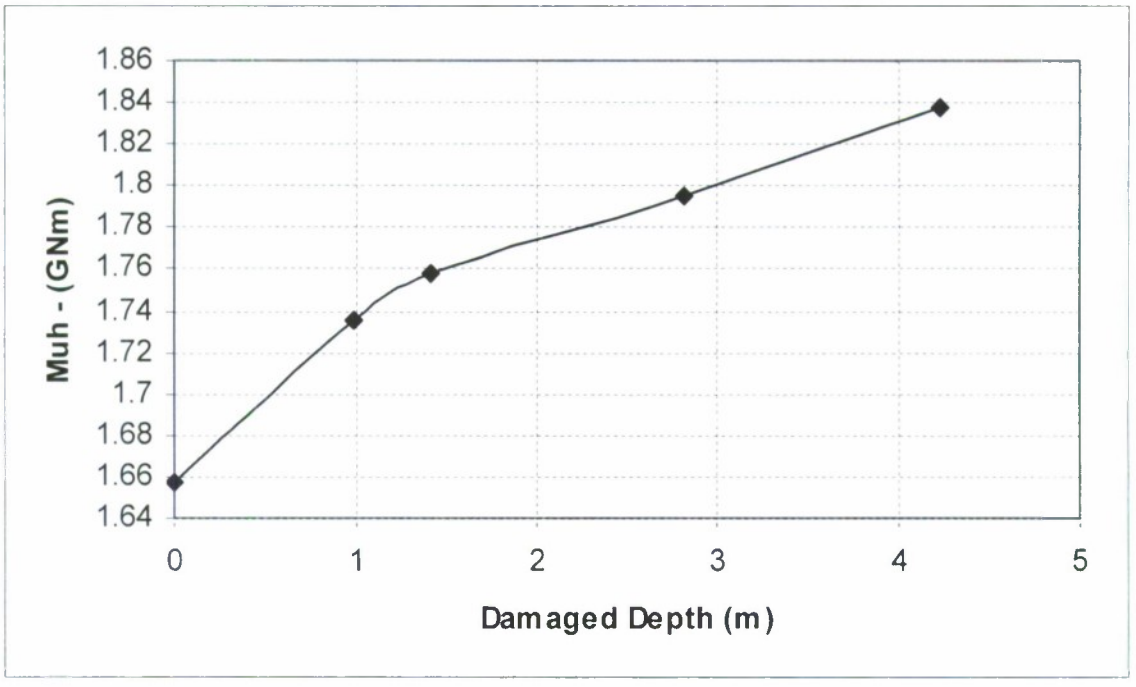

Figure 5.6.2-15: Ultimate horizontal bending moment as a function of damaged depth

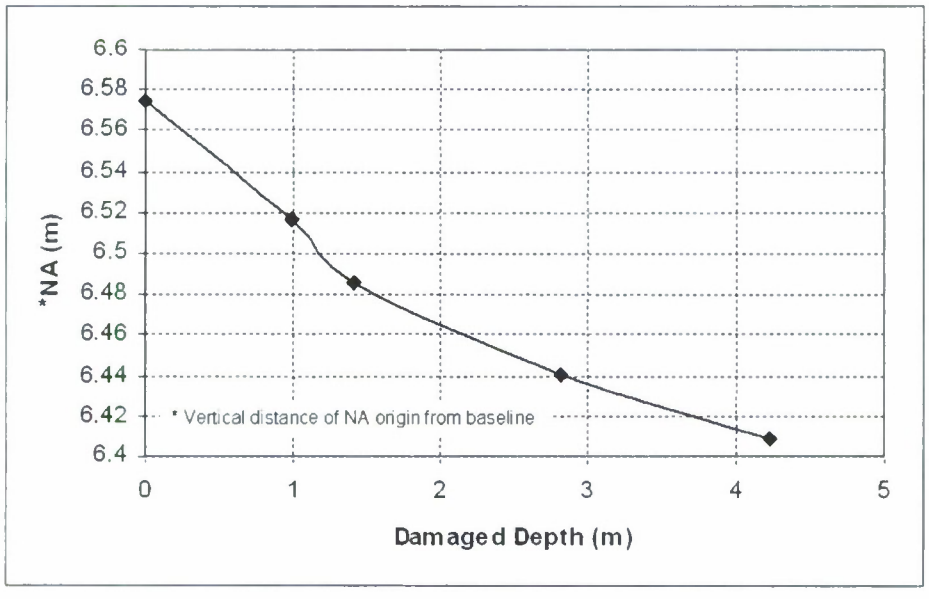

Figure 5.6.2-16: Shift in vertical location of neutral axis as a function of damaged depth

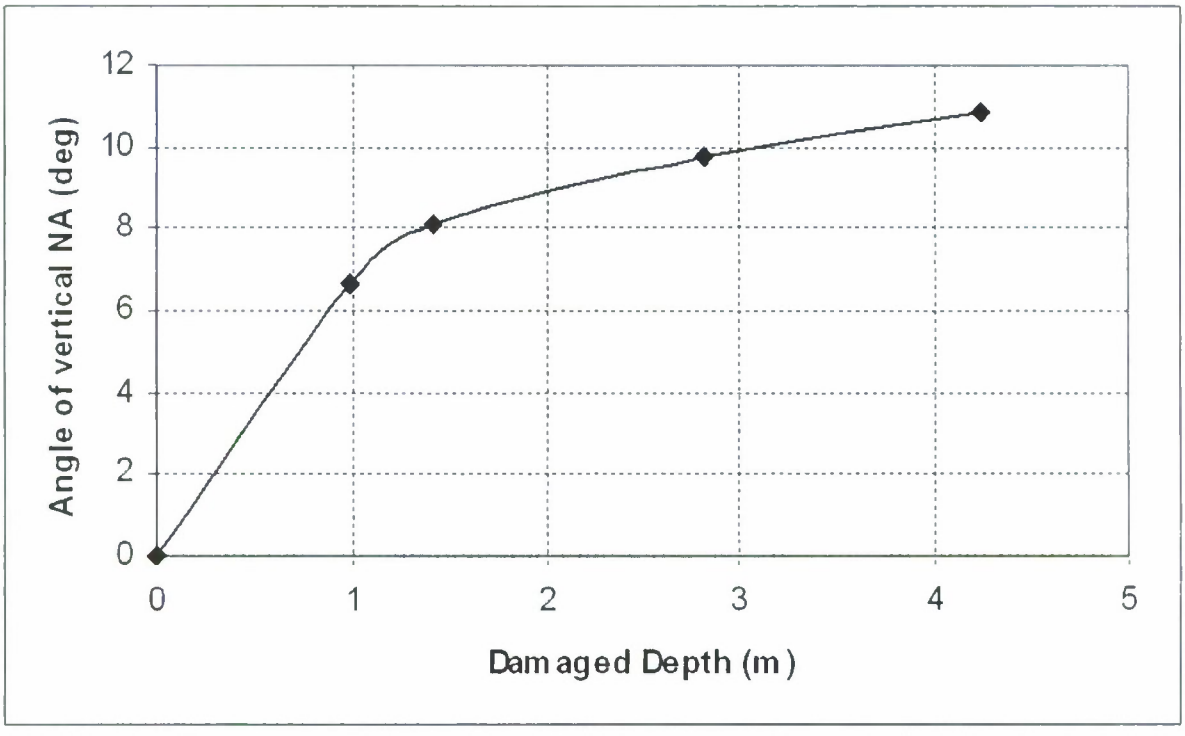

Figure 5.6.2-17: Incalination angle of neutral axis as a function of damaged depth

5.6.3 Ultimate Hull Girder Strength – using ANSYS

The ANSYS is used for finite element analysis of Hull 5415 to determine ultimate strength of the hull girder. In FE analysis, the size of ship structure to be used in FE model requires to be carefully determined. Some suggestions were made in the kick-off meeting (21 Aug 2006) to develop model of a complete ship using top-down procedure starting from a coarse model to fine mesh. Considering the enormous amount of computing time in non-linear analysis, this procedure was not considered realistic for the project because of budget constraints and enormous amount of computing time and effort. It was decided that a three compartment model shall be sufficient as similar extent of structure is mostly recommended by classification societies for direct strength assessment of the primary supporting structure. Three compartment part of the Hull 5415 as shown in Figure 5.6.3-1 is modelled for finite element analysis.

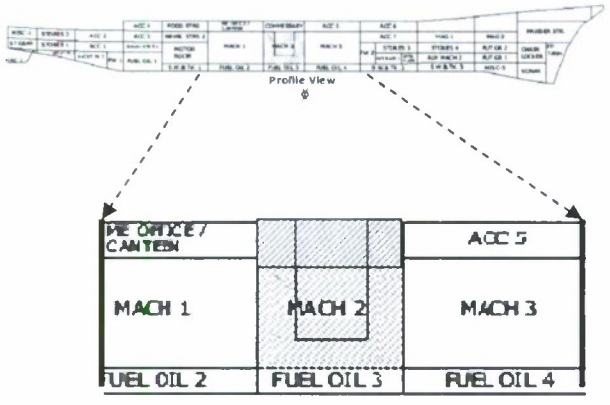

Figure 5.6.3-1: The range of ship for FE modelling of damaged ship analysis

However, structural details of the Hull 5415 are only available for midship section and the three compartments are considered to be same in cross section as the midship in these studies. Further, no FE based design assessment of intact ship is available to compare the results with that of the damaged ship. The FE analysis for ultimate strength of hull girder shall be carried out for both intact and damaged conditions.

5.6.3.1 Finite Element Model for nonlinear ultimate strength assessment

Three compartment models being large in term of FE computational time and since reliability based assessment of residual strength of damaged ship using FE analysis require a number of run to generate response surface and again because of budget constraint and time available for project completion, a three levels finite element modelling approach was adopted for this project, with a planning to compare the results from the large model with that of small model to assess influence of boundary conditions. The reduced/small model was used for large number of calculations for response surface development and reliability analysis. The reduced/small model analysis was however only possible for intact ship. The three levels of finite element models of ship in intact condition are shown in figure 5.6.3.1-1 which are the following:

- Three compartment model
- One compartment model

- Two frame model

A full three compartment model was used for finite element analysis of ship in damaged condition (see figure 5.6.3.1-2). All the three models developed were for both port and starboard part of the ship, i.e. no recourse was made to symmetry of structure about centre line, as apart form vertical and horizontal moment, torsion is also considered to be dominant load for damaged ship.

The ANSYS SHELL181 element is used in this analysis. SHELL181 is suitable for analyzing thin to moderately-thick shell structures. It is a 4-node element with six degrees of freedom at each node: translations in the x, y, and z directions, and rotations about the x, y, and z-axes. SHELL181 is well-suited for linear, large rotation, and/or large strain nonlinear applications. Change in shell thickness is accounted for in nonlinear analyses. In the element domain, both full and reduced integration schemes are supported. SHELL181 counts for follower (load stiffness) effects of distributed pressures.

The three compartment FE model of ship structure is discretized in two major meshing sizes. The middle part of the middle compartment up to one frame inside of bulkheads is fine meshed with average element size of 8 to 10 cm. For remaining part of the model a comparative coarse mesh of 35 to 40 cm was used in order to reduce the number of nodes and elements of the FE model. Three compartment model in total consists of around 0.4 million nodes and 0.41 million elements. The fine mesh in the middle compartment was required to suitably simulate structural damage using ANSYS/LS DYNA explicit finite element analysis.

The one compartment model mainly consists of coarse mesh of average size between 50 to 70cm. The FE model consists of about 45 thousands nodes and 42 thousand elements.

A fine FE mesh was used for two frame model which consists of 52 thousands nodes and 51 thousand elements.

The ships structural model for damaged case analysis was generated using explicit dynamic finite element simulation of collision between two ships. A typical bow structure for merchant vessel was modelled for collision impact approximately in the centre of the middle compartment at right angle to longitudinal-central vertical plane of hull 5415. The damaged part of hull 5415 as obtained subsequent to collision simulation is shown in figure 5.6.3.1-2. The figure 5.6.3.1-3 shows residual stress distribution in the deformed structure. The overly deformed elements from the damaged part of the damaged model were removed in order to avoid computational divergence in subsequent static nonlinear finite element analysis to determine ultimate moment capacity of the damaged hull. The refined element mesh of damaged structural model is shown in figure 5.6.3.1-4 along with residual stress vectors.

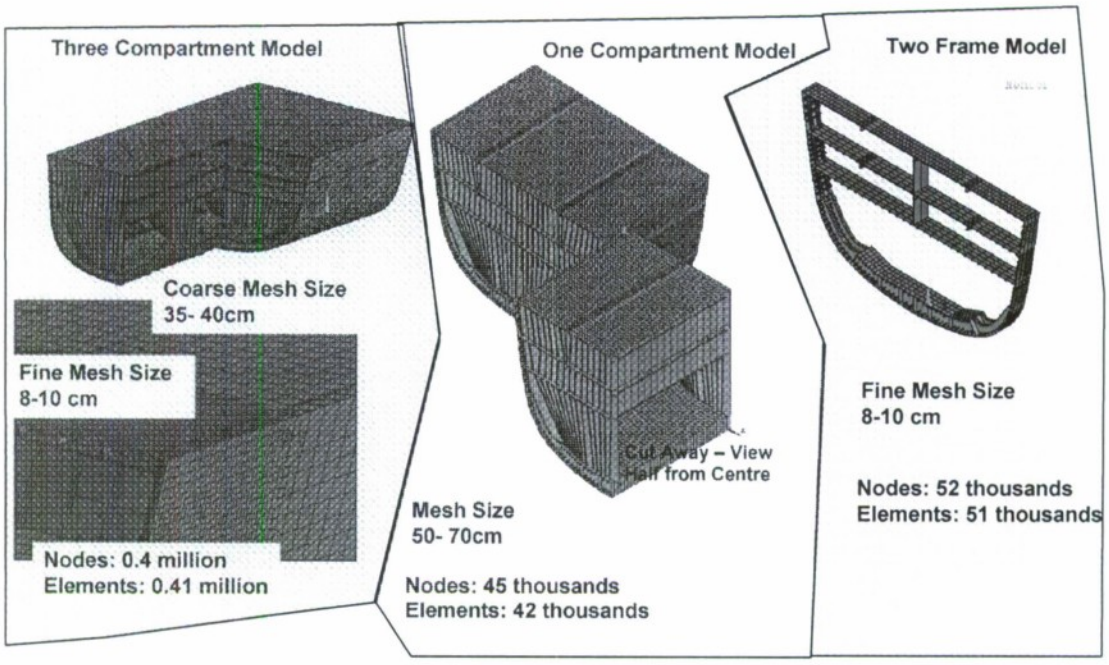

Figure 5.6.3.1-1: Different model for Finite Element Analysis.

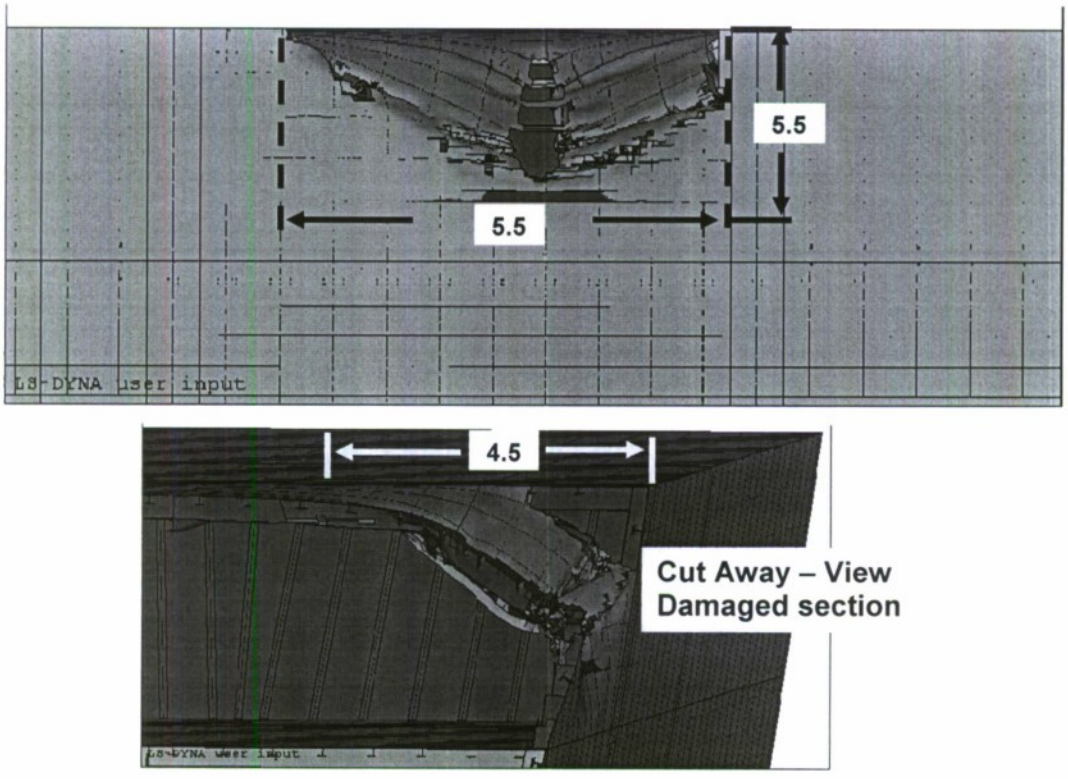

Figure 5.6.3.1-2: Damaged structural model ANSYS/LS DYNA simulation.

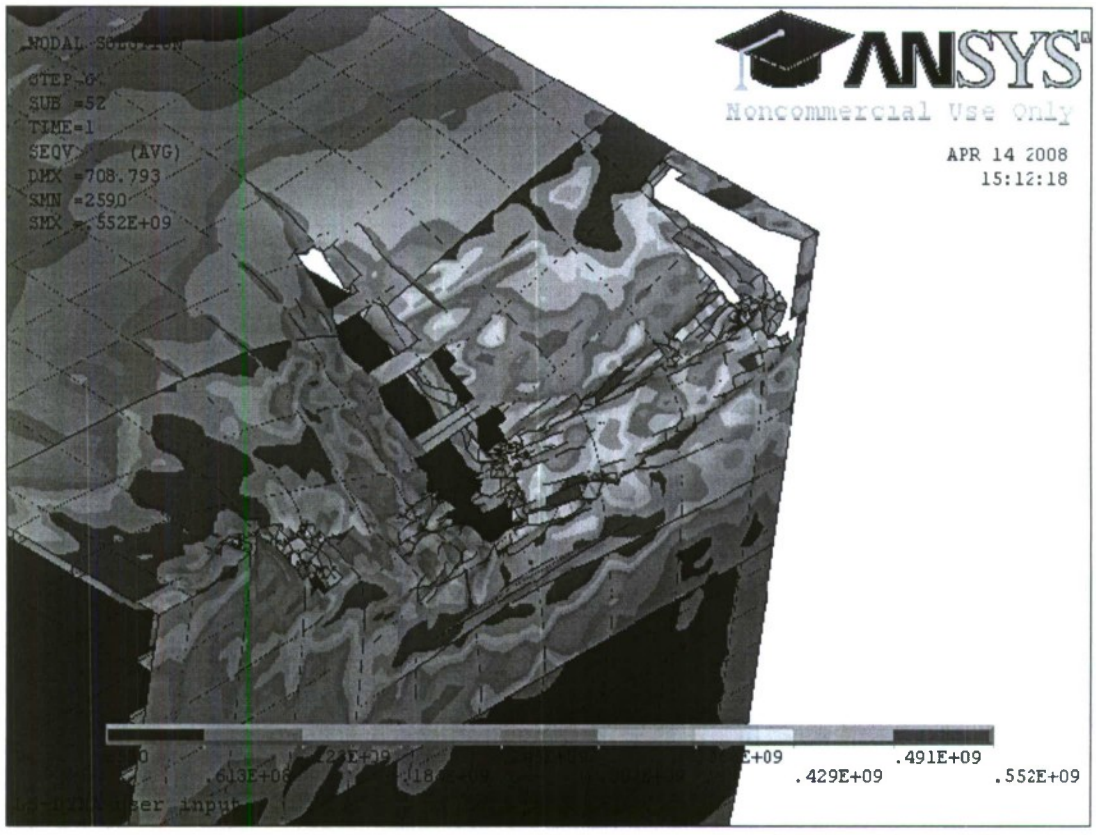

Figure 5.6.3.1-3: Residual stress in the damaged part of model structure

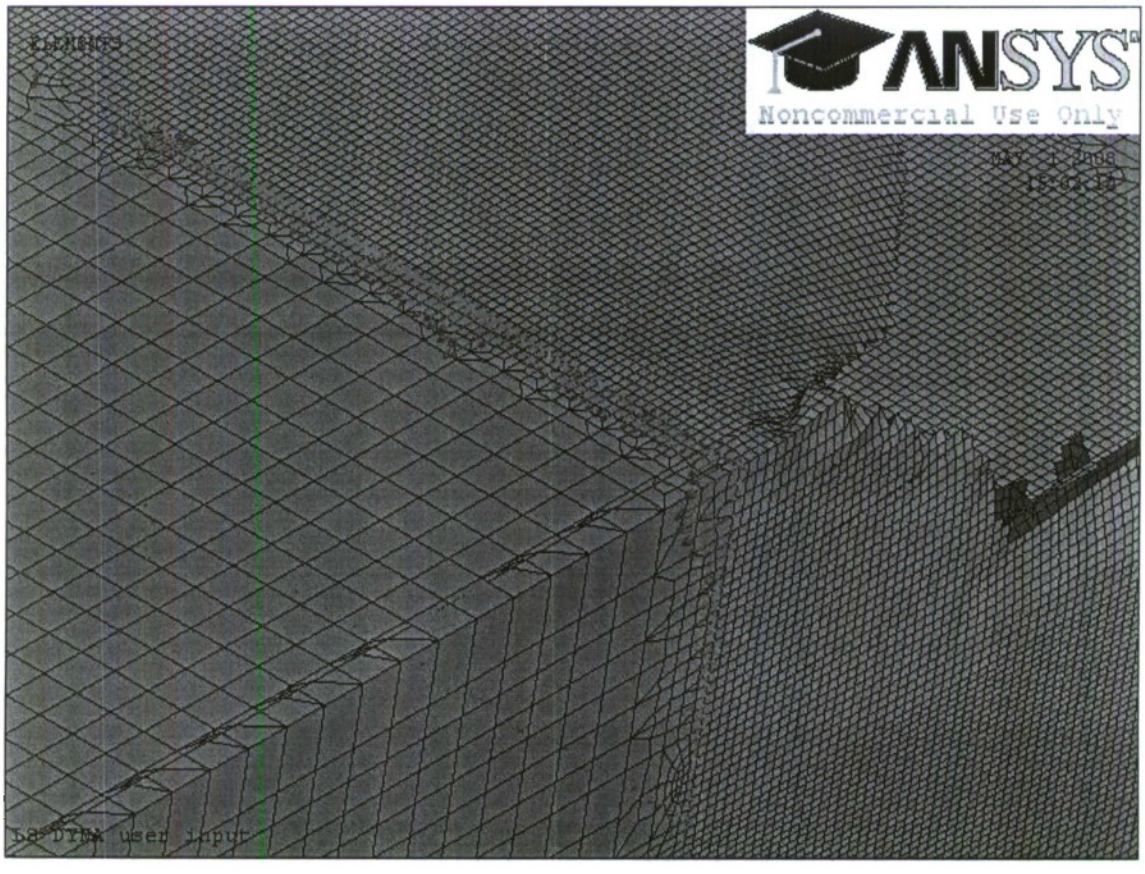

Figure 5.6.3.1-4: Refined mesh of damaged structure

5.6.3.2 Initial Deformations

The steel ship production process involve flame cutting and welding methods causing uneven rapid heating and cooling resulting in imperfection in the formed structural material. Initial deformation arising out of production process may considerably reduce the load bearing capacity of ship structure. There are a number efforts made to model initial deformation of welded structure based on analytical methods, numerical methods and experimental/practical measurements e.g. Faulkner (1975), Carlsen & Czujko (1978), Antoniou (1980), Smith et al (1988) and Masaoka (1996). Further, classification societies also specify limitation on maximum initial deflection of plate on completion of fabrication. The post weld initial deflections are represented by the following formula:

$$w_0 = w_{0pl} \sum_{i=0}^{M} \sum_{j=0}^{N} B_{0ij} \sin \frac{i\pi x}{a} \sin \frac{j\pi y}{b} \qquad (5.6.3.2.1)$$

Where a is plate length, b is plate breath. B_{oij} indicates the welding induced initial deformation normalized by the maximum initial deflection, w_{0pl}. The i and j are half wave number in the x and y direction.

The values of maximum initial deflection proposed by different sources are given in figure 5.6.3.2-1. Statistical analysis of proposed values relevant to structural plates of hull 5415 resulted in an average value of 0.00461m with a coefficient of variance of 0.508 which approximately follows normal distribution as it is apparent from the histogram in the figure. The figure 5.6.3.2-2 also shows the deflection wave pattern that is applied as initial deformation to the FE model with random maximum amplitude with normal distribution as described above. The initial deformation is applied only to middle part of three compartment model. In case of one compartment and two frame model, the initial deformation is applied for whole structure.

Source	Wopl
Faulkner (1975)	0.00705
Antoniou (basis Faulkner) (1980)	0.00369
Carlsen et al (1978)	0.00592
Antoniou (basis Carlsen et al) (1980)	0.00505
Smith et al (1988) (Slight level)	0.00064
Smith et al (1988) (Average level)	0.00256
Smith et al (1988) (Severe level)	0.00767
Masaoka (1996)	0.00277
DnV	0.00620
Mean	0.00461
Standard Deviation	0.00234
Variance	5.49496E-06
CoV	0.50798266

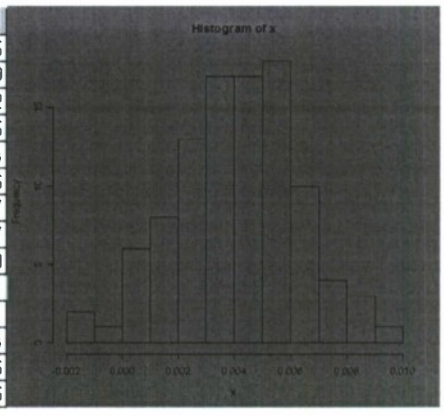

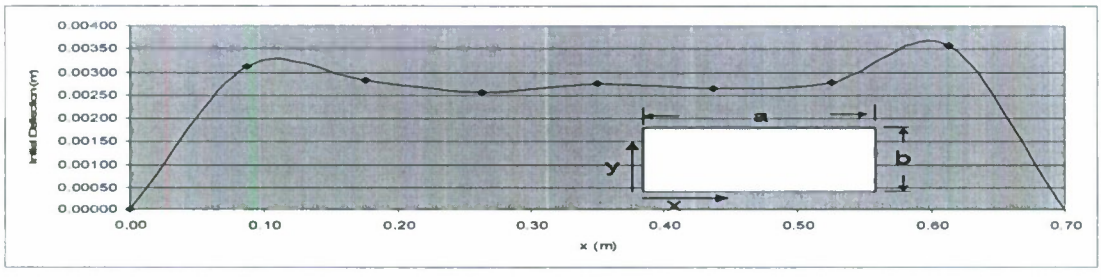

Figure 5.6.3.2-1: Initial deformation model for FE analysis

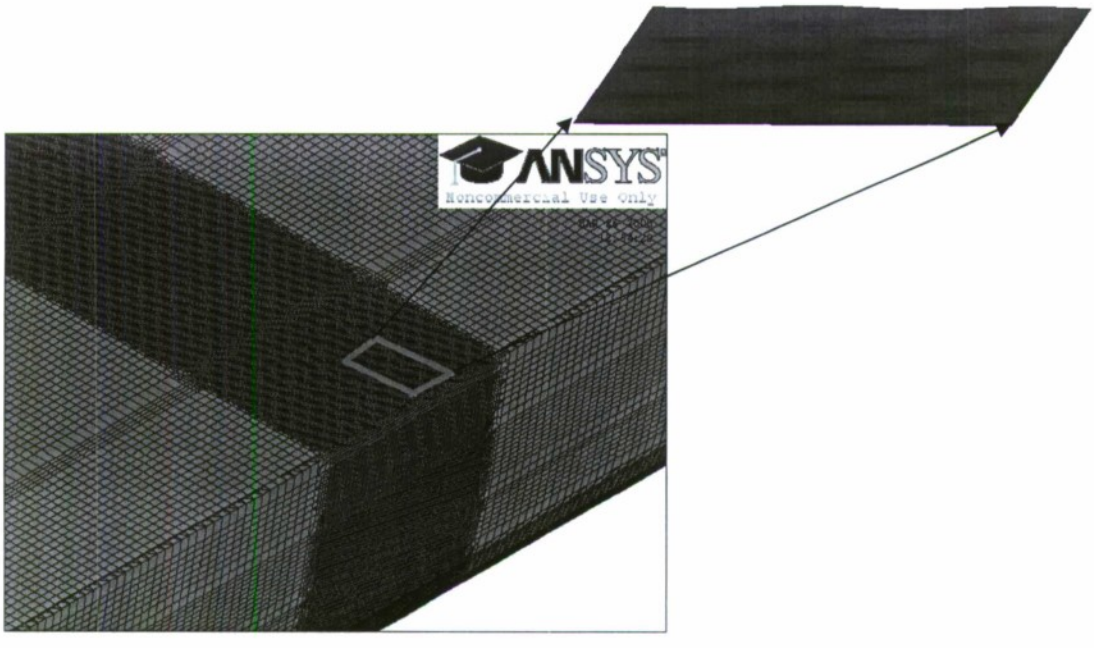

Figure 5.6.3.2-2: Initial deformation as applied to mid part of 3 compartment model.

5.6.3.3 Material Model

The ships hull structure is designed for two types of steels. The properties of steels are listed in the Table 5.6.3.3-1 below. Both the types of steel materials are modelled as elastic-perfectly-plastic. Production related variations in strength of material such as residual stress due to welding, cold working etc are not considered directly as a random parameter in FE analysis but shall be counted for in reliability analysis using uncertainty factors. Therefore, the yield strength and modulus of elasticity were taken as deterministic values in finite element analysis.

Table 0-1: Properties of steel materials

Parameter	Mean	COV	Distribution	Correlation
HY80 σ_y (MN/m^2)	552	0.08	Lognormal	Independent
HSS σ_y (MN/m^2)	351	0.08	Lognormal	Independent

5.6.3.4 Load modelling and boundary conditions

As already discussed in section 4.3, in present study only vertical bending moment, horizontal bending moment and torsion is considered. The finite element analysis shall be carried out to determine ultimate strength for the following conditions:

- Vertical bending moment to determine ultimate vertical bending moment capacity
- Horizontal bending moment to determine ultimate horizontal bending moment capacity.
- Torsion to determine ultimate capacity of the section in torsion
- Combined load to determine response function for hull structure in the form similar to equation 3.3-6 and also for interaction of three moments mentioned above.

The incrementally moment equivalent displacement were applied as loads on boundary nodes for nonlinear analysis and to achieve ultimate failure as shown in figure 5.6.3.4-1.

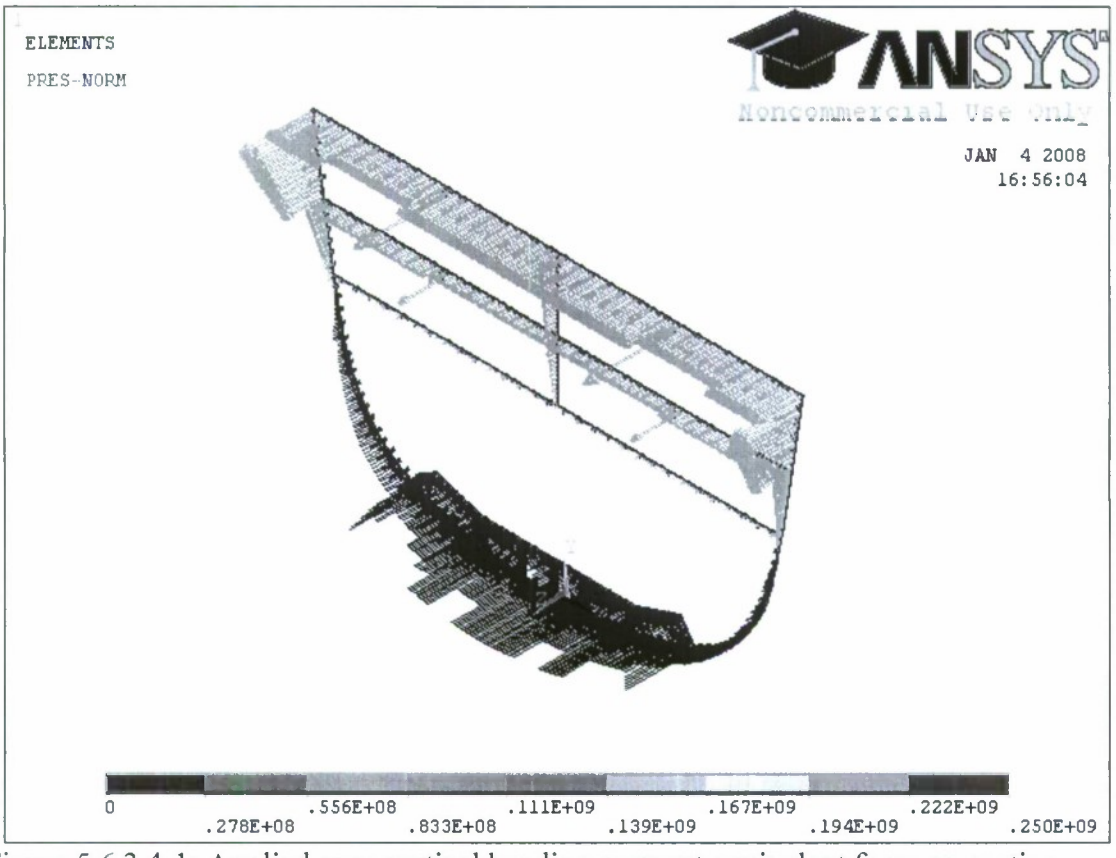

Figure 5.6.3.4-1: Applied pure vertical bending moment equivalent force on section

5.6.3.5 FE Analysis Results & Discussion

As discussed earlier, three different levels of finite element models were adopted for these studies considering available computing resources and project time to achieve good estimates for ultimate strength of intact and residual ultimate strength of damaged ship and comparison of results. Comparatively small 2 frame finite element model was used to carry out extensive FE runs to develop response surface for reliability based assessment and for comparison of results with conventional beam-column methods for both intact as well as for damaged condition. The one compartment and three compartment models were used to established influence of boundary conditions to infer the results obtained from two frame model.

The figure 5.6.3.5-1 and 5.6.3.5-2 show the one compartment coarse mesh FE model and analysis results for pure ultimate vertical and horizontal moment, respectively. Whereas, figure 5.6.3.5-3 show the ultimate horizontal moment of the hull girder using two frame finite element model. The FE model and stress distribution at ultimate failure for damaged structure of three compartment model is shown in figure 5.6.3.5-4. The plot in figures 5.6.3.5-5 and 5.6.3.5-6 show the torsion bending moment against load steps as structure approach to progressive collapse for three compartment and 2 frame models, respectively.

Two types of moment interaction functions were developed, one set of two combinations of moments such as interaction of vertical and horizontal moments, and one set for interaction of all the moments viz. vertical, horizontal and torsion moment. Since only vertical and horizontal interaction function was possible using conventional beam-column, the similar results were obtained from FE analysis to compare with that of MARS calculations.

The figure 5.6.3.5-7 show the vertical and horizontal moment interaction diagram developed using finite element analysis results of two frame model. The vertical/horizontal moment interaction function is as follows:

$$\left(\frac{M_v}{M_{uv}}\right)^{2.9543} + \left(\frac{M_h}{M_{uh}}\right)^{1.0751} = 1 \qquad (5.6.3.5\text{-}1)$$

It may be observed that one point (0.577, 0.44) considerably depart from the trend followed by the remaining data points. This point was excluded from response function evolution. The residual standard error of 0.056 in fitting of remaining data points was achieved.

The vertical and horizontal moment interaction function obtained from finite element analysis is compared with that of MARS beam-column and elastic-plastic interaction diagram in figure 5.6.3.5-8. The comparison of ultimate moment capacity estimate obtained using the two methods, FE and beam-column method of MARS are given in figure 5.6.3.5-9 for various M_v/M_h ratio. The percentage difference of the two is plotted in figure 5.6.3.5-10 where it is apparent that a maximum difference of 14% in estimate of ultimate moment capacity of hull girder is for M_v/M_h ratio around 0.6. The ultimate moment estimates obtained using beam-column method are higher than that form the two frame finite element analysis. The difference between the two results diminishes as M_v/M_h moment ratio increases.

The other interaction formulae obtained from two frame finite element analysis are the followings:

- Vertical moment and torsion interaction

$$\left(\frac{M_v}{M_{uv}}\right)^{1.9329} + \left(\frac{M_T}{M_{uT}}\right)^{1.176} = 1 \qquad (5.6.3.5.2)$$

- Horizontal moment and torsion interaction

$$\left(\frac{M_h}{M_{uh}}\right)^{2.438} + \left(\frac{M_T}{M_{uT}}\right)^{2.8946} = 1 \qquad (5.6.3.5.3)$$

- Vertical moment, horizontal moment and torsion, also see figure 0-11

$$\left(\frac{M_v}{M_{uv}\left(1-\left(\frac{M_T}{M_{uT}}\right)^{1.176}\right)^{0.5174}}\right)^{2.9543} + \left(\frac{M_h}{M_{uh}\left(1-\left(\frac{M_T}{M_{uT}}\right)^{2.8946}\right)^{0.5174}}\right)^{1.0751} = 1 \qquad (5.6.3.5.4)$$

The comparison of ultimate moment capacity of the hull girder in intact and damaged conditions is given in table 5.6.3.5-1. Further, table 5.6.3.5-2 gives % age of ultimate strength of damaged hull in comparison to ultimate strength of intact ship. The ultimate moment capacity in torsion for damaged hull is only 8% of the ship in intact condition.

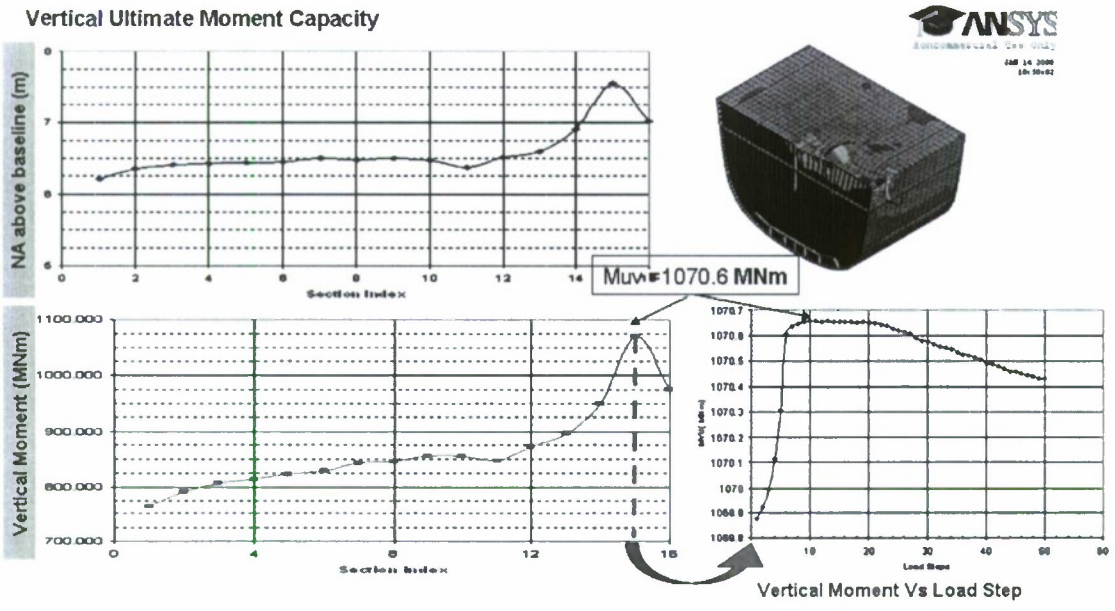

Figure 5.6.3.5-1: Ultimate vertical moment capacity of one compartment model

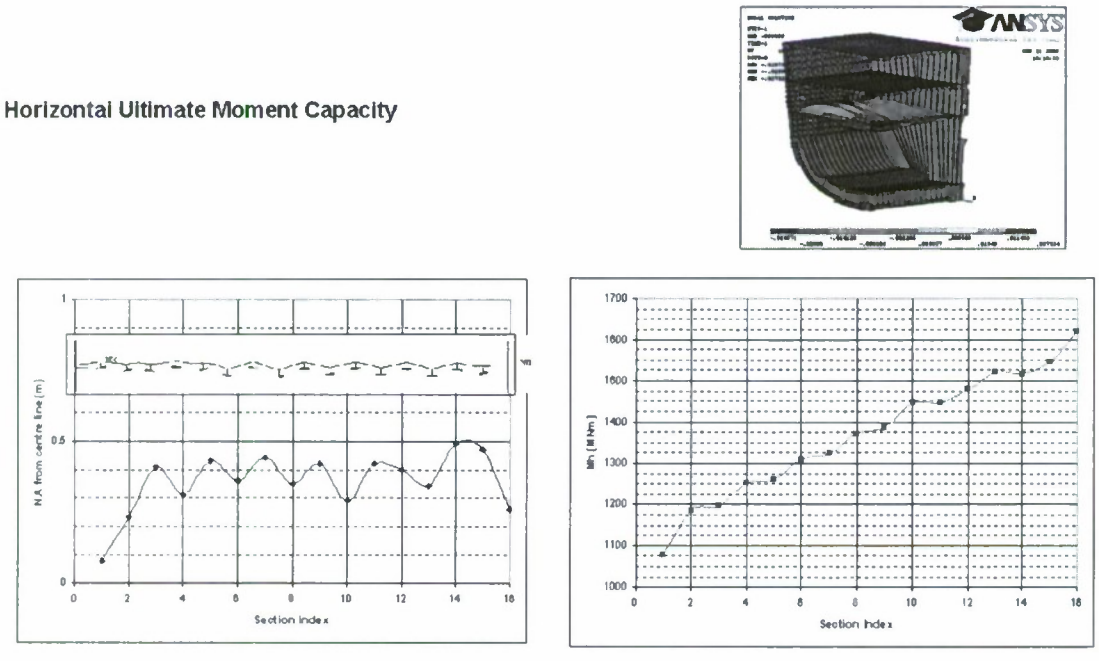

Figure 5.6.3.5-2: Horizontal ultimate moment capacity - one compartment model

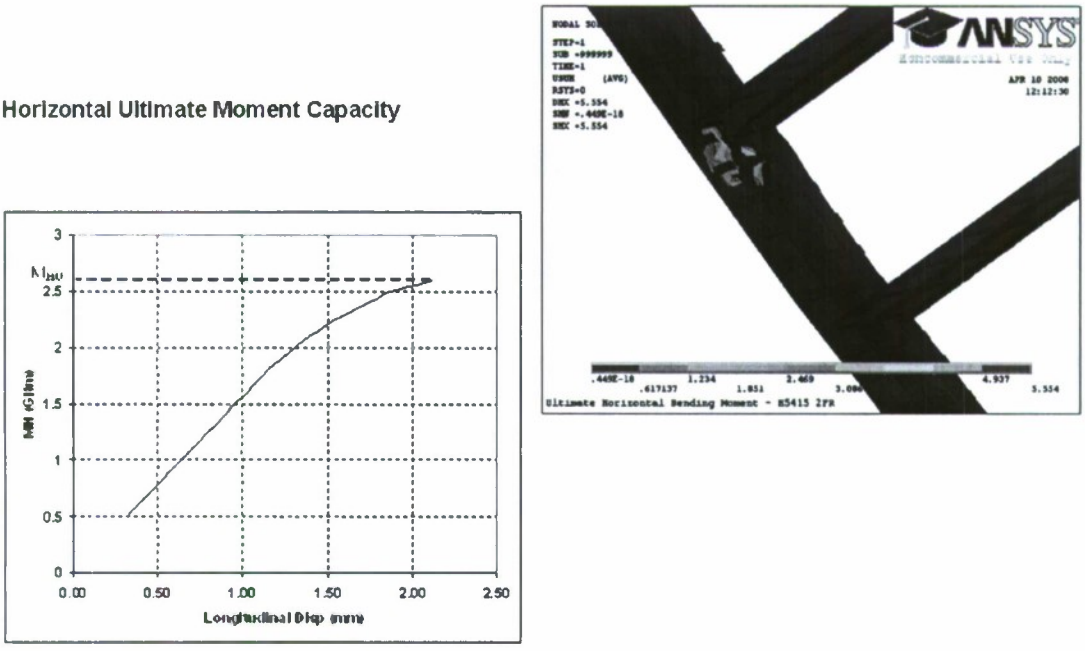

Figure 5.6.3.5-3: Horizontal ultimate moment capacity of 2 Fr model

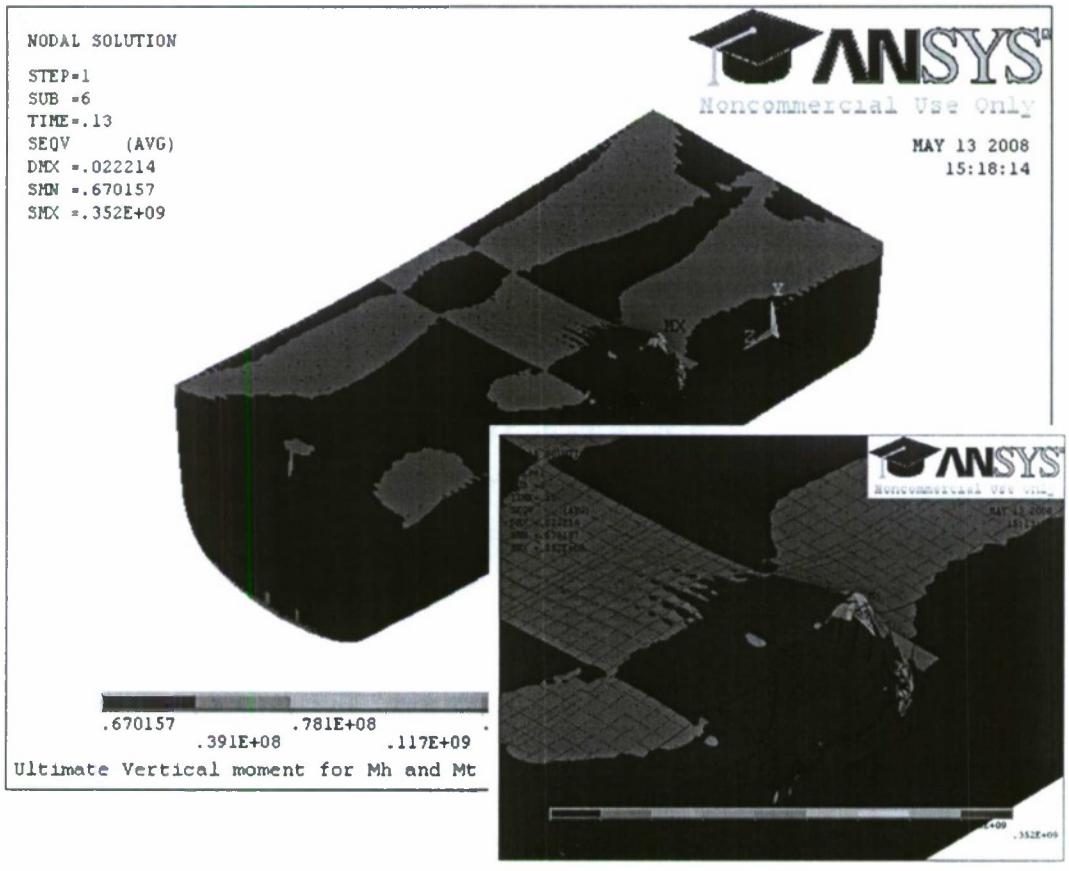

Figure 5.6.3.5-4: Deformation and stress distribution of damaged 3 compt. model

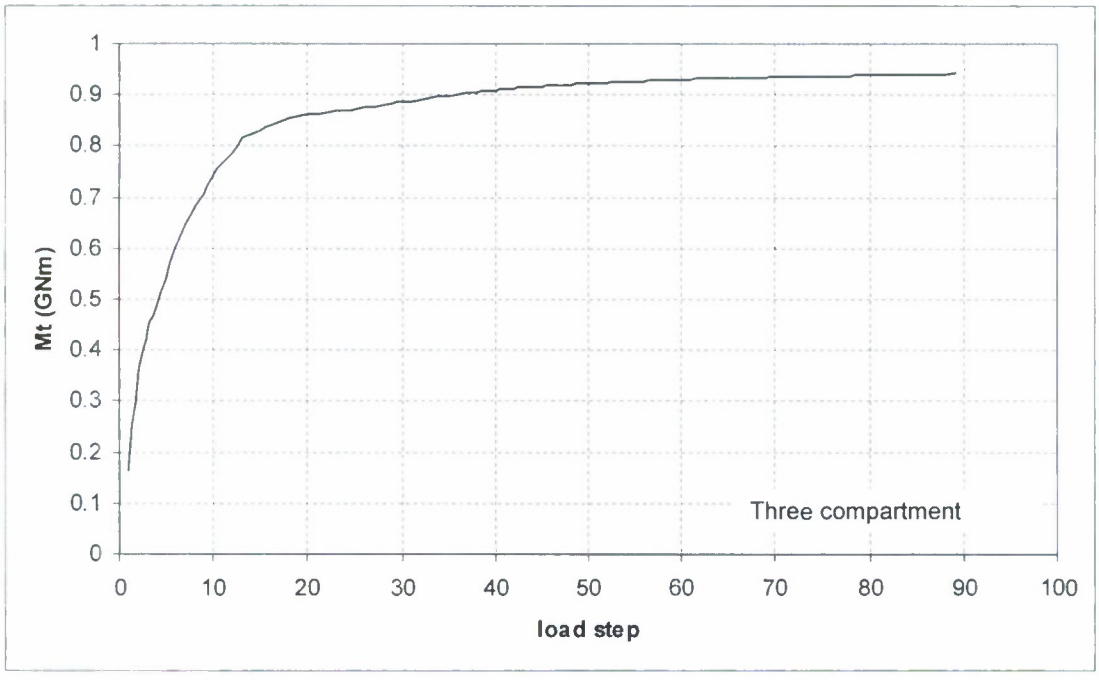

Figure 5.6.3.5-5: Ultimate torsion – three compartment FE analysis

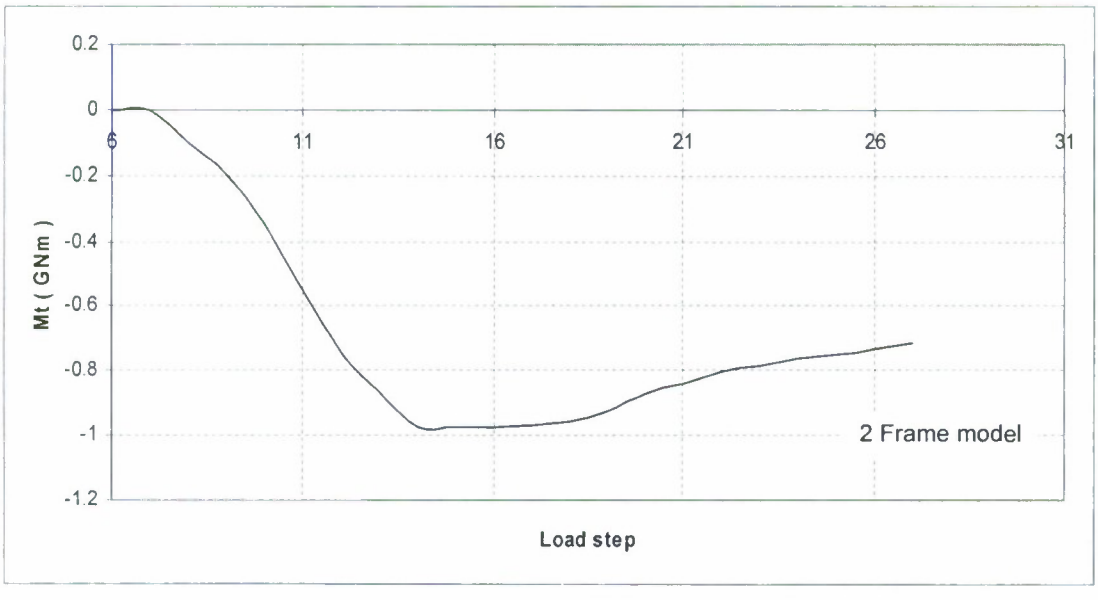

Figure 5.6.3.5-6: Ultimate torsion – 2 Frame FE model

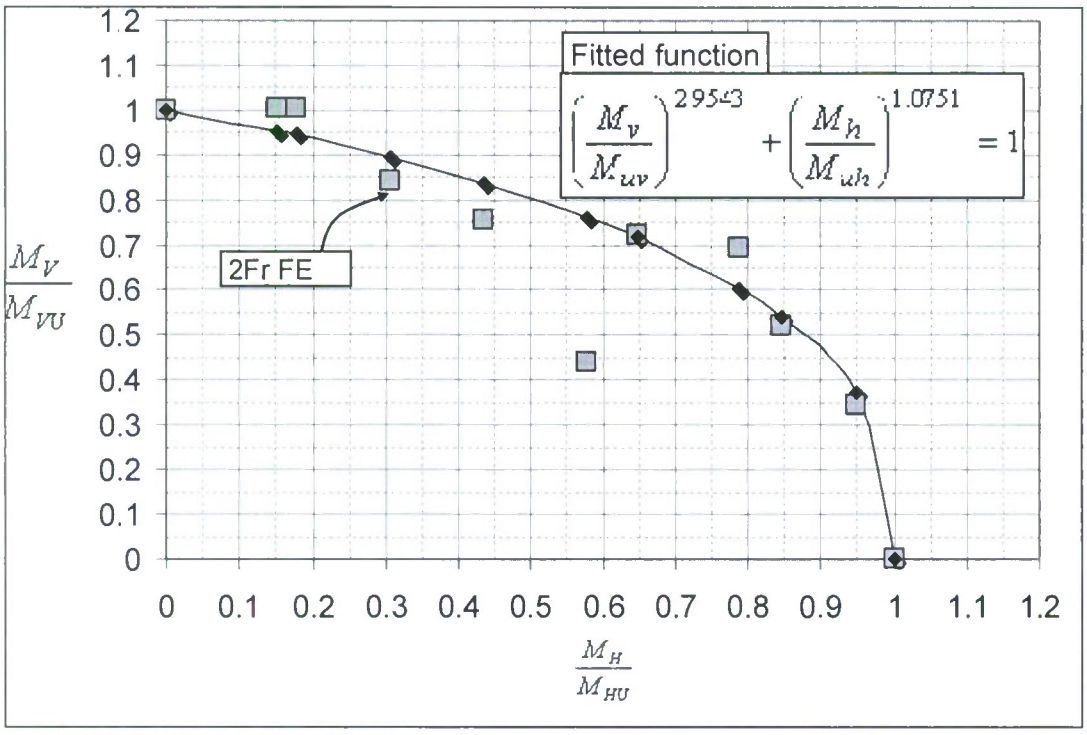

Figure 5.6.3.5-7: Mv and Mh interaction – 2 Frame FE analysis results

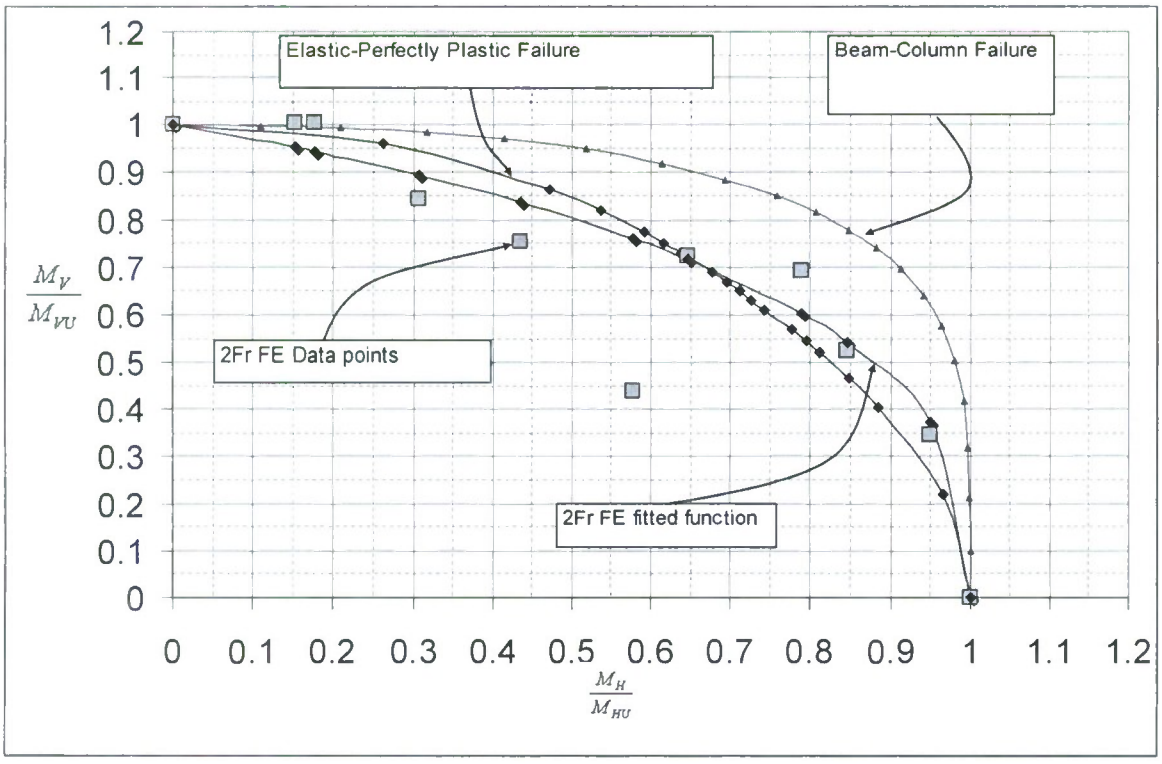

Figure 5.6.3.5-8: Comparison MARS results with 2 Frame FE analysis results

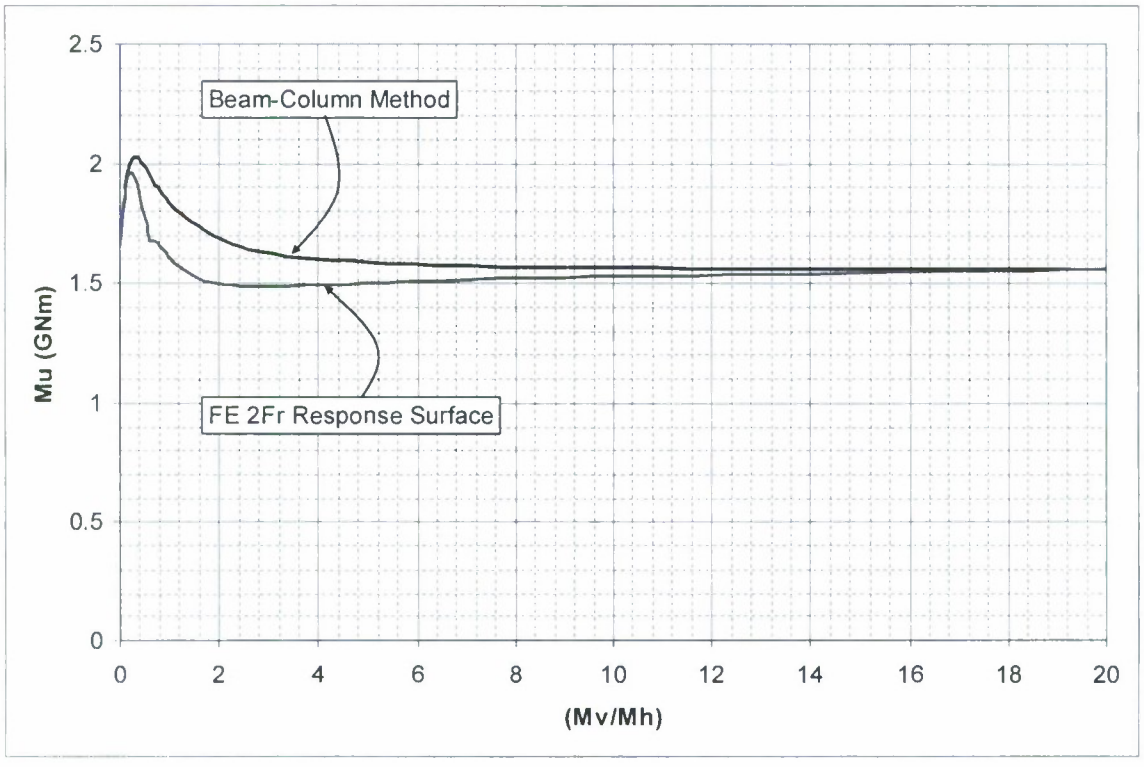

Figure 5.6.3.5-9 : Comparison Ultimate Moment, MARS and 2 Frame FE results

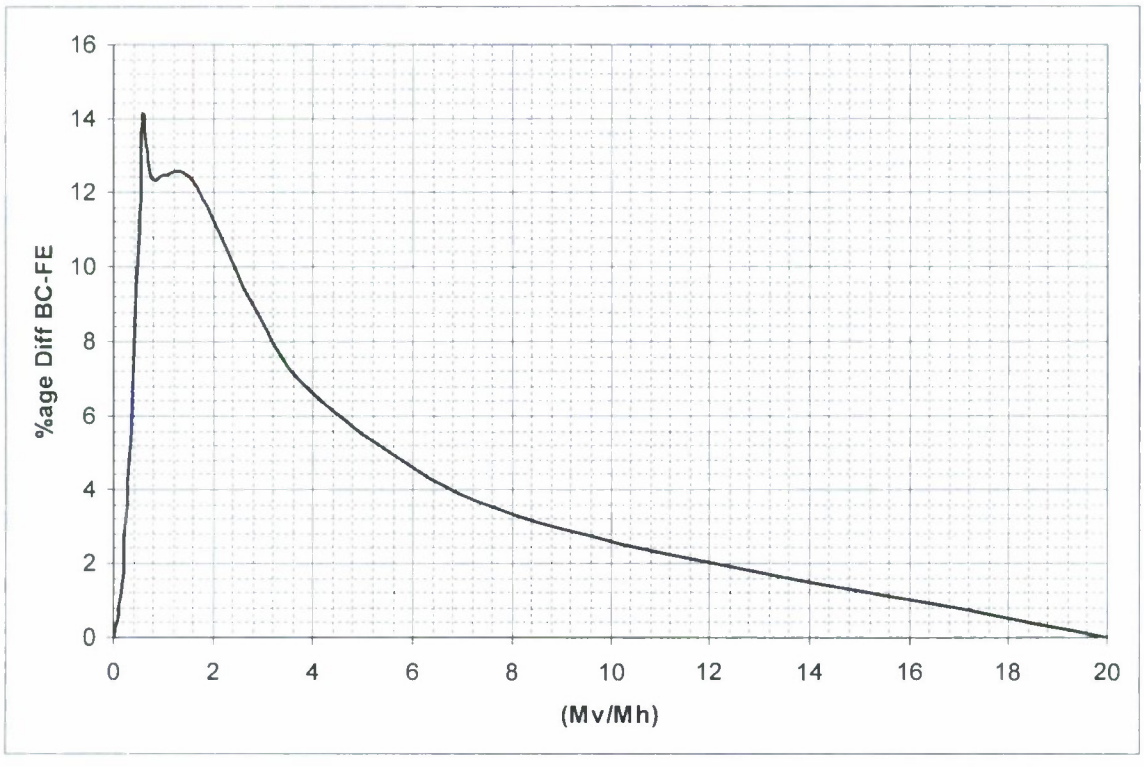

Figure 5.6.3.5-10: Ultimate moment, % age difference MARS and FE results

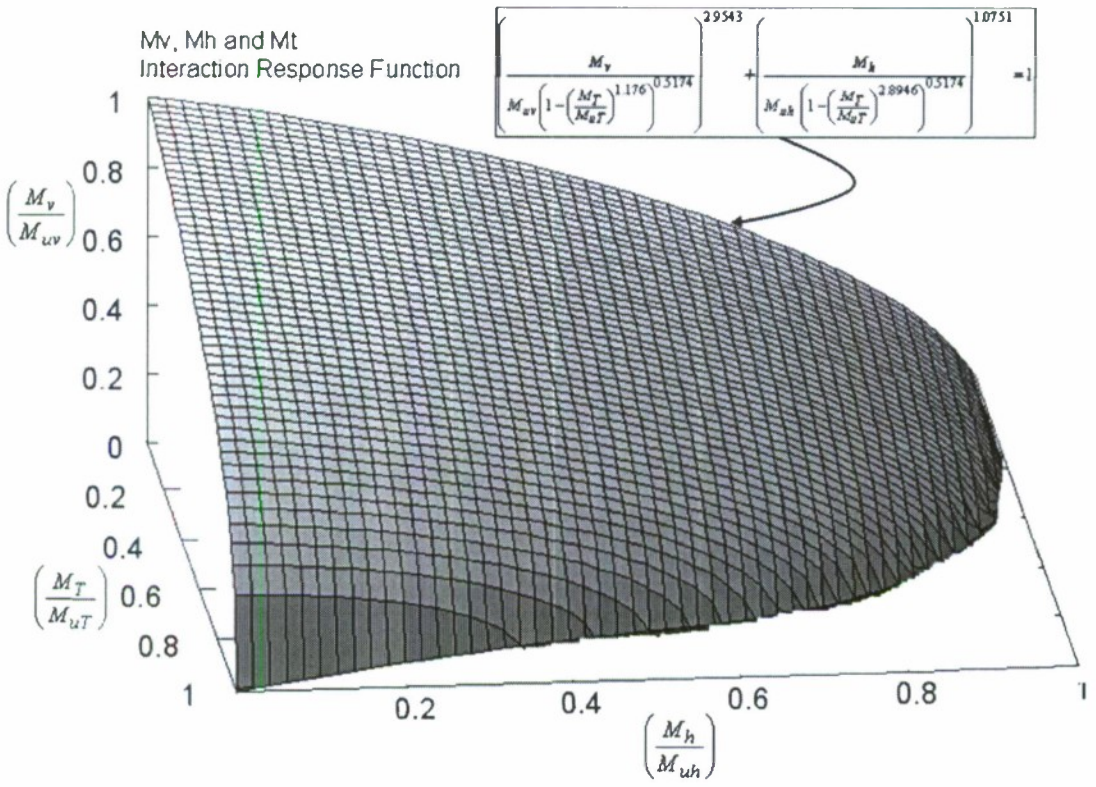

Figure 5.6.3.5-11: Interaction response surface for M_v, M_h and M_t moment; FE results

Table 5.6.3.5-1: Comparison of ultimate vertical bending moment from different methods

Method		MARS			ANSYS			
Item		EIP	BC	FPMC	CM	2 FrM	3C Intact	3C Dmg
M_{VU} (GNm)	Hogging	2.3405	1.5609	2.1859	1.389	2.095	1.46	0.16
	Sagging	-2.3405	-1.3273	-2.1859	-1.0701	-1.1445	-1.28	-0.214
$M_{HU\ (GNm)}$		2.5587	1.657	2.5878	1.625	1.3199	1.079	+0.341 -0.281
$M_{TU\ (GNm)}$		-	-	-	1.251	1.5611	0.898	0.0728

Key:

EIP	Elastic- Ideally Plastic Failure Mode
BC	Beam Column Failure Mode (Smith's Method)
FPMC	Full Plastic Moment Capacity of the section
CM	Coarse Mesh Model
2FrM	2Frame Model – fine mesh
FM	Failure Mode
Dmg	Damaged condition

Table 5.6.3.5-2: Comparison of ultimate strength of intact and damaged ship

Ultimate Moment (GNm)	Intact	Damaged	Damage %age of Intact
Vertical (saging)	-1.28	-0.214	17%
Horizontal	-1.079	0.341	32%
		-0.281	26%
Torsion	0.898	-0.0728	8%

5.6.3.6 Reliability Based Assessment of Intact and Damaged Structure

The reliability based assessment of hull structure was made for both intact and damaged condition. The reliability assessment for intact condition is made for worse case scenario i.e. sea state 7 including three combinations as identified from ship loading analysis.
The reliability analysis was carried out using the moment interaction formula given in (equation 5.6.3.5-4). Accordingly, limit state function is defined as follows:

$$g(M_v, M_h, M_t) = \chi_S \left(\frac{M_v}{M_{uv}\left(1-\left(\frac{M_T}{M_{uT}}\right)^{1.176}\right)^{0.5174}} \right)^{2.9543} + \left(\frac{M_h}{M_{uh}\left(1-\left(\frac{M_T}{M_{uT}}\right)^{2.8946}\right)^{0.5174}} \right)^{1.0751} - 1 \times \chi_R \qquad (5.6.3.6\text{-}1)$$

Where χ_S and χ_R are the modelling uncertainty parameters (Faulkner et. al., 1988) defined as follows:

$$\chi = \frac{actual\ response}{predicted\ response} \qquad (5.6.3.6\text{-}2)$$

It is usual to assume normal distribution for uncertainty parameters, the 10% variance Teixeira (1997) in ultimate strength modelling and 15% variance (Mansour et al., 1994) in load modelling as suggested in the reference above are taken in reliability analysis. The still water bending moment is considered normally distributed. The extreme value Type-II distribution is taken for vertical, horizontal and torsion moment loads. For ultimate moment capacity of the hull, Weibull distribution is assumed.

Because of time constraints, complete interaction diagram for vertical moment, horizontal moment and torsion for damaged case using finite element analysis was not possible. Considering comparison of vertical/horizontal moment for damaged and intact condition using beam-column method as shown in figure 0-9), giving small difference in moment ratio, around 11%, the limit state function in (equation 0.1) was used for reliability analysis for damaged condition as well with scaling that is built into function because of ultimate vertical, horizontal and torsion moment capacities of structure used in evaluation. This assumption is considered reasonable to derive reliability index in absence of more accurate moment interaction function for damaged condition.

The reliability analysis was carried out using CALREL software, the First Order Reliability Method (FORM) and Monte Carlo Simulation (MCS). The reliability index and relevant probabilities as calculated are given in table 5.6.3.6.1 for both intact and damaged case.

The reliability index for intact condition is a minimum 3.771 for load combination 1 (LC1) for sea state 7 that is worse operating scenario for the ship. In case of damaged scenario, the reliability index against various sea states are plotted in figure 5.6.3.6-1. As it is given in table 5.6.3.6-1, the FORM calculation did not converge for load combination LC2 for sea state 5, and for all the load combination of sea state 6 & 7. The minimum value of reliability index is 0.30812 with a probability of failure 0.621 for load combination case 1 (LC1) of sea state 3. It is interesting to note that reliability index for LC1 and LC2 of damaged ship structure for sea state 4 is higher then that in sea state 3.

Table 5.6.3.6-1: Reliability analysis results

Particulars	Load combination	B	Probability
Intact Condition			
Sea state 7	LC1	3.771	8.1434E-5
	LC2	4.643	1.7154E-6
	LC3	5.389	3.5375E-8
Damaged Case 1			
Sea State 3	LC1	FORM =-0.30812	6.2100E-1
		MCS =-0.118	5.4700E-1
	LC2	FORM =0.13623	5.5418E-1
		MCS =-0.0277	4.8900E-1
	LC3	FORM =-1.4114	9.2094E-1
		MCS =-1.3047	9.0400E-1
Sea State 4	LC1	FORM =3.7956	7.3629E-5
		MCS =3.8905	5.0000E-5
	LC2	FORM =4.3257	7.6008E-6
		MCS =3.2905	5.0000E-4
	LC3	FORM =1.0294	1.5165E-1
		MCS =1.2873	9.9000E-2
Sea State 5	LC1	FORM =9.658	1.0000E-10
		MCS =3.3201	4.5000E-4
	LC2	FORM = 0	Failed
		MCS = 2.144	1.3400E-2
	LC3	FORM = 4.3915	5.6296E-6
		MCS = 3.194	7.0000E-4
Sea State 6	LC1	FORM = 0	Failed
		MCS = 2.6256	4.3000E-3
	LC2	FORM = 0	Failed
		MCS = 1.1838	1.825E-1
	LC3	FORM = 0	Failed
		MCS = 2.3888	8.4500E-3
Sea State 7	LC1	FORM = 0	Failed
		MCS = 1.9943	2.3059E-2

	LC2	FORM = 0	Failed
		MCS = 0.1917	4.2400E-1
	LC3	FORM = 0	Failed
		MCS = 1.6919	4.5333E-2

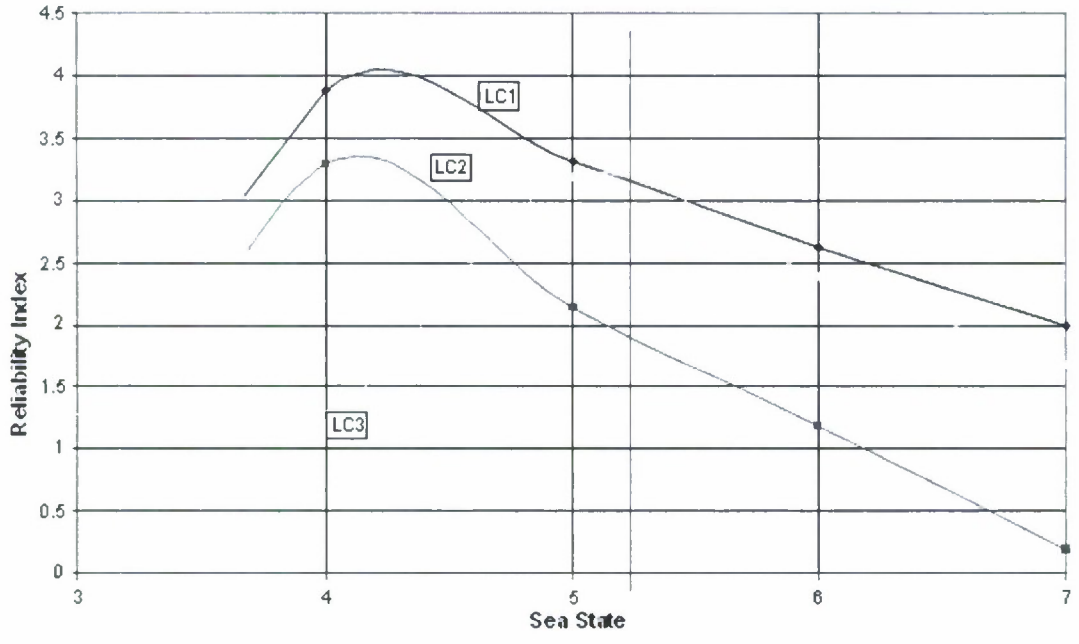

Figure 5.6.3.6-1: The reliability index for different sea state – damaged case

6. CONCLUSIONS

In the previous NICOP project, a procedure has been developed to assess structural integrity of damaged ships. The state of the art of the methods for predicting environmental loads and assessing the structural safety has been reviewed. The developed procedure has been applied to a sample vessel, HULL5415, to demonstrate the accuracy of these methods.

In the current project, some tools for predicting wave-induced loads and assessing ultimate hull girder strength have been further developed. In particular, a 2D linear and non-linear method have been applied to the ship model to calculate the wave-induced loads in regular waves at the cut where the force gauge is installed to measure the loads in the experimental tests. The numerical results have been compared with the experimental results.

The 2D linear method can accurately predict wave-induced vertical bending moment in head seas and stern quartering seas, but the accuracy is deteriorating with the increase of wave amplitude. The accuracy in predicting horizontal bending moment is not as good as that for vertical bending moment, but is acceptable in most cases. However, the predictions of torsion moment are not satisfactory.

The experimental results have revealed that majority of the response RAOs show non-linear trend, in which the non-dimensional responses are decreasing as wave amplitude increases in most frequency range, especially at the frequency where the responses achieve the maximum. For vertical bending moment this trend is very remarkable. It may be said that the high non-linearity is an inherent feature of the sample vessel with a very fine hull form.

Because the damage on the ship is unsymmetrical transversely, it is expected that the wave-induced loads might be different when the wave is approaching the ship model from different sides due to the dynamic behaviour of the flooded water in the damaged compartment. The test results have shown that the vertical bending moment at 45° wave heading at most of frequencies was slightly larger than that at 315° wave heading. There was no clear trend for horizontal bending moment at 45° and 315° wave headings. However, the horizontal bending moment in beam seas at 90° wave headings is slightly larger than that at 270° wave headings. The torsion moment at 315° wave headings is larger than that at 45° wave headings.

The 2D nonlinear method does not produce satisfactory results for vertical bending moment, horizontal bending moment and torsion moment in regular waves. Although this conclusion was largely based on the analysis of the results of 2 metres wave height, it was equally applicable to the results of 2.5 metres wave height. Again the predictions of torsion moment are the worst among the three components of the wave-induced loads, while the predictions of vertical bending moment have similar level of accuracy to those of horizontal bending moment. The nonlinear method tends to produce better results at the resonant frequencies than at the other frequencies. However it should be pointed out that the measured wave heights were not equal to 2.0 metres, which was used in the numerical calculations, at most frequencies.

Model uncertainties of both 2D linear and non-linear method have been calculated. For the 2D linear method, it is observed that the accuracy, which is measured by the mean and COV of the model uncertainty factor, of vertical bending moment is generally better than that of horizontal bending moment and torsion moment, and the accuracy for loads in head seas is much better than those in stern quartering seas and beam seas. This could be mainly caused by the underwater hull form of the ship model with a small C_b compared with conventional ships. The

COV of horizontal bending moment is almost as twice as that of vertical bending moment. The COV of torsion moment is the largest of the three. Because of the large difference in COV for different force components it is more rational to consider the model uncertainties for vertical bending moment, horizontal bending moment and torsion moment separately in reliability analysis rather than using one combined model uncertainty for all the components. It can be seen that the 2D linear method has better mean and COV of X_m in the predictions of vertical bending moment and horizontal bending moment in both intact condition and damage scenario 2 than the 2D nonlinear method, and both 2D linear and nonlinear methods have produced unsatisfactory results in torsion moment. Based on the current results, it may be said that the 2D linear method is more accurate than the nonlinear method. However the nonlinear method can distinguish the difference between the positive and negative responses, but linear methods can't. This advantage of the nonlinear method is especially important for ships with small block coefficient, such as frigate etc. For a frigate the ratio of sagging bending moment to hogging bending moment could be as large as 1.78 (Clarke, 1986). In addition, hull girder strength in hogging is normally different from that in sagging. Therefore the nonlinear method is preferred. This slight preference of the nonlinear method was also based on another fact that the nonlinear method tends to produce better results in the resonant region than at other frequencies. Based on the current method for combining different load components, the accuracy in resonant region is more important than that at other frequencies.

Extreme design loads in irregular waves based on the RAO from the 2D linear method, 2D non-linear method and experiment have been calculated for the ship model at the cut under intact condition and damage scenario 2. The formulae recommended in the Lloyds Register's rule for Navy vessels (Lloyds Register of shipping, 2002) have also been used to calculate the wave-induced extreme design loads. The results have demonstrated that the difference of extreme design loads (both hogging and sagging) between 2m and 2.5m wave height was increasing with the increase of sea roughness, but always less than 6.62% in intact condition and 6.60% in damage scenario 2. For hogging bending moment, the extreme design value based on 2m wave height is greater than that based on 2.5m wave height, but it was opposite for sagging bending moment. Hence the effects of wave amplitude on the prediction of extreme design loads are modest.

Both 2D linear and nonlinear methods overestimate extreme design loads. The results are slightly in favour of the 2D linear method in intact condition, while the accuracy of the 2D linear method is almost as good as that of the 2D nonlinear method in damage scenario 2. Both hogging and sagging bending moments predicted by the 2D nonlinear method agree well with those of LR Rules' formulae. However hogging bending moment of the 2D linear method agrees well with that of LR Rules' formulae, but agreement in sagging bending moment is not as good as in hogging bending moment because in the 2D linear method the sagging bending moment is the same as hogging bending moment. It should be noted that the extreme design value predicted by LR Rules is the maximum value for the ship model. In another word, the extreme design value at the cut is the same as that of the sections at the amidships because the cut is not far away from amidships. However the extreme design value predicted by the 2D nonlinear method at the cut could potentially be quite different from that of the sections at amidships, where the maximum vertical bending moment would occur. This might, at least partly, explain that LR Rules produces the largest extreme design hogging and sagging moments in intact condition.

The ratio of sagging bending moment to hogging bending moment of the 2D nonlinear method is in good agreement with that of the experimental tests. This is an advantage of the 2D nonlinear method over the 2D linear method. It should be pointed out that the reason for using

the RAO of the 2D linear method rather than 2D non-linear method in strength assessment in this project is that the 2D non-linear results were not available at that moment.

The 2D linear method has also been applied to the original ship (not the model) in order to predict the extreme design loads for the strength assessment. The extreme design loads at sea states 3 - 7 have been calculated using short term prediction. An 'equivalent wave system' has been used to combine vertical bending moment, horizontal bending moment and torsion moment.

The ultimate bending moment for intact ship using the Smith Method like approach using the MARS software of BV classification society have been calculated for various load combinations. Further, equations for interaction of horizontal and vertical bending moment are also developed for the hull 5415 using conventional methods and finite element methods.

Using the conventional beam-column method for ultimate strength of hull girder, only vertical and horizontal moment interaction can be assessed. The difference between intact and damaged case ultimate strength found through beam-column is around 10% for sagging condition.

Finite element methods were used to get an accurate assessment of residual strength of damaged ship. Initial deformation, deformation due to collision impact and residual stresses were all included in finite element modelling and simulation. For the studied case scenario, the ultimate torsion is found to 8% of the strength in intact case. Whereas, the ultimate vertical moment is 17% and horizontal moment for compress in the damaged part of hull is 26% of the intact condition. The large difference in the damaged ship strength estimated using beam-column method and finite element method suggest requirement to update load shortening curves for beam-column methods to improve estimation for damaged condition.

ACKNOWLEDGEMENT

We would like to thank Dr Paul Hess of ONR for his enthusiasm and enormous efforts. We benefit greatly from his in-depth knowledge in both loading and strength assessment, his vision for determining the way forward, and his guidance and support. His contribution could not be overstated. We are also grateful to Professor Atilla Incecik for his great contribution to this project.

REFERENCES

Adegeest, L. J. M. (1995). *"Non-linear hull girder loads in ships",* Thesis, Delft Univ. Technology.

ANSYS User Manuals version 9

Aryawan, I. D. (2000). *"Development of Analysis Methods for the Assessment of Hull Girder Loading and Strength of a Turret Moored FPSO",* PhD thesis, University of Newcastle upon Tyne.

Bhattacharyya, R. (1978). *"Dynamics of Marine Vehicles"*, John Wiley and Sons, Chichester.

Box, G.E.P. & Wilson, K.B. 1951. "On the experimental attainment of optimum conditions", Journal of the Royal Statistical Society, Series B,13:1–45.

Brebbia, C. A. & Walker, S. (1979). *"Dynamic analysis of offshore structures",* Butterworth & Co. ISBN: 0-408-00393-6.

Bucher, C., Macke, M. & Most, T., 2006. "Application of approximate response functions in structural reliability analysis", 3rd Inetrnational ASRANet Colloquium, 10-12th July 2006, Glasgow, UK.

Bureau Veritas, (2003). *"Rules for the Classification of Steel Ships"*, Bureau Veritas, France.

Chan, H. S. (1992). "Dynamic structural responses of a mono-hull vessel to regular waves", *International Shipbuilding Progress, Vol.* 39, pp.287-315.

Chan, H. S. (1993). "Prediction of motion and wave loads of twin-hulled ships", *J Marine Structures, Vol. 16*, pp.75-102.

Chan, H. S. (1995). "On the calculations of ship motions and wave loads of high-speed catamarans", *International Shipbuilding Progress, Vol. 42*, pp.181-95.

Chan, H. S. (1998). "Prediction of large amplitude motions and wave loads on a RoRo ship in regular oblique waves in intact and damage conditions", *DTR-4.1-UNEW-12.98, DEXTREMEL project BE97-4375.*

Chan, H. S., Voudouris, G.; Servis, D. P. and Samuelides, M. (2000). "Residual Strength of a Damaged RO RO Ship", *DTR-4.3-UNEW-04.00, DEXTREMEL project BE97-4375.*

Chan, H. S.; Atlar, M. and Incecik, A. (2002). "Large-amplitude motion responses of a Ro-Ro ship to regular oblique waves in intact and damaged conditions", *J Marine Science and Technology Vol. 7*, pp.91-99.

Chan, H. S.; Atlar, M. and Incecik, A. (2003). "Global wave loads on intact and damaged RO-RO ships in regular oblique waves", *J Marine Structures Vol. 16*, pp.323-344.

Chan, H.S., Incecik, A. and Atlar, M. (2001). "Structural Integrity of a Damaged Ro-Ro Vessel" Proceedings of the second international conference on collision and grounding of ships, Technical University of Denmark, Lybgby, pp. 253-258.

Clarke, J. D. (1986). "*Wave Loading in Warships", in Advances in Marine Structures*, edited by Clarke, J. D and Smith, C. S, Elsevier Applied Science Publishers, pp. 1–25

Das P.K., Zheng Y. (2000). "Cumulative formation of Response Surface and its use in Reliability Analysis", *Probabilistic Engineering Mechanics*, Elsevier Science Ltd., 15 (309-315).

Ditlevsen, H.O.Madsen.(1996). *"Structural Reliability Methods"*, John Wiley & Sons, England.

DNV (2000). *"DNV Classification Note 30.5: Environmental Conditions and Environmental Loads".*

Faltinsen, O.M. (1990). *"Sea Loads on Ships and Offshore Structures"*, Cambridge Ocean Technology Series, Cambridge University Press.

Faulkner D, Adamchak JC, Snyder GJ, Vetter MF. (1973). "Synthesis of Welded Grillages to Withstand Compression and Normal Loards". *Computers and Structures*, Vol. 3, No. 2, pp.221-246.

Frank, W. (1967). "Oscillation of Cylinders in or Below the Free Surface of Deep Fluids", *Hydromechanics Laboratory Research and Development Report.*

Fujino, M. and Yoo, B. S. (1985). "A study on wave loads acting on ship in large amplitude (3rd Report) ", *J Society of Naval Architects of Japan, Vol. 158.*

Fukasawa,T., Kawabe,H and Moan,T (2007). "On extreme ship response in severe short-term sea state", *Advancements in Marine Structures*, pp.33-40

Ghoneim, G. A.; Tadros, G. (1992). "Finite element analysis of damaged ship hull structures". *Proceedings of the International Offshore Mechanics and Arctic Engineering*, Vol. 1, pt B, (1992), pp. 611-620.

Ghose, D.J., Nappi, N.S. and Wiernicki, C.J. (1995). "Residual strength of damaged marine structures". *Report of Ship Structures Committee*, SSC-381.

Hasselmann, K. at al (1973). "Measurements of wind wave growth and swell decay during the Joint North Sea Wave Project (JONSWAP)". *Deutsches Hydrographisches institut*, Hamburg, Report Series A. No. 12.

Holyland.A. & Marvin R. 1994. "System Reliability Theory Models and Statistical Methods", John Wiley & Sons Ltd.

Incecik, A.; Pu, Y. Aryawan, I. D. (2001). "Hydro-Structural Aspects of Floating Production Storage and Offloading Systems (FPSOs)", *Proc the 1st PNU International Colloquium*, Pusan National Unv., Korea, pp.7-17.

ISSC, 1997. "Ultimate Strength". Report of Committee III.1, *International Ships and Offshore Structures Congress*.

Jacobs, W.R. (1958). "The analytical calculation of ship bending moments in regular waves". J Ship Research, June, pp.20-29.

Jacobs, W.R.; Dalzell, J. & Lalangas, P. (1960). "Guide to computational procedure for analytical evaluation of ship bending-moments in regular waves", *US Navy, Davidson Laboratory*, Report No.791.

Jensen J.J. et al. (1994). "Report of Committee III.1, Ductile Collapse", *Proc. 12th International Ship and Offshore Structures Congress*, Vol. 1, pp.229-387.

Lee, Y. W. ; Pu, Y. ; Chan, H. S. ; Incecik, A. ; Dow, R. S. ; Khan, I. ; Das, P. K. and Hess, P. E. (2006). "Reliability – Based Performance Assessment of Damaged Ships", Research Report of Office of Naval Research (USA), Contract number N00014-04-1-0757.

Lloyd's Register of Shipping, 2002, *"Rule and Regulations for Classification of Naval Ships"* Vol.1.

Lloyd's Register, (2000). *"World Casualty Statistics: annual statistical summary of reported loses and disposals of propelled sea-going merchant ships of not less than 100 GT".*

Mano, H., Kawabe, H., Iwakawa, K., Mitsumune, N. (1977). "Statistical character of the demand on longitudinal strength (second report)-long term distribution of still water bending moment", *Journal of the Society of Naval Architects of Japan*, Vol. 142, in Japanese.

Mansour, A.E., Thayambaili, A., 1994. "Probability-based ship design procedures: loads and load combinations", Report to Ship Structures Committee, SSC-373.

Melchers, R.E. (1999). *"Structural Reliability Analysis and Prediction 2nd Edition"*, John Wiley & Sons, Chichester, England.

Myers, R. H. & Montgomery, D. C. 2002. "Response Surface Methodology: Process and Product Optimization Using Designed Experiments", Wiley, New York.

Ochi, M.K. (1973). "On prediction of extreme values". *J Ship Research*, v.17 n.1, Mar, pp.29-37.

Ochi, M.K. (1981). "Principles of extreme value statistics and their application". *Extreme Loads Response Symposium (SNAME)*, Arlington, VA, October 19-20, SNAME, pp.15-30.

Paik J.K. (1992). "Ultimate hull girder strength analysis using Idealized Structural Unit Method: A case study for double hull girder with transverseless system", *PRADS '92*, Elsevier, Vol. 2, pp.745-763, Newcastle upon Tyne.

Paik J.K. (1993). "Hull Collapse of an aging Bulk Carrier under combined Longitudinal Bending and Shearing Force", *Trans. RINA.*

Paik J.K. (1999). "SPINE, A computer program for analysis of elastic –plastic large deflection behaviour of stiffened panels". User's Manual", *Pusan National Univ.,* Korea.

Paik J.K., Kim D.H., Bong H.S., Kim M.S., Han S.K. (1992). "Deterministic and probabilistic safety evaluation for a new double-hull tanker with transverseless system". *Trans. SNAME*, Vol. 100, pp.173-198.

Paik J.K., Kim S.K., Yang S. H., Thayamballi A.K. (1997). "Ultimate Strength Reliability of Corroded Ship Hulls", *Trans. RINA.*

Paik J.K., Lee D.H. (1990). "Ultimate strength-based safety and reliability assessment of ship's hull girder", *Journal Soc. Naval Arch. Of Japan*, Vol. 168, pp.397-409, in Japanese.

Paik J.K., Lee J.M.(1995). "An empirical formulation for predicting ultimate compressive strength of plates and stiffened plates", *Journal of Ship Research.*

Paik JK, Thayamballi A and Che JS. (1996). "Ultimate Strength of Ship Hulls Under Combined Vertical Bending, Horizontal Bending and Shearing Forces". *Transactions of SNAME* 1996, Vol. 104, pp.31-59.

Paik, J. K.; Thayamballi, A. K.; Yang, S. H. (1998). "Residual strength assessment of ships after collision and grounding". *Marine Technology*, v 35, n 1, pp. 38-54.

Paik, J.K., Pedersen, T. (1996). "A simplified method for predicting ultimate compressive strength of ship panels". *Int. Shipbuilding Progress*, Vol. 43, No. 434, pp.139-157.

Paik, Jeom K. (1992). "Reserve/residual strength of a double hull girder in intact/damaged condition". *Proceedings of the Second International Offshore and Polar Engineering Conference*, Jun 14-19 1992.

Paik, Jeom K.; Lee, Tak K. (1995). "Damage and residual strength of double-hull tankers in grounding". *International Journal of Offshore and Polar Engineering*, v 5, 4, Dec 1995, pp. 286-293.

Pu, Y. (1995). "Reliability analysis and reliability-based optimization design of SWATH ships," PhD thesis, University of Glasgow, Glasgow.

Qi, Enrong; Cui, Weicheng; Peng, Xingning; Xu, Xiangdong. (1999). "Reliability assessment of ship residual strength after collision and grounding". *Journal of Ship Mechanics*, v 3, n 5, pp. 40-46.

Raff, A. I., (1972). "Program Scores-Ship structural response in waves", Final report on Project SR-174, "Ship Computer Response" to Report of the Ship Structure Committee, SSC-230, Washington D.C.

Reilly, E., Shin, Y.S. and Kotte, E.H. (1988): "A prediction of structural load and response of a SWATH ship in waves", Naval Engineering Journal, ASNE, May, pp251-264.

Samuelides, M.S., Voudouris, G., Toulios, M., Amdahl, J. and Dow, R. (2007). "Simulation of the behaviour of double bottom subjected to grounding actions", 4th International Conference on Collision and Grounding of Ships, Hamburg University of Technology, pp.93-102.

Salvesen, N.; Tuck, E.O. & Faltinsen, O. (1970). "Ship motion and sea loads", *SNAME Trans v.78*, pp.1-30.

Santos,T.A and Soares,C.G (2007). "Time domain simulation of ship global loads due to progressive flooding". *Advancements in Marine Structures*, pp.79-88.

Shahid, M. & Das, P.K.. 2007. "Structural system reliability using FEM and reliability processors" MARSTUCT Conference on Advancements in Marine Structures, 12-14th of March 2007, Glasgow, UK.

Smith C.S., Dow R.S. (1986): "Ultimate Strength of Ship's Hull under Biaxial Bending", ARE TR86204, *ARE Dunfermline*, Scotland.

Smith, C.S. (1977). "Influence of Local Compressive Failure on Ultimate Longitudinal Strength of a Ship's Hull". *Proceedings of the PRADS*: International Symposium on Practical Design in Shipbuilding; 18-20 October 1977; Tokyo, Japan: Society of Naval Architects of Japan, pp. 73-79.

Smith, C.S. and Dow, R., 1981. "Residual Strength of Damaged Steel Ships and Offshore Structures". *Journal of Constructional Steel Research*, Vol. 1, No. 4, September.

Smith, T.W.P.; Drake, K.R & Rusling, S (2007). "Investigation of the variation of loads experienced by a damaged ship in waves". *Advancements in Marine Structures*, pp.89-98.

Teixeira, A., 1997. "Reliability of marine structures in the context of risk based design", MSc Thesis, University of Glasgow, UK.

Thoft-Christensen. P. & Murotsu Y. 1986. "Application of Structural System Reliability Theory", Springer-Verlag Berlin Heidelberg New York Tokyo.

Ueda Y., Rashed S.M.H., Paik J.K.(1984). "Plate and stiffened plate units of the idealized structural unit method-Under in-plane loading", *Journal Soc. Naval Arch. Of Japan*, Vol. 156, pp.336-375, in Japanese.

Ueda, Y. and Rashed, SMH. (1984). "The idealised structural unit method and its application to deep girder structures". *Computers and Structures*, Vol. 18, No. 2, pp.227-293.

Wang, Ge; Chen, Yongjun; Zhang, Hanqing; Peng, Hua. (2002). "Longitudinal strength of ships with accidental damages". *Marine Structures*, v 15, n 2, 2002, p 119-138.

Wang, Xiaozhi and Moan, Torgeir (1996). "Stochastic and deterministic combinations of still water and wave bending moment in ships", Marine Structures, Vol. 9, pp.787-810.

Zheng, Y., Das, P. K., Yu, L. and Leira, B. (2005). "A benchmark study on response surface method", Maritime Transportation and Exploitation of Ocean and Coastal Resources, © Taylor & Francis Group, London.

Zhang, Sheng-Kun; Yu, Qing; Mu, Yang. (1996). "Semi-analytical method of assessing the residual longitudinal strength of damaged ship hull". *Proceedings of the International Offshore and Polar Engineering Conference,* v 4, pp. 510-516.

Zheng, Y. and Das, P. K. (2000). "Improved response surface method and its application to stiffened plate reliability analysis", Engineering Structures, Vol. 22, No.5, pp.446-458.

APPENDIX A:
RAOs OF WAVE-INDUCED LOADS OF THE SAMPLE VESSEL

This appendix presents the RAOs, which were predicted by the 2D linear method, of wave-induced vertical bending moment, horizontal bending moment and torsion moment of the sample vessel at the midship section, which was 70.5 metres from AP, in intact condition and damage scenario 1. These data were used to calculate the extreme design loads by short term prediction.

RAO in Intact Condition

Head sea

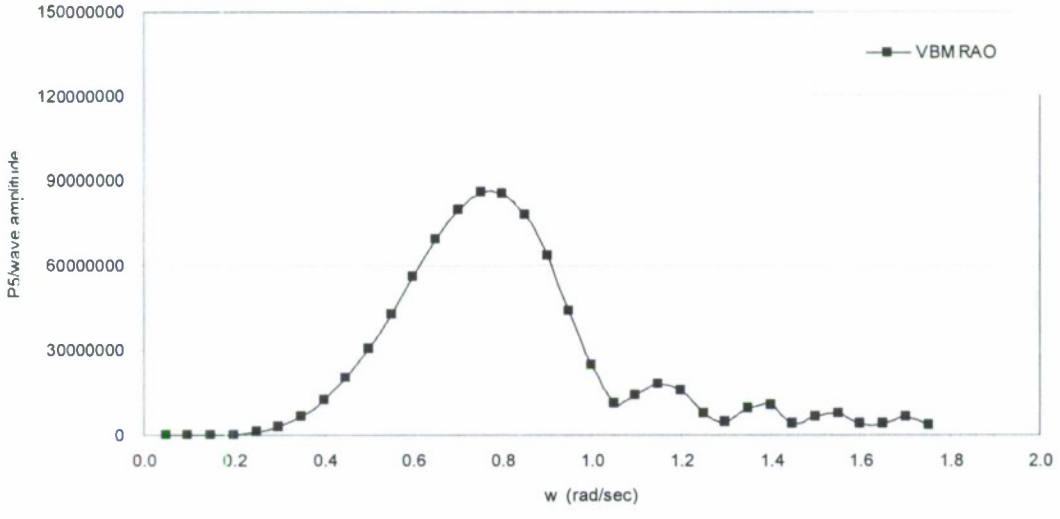

Figure A.1: Vertical bending moment RAO at head waves in intact condition

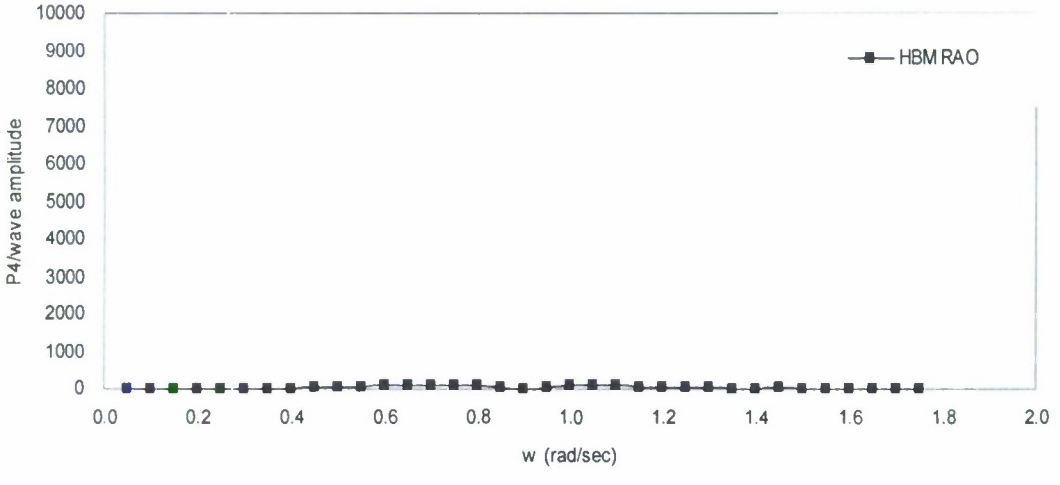

Figure A.2: Horizontal bending moment RAO at head waves in intact condition

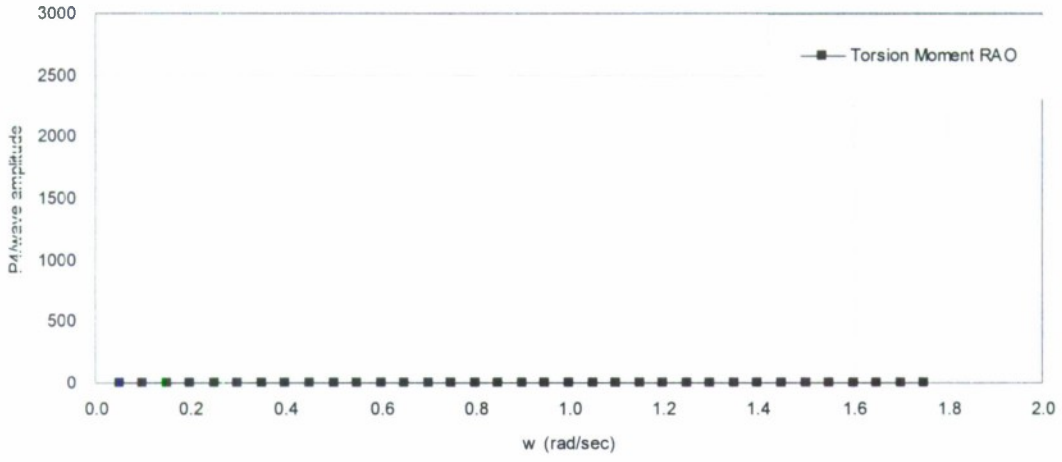

Figure A.3: Torsion moment RAO at head waves in intact condition

Stern quartering sea

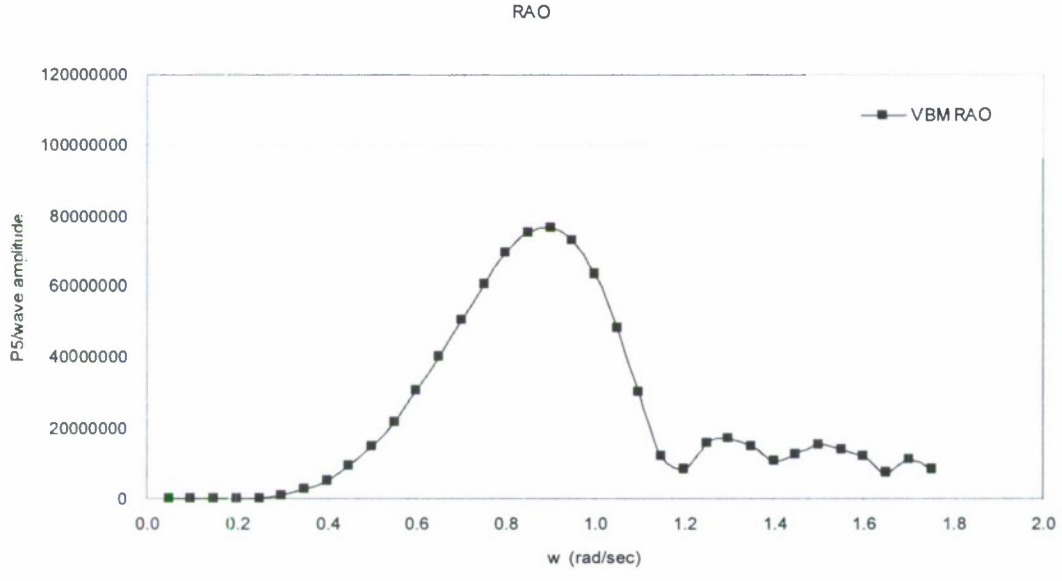

Figure A.4: Vertical bending moment RAO at stern quartering waves in intact condition

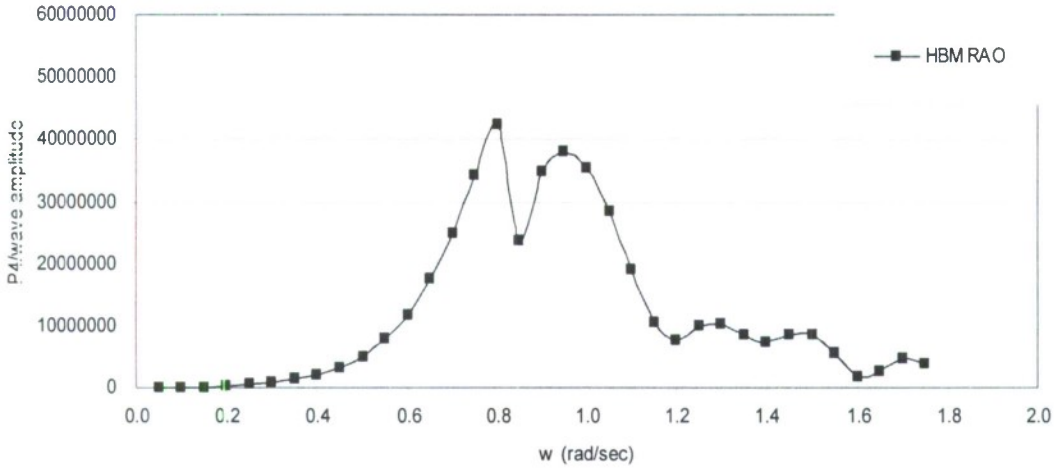

Figure A.5: Horizontal bending moment RAO at stern quartering waves in intact condition

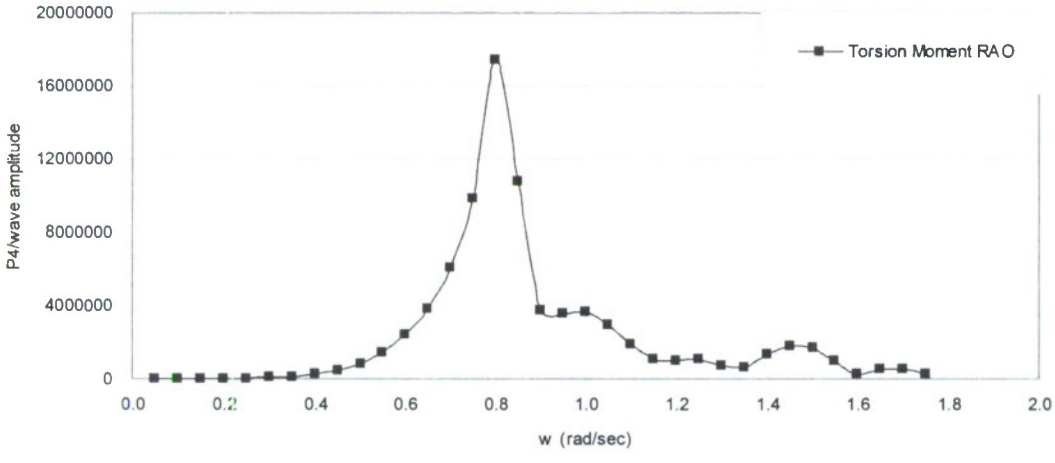

Figure A.6: Torsion moment RAO at stern quartering waves in intact condition

Beam sea

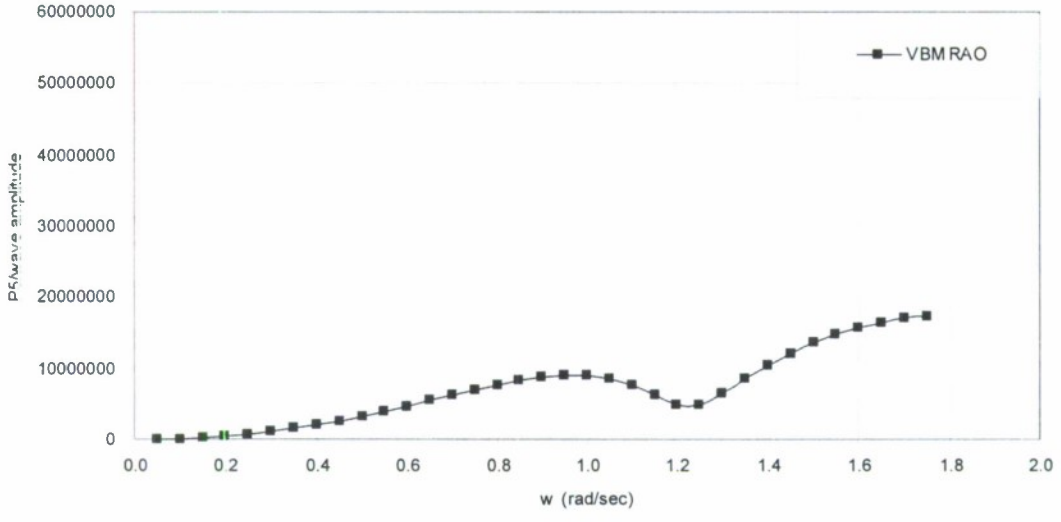

Figure A.7: Vertical bending moment RAO at beam waves in intact condition

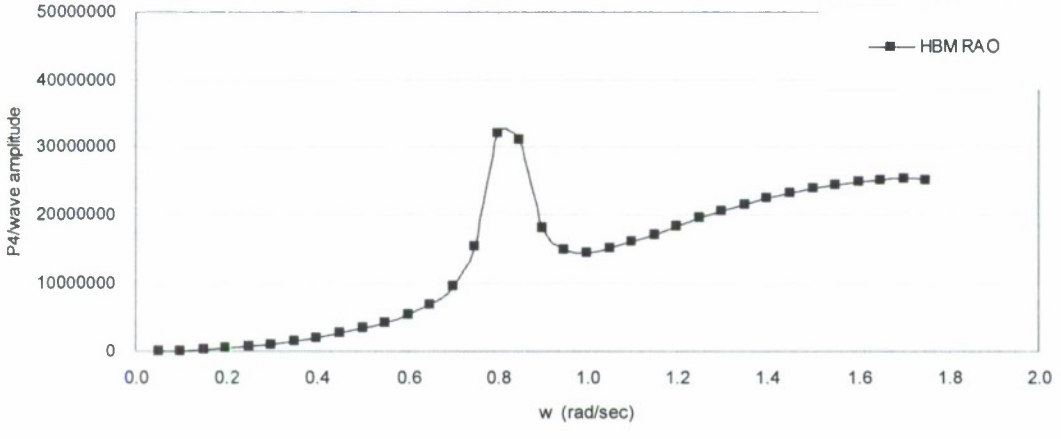

Figure A.8: Horizontal bending moment RAO at beam waves in intact condition

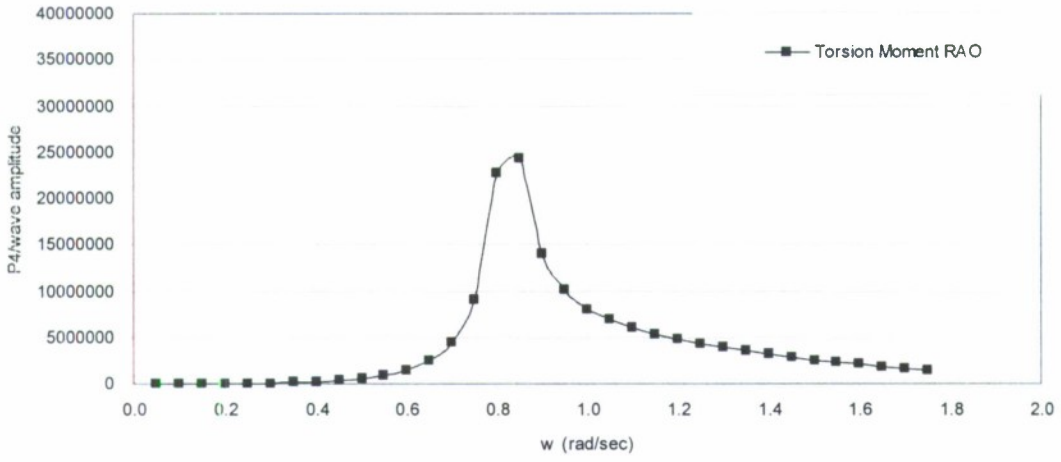

Figure A.9: Torsion moment RAO at beam waves in intact condition

RAO in Damage Scenario 1

Head sea

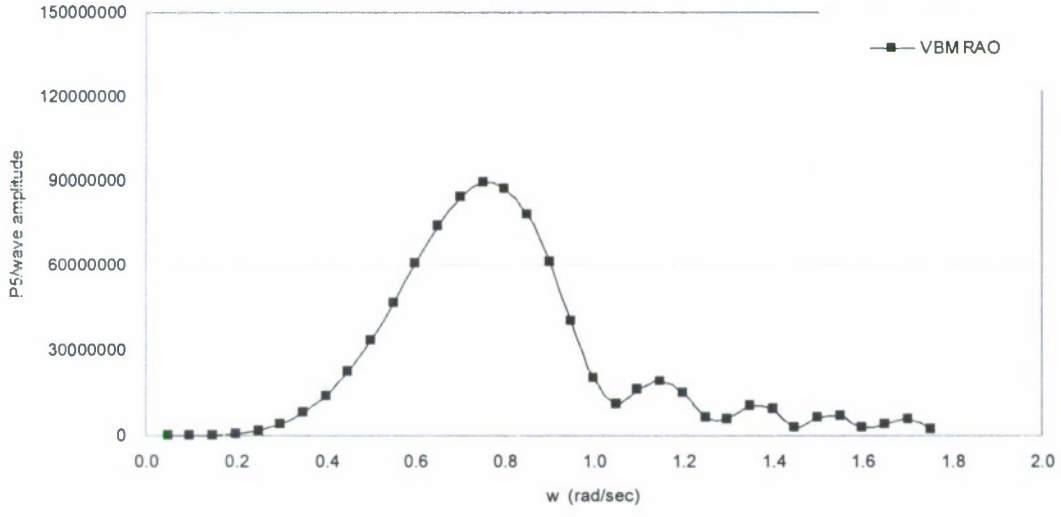

Figure A.10: Vertical bending moment RAO at head waves in damage scenario 1

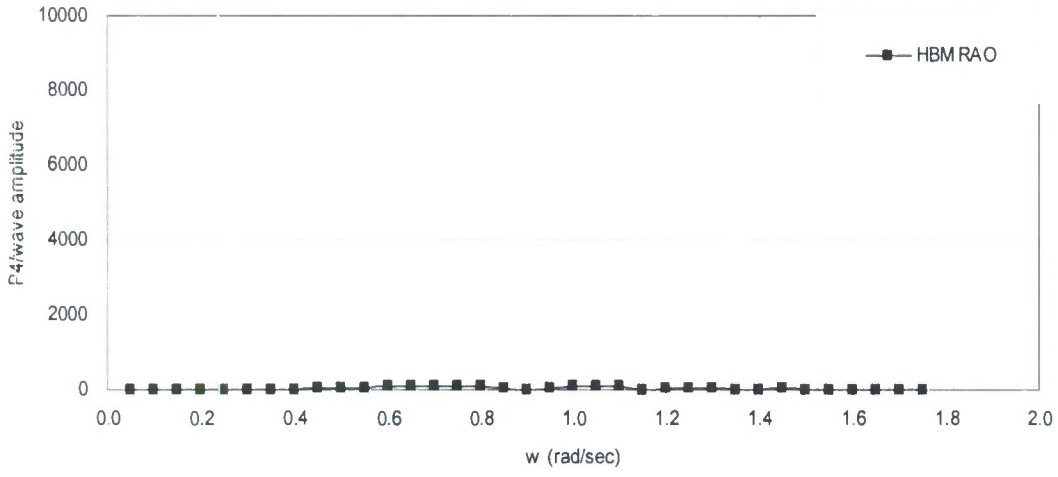

Figure A.11: Horizontal bending moment RAO at head waves in damage scenario 1

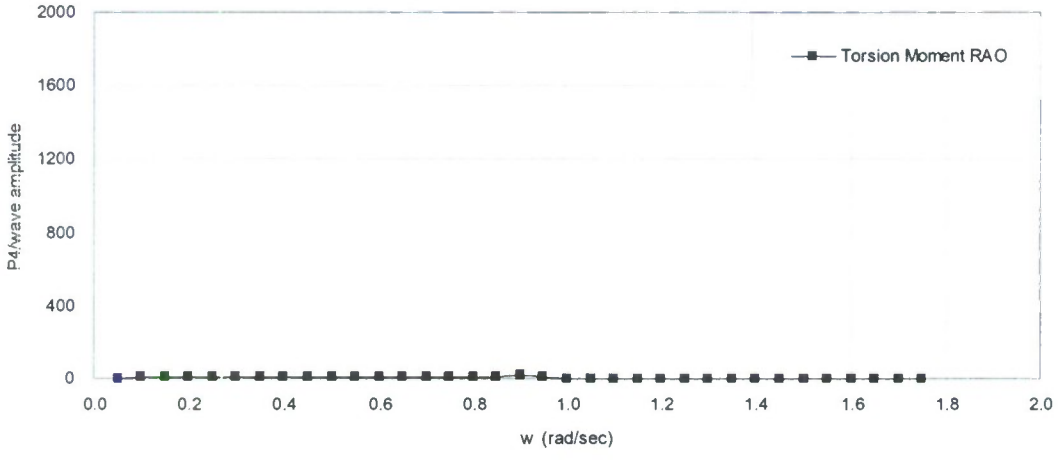

Figure A.12: Torsion moment RAO at head waves in damage scenario 1

Stern quartering sea

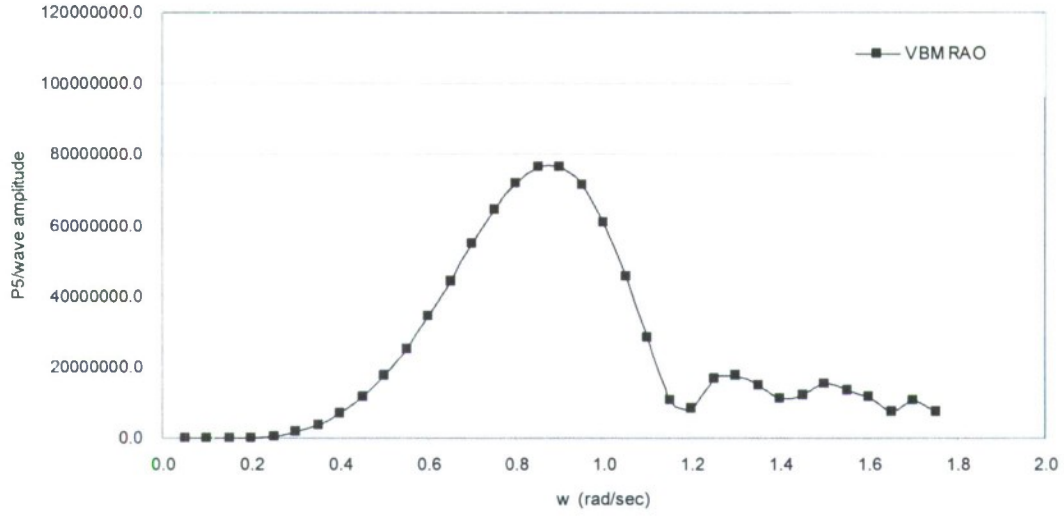

Figure A.13: Vertical bending moment RAO at stern quartering waves in damage scenario 1

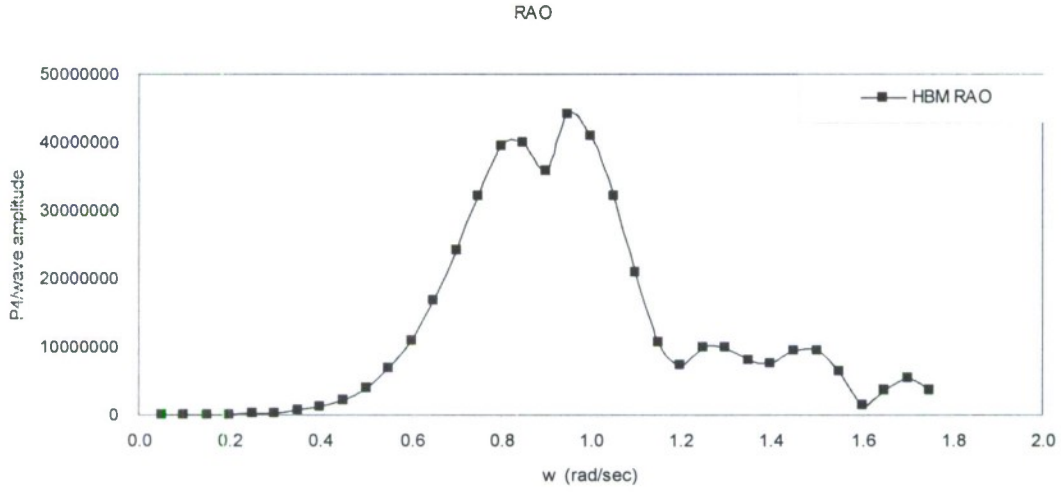

Figure A.14: Horizontal bending moment RAO at stern quartering waves in damage scenario 1

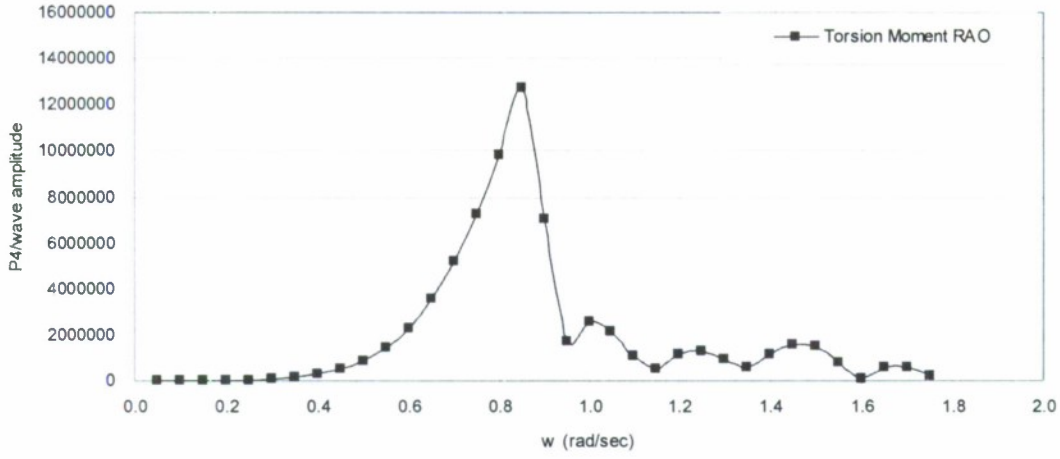

Figure A.15: Torsion moment RAO at stern quartering waves in damage scenario 1

Beam sea

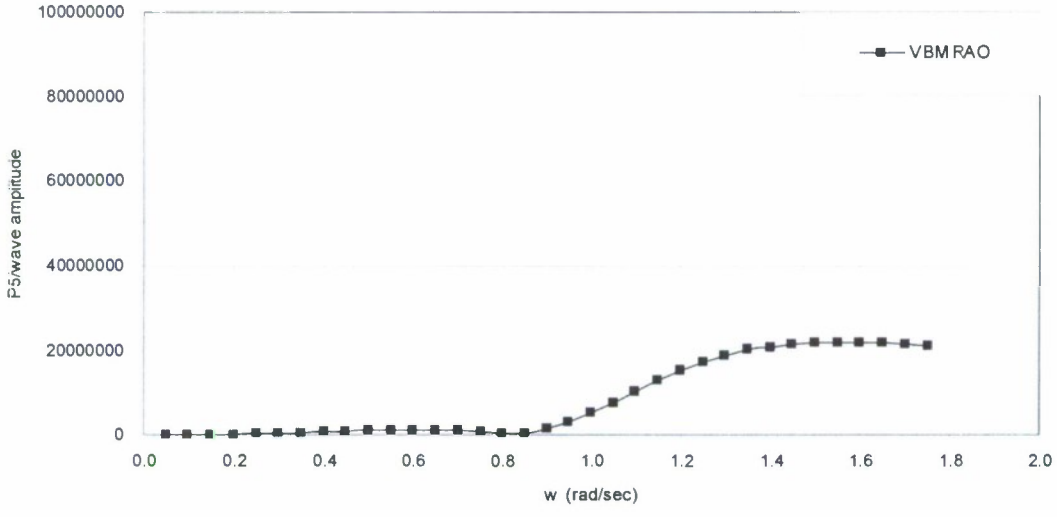

Figure A.16: Vertical bending moment RAO at beam waves in damage scenario 1

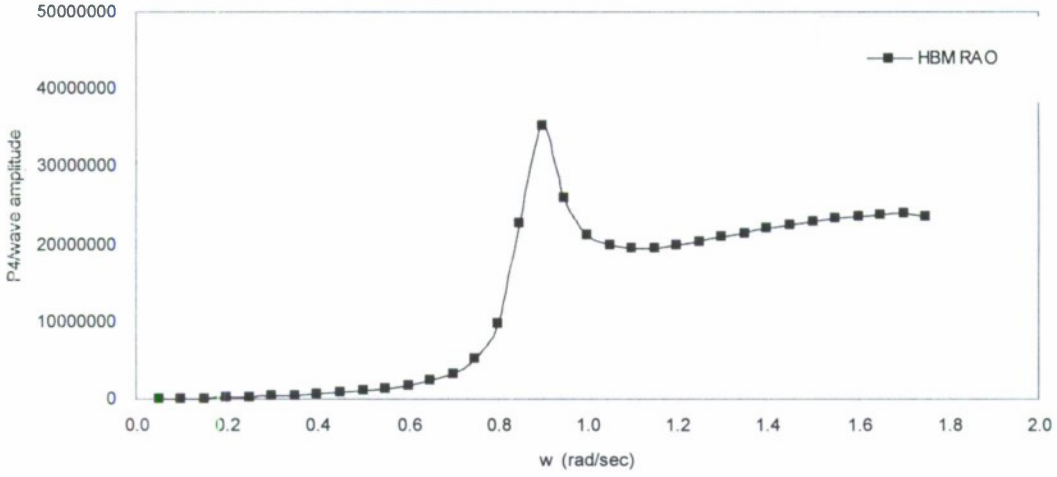

Figure A.17: Horizontal bending moment RAO at beam waves in damage scenario 1

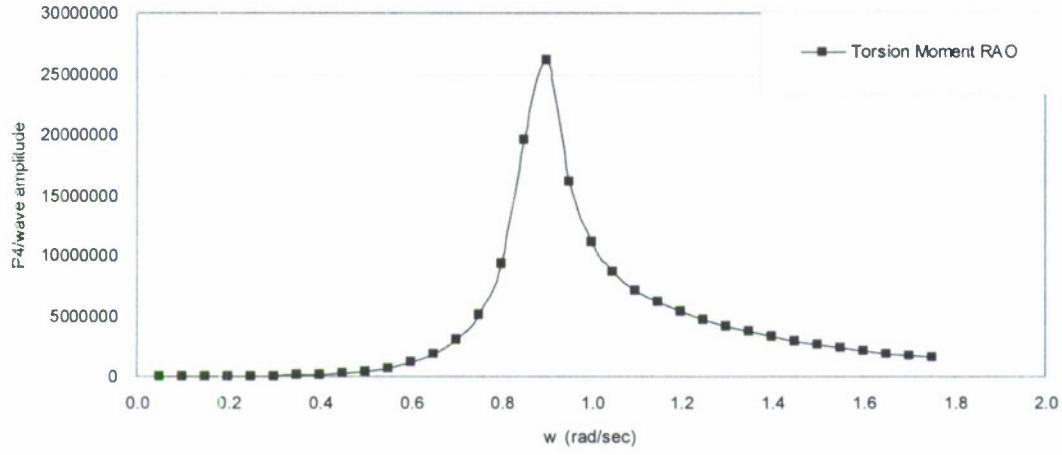

Figure A.18: Torsion moment RAO at beam waves in damage scenario 1

APPENDIX B:
MODEL UNCERTAINTIES OF THE 2D LINEAR METHOD

This appendix presents the details of the calculation of model uncertainties of the 2D linear method at various floating conditions. In the tables below, following symbols are used:

β – Wave heading angle
Hw – Wave height
Exp – Non-dimensional dynamic force response RAO from the experiment
Pred – Non-dimensional dynamic force response RAO from the 2D linear method
Xm – Model uncertainty of the 2D linear method
Mean – Mean model uncertainty of each force component
COV – Coefficient of variation
mean, L1 – mean value including all three sets of wave amplitudes
COV, L1 – COV including all three sets of wave amplitudes

Table B.1: Model uncertainties of the 2D linear method in intact condition

	load	β	Hw	exp.	pred.	Xm	mean	COV	mean, L1	COV, L1
				4.867E-03	4.000E-03	1.217E+00				
				1.186E-02	1.180E-02	1.005E+00				
				1.680E-02	1.740E-02	9.656E-01				
				1.761E-02	1.990E-02	8.849E-01				
			small	1.271E-02	1.890E-02	6.727E-01				
				1.144E-02	1.460E-02	7.834E-01				
				7.360E-03	8.200E-03	8.976E-01				
				1.525E-03	1.700E-03	8.972E-01				
		180		2.538E-03	3.800E-03	6.678E-01	8.879E-01	1.926E-01		
				4.650E-03	4.000E-03	1.163E+00				
				1.186E-02	1.180E-02	1.005E+00				
				1.247E-02	1.740E-02	7.169E-01				
				1.469E-02	1.990E-02	7.382E-01				
			large	1.257E-02	1.890E-02	6.652E-01				
				1.039E-02	1.460E-02	7.119E-01				
				6.115E-03	8.200E-03	7.457E-01				
				9.588E-04	1.700E-03	5.640E-01				
				2.456E-03	3.800E-03	6.462E-01	7.729E-01	2.446E-01		
				4.578E-03	4.000E-03	1.144E+00				
				1.105E-02	1.180E-02	9.365E-01				
				1.298E-02	1.740E-02	7.457E-01				
				1.085E-02	1.990E-02	5.454E-01				
			Very large	1.154E-02	1.890E-02	6.107E-01				
				8.678E-03	1.460E-02	5.944E-01				
				5.870E-03	8.200E-03	7.158E-01				
				1.537E-03	1.700E-03	9.043E-01				
	VBM			2.109E-03	3.800E-03	5.551E-01	7.503E-01	2.743E-01	8.037E-01	2.387E-01

				2.689E-03	1.800E-03	1.494E+00				
				6.798E-03	6.200E-03	1.096E+00				
				9.915E-03	1.050E-02	9.443E-01				
				1.337E-02	1.480E-02	9.036E-01				
			small	1.806E-02	1.690E-02	1.069E+00				
				2.445E-02	1.780E-02	1.374E+00				
				1.375E-02	1.660E-02	8.281E-01				
				4.379E-03	1.180E-02	3.711E-01				
		45		6.105E-03	6.000E-03	1.018E+00	1.011E+00	3.194E-01		
				3.024E-03	1.800E-03	1.680E+00				
				6.168E-03	6.200E-03	9.949E-01				
				7.961E-03	1.050E-02	7.582E-01				
				1.195E-02	1.480E-02	8.075E-01				
			large	1.194E-02	1.690E-02	7.065E-01				
				1.870E-02	1.780E-02	1.050E+00				
				1.657E-02	1.660E-02	9.983E-01				
				6.076E-03	1.180E-02	5.149E-01				
				3.871E-03	6.000E-03	6.452E-01	9.062E-01	3.760E-01		
				2.113E-03	1.800E-03	1.174E+00				
				6.281E-03	6.200E-03	1.013E+00				
				7.821E-03	1.050E-02	7.448E-01				
				9.712E-03	1.480E-02	6.562E-01				
			Very large	8.557E-03	1.690E-02	5.063E-01				
				1.365E-02	1.780E-02	7.668E-01				
				1.624E-02	1.660E-02	9.782E-01				
				1.836E-02	1.180E-02	1.556E+00				
				5.469E-03	6.000E-03	9.114E-01	9.230E-01	3.374E-01	9.467E-01	3.337E-01
				2.224E-03	1.700E-03	1.308E+00				
				6.698E-03	6.100E-03	1.098E+00				
				8.182E-03	1.050E-02	7.792E-01				
				1.162E-02	1.430E-02	8.128E-01				

			small	1.225E-02	1.620E-02	7.564E-01				
				9.961E-03	1.720E-02	5.791E-01				
				1.357E-02	1.650E-02	8.222E-01				
				1.113E-02	1.330E-02	8.372E-01				
		135		2.447E-03	3.100E-03	7.894E-01	8.647E-01	2.462E-01		
			large	2.088E-03	1.700E-03	1.228E+00				
				6.093E-03	6.100E-03	9.988E-01				
				5.611E-03	1.050E-02	5.344E-01				
				1.033E-02	1.620E-02	6.375E-01				
				1.372E-02	1.650E-02	8.317E-01				
				1.180E-02	1.330E-02	8.875E-01				
				2.455E-03	3.100E-03	7.920E-01	8.443E-01	2.714E-01		
			Very large	2.085E-03	1.700E-03	1.226E+00				
				4.335E-03	6.100E-03	7.106E-01				
				5.388E-03	1.050E-02	5.131E-01				
				3.563E-03	1.430E-02	2.492E-01				
				5.560E-03	1.620E-02	3.432E-01				
				7.780E-03	1.720E-02	4.523E-01				
				1.195E-02	1.650E-02	7.244E-01				
				1.309E-02	1.330E-02	9.841E-01				
				6.337E-03	3.100E-03	2.044E+00	8.053E-01	6.931E-01	8.376E-01	4.350E-01
			small	1.078E-03	5.000E-04	2.157E+00				
				9.756E-04	8.000E-04	1.220E+00				
				1.013E-03	1.100E-03	9.207E-01				
				1.938E-03	1.300E-03	1.491E+00				
				5.988E-03	1.500E-03	3.992E+00				
				1.974E-03	1.400E-03	1.410E+00				
				1.649E-03	1.200E-03	1.374E+00				
				2.728E-03	9.000E-04	3.031E+00	1.949E+00	5.833E-01		
				8.170E-04	5.000E-04	1.634E+00				
		90		9.305E-04	7.000E-04	1.329E+00				

			large	1.102E-03	1.100E-03	1.001E+00				
				4.897E-03	1.400E-03	3.498E+00				
				3.051E-03	1.400E-03	2.180E+00				
				1.134E-03	1.400E-03	8.098E-01				
				2.738E-03	9.000E-04	3.042E+00	1.928E+00	5.325E-01		
			Very large	5.476E-04	5.000E-04	1.095E+00				
				8.141E-04	7.000E-04	1.163E+00				
				1.227E-03	1.100E-03	1.116E+00				
				4.588E-03	1.400E-03	3.277E+00				
				3.593E-03	1.400E-03	2.567E+00				
				4.218E-03	1.400E-03	3.013E+00				
				2.911E-03	1.000E-03	2.911E+00	2.163E+00	4.593E-01	2.010E+00	4.890E-01
		180	small	small values ≈ 0						
			large	small values ≈ 0						

Intact	HBM		Very large	small values ≈ 0						
		45	small	1.002E-03	6.000E-04	1.670E+00				
				1.084E-03	2.200E-03	4.929E-01				
				2.366E-03	5.100E-03	4.640E-01				
				3.925E-03	8.200E-03	4.786E-01				
				7.309E-03	3.800E-03	1.923E+00				
				1.404E-02	5.300E-03	2.649E+00				
				5.480E-03	6.100E-03	8.983E-01				
				2.391E-03	4.800E-03	4.982E-01				
				3.388E-03	3.400E-03	9.965E-01	1.119E+00	7.045E-01		
			large	1.073E-03	6.000E-04	1.788E+00				
				1.003E-03	2.200E-03	4.561E-01				
				2.322E-03	5.100E-03	4.552E-01				
				4.755E-03	8.200E-03	5.799E-01				
				7.370E-03	3.800E-03	1.939E+00				
				1.106E-02	5.300E-03	2.086E+00				
				5.262E-03	6.100E-03	8.627E-01				
				1.554E-03	4.800E-03	3.238E-01				
				2.315E-03	3.400E-03	6.809E-01	1.019E+00	6.962E-01		
			very large	3.976E-04	6.000E-04	6.627E-01				
				1.006E-03	2.200E-03	4.572E-01				
				3.012E-03	5.100E-03	5.907E-01				
				5.636E-03	8.200E-03	6.873E-01				
				6.352E-03	3.800E-03	1.672E+00				

				9.191E-03	5.300E-03	1.734E+00				
				7.537E-03	6.100E-03	1.236E+00				
				7.283E-03	4.800E-03	1.517E+00				
				2.666E-03	3.400E-03	7.842E-01	1.038E+00	4.842E-01	1.059E+00	6.164E-01
		135	small	2.333E-04	5.000E-04	4.666E-01				
				8.775E-04	2.100E-03	4.178E-01				
				1.986E-03	5.500E-03	3.610E-01				
				3.165E-03	8.000E-03	3.957E-01				
				6.466E-03	3.200E-03	2.021E+00				
				5.508E-03	5.500E-03	1.001E+00				
				6.665E-03	7.000E-03	9.521E-01				
				5.317E-03	6.400E-03	8.307E-01				
				1.110E-03	1.900E-03	5.844E-01	7.812E-01	6.730E-01		
			large	1.572E-04	5.000E-04	3.145E-01				
				7.759E-04	2.100E-03	3.695E-01				
				1.571E-03	5.500E-03	2.856E-01				
				6.331E-03	3.200E-03	1.979E+00				
				9.656E-03	7.000E-03	1.379E+00				
				8.998E-03	6.400E-03	1.406E+00				
				1.247E-03	1.900E-03	6.564E-01	9.129E-01	7.361E-01		
			very large	2.373E-04	5.000E-04	4.746E-01				
				6.922E-04	2.100E-03	3.296E-01				
				1.891E-03	5.500E-03	3.438E-01				
				2.435E-03	8.000E-03	3.044E-01				
				3.471E-03	3.200E-03	1.085E+00				
				5.371E-03	5.500E-03	9.766E-01				
				7.970E-03	7.000E-03	1.139E+00				
				8.890E-03	6.400E-03	1.389E+00				
				4.338E-03	1.900E-03	2.283E+00	9.249E-01	7.063E-01	8.698E-01	6.820E-01
				3.888E-04	5.000E-04	7.776E-01				
				3.244E-04	1.300E-03	2.496E-01				

				7.262E-04	3.200E-03	2.269E-01					
				1.957E-03	1.010E-02	1.938E-01					
			small	8.011E-03	3.200E-03	2.503E+00					
				4.247E-03	2.600E-03	1.634E+00					
				1.510E-03	2.300E-03	6.567E-01					
		90		7.781E-03	2.700E-03	2.882E+00	1.140E+00	9.388E-01			
				2.381E-04	5.000E-04	4.762E-01					
				3.209E-04	9.000E-04	3.565E-01					
				8.322E-04	3.200E-03	2.601E-01					
				2.281E-03	6.200E-03	3.679E-01					
			large	2.185E-03	2.500E-03	8.742E-01					
				1.663E-03	2.300E-03	7.232E-01					
				1.525E-03	2.700E-03	5.650E-01	5.176E-01	4.233E-01			
				2.177E-04	6.000E-04	3.629E-01					
				3.230E-04	1.000E-03	3.230E-01					
				8.332E-04	3.200E-03	2.604E-01					
				3.040E-03	5.800E-03	5.241E-01					
			very large	1.848E-03	2.300E-03	8.035E-01					
				2.084E-03	2.300E-03	9.062E-01					
				1.736E-03	2.700E-03	6.431E-01	5.462E-01	4.551E-01	7.532E-01	9.420E-01	
			small	small values ≈ 0							
		180									

			large	small values ≈ 0						
	TM									
		45	small	1.707E-04	2.000E-04	8.535E-01				
				2.831E-04	9.000E-04	3.145E-01				
				8.780E-04	3.000E-03	2.927E-01				
				1.613E-03	8.800E-03	1.833E-01				
				6.303E-03	3.900E-03	1.616E+00				
				3.397E-03	8.000E-04	4.246E+00				
				2.769E-04	7.000E-04	3.956E-01				
				2.774E-04	1.100E-03	2.522E-01				
				3.645E-04	7.000E-04	5.207E-01	9.638E-01	1.359E+00		
			large	1.216E-04	2.000E-04	6.078E-01				
				4.404E-04	9.000E-04	4.893E-01				
				9.543E-04	3.000E-03	3.181E-01				
				1.735E-03	8.800E-03	1.972E-01				
				4.035E-03	3.900E-03	1.035E+00				
				3.399E-03	8.000E-04	4.249E+00				
				3.864E-04	7.000E-04	5.519E-01				
				1.221E-04	1.100E-03	1.110E-01				
				1.646E-04	7.000E-04	2.351E-01	8.660E-01	1.500E+00		
			large	1.240E-04	2.000E-04	6.201E-01				
				4.557E-04	9.000E-04	5.063E-01				
				9.992E-04	3.000E-03	3.331E-01				
				2.184E-03	8.800E-03	2.482E-01				
				2.188E-03	3.900E-03	5.611E-01				
				3.112E-03	8.000E-04	3.890E+00				

				5.288E-04	7.000E-04	7.554E-01			
				9.430E-04	1.100E-03	8.573E-01			
				3.148E-04	7.000E-04	4.497E-01	9.135E-01	1.240E+00	9.144E-01	1.314E+00
				9.246E-05	2.000E-04	4.623E-01			
				2.958E-04	9.000E-04	3.287E-01			
				6.583E-04	3.300E-03	1.995E-01			
				1.251E-03	1.010E-02	1.239E-01			
			small	4.065E-03	4.100E-03	9.915E-01			
				1.471E-03	1.300E-03	1.131E+00			
				1.262E-04	2.000E-04	6.309E-01			
				7.629E-04	1.200E-03	6.357E-01			
		135		5.266E-04	1.000E-03	5.266E-01	5.590E-01	6.027E-01		
				7.473E-05	2.000E-04	3.736E-01			
				2.990E-04	9.000E-04	3.322E-01			
				6.711E-04	3.300E-03	2.034E-01			
				1.792E-03	4.100E-03	4.372E-01			
			large	7.969E-04	2.000E-04	3.985E+00			
				7.085E-04	1.200E-03	5.904E-01			
				5.096E-04	1.000E-03	5.096E-01	9.187E-01	1.478E+00		
				1.272E-04	2.000E-04	6.358E-01			
				3.122E-04	9.000E-04	3.469E-01			
				7.110E-04	3.300E-03	2.155E-01			
				1.091E-03	1.010E-02	1.080E-01			
			large	1.388E-03	4.100E-03	3.385E-01			
				1.226E-03	1.300E-03	9.431E-01			
				1.130E-03	2.000E-04	5.649E+00			
				5.033E-04	1.200E-03	4.195E-01			
				7.765E-04	1.000E-03	7.765E-01	1.048E+00	1.666E+00	8.358E-01	1.496E+00
				1.095E-04	1.000E-04	1.095E+00			
				2.284E-04	8.000E-04	2.855E-01			
				6.757E-04	2.700E-03	2.502E-01			

				2.358E-03	1.150E-02	2.050E-01					
			small	8.485E-03	4.900E-03	1.732E+00					
				4.346E-03	3.800E-03	1.144E+00					
				1.273E-03	3.200E-03	3.977E-01					
		90		3.363E-03	2.600E-03	1.294E+00	8.003E-01	7.316E-01			
				8.906E-05	1.000E-04	8.906E-01					
				1.242E-04	4.000E-04	3.104E-01					
				7.417E-04	3.000E-03	2.472E-01					
				3.901E-03	7.300E-03	5.343E-01					
			large	3.084E-03	3.800E-03	8.116E-01					
				1.791E-03	3.300E-03	5.427E-01					
				1.136E-03	2.600E-03	4.368E-01	5.391E-01	4.453E-01			
				1.176E-04	2.000E-04	5.878E-01					
				1.459E-04	5.000E-04	2.919E-01					
				8.052E-04	2.900E-03	2.776E-01					
				2.829E-03	7.400E-03	3.823E-01					
			large	2.697E-03	3.500E-03	7.705E-01					
				3.620E-03	3.300E-03	1.097E+00					
				1.217E-03	2.600E-03	4.680E-01	5.536E-01	5.342E-01	6.387E-01	6.482E-01	

Table B.2: Model uncertainties of the 2D linear method in Damage Scenario 2

	load	β	Hw	exp.	pred.	Xm	mean	COV	mean, L1	COV, L1
				4.274E-03	4.800E-03	8.905E-01				
				1.454E-02	1.410E-02	1.031E+00				
				1.687E-02	2.020E-02	8.350E-01				
				1.592E-02	2.150E-02	7.405E-01				
			small	1.255E-02	1.840E-02	6.823E-01				
				1.099E-02	1.240E-02	8.864E-01				
				4.865E-03	5.100E-03	9.539E-01				
				1.162E-03	3.900E-03	2.978E-01				

		180		1.967E-03	2.500E-03	7.867E-01	7.894E-01	2.698E-01		
			large	3.804E-03	4.800E-03	7.926E-01				
				1.380E-02	1.410E-02	9.789E-01				
				1.650E-02	2.020E-02	8.170E-01				
				1.446E-02	2.150E-02	6.725E-01				
				1.241E-02	1.840E-02	6.742E-01				
				7.896E-03	1.240E-02	6.368E-01				
				4.268E-03	5.100E-03	8.369E-01				
				1.654E-03	3.900E-03	4.240E-01				
				2.053E-03	2.500E-03	8.212E-01	7.393E-01	2.145E-01		
			Very large	4.399E-03	4.800E-03	9.165E-01				
				1.314E-02	1.410E-02	9.317E-01				
				1.628E-02	2.020E-02	8.060E-01				
				1.328E-02	2.150E-02	6.175E-01				
				1.107E-02	1.840E-02	6.016E-01				
				8.950E-03	1.240E-02	7.217E-01				
				5.147E-03	5.100E-03	1.009E+00				
				2.692E-03	3.900E-03	6.903E-01				
	VBM			1.887E-03	2.500E-03	7.546E-01	7.832E-01	1.834E-01	7.707E-01	2.193E-01
		45	small	2.265E-03	2.400E-03	9.436E-01				
				8.682E-03	8.200E-03	1.059E+00				
				1.190E-02	1.300E-02	9.155E-01				
				1.610E-02	1.680E-02	9.582E-01				
				2.489E-02	1.820E-02	1.367E+00				
				2.202E-02	1.780E-02	1.237E+00				
				1.590E-02	1.590E-02	9.998E-01				
				5.444E-03	1.040E-02	5.235E-01				
				9.711E-03	6.200E-03	1.566E+00	1.063E+00	2.818E-01		
				2.201E-03	2.400E-03	9.172E-01				
				9.642E-03	8.200E-03	1.176E+00				
				1.163E-02	1.300E-02	8.950E-01				

	large	1.435E-02	1.680E-02	8.542E-01					
		1.662E-02	1.820E-02	9.132E-01					
		1.688E-02	1.780E-02	9.482E-01					
		1.876E-02	1.590E-02	1.180E+00					
		6.898E-03	1.040E-02	6.633E-01					
		7.578E-03	6.200E-03	1.222E+00	9.744E-01	1.884E-01			
	Very large	2.552E-03	2.400E-03	1.063E+00					
		9.285E-03	8.200E-03	1.132E+00					
		1.186E-02	1.300E-02	9.124E-01					
		1.354E-02	1.680E-02	8.058E-01					
		1.218E-02	1.820E-02	6.693E-01					
		1.521E-02	1.780E-02	8.545E-01					
		1.907E-02	1.590E-02	1.199E+00					
		1.492E-02	1.040E-02	1.435E+00					
		6.318E-03	6.200E-03	1.019E+00	1.010E+00	2.284E-01	1.016E+00	2.324E-01	
315	small	2.108E-03	2.600E-03	8.107E-01					
		9.834E-03	8.000E-03	1.229E+00					
		9.710E-03	1.300E-02	7.469E-01					
		1.546E-02	1.700E-02	9.095E-01					
		1.560E-02	1.840E-02	8.478E-01					
		1.326E-02	1.810E-02	7.327E-01					
		2.198E-02	1.580E-02	1.391E+00					
		1.513E-02	1.050E-02	1.441E+00					
		4.295E-03	6.100E-03	7.041E-01	9.792E-01	2.991E-01			
	large	2.228E-03	2.600E-03	8.568E-01					
		7.900E-03	8.000E-03	9.875E-01					
		8.311E-03	1.300E-02	6.393E-01					
		1.326E-02	1.700E-02	7.803E-01					
		1.270E-02	1.840E-02	6.901E-01					
		1.229E-02	1.810E-02	6.788E-01					
		3.420E-02	1.580E-02	2.164E+00					

		1.640E-02	1.050E-02	1.562E+00				
		4.177E-03	6.100E-03	6.847E-01	1.005E+00	5.182E-01		
	Very large	2.170E-03	2.600E-03	8.347E-01				
		7.314E-03	8.000E-03	9.143E-01				
		9.800E-03	1.300E-02	7.538E-01				
		1.079E-02	1.700E-02	6.347E-01				
		1.100E-02	1.840E-02	5.978E-01				
		1.398E-02	1.810E-02	7.725E-01				
		2.159E-02	1.580E-02	1.366E+00				
		1.855E-02	1.050E-02	1.767E+00				
		5.478E-03	6.100E-03	8.981E-01	9.488E-01	3.998E-01	9.776E-01	4.022E-01
90	small	4.884E-04	1.000E-04	4.884E+00				
		4.347E-04	2.000E-04	2.174E+00				
		5.341E-04	6.000E-04	8.902E-01				
		2.297E-03	1.100E-03	2.088E+00				
		4.413E-03	1.700E-03	2.596E+00				
		3.284E-03	2.500E-03	1.314E+00				
		5.734E-03	3.700E-03	1.550E+00				
		4.535E-03	5.600E-03	8.098E-01				
		7.804E-03	7.400E-03	1.055E+00	1.929E+00	6.578E-01		
	large	4.031E-04	1.000E-04	4.031E+00				
		4.656E-04	2.000E-04	2.328E+00				
		8.675E-04	6.000E-04	1.446E+00				
		2.665E-03	1.100E-03	2.422E+00				
		5.049E-03	1.700E-03	2.970E+00				
		2.178E-03	2.500E-03	8.714E-01				
		6.303E-03	3.700E-03	1.703E+00				
		5.278E-03	5.600E-03	9.424E-01				
		7.290E-03	7.400E-03	9.851E-01	1.967E+00	5.440E-01		
		2.920E-04	1.000E-04	2.920E+00				
		5.946E-04	2.000E-04	2.973E+00				

		1.515E-03	6.000E-04	2.525E+00				
		2.108E-03	1.100E-03	1.916E+00				
	Very large	4.434E-03	1.700E-03	2.608E+00				
		7.285E-03	2.500E-03	2.914E+00				
		4.454E-03	3.700E-03	1.204E+00				
		1.205E-02	5.600E-03	2.152E+00				
		5.379E-03	7.400E-03	7.269E-01	2.215E+00	3.618E-01	2.037E+00	5.059E-01
		4.452E-04	1.000E-04	4.452E+00				
		5.309E-04	3.000E-04	1.770E+00				
		9.321E-04	6.000E-04	1.553E+00				
		2.054E-03	1.200E-03	1.712E+00				
	small	2.515E-03	1.800E-03	1.397E+00				
		1.925E-03	2.400E-03	8.021E-01				
		1.049E-03	3.600E-03	2.914E-01				
		4.509E-03	5.500E-03	8.198E-01				
	270	2.554E-03	7.400E-03	3.451E-01	1.460E+00	8.586E-01		
		4.185E-04	1.000E-04	4.185E+00				
		4.973E-04	3.000E-04	1.658E+00				
		1.401E-03	6.000E-04	2.335E+00				
		1.968E-03	1.200E-03	1.640E+00				
	large	3.489E-03	1.800E-03	1.939E+00				
		1.836E-03	2.400E-03	7.649E-01				
		2.442E-03	3.600E-03	6.782E-01				
		6.231E-03	5.500E-03	1.133E+00				
		3.107E-03	7.400E-03	4.199E-01	1.639E+00	6.985E-01		
		3.291E-04	1.000E-04	3.291E+00				
		7.883E-04	3.000E-04	2.628E+00				
		1.913E-03	6.000E-04	3.188E+00				
		2.647E-03	1.200E-03	2.206E+00				
	Very large	3.288E-03	1.800E-03	1.827E+00				
		5.824E-03	2.400E-03	2.427E+00				

				2.282E-03	3.600E-03	6.338E-01				
				5.308E-03	5.500E-03	9.650E-01				
				3.483E-03	7.400E-03	4.706E-01	1.959E+00	5.409E-01	1.686E+00	6.701E-01
		180	small	small values ≈ 0						
			large	small values ≈ 0						
			Very large	small values ≈ 0						
Damage Scenario 2	HBM			7.742E-04	3.000E-04	2.581E+00				

			1.290E-03	2.000E-03	6.448E-01					
			3.043E-03	4.900E-03	6.211E-01					
			7.043E-03	8.200E-03	8.589E-01					
		small	1.004E-02	7.800E-03	1.287E+00					
			1.061E-02	8.800E-03	1.206E+00					
			6.764E-03	9.700E-03	6.973E-01					
			1.981E-03	6.600E-03	3.001E-01					
	45		9.366E-03	4.100E-03	2.284E+00	1.164E+00	6.721E-01			
			6.034E-04	3.000E-04	2.011E+00					
			1.116E-03	2.000E-03	5.581E-01					
			3.203E-03	4.900E-03	6.537E-01					
			5.014E-03	8.200E-03	6.114E-01					
		large	7.492E-03	7.800E-03	9.605E-01					
			6.594E-03	8.800E-03	7.493E-01					
			6.372E-03	9.700E-03	6.569E-01					
			2.699E-03	6.600E-03	4.089E-01					
			6.816E-03	4.100E-03	1.662E+00	9.192E-01	5.960E-01			
			5.192E-04	3.000E-04	1.731E+00					
			1.171E-03	2.000E-03	5.855E-01					
			3.484E-03	4.900E-03	7.110E-01					
			4.417E-03	8.200E-03	5.387E-01					
		very large	5.552E-03	7.800E-03	7.118E-01					
			7.564E-03	8.800E-03	8.596E-01					
			2.988E-03	9.700E-03	3.080E-01					
			6.100E-03	6.600E-03	9.242E-01					
			5.172E-03	4.100E-03	1.261E+00	8.479E-01	5.020E-01	9.772E-01	6.103E-01	
			6.391E-04	3.000E-04	2.130E+00					
			2.043E-03	2.100E-03	9.729E-01					
			3.660E-03	4.800E-03	7.625E-01					
			7.663E-03	8.500E-03	9.016E-01					
		small	7.118E-03	8.100E-03	8.787E-01					

			6.232E-03	8.800E-03	7.082E-01				
			9.571E-03	9.800E-03	9.766E-01				
			7.013E-03	7.000E-03	1.002E+00				
	315		3.408E-03	4.200E-03	8.115E-01	1.016E+00	4.230E-01		
			6.215E-04	3.000E-04	2.072E+00				
			2.203E-03	2.100E-03	1.049E+00				
			3.789E-03	4.800E-03	7.894E-01				
			8.214E-03	8.500E-03	9.663E-01				
		large	6.662E-03	8.100E-03	8.225E-01				
			5.636E-03	8.800E-03	6.404E-01				
			1.826E-02	9.800E-03	1.863E+00				
			7.556E-03	7.000E-03	1.079E+00				
			3.486E-03	4.200E-03	8.301E-01	1.124E+00	4.450E-01		
			5.451E-04	3.000E-04	1.817E+00				
			1.990E-03	2.100E-03	9.476E-01				
			4.823E-03	4.800E-03	1.005E+00				
			7.355E-03	8.500E-03	8.652E-01				
		very large	6.455E-03	8.100E-03	7.970E-01				
			6.531E-03	8.800E-03	7.421E-01				
			1.186E-02	9.800E-03	1.211E+00				
			1.094E-02	7.000E-03	1.562E+00				
			4.940E-03	4.200E-03	1.176E+00	1.125E+00	3.217E-01	1.088E+00	3.864E-01
			2.978E-04	2.000E-04	1.489E+00				
			4.451E-04	1.000E-04	4.451E+00				
			9.587E-04	5.000E-04	1.917E+00				
			5.601E-03	1.900E-03	2.948E+00				
		small	1.026E-02	7.300E-03	1.405E+00				
			4.103E-03	7.900E-03	5.194E-01				
			5.973E-03	5.100E-03	1.171E+00				
			5.017E-03	4.200E-03	1.195E+00				
	90		9.499E-03	4.000E-03	2.375E+00	1.941E+00	6.086E-01		

		large	2.303E-04	2.000E-04	1.152E+00				
			4.466E-04	1.000E-04	4.466E+00				
			1.171E-03	5.000E-04	2.343E+00				
			4.186E-03	1.900E-03	2.203E+00				
			6.689E-03	7.300E-03	9.163E-01				
			3.588E-03	7.900E-03	4.542E-01				
			6.006E-03	5.100E-03	1.178E+00				
			4.945E-03	4.200E-03	1.177E+00				
			7.544E-03	4.000E-03	1.886E+00	1.753E+00	6.792E-01		
		very large	1.059E-04	2.000E-04	5.295E-01				
			5.345E-04	1.000E-04	5.345E+00				
			1.607E-03	5.000E-04	3.215E+00				
			3.027E-03	1.900E-03	1.593E+00				
			5.390E-03	7.300E-03	7.384E-01				
			9.406E-03	7.900E-03	1.191E+00				
			4.699E-03	5.100E-03	9.214E-01				
			9.877E-03	4.200E-03	2.352E+00				
			5.066E-03	4.000E-03	1.266E+00	1.906E+00	8.084E-01	1.867E+00	6.783E-01
	270	small	4.282E-04	1.000E-04	4.282E+00				
			2.489E-04	1.000E-04	2.489E+00				
			4.802E-04	5.000E-04	9.604E-01				
			4.585E-03	2.100E-03	2.183E+00				
			8.399E-03	8.400E-03	9.998E-01				
			3.302E-03	7.600E-03	4.345E-01				
			3.530E-03	5.000E-03	7.061E-01				
			4.872E-03	4.100E-03	1.188E+00				
			4.047E-03	3.900E-03	1.038E+00	1.587E+00	7.633E-01		
			4.213E-04	1.000E-04	4.213E+00				
			3.734E-04	1.000E-04	3.734E+00				
			8.477E-04	5.000E-04	1.695E+00				
			2.738E-03	2.100E-03	1.304E+00				

			large	5.432E-03	8.400E-03	6.467E-01				
				3.180E-03	7.600E-03	4.184E-01				
				3.161E-03	5.000E-03	6.323E-01				
				5.233E-03	4.100E-03	1.276E+00				
				3.489E-03	3.900E-03	8.947E-01	1.646E+00	8.403E-01		
			very large	1.535E-04	1.000E-04	1.535E+00				
				4.190E-04	1.000E-04	4.190E+00				
				9.091E-04	5.000E-04	1.818E+00				
				2.345E-03	2.100E-03	1.117E+00				
				5.410E-03	8.400E-03	6.441E-01				
				7.576E-03	7.600E-03	9.969E-01				
				2.972E-03	5.000E-03	5.943E-01				
				5.411E-03	4.100E-03	1.320E+00				
				3.097E-03	3.900E-03	7.940E-01	1.445E+00	7.656E-01	1.559E+00	7.653E-01
		180	small	small values ≈ 0						
			large	small values ≈ 0						

TM		Very large	small values ≈ 0						
	45	small	1.423E-04	1.000E-04	1.423E+00				
			2.581E-04	6.000E-04	4.301E-01				
			7.364E-04	1.600E-03	4.603E-01				
			2.169E-03	3.000E-03	7.231E-01				
			8.258E-04	4.500E-03	1.835E-01				
			1.566E-03	1.800E-03	8.700E-01				
			6.408E-04	1.500E-03	4.272E-01				
			3.517E-04	1.800E-03	1.954E-01				
			6.887E-04	7.000E-04	9.839E-01	6.329E-01	6.414E-01		
		large	1.289E-04	1.000E-04	1.289E+00				
			1.980E-04	6.000E-04	3.301E-01				
			7.037E-04	1.600E-03	4.398E-01				
			9.831E-04	3.000E-03	3.277E-01				
			6.482E-04	4.500E-03	1.441E-01				
			9.164E-04	1.800E-03	5.091E-01				
			8.816E-04	1.500E-03	5.877E-01				
			4.838E-04	1.800E-03	2.688E-01				
			3.520E-04	7.000E-04	5.028E-01	4.888E-01	6.754E-01		
			1.079E-04	1.000E-04	1.079E+00				
			1.754E-04	6.000E-04	2.924E-01				
			6.552E-04	1.600E-03	4.095E-01				

	Very large	7.495E-04	3.000E-03	2.498E-01				
		6.707E-04	4.500E-03	1.490E-01				
		7.758E-04	1.800E-03	4.310E-01				
		1.395E-03	1.500E-03	9.301E-01				
		9.425E-04	1.800E-03	5.236E-01				
		3.468E-04	7.000E-04	4.954E-01	5.067E-01	6.093E-01	5.428E-01	6.324E-01
315	small	1.543E-04	1.000E-04	1.543E+00				
		7.723E-04	7.000E-04	1.103E+00				
		1.163E-03	1.400E-03	8.304E-01				
		3.930E-03	3.000E-03	1.310E+00				
		4.472E-03	4.700E-03	9.516E-01				
		8.564E-04	1.800E-03	4.758E-01				
		5.149E-04	1.800E-03	2.861E-01				
		9.498E-04	1.700E-03	5.587E-01				
		2.343E-04	6.000E-04	3.904E-01	8.277E-01	5.260E-01		
	large	1.575E-04	1.000E-04	1.575E+00				
		7.967E-04	7.000E-04	1.138E+00				
		1.344E-03	1.400E-03	9.601E-01				
		4.015E-03	3.000E-03	1.338E+00				
		2.660E-03	4.700E-03	5.660E-01				
		7.803E-04	1.800E-03	4.335E-01				
		1.104E-03	1.800E-03	6.131E-01				
		1.100E-03	1.700E-03	6.472E-01				
		3.538E-04	6.000E-04	5.896E-01	8.734E-01	4.568E-01		
	Very large	1.752E-04	1.000E-04	1.752E+00				
		8.336E-04	7.000E-04	1.191E+00				
		1.752E-03	1.400E-03	1.251E+00				
		2.580E-03	3.000E-03	8.599E-01				
		1.815E-03	4.700E-03	3.862E-01				
		1.100E-03	1.800E-03	6.112E-01				
		8.802E-04	1.800E-03	4.890E-01				

		1.451E-03	1.700E-03	8.534E-01				
		6.079E-04	6.000E-04	1.013E+00	9.341E-01	4.567E-01	8.784E-01	4.628E-01
90	small	2.512E-04	1.000E-04	2.512E+00	9.148E-01	7.563E-01		
		4.525E-04	5.000E-04	9.050E-01				
		1.218E-03	1.300E-03	9.371E-01				
		5.147E-03	3.500E-03	1.470E+00				
		6.353E-03	1.160E-02	5.477E-01				
		4.174E-03	1.060E-02	3.937E-01				
		3.260E-03	5.800E-03	5.620E-01				
		1.561E-03	4.100E-03	3.808E-01				
		1.520E-03	2.900E-03	5.243E-01				
	large	1.434E-04	1.000E-04	1.434E+00	7.107E-01	5.570E-01		
		4.730E-04	5.000E-04	9.459E-01				
		1.313E-03	1.300E-03	1.010E+00				
		3.455E-03	3.500E-03	9.871E-01				
		3.873E-03	1.160E-02	3.339E-01				
		3.101E-03	1.060E-02	2.926E-01				
		2.879E-03	5.800E-03	4.964E-01				
		1.552E-03	4.100E-03	3.786E-01				
		1.503E-03	2.900E-03	5.184E-01				
	Very large	1.250E-04	1.000E-04	1.250E+00	6.675E-01	5.847E-01	7.644E-01	6.600E-01
		5.290E-04	5.000E-04	1.058E+00				
		1.459E-03	1.300E-03	1.123E+00				
		2.018E-03	3.500E-03	5.766E-01				
		2.319E-03	1.160E-02	2.000E-01				
		2.822E-03	1.060E-02	2.662E-01				
		2.227E-03	5.800E-03	3.839E-01				
		2.893E-03	4.100E-03	7.056E-01				
		1.289E-03	2.900E-03	4.446E-01				
		8.888E-05	1.000E-04	8.888E-01				
		4.032E-04	5.000E-04	8.065E-01				

		270	small	9.624E-04	1.200E-03	8.020E-01				
				5.139E-03	3.700E-03	1.389E+00				
				5.835E-03	1.200E-02	4.862E-01				
				3.026E-03	1.080E-02	2.801E-01				
				2.489E-03	5.700E-03	4.366E-01				
				2.303E-03	4.000E-03	5.757E-01				
				6.304E-04	3.100E-03	2.034E-01	6.520E-01	5.595E-01		
			large	6.446E-05	1.000E-04	6.446E-01				
				6.461E-04	5.000E-04	1.292E+00				
				1.066E-03	1.200E-03	8.881E-01				
				3.072E-03	3.700E-03	8.303E-01				
				3.946E-03	1.200E-02	3.288E-01				
				2.576E-03	1.080E-02	2.386E-01				
				2.088E-03	5.700E-03	3.663E-01				
				3.097E-03	4.000E-03	7.742E-01				
				7.968E-04	3.100E-03	2.570E-01	6.245E-01	5.714E-01		
			Very large	1.019E-04	1.000E-04	1.019E+00				
				5.808E-04	5.000E-04	1.162E+00				
				1.224E-03	1.200E-03	1.020E+00				
				2.076E-03	3.700E-03	5.611E-01				
				2.487E-03	1.200E-02	2.072E-01				
				3.365E-03	1.080E-02	3.116E-01				
				2.141E-03	5.700E-03	3.755E-01				
				2.605E-03	4.000E-03	6.514E-01				
				1.252E-03	3.100E-03	4.038E-01	6.346E-01	5.536E-01	6.370E-01	5.398E-01

Table B.3: Model uncertainties of the 2D linear method in damage scenario 3

	load	β	Hw	exp.	pred.	Xm	mean	COV	mean, L1	COV, L1
				4.794E-03	4.000E-03	1.198E+00				
				1.216E-02	1.190E-02	1.022E+00				
				1.421E-02	1.790E-02	7.938E-01				
				1.442E-02	2.050E-02	7.036E-01				
			small	1.265E-02	1.880E-02	6.730E-01				
				1.226E-02	1.460E-02	8.394E-01				
				5.587E-03	8.700E-03	6.422E-01				
				1.177E-03	2.100E-03	5.603E-01				
		180		1.476E-03	3.500E-03	4.218E-01	7.616E-01	3.104E-01		
				4.509E-03	4.000E-03	1.127E+00				
				1.126E-02	1.190E-02	9.464E-01				
				1.417E-02	1.790E-02	7.914E-01				
				1.338E-02	2.050E-02	6.527E-01				
			large	1.259E-02	1.880E-02	6.695E-01				
				1.008E-02	1.460E-02	6.906E-01				
				5.329E-03	8.700E-03	6.125E-01				
				1.213E-03	2.100E-03	5.774E-01				
				1.181E-03	3.500E-03	3.374E-01	7.117E-01	3.173E-01		
				4.228E-03	4.000E-03	1.057E+00				
				6.315E-03	1.190E-02	5.307E-01				
				9.580E-03	1.790E-02	5.352E-01				
				1.103E-02	2.050E-02	5.380E-01				
			Very large	1.199E-02	1.880E-02	6.375E-01				
				1.568E-02	1.460E-02	1.074E+00				
				1.164E-02	8.700E-03	1.338E+00				
				1.077E-02	2.100E-03	5.128E+00				
	VBM			4.968E-03	3.500E-03	1.419E+00	1.362E+00	1.068E+00	9.4513E-01	9.3160E-01
				2.473E-03	2.000E-03	1.237E+00				

			6.746E-03	6.600E-03	1.022E+00				
			9.396E-03	1.110E-02	8.465E-01				
			1.160E-02	1.530E-02	7.579E-01				
		small	2.055E-02	1.780E-02	1.154E+00				
			1.745E-02	1.850E-02	9.432E-01				
			1.666E-02	1.660E-02	1.003E+00				
			7.131E-03	1.090E-02	6.542E-01				
	45		5.776E-03	6.500E-03	8.886E-01	9.452E-01	1.946E-01		
			2.507E-03	2.000E-03	1.253E+00				
			6.513E-03	6.600E-03	9.869E-01				
			8.386E-03	1.110E-02	7.555E-01				
			1.214E-02	1.530E-02	7.935E-01				
		large	1.800E-02	1.780E-02	1.011E+00				
			1.379E-02	1.850E-02	7.457E-01				
			1.806E-02	1.660E-02	1.088E+00				
			8.606E-03	1.090E-02	7.895E-01				
			4.944E-03	6.500E-03	7.607E-01	9.094E-01	2.009E-01		
			2.273E-03	2.000E-03	1.136E+00				
			6.315E-03	6.600E-03	9.569E-01				
			9.580E-03	1.110E-02	8.630E-01				
			1.103E-02	1.530E-02	7.208E-01				
		Very large	1.199E-02	1.780E-02	6.733E-01				
			1.568E-02	1.850E-02	8.478E-01				
			1.164E-02	1.660E-02	7.015E-01				
			1.077E-02	1.090E-02	9.880E-01				
			4.968E-03	6.500E-03	7.643E-01	8.502E-01	1.812E-01	9.0161E-01	1.9077E-01
			6.925E-04	5.000E-04	1.385E+00				
			7.556E-04	1.000E-03	7.556E-01				
			1.420E-03	1.400E-03	1.015E+00				
			2.521E-03	1.600E-03	1.576E+00				
		small	4.285E-03	1.800E-03	2.381E+00				

				5.234E-03	1.900E-03	2.754E+00				
				2.966E-03	2.000E-03	1.483E+00				
				1.931E-03	1.600E-03	1.207E+00				
		90		7.858E-03	4.000E-04	1.964E+01	3.578E+00	1.693E+00		
				5.799E-04	5.000E-04	1.160E+00				
				7.546E-04	1.000E-03	7.546E-01				
				1.377E-03	1.400E-03	9.837E-01				
				3.064E-03	1.600E-03	1.915E+00				
			iarge	5.025E-03	1.800E-03	2.792E+00				
				6.303E-03	1.900E-03	3.317E+00				
				4.100E-03	2.000E-03	2.050E+00				
				6.003E-04	1.600E-03	3.752E-01				
				1.523E-03	4.000E-04	3.808E+00	1.906E+00	6.288E-01		
				5.121E-04	5.000E-04	1.024E+00				
				6.886E-04	1.000E-03	6.886E-01				
				1.228E-03	1.400E-03	8.770E-01				
				2.513E-03	1.600E-03	1.571E+00				
			Very large	5.922E-03	1.800E-03	3.290E+00				
				7.755E-03	1.900E-03	4.082E+00				
				5.685E-03	2.000E-03	2.842E+00				
				1.847E-03	1.600E-03	1.154E+00				
				2.828E-03	4.000E-04	7.071E+00	2.511E+00	8.318E-01	2.6650E+00	1.3824E+00
			small	small values ≈ 0						
		180								

			large	small values ≈ 0						
			Very large	small values ≈ 0						
Damage Scenario 3	HBM	45	small	4.327E-04	6.000E-04	7.211E-01	7.320E-01	5.978E-01		
				1.012E-03	2.300E-03	4.402E-01				
				2.079E-03	4.700E-03	4.424E-01				
				3.740E-03	9.100E-03	4.110E-01				
				8.491E-03	5.400E-03	1.572E+00				
				8.093E-03	6.100E-03	1.327E+00				
				5.126E-03	7.100E-03	7.220E-01				
				1.658E-03	5.700E-03	2.909E-01				
				2.315E-03	3.500E-03	6.614E-01				
				4.343E-04	6.000E-04	7.239E-01				
				9.436E-04	2.300E-03	4.103E-01				
				2.221E-03	4.700E-03	4.725E-01				
				4.351E-03	9.100E-03	4.781E-01				

		large	7.721E-03	5.400E-03	1.430E+00				
			6.180E-03	6.100E-03	1.013E+00				
			7.815E-03	7.100E-03	1.101E+00				
			2.336E-03	5.700E-03	4.098E-01				
			2.009E-03	3.500E-03	5.739E-01	7.347E-01	4.969E-01		
		very large	2.266E-04	6.000E-04	3.777E-01				
			1.073E-03	2.300E-03	4.667E-01				
			3.225E-03	4.700E-03	6.863E-01				
			5.681E-03	9.100E-03	6.243E-01				
			6.312E-03	5.400E-03	1.169E+00				
			8.554E-03	6.100E-03	1.402E+00				
			8.354E-03	7.100E-03	1.177E+00				
			6.876E-03	5.700E-03	1.206E+00				
			3.284E-03	3.500E-03	9.383E-01	8.942E-01	4.106E-01	7.8695E-01	4.8781E-01
	90	small	2.451E-04	6.000E-04	4.085E-01				
			4.034E-04	1.300E-03	3.103E-01				
			9.444E-04	2.600E-03	3.632E-01				
			2.048E-03	6.900E-03	2.968E-01				
			4.421E-03	8.500E-03	5.202E-01				
			5.251E-03	4.300E-03	1.221E+00				
			4.087E-03	2.700E-03	1.514E+00				
			1.835E-03	2.200E-03	8.341E-01				
			4.509E-03	2.500E-03	1.804E+00	8.080E-01	7.070E-01		
		large	2.031E-04	6.000E-04	3.386E-01				
			3.321E-04	1.300E-03	2.554E-01				
			8.707E-04	2.600E-03	3.349E-01				
			1.963E-03	6.900E-03	2.845E-01				
			3.060E-03	8.500E-03	3.600E-01				
			5.340E-03	4.300E-03	1.242E+00				
			4.209E-03	2.700E-03	1.559E+00				
			1.552E-03	2.200E-03	7.055E-01				

				1.901E-03	2.500E-03	7.605E-01	6.489E-01	7.230E-01		
			very large	1.476E-04	6.000E-04	2.459E-01				
				3.548E-04	1.300E-03	2.729E-01				
				8.572E-04	2.600E-03	3.297E-01				
				2.205E-03	6.900E-03	3.195E-01				
				5.063E-03	8.500E-03	5.956E-01				
				9.134E-03	4.300E-03	2.124E+00				
				4.438E-03	2.700E-03	1.644E+00				
				2.118E-03	2.200E-03	9.627E-01				
				2.206E-03	2.500E-03	8.826E-01	8.197E-01	8.154E-01	7.5884E-01	7.3594E-01
		180	small	small values ≈ 0						
			large	small values ≈ 0						

	TM		Very large	small values ≈ 0						
		45	small	1.458E-04	1.000E-04	1.458E+00				
				3.699E-04	7.000E-04	5.284E-01				
				8.153E-04	1.800E-03	4.529E-01				
				1.938E-03	5.300E-03	3.656E-01				
				5.268E-03	4.700E-03	1.121E+00				
				3.550E-03	7.000E-04	5.071E+00				
				5.602E-04	9.000E-04	6.224E-01				
				2.918E-04	1.400E-03	2.084E-01				
				3.354E-04	7.000E-04	4.792E-01	1.145E+00	1.330E+00		
			large	1.139E-04	1.000E-04	1.139E+00				
				3.466E-04	7.000E-04	4.952E-01				
				7.851E-04	1.800E-03	4.362E-01				
				1.671E-03	5.300E-03	3.153E-01				
				3.048E-03	4.700E-03	6.485E-01				
				2.838E-03	7.000E-04	4.054E+00				
				4.591E-04	9.000E-04	5.101E-01				
				3.004E-04	1.400E-03	2.146E-01				
				3.567E-04	7.000E-04	5.096E-01	9.247E-01	1.300E+00		
			large	6.914E-05	1.000E-04	6.914E-01				
				3.889E-04	7.000E-04	5.555E-01				
				9.648E-04	1.800E-03	5.360E-01				
				1.310E-03	5.300E-03	2.471E-01				
				1.862E-03	4.700E-03	3.962E-01				
				2.155E-03	7.000E-04	3.078E+00				
				3.393E-04	9.000E-04	3.771E-01				

				5.474E-04	1.400E-03	3.910E-01				
				5.867E-04	7.000E-04	8.381E-01	7.901E-01	1.109E+00	9.5333E-01	1.2489E+00
				1.525E-04	1.000E-04	1.525E+00				
				3.361E-04	5.000E-04	6.722E-01				
				7.425E-04	1.600E-03	4.641E-01				
				2.162E-03	6.300E-03	3.431E-01				
			small	5.477E-03	9.900E-03	5.532E-01				
				6.283E-03	6.100E-03	1.030E+00				
				4.125E-03	4.200E-03	9.821E-01				
				1.652E-03	3.400E-03	4.859E-01				
		90		3.054E-03	2.700E-03	1.131E+00	7.985E-01	4.887E-01		
				5.973E-05	1.000E-04	5.973E-01				
				2.564E-04	5.000E-04	5.128E-01				
				6.431E-04	1.600E-03	4.019E-01				
				2.262E-03	6.300E-03	3.591E-01				
			large	3.876E-03	9.900E-03	3.915E-01				
				4.902E-03	6.100E-03	8.036E-01				
				4.270E-03	4.200E-03	1.017E+00				
				1.510E-03	3.400E-03	4.441E-01				
				1.136E-03	2.700E-03	4.209E-01	5.498E-01	4.052E-01		
				5.027E-05	1.000E-04	5.027E-01				
				3.390E-04	5.000E-04	6.779E-01				
				7.736E-04	1.600E-03	4.835E-01				
				1.640E-03	6.300E-03	2.603E-01				
			large	2.609E-03	9.900E-03	2.636E-01				
				3.806E-03	6.100E-03	6.240E-01				
				4.973E-03	4.200E-03	1.184E+00				
				2.068E-03	3.400E-03	6.083E-01				
				1.111E-03	2.700E-03	4.116E-01	5.573E-01	4.989E-01	6.3520E-01	4.9728E-01

APPENDIX C:
MODEL UNCERTAINTIES OF THE 2D NON-LINEAR METHOD

This appendix presents the details of the calculation of model uncertainties of the 2D non-linear method at various floating conditions. In the tables below, following symbols are used:

β – Wave heading angle
Hw (exp) – Wave height (Experiment)
Hw (pred) – Wave height (2D non-linear theory)
Exp(+) – Positive non-dimensional dynamic force response RAO from the experiment
Exp(-) – Negative non-dimensional dynamic force response RAO from the experiment
Pred (+) – Positive non-dimensional dynamic force response RAO from the 2D non-linear method
Pred (-) – Negative non-dimensional dynamic force response RAO from the 2D non-linear method
Xm(+) – Model uncertainty of the non-linear method for positive responses
Xm(-) – Model uncertainty of the non-linear method for negative responses
Mean(+) – Mean model uncertainty of each force component for positive responses under one wave weight
Mean(-) – Mean model uncertainty of each force component for negative responses under one wave weight
COV(+) – Coefficient of variation of model uncertainty for positive responses under one wave height
COV(-) – Coefficient of variation of model uncertainty for negative responses under one wave height
Mean(+) L1 – Mean model uncertainty of each force component for positive responses under both wave weights
Mean(-) L1 – Mean model uncertainty of each force component for negative responses under both wave weight
COV(+) L1 – Coefficient of variation of model uncertainty for positive responses under both wave height
COV(-) L1 – Coefficient of variation of model uncertainty for negative responses under both wave height

Table C.1: Model uncertainties of the 2D non-linear method in intact condition

	load	β	Hw (exp)	Hw (pred)	exp.(+)	exp.(-)	pred.(+)	pred.(-)	Xm (+)	Xm (-)	mean (+)	mean (-)	COV (+)	COV (-)	mean (+), L1	mean (-), L1	COV (+), L1	COV (-), L1
			1.160E+00		3.295E-03	6.174E-03	2.800E-03	6.300E-03	1.177E+00	9.800E-01								
			1.622E+00		1.039E-02	1.300E-02	1.260E-02	1.550E-02	8.246E-01	8.390E-01								
			2.483E+00		1.053E-02	1.486E-02	1.760E-02	1.880E-02	5.984E-01	7.906E-01								
			2.168E+00		1.223E-02	1.771E-02	1.680E-02	2.290E-02	7.282E-01	7.733E-01								
			2.029E+00	2m	1.145E-02	1.388E-02	1.470E-02	2.040E-02	7.789E-01	6.803E-01								
			8.445E-01		7.605E-03	1.247E-02	1.130E-02	1.600E-02	6.730E-01	7.796E-01								
			7.437E-01		3.470E-03	8.643E-03	9.000E-03	8.800E-03	3.856E-01	9.822E-01								
			6.206E-01		2.265E-03	4.294E-03	3.300E-03	9.000E-04	6.862E-01	4.771E+00								
		180	3.529E-01		3.045E-03	7.874E-03	1.300E-03	8.500E-03	2.342E+00	9.263E-01	9.104E-01	1.280E+00	6.332E-01	1.025E+00				
			2.370E+00		4.039E-03	4.665E-03	3.000E-03	7.000E-03	1.346E+00	6.664E-01								
			3.294E+00		9.363E-03	1.316E-02	1.130E-02	1.770E-02	8.286E-01	7.435E-01								
			4.202E+00		1.051E-02	1.616E-02	1.830E-02	1.930E-02	5.741E-01	8.371E-01								
			4.437E+00		9.041E-03	1.270E-02	1.660E-02	2.310E-02	5.447E-01	5.496E-01								
			3.929E+00	2.5m	9.807E-03	1.353E-02	1.430E-02	2.050E-02	6.858E-01	6.600E-01								
			3.445E+00		7.890E-03	9.552E-03	1.070E-02	1.620E-02	7.374E-01	5.896E-01								
			1.912E+00		5.549E-03	6.869E-03	8.700E-03	9.400E-03	6.379E-01	7.307E-01								
	VBM		1.419E+00		9.466E-04	1.891E-03	3.400E-03	1.900E-03	2.784E-01	9.955E-01								
			9.769E-01		1.855E-03	2.246E-03	5.000E-04	8.400E-03	3.710E+00	2.674E-01	1.038E+00	6.711E-01	1.004E+00	3.009E-01	9.743E-01	9.757E-01	8.413E-01	9.876E-01
			1.168E+00		2.319E-03	3.456E-03	7.000E-04	1.040E-02	3.313E+00	3.323E-01								
			1.617E+00		6.038E-03	5.853E-03	7.900E-03	1.410E-02	7.643E-01	4.151E-01								
			2.343E+00		7.124E-03	8.450E-03	1.120E-02	1.700E-02	6.361E-01	4.971E-01								

			2.297E+00		9.499E-03	1.353E-02	1.370E-02	1.820E-02	6.934E-01	7.434E-01								
			2.168E+00	2m	9.270E-03	1.457E-02	1.820E-02	1.690E-02	5.093E-01	8.619E-01								
			7.862E-01		1.666E-02	1.993E-02	1.830E-02	1.740E-02	9.106E-01	1.145E+00								
			7.960E-01		1.309E-02	1.874E-02	2.010E-02	1.590E-02	6.510E-01	1.179E+00								
			8.288E-01		5.223E-03	7.737E-03	1.240E-02	1.120E-02	4.212E-01	6.908E-01								
		45	6.215E-01		2.419E-03	5.957E-03	4.200E-03	7.800E-03	5.761E-01	7.637E-01	9.416E-01	7.365E-01	9.562E-01	4.032E-01				
			2.386E+00		2.587E-03	1.733E-03	6.800E-03	1.140E-02	3.804E-01	1.520E-01								
			3.296E+00		5.613E-03	6.600E-03	1.280E-02	8.700E-03	4.385E-01	7.586E-01								
			4.038E+00		6.492E-03	9.285E-03	1.070E-02	1.540E-02	6.067E-01	6.029E-01								
			4.187E+00		7.324E-03	1.000E-02	1.530E-02	1.770E-02	4.787E-01	5.651E-01								
			4.730E+00	2.5m	7.421E-03	1.016E-02	2.100E-02	1.700E-02	3.534E-01	5.976E-01								
			2.787E+00		1.252E-02	1.612E-02	1.820E-02	1.640E-02	6.879E-01	9.827E-01								
			2.013E+00		1.363E-02	1.931E-02	2.030E-02	1.720E-02	6.714E-01	1.123E+00								
			1.283E+00		1.574E-02	1.923E-02	1.330E-02	1.160E-02	1.184E+00	1.658E+00								
			1.120E+00		4.929E-03	5.068E-03	5.100E-03	7.300E-03	9.664E-01	6.943E-01	6.408E-01	7.926E-01	4.354E-01	5.354E-01	7.912E-01	7.646E-01	8.404E-01	4.662E-01
Intact			1.168E+00		1.064E-03	1.065E-03	2.200E-03	1.800E-03	4.836E-01	5.915E-01								
			1.617E+00		1.083E-03	9.661E-04	4.200E-03	3.900E-03	2.580E-01	2.477E-01								
			2.343E+00		2.674E-03	1.817E-03	4.100E-03	8.000E-03	6.522E-01	2.272E-01								
			2.297E+00		2.698E-03	6.973E-03	3.900E-03	1.320E-02	6.919E-01	5.283E-01								
			2.168E+00	2m	9.009E-03	5.315E-03	3.100E-03	1.640E-02	2.906E+00	3.241E-01								
			7.862E-01		1.323E-02	8.936E-03	2.800E-03	1.620E-02	4.726E+00	5.516E-01								
			7.960E-01		5.978E-03	6.584E-03	6.000E-03	6.600E-03	9.963E-01	9.975E-01								
			8.288E-01		1.610E-03	1.767E-03	4.300E-03	8.200E-03	3.745E-01	2.155E-01								
	HBM	45	6.215E-01		2.131E-03	2.461E-03	1.900E-03	2.300E-03	1.122E+00	1.070E+00	1.357E+00	5.282E-01	1.100E+00	6.088E-01				
			2.386E+00		2.428E-04	6.330E-04	2.300E-03	1.700E-03	1.056E-01	3.724E-01								
			3.296E+00		1.161E-03	7.979E-04	5.500E-03	5.400E-03	2.112E-01	1.478E-01								

			4.038E+00		3.628E-03	1.999E-03	5.800E-03	6.500E-03	6.254E-01	3.075E-01								
			4.187E+00		7.113E-03	3.148E-03	4.400E-03	1.340E-02	1.617E+00	2.349E-01								
			4.730E+00	2.5m	7.281E-03	5.340E-03	3.800E-03	1.630E-02	1.916E+00	3.276E-01								
			2.787E+00		7.328E-03	1.156E-02	3.200E-03	1.590E-02	2.290E+00	7.271E-01								
			2.013E+00		6.326E-03	8.792E-03	3.200E-03	1.290E-02	1.977E+00	6.816E-01								
			1.283E+00		5.729E-03	8.013E-03	4.800E-03	6.300E-03	1.194E+00	1.272E+00								
			1.120E+00		1.395E-03	2.974E-03	1.500E-03	2.300E-03	9.299E-01	1.293E+00	1.207E+00	5.960E-01	6.585E-01	7.275E-01	1.282E+00	5.621E-01	9.067E-01	6.617E-01
			1.168E+00		4.425E-05	3.026E-04	8.000E-04	6.000E-04	5.531E-02	5.043E-01								
			1.617E+00		3.891E-04	4.961E-04	1.500E-03	9.000E-04	2.594E-01	5.512E-01								
			2.343E+00		1.247E-03	8.299E-04	1.100E-03	2.600E-03	1.133E+00	3.192E-01								
			2.297E+00		1.399E-03	2.285E-03	1.900E-03	3.800E-03	7.365E-01	6.013E-01								
			2.168E+00	2m	4.159E-03	3.372E-03	3.100E-03	4.200E-03	1.342E+00	8.028E-01								
			7.862E-01		3.498E-03	3.105E-03	4.200E-03	3.900E-03	8.329E-01	7.962E-01								
			7.960E-01		1.993E-04	6.185E-04	5.100E-03	3.200E-03	3.909E-02	1.933E-01								
			8.288E-01		3.927E-05	3.096E-04	1.600E-03	1.800E-03	2.455E-02	1.720E-01								
	TM	45	6.215E-01		3.273E-05	4.171E-04	9.000E-04	9.000E-04	3.637E-02	4.634E-01	4.955E-01	4.893E-01	1.055E+00	4.721E-01				
			2.386E+00		3.138E-05	2.162E-04	7.000E-04	6.000E-04	4.483E-02	3.604E-01								
			3.296E+00		5.316E-04	3.930E-04	6.000E-04	5.000E-04	8.861E-01	7.861E-01								
			4.038E+00		1.500E-03	6.760E-04	2.300E-03	4.900E-03	6.523E-01	1.380E-01								
			4.187E+00		2.446E-03	1.370E-03	1.800E-03	4.600E-03	1.359E+00	2.978E-01								
			4.730E+00	2.5m	2.336E-03	1.921E-03	2.500E-03	4.300E-03	9.345E-01	4.468E-01								
			2.787E+00		3.099E-03	3.176E-03	2.500E-03	3.400E-03	1.239E+00	9.343E-01								
			2.013E+00		5.767E-04	8.193E-04	4.400E-03	2.900E-03	1.311E-01	2.825E-01								
			1.283E+00		8.445E-04	9.641E-04	1.600E-03	2.300E-03	5.278E-01	4.192E-01								
			1.120E+00		1.783E-04	4.868E-04	8.000E-04	8.000E-04	2.229E-01	6.085E-01	6.664E-01	4.748E-01	7.152E-01	5.393E-01	5.810E-01	4.821E-01	8.488E-01	4.910E-01

Table C.2: Model uncertainties of the 2D non-linear method in damage condition 2

	load	β	Hw (exp)	Hw (pred)	exp.(+)	exp.(-)	pred.(+)	pred.(-)	Xm (+)	Xm (-)	mean (+)	mean (-)	COV (+)	COV (-)	mean (+), L1	mean (-), L1	COV (+), L1	COV (-), L1
			1.148E+00		4.400E-03	3.500E-03	2.000E-04	2.000E-04	2.211E+01	1.757E+01								
			1.626E+00		1.260E-02	1.490E-02	1.210E-02	1.630E-02	1.044E+00	9.135E-01								
			2.297E+00		1.390E-02	1.790E-02	2.240E-02	2.130E-02	6.200E-01	8.383E-01								
			2.090E+00		1.460E-02	1.430E-02	1.760E-02	2.390E-02	8.316E-01	5.994E-01								
			2.065E+00	2m	1.110E-02	1.210E-02	1.460E-02	2.000E-02	7.626E-01	6.060E-01								
			1.758E+00		8.900E-03	8.700E-03	1.040E-02	1.430E-02	8.545E-01	6.085E-01								
			1.136E+00		5.200E-03	4.400E-03	7.400E-03	6.200E-03	6.972E-01	7.027E-01								
			1.015E+00		2.900E-03	1.200E-03	3.700E-03	2.800E-03	7.784E-01	4.262E-01								
		180	7.025E-01		3.400E-03	7.000E-04	1.100E-03	1.020E-02	3.082E+00	6.940E-02	1.084E+00	5.955E-01	7.537E-01	4.385E-01				
			2.400E+00		3.700E-03	4.900E-03	6.000E-03	1.210E-02	6.131E-01	4.021E-01								
			3.277E+00		1.130E-02	1.470E-02	7.000E-03	1.960E-02	1.617E+00	7.499E-01								
			4.065E+00		1.350E-02	1.700E-02	1.390E-02	1.870E-02	9.679E-01	9.078E-01								
			3.936E+00		1.170E-02	1.350E-02	1.950E-02	2.490E-02	5.991E-01	5.439E-01								
			4.129E+00	2.5m	1.090E-02	1.210E-02	1.120E-02	2.300E-02	9.713E-01	5.278E-01								
			3.045E+00		7.900E-03	9.400E-03	9.200E-03	1.410E-02	8.597E-01	6.671E-01								
			1.600E+00		3.700E-03	6.300E-03	8.300E-03	7.700E-03	4.473E-01	8.124E-01								
	VBM		1.445E+00		1.700E-03	3.900E-03	1.600E-03	4.100E-03	1.073E+00	9.544E-01								
			1.084E+00		6.000E-04	3.000E-03	3.000E-04	1.020E-02	2.127E+00	2.907E-01	1.031E+00	6.507E-01	5.186E-01	3.490E-01	1.056E+00	6.247E-01	6.251E-01	3.802E-01
			1.161E+00		1.100E-03	3.300E-03	1.100E-03	1.220E-02	1.019E+00	2.665E-01								
			1.594E+00		8.800E-03	1.030E-02	1.280E-02	2.050E-02	6.862E-01	5.032E-01								

			2.194E+00		1.100E-02	1.340E-02	1.280E-02	2.220E-02	8.622E-01	6.057E-01									
			2.310E+00		1.270E-02	1.690E-02	1.900E-02	2.180E-02	6.675E-01	7.757E-01									
			1.936E+00	2m	1.480E-02	2.090E-02	1.620E-02	2.280E-02	9.135E-01	9.146E-01									
			8.516E-01		1.490E-02	2.030E-02	1.600E-02	2.030E-02	9.316E-01	9.978E-01									
			8.774E-01		1.480E-02	2.080E-02	1.580E-02	1.670E-02	9.391E-01	1.244E+00									
			2.735E-01		5.000E-04	1.480E-02	1.000E-02	1.200E-02	5.210E-02	1.233E+00									
		45	5.806E-01		1.800E-03	1.030E-02	4.600E-03	8.200E-03	3.960E-01	1.254E+00	7.186E-01	8.661E-01	4.387E-01	4.113E-01					
			2.323E+00		2.400E-03	3.200E-03	2.300E-03	1.200E-02	1.024E+00	2.663E-01									
			3.200E+00		7.900E-03	1.060E-02	2.030E-02	1.170E-02	3.908E-01	9.041E-01									
			3.774E+00		9.800E-03	1.460E-02	1.230E-02	2.280E-02	7.975E-01	6.383E-01									
			3.903E+00		1.180E-02	1.570E-02	1.930E-02	2.330E-02	6.103E-01	6.755E-01									
			4.500E+00	2.5m	1.130E-02	1.390E-02	2.530E-02	1.950E-02	4.460E-01	7.122E-01									
			2.839E+00		1.420E-02	1.590E-02	1.730E-02	2.170E-02	8.202E-01	7.331E-01									
			1.952E+00		1.630E-02	1.970E-02	1.540E-02	1.590E-02	1.061E+00	1.238E+00									
			1.497E+00		1.280E-02	1.500E-02	1.190E-02	1.110E-02	1.078E+00	1.352E+00									
			1.058E+00		4.200E-03	6.300E-03	5.500E-03	8.300E-03	7.607E-01	7.561E-01	7.765E-01	8.083E-01	3.288E-01	4.025E-01	7.475E-01	8.372E-01	3.744E-01	3.969E-01
Damage Scenario2			1.161E+00		5.000E-04	8.000E-04	1.100E-03	2.200E-03	4.688E-01	3.414E-01									
			1.594E+00		2.100E-03	2.000E-04	4.100E-03	5.600E-03	5.019E-01	3.190E-02									
			2.194E+00		3.600E-03	2.400E-03	4.300E-03	1.170E-02	8.420E-01	2.080E-01									
			2.310E+00		4.200E-03	6.300E-03	3.700E-03	1.850E-02	1.147E+00	3.418E-01									
			1.936E+00	2m	7.400E-03	7.400E-03	3.900E-03	1.730E-02	1.897E+00	4.277E-01									
			8.516E-01		7.800E-03	8.100E-03	5.000E-03	1.190E-02	1.559E+00	6.809E-01									
			8.774E-01		5.400E-03	8.100E-03	5.500E-03	7.000E-03	9.864E-01	1.159E+00									
			2.735E-01		1.500E-03	3.700E-03	4.400E-03	8.700E-03	3.313E-01	4.206E-01									
	HBM	45	5.806E-01		5.400E-03	6.500E-03	2.400E-03	3.600E-03	2.242E+00	1.806E+00	1.109E+00	6.020E-01	6.034E-01	9.186E-01					
			2.323E+00		1.500E-03	3.000E-04	5.900E-03	4.800E-03	2.577E-01	5.400E-02									

			3.200E+00		1.800E-03	7.000E-04	8.100E-03	8.400E-03	2.260E-01	8.230E-02								
			3.774E+00		3.900E-03	3.400E-03	5.900E-03	9.300E-03	6.578E-01	3.709E-01								
			3.903E+00		4.500E-03	3.800E-03	5.200E-03	1.510E-02	8.660E-01	2.540E-01								
			4.500E+00	2.5m	4.800E-03	6.100E-03	4.100E-03	1.740E-02	1.164E+00	3.492E-01								
			2.839E+00		1.020E-02	4.700E-03	4.900E-03	1.340E-02	2.091E+00	3.476E-01								
			1.952E+00		6.000E-03	9.700E-03	5.700E-03	9.600E-03	1.053E+00	1.008E+00								
			1.497E+00		6.700E-03	5.500E-03	4.400E-03	4.300E-03	1.520E+00	1.277E+00								
			1.058E+00		6.700E-03	3.400E-03	2.700E-03	3.900E-03	2.495E+00	8.598E-01	1.148E+00	5.114E-01	6.758E-01	8.428E-01	1.128E+00	5.567E-01	6.231E-01	8.680E-01
			1.161E+00		1.000E-04	3.000E-04	1.900E-03	2.200E-03	2.880E-02	1.471E-01								
			1.594E+00		0.000E+00	4.000E-04	1.100E-03	3.500E-03	3.020E-02	1.101E-01								
			2.194E+00		4.000E-04	9.000E-04	5.400E-03	8.800E-03	7.690E-02	9.950E-02								
			2.310E+00		9.000E-04	1.400E-03	2.700E-03	8.000E-03	3.340E-01	1.726E-01								
			1.936E+00	2m	8.000E-04	5.000E-04	3.600E-03	6.300E-03	2.131E-01	8.510E-02								
			8.516E-01		1.000E-03	1.400E-03	4.200E-03	3.600E-03	2.298E-01	3.902E-01								
			8.774E-01		7.000E-04	1.300E-03	5.300E-03	2.100E-03	1.347E-01	6.227E-01								
			2.735E-01		4.000E-04	1.400E-03	3.600E-03	2.200E-03	1.107E-01	6.355E-01								
	TM	45	5.806E-01		0.000E+00	7.000E-04	1.200E-03	8.000E-04	7.000E-03	8.233E-01	1.295E-01	3.429E-01	8.507E-01	8.275E-01				
			2.323E+00		0.000E+00	2.000E-04	5.800E-03	2.300E-03	5.600E-03	7.810E-02								
			3.200E+00		1.000E-04	3.000E-04	3.800E-03	1.500E-03	1.940E-02	1.950E-01								
			3.774E+00		4.000E-04	8.000E-04	3.700E-03	1.500E-03	1.180E-01	5.282E-01								
			3.903E+00		8.000E-04	5.000E-04	3.000E-03	1.200E-03	2.668E-01	3.752E-01								
			4.500E+00	2.5m	7.000E-04	4.000E-04	3.000E-03	1.200E-03	2.218E-01	3.616E-01								
			2.839E+00		8.000E-04	7.000E-04	3.500E-03	1.400E-03	2.191E-01	4.658E-01								
			1.952E+00		1.400E-03	1.400E-03	5.100E-03	2.000E-03	2.812E-01	6.838E-01								
			1.497E+00		1.200E-03	8.000E-04	4.200E-03	1.700E-03	2.744E-01	4.477E-01								
			1.058E+00		2.000E-04	5.000E-04	1.400E-03	6.000E-04	1.291E-01	8.652E-01	1.706E-01	4.445E-01	6.280E-01	5.335E-01	1.500E-01	3.937E-01	7.165E-01	6.579E-01

APPENDIX D

THE RULE-BASED FORMULAE FOR PREDICTING EXTREME DESIGN LOADS

This appendix presents the detailed formulae, which were recommended by Lloyds Register of Shipping (2002) to calculate extreme design loads.

In intact condition, the minimum value of vertical wave-induced bending moment, M_w, at any position along the ship may be taken as follows:

$$M_W = F_f D_f M_o \quad \text{kNm} \qquad \text{[D-1]}$$

Where F_f is the hogging, F_{fH}, or sagging, F_{fS}, correction factor based on the amount of bow flare, stern flare, length and effective buoyancy of the aft end of the ship above the waterline.

D_f the longitudinal distribution factor

$= 0$ at aft end of L_R [D-2a]

$= 1.0$ between $0.4\,L_R$ and $0.65\,L_R$ [D-2b]

$= 0$ at forward end of L_R [D-2c]

$$M_O = 0.1 L_f f_s L_R{}^2 B_{WL} (C_{b1} + 0.7) \text{ kNm} \qquad \text{[D-3]}$$

$$L_f = 0.0412 L_R + 4.0 \quad \text{for } L_R \le 90 \text{ m} \qquad \text{[D-4a]}$$

$$= 10.75 - \left(\frac{300 - L_R}{100}\right)^{1.5} \quad \text{for } L_R > 90 \text{ m} \qquad \text{[D-4b]}$$

$$= 10.75 \quad \text{for } L_R > 300 \text{ m} \qquad \text{[D-4c]}$$

$$= 10.75 - \left(\frac{L_R - 350}{150}\right)^{1.5} \quad \text{for } L_R > 350 \text{ m} \qquad \text{[D-4d]}$$

f_s = service area factor applicable to the service area notation

B_{WL} = maximum waterline breadth, in metres

L_R = rule length, taken as 0.965 of length between perpendicular, in metres

$C_{b1} = C_b$ but is not to be taken less than 0.6

Extreme vertical wave bending moments

$$M_{WEX} = K_{fEX} M_W \quad \text{kNm} \qquad \text{[D-5]}$$

K_{fEX} = 1.5, is called extreme scaling factor

In damaged conditions, the so-called residual strength vertical wave bending moment should be used to assess damaged strength. A residual strength reduction factor, K_{fRS}, is given by the following:

$$K_{fRS} = 1.1 H_{rw} L_R{}^{-0.48} \qquad \text{[D-6]}$$

Where, H_{rw}, residual wave height, is taken as the significant wave height that has a 20 percent probability being exceeded for the service area,

$$H_{rw} = 0.9H_S \qquad \text{m} \qquad \text{[D-7]}$$

The residual strength vertical wave bending moment, M_{WRS}, at any position along the ship is given by:

$$M_{WRS} = K_{fRS} M_W \qquad \text{Kn m} \qquad \text{[D-8]}$$

In damaged conditions, a duration of 12 hours is recommended for short term prediction of extreme design loads.